HYDRODYNAMICS OF AN UNCONSTRAINED CYLINDER IN FORCED ROLL

by

Jakub Cichowicz

A Thesis Submitted for the Degree of Doctor of Philosophy

Department of Naval Architecture and Marine Engineering

University of Strathclyde

2012

This thesis is the result of the author's original research. It has been composed by the author and has not been previously submitted for examination which has led to the award of a degree.

Signed:

Date:

Nature uses as little as possible of anything.

Johannes Kepler
Harmonice Mundi, 1619

To my mother

To my wife, Ania

TABLE OF CONTENTS

Acknowledgments

There are many people, who contributed to this work, to whom I owe gratitude.

In particular:

Professor Dracos Vassalos for giving me the opportunity and supervising this work

Dr Andrzej Jasionowski for his encouragement and teaching me basic principles of research

Dr Sandy Day and David Clelland for continuous support and effort put in the process

Charles Key for organising experimental work

William McGuffy for his work on the ‘gyro’

Edward Nixon, Grant Dunning and William Wright for help with measurements

Professor Maciej Pawłowski for valuable discussions, support and informal lectures in science

My friends from the SSRC, Department and those scattered all around the world for being my friends

My wife Ania, daughter Jagoda and son Jan for their patience and for being my pride and joy

My parents for their love, effort and for giving me the most important lectures in life

Abstract

The research summarised in this thesis addresses the problem of determining the hydrodynamic properties of damaged ships subjected to forced oscillations in calm water.

Traditionally forces of hydrodynamic reaction acting on a rigid body moving through a fluid are derived either analytically or numerically. The former approach is usually restricted to small amplitude motions of the body moving through an unbounded domain of ideal fluid. The methodology is relatively simple and computationally effective but, as experimental results suggest, accuracy of the prediction, particularly for roll motion is unsatisfactory even for intact ships. The advanced CFD-based techniques are more suitable in addressing this problem, particularly the case of a damaged ship, but they are computationally demanding. Therefore, in order to tackle the issue efficiently, there is a need for high-quality experimental data for validation of the numerical results. However, the experiments, particularly in roll, are very difficult and there is very little data available for the simpler case of intact ships and virtually none for damaged ships. As the problem involves complex nonlinear phenomena, the physical tests should be performed in a controllable environment and therefore, the 'classical' sea-keeping tests have very limited applicability in this respect. Furthermore, the calm-water experiments are usually performed with oscillations about a fixed axis and the adequacy of such an approach for investigating hydrodynamic properties of damaged ships can be questioned. That is, the physical tests on partially restricted models are of great value, particularly for validating analytical / numerical approaches, but the presence of constraints may introduce artificial conditions affecting the dynamical characteristics of the system.

Accounting for this, the approach adopted in this thesis involves a freely-floating body subjected to harmonic excitations generated by an internal forcing mechanism. It is postulated that by removing all kinematic constraints the system can be analysed in the most realistic (achievable in calm water) and controllable configuration.

Although use of gyroscopic moment generators for forced roll experiments is not a novelty, this methodology has never been fully exploited for measurements of hydrodynamic reaction forces acting on an unconstrained model of a damaged ship. As the experiments were unprecedented, they resulted in a modest amount of collected data but provided great opportunity for examining the nature and scale of the underlying phenomena. Furthermore, in the course of the research the methodology has been refined and has eventually reached the point at which it can be utilised to produce large amount of experimental data in an accurate and efficient way. From this perspective, the research is prenormative.

Nomenclature

A, P - arbitrary points in space

A - point on the natural axis of rotation

a_{ii} - added mass/inertia in i-th mode of motion

a_{ij} - added mass/inertia the coupling of j-th into i-th mode of motion

b_{ii} - damping i-th mode of motion

b_{ij} - damping in the coupling of j-th into i-th mode of motion

c_{ii} - restoring coefficient in i-th mode of motion

c_{ij} - restoring coefficient in coupling of j-th into i-th mode of motion

B - beam of the vessel

B - centre of buoyancy

B_1, B_L - linear term in damping moment

B_2, B_Q - quadratic term in damping moment

D - Rayleigh's dissipation function

E_w - period-average total energy of a wave per unit area

$\mathbf{F}$ - body (mass) force

Fn - Froude number

Fh - depth Froude number

F_2 - horizontal force (to sustain motion)

F_3 - vertical force (to sustain motion)

$\mathbf{f}_h$ - force of hydrodynamic reaction

G - centre of gravity

g - gravity acceleration

h - depth below free surface

H - depth of the fluid domain

I - unit matrix

I - moment of inertia

I_{44} - inertia about the roll axis

$\mathbf{i}, \mathbf{j}, \mathbf{k}$ - unit vectors of standard Cartesian basis

$\mathbf{i}_i$ - unit vectors of arbitrary orthonormal basis

k - wave number

$\mathbf{L}, \mathbf{L}^I$ - vector of angular momentum

M - metacentre

M_{ij} - generalised mass

M_{44} - moment to sustain roll motion

$\mathbf{M}_h$ - moment of hydrodynamic reaction

m - mass

$\mathbf{n}$ - normal vector

$\mathbf{n}_B$ - vector normal to a body surface

$\mathbf{n}_F$ - vector normal to a fluid surface

O - origin of the inertial coordinate system

$\overline{OA}$ - elevation of the natural axis of rotation

$\overline{OG}$ - vertical postion of centre of gravity above waterplane

P - point on the axis of gyro pivoting

$\mathbf{P}, \mathbf{P}^I$ - vector of linear momentum

$\mathbf{P}_n$ - vector of normal stresses

P_S - stress tensor

p - pressure

q_k - generalised coordinates

R_w - magnitude of a wave resistance force

$\mathbf{r}$ - radius vector

$\mathbf{r}_S$ - radius vector of a surface element

S_B - surface of a body

∂S_B - boundary curve

S_F - surface bounding a fluid element

S_Σ - surface bounding system comprising a fluid element and a body

t - time

T - kinetic energy

T - draught of the vessel

T_0 - period of oscillations

U - gravitational potential

u - group velocity of a wave

V_B - volume of a body

V_F - volume of a fluid domain at the initial time $t = 0$

$\mathbf{v}$ - velocity vector

$\mathbf{v}_O$ - translational velocity

v - magnitude of a velocity vector

v_k - generalised velocities

v_{nB} - magnitude of a velocity in direction normal to the body surface

v_{nF} - magnitude of a velocity in direction normal to the fluid surface

$\mathbf{v}_S$ - velocity vector of a surface element

W_0 - work of dissipative forces

x, y, z - Cartesian coordinates

x_1, x_2, x_3 - rectangular coordinates

y, z, φ - sway, heave, roll

ε - phase angle

Γ - intensity of vortex filament

Λ - Lagrangian function

λ - wave length

ζ_0 - wave amplitude

ϕ - velocity potential

ρ - density

μ - viscosity

$\boldsymbol{\omega}$ - vector of instantaneous angular velocity

ω - circular frequency

ω_B - nondimensional frequency

∇ - gradient operator

$\otimes$ - outer product

$\times$ - vector product

$\hat{}$ - nondimensional quantity

$[.]_{ij}$ - experimental estimates of added inertia and damping

Chapter 1 Introduction

Determining forces of hydrodynamic reaction acting on a damaged ship is a very important but complex task. To date, even accurate prediction of hydrodynamics of intact ships is challenging. The existing analytical or numerical methods are either inaccurate or so computationally demanding that they cannot be used in day-to-day engineering practice. On one hand, we are used to accept uncertainty as an inherent part of engineering and therefore we might accept the facts and assume that tools at our disposal offer 'sufficient accuracy for engineering purposes'. However, in so doing we admit that we do not know *how* - the expensive and technologically advanced ships we build, carrying often several thousands of people on board, will behave in a seaway. Concerning the dynamic response of ships carrying liquid cargo or being subjected to flooding in a consequence of a damage we know even less. This leads to a serious dissonance between technological advances and our knowledge about the dynamics of ships we design and build. The fundamental research carried out in the 1960's and 1970's gave us great opportunities to benchmark our understanding of hydrodynamics of ships. We learnt that we could reproduce theoretical predictions obtained for basic geometries with reasonable accuracy. We learnt also, that the prediction did not actually match up with reality and the differences were not small. In particular, we were unable to predict the hydrodynamic properties of a ship rolling with moderate and large amplitudes and subsequently we had to introduce empirical corrections to our predictions. Unfortunately, the corrections are applicable only to 'typical' ships in intact condition. There is no such a methodology available for ships in damaged condition. Given the continuous advances in CFD techniques as well as always-increasing availability of computational power, we are capable of addressing many issues numerically, although not on an industrial scale. Moreover, CFD codes are not perfect either and they need to be benchmarked against *some* high-quality data. On the other hand, such reliable data is available only for simple cases – those for which we *can* obtain reasonable predictions with the use of simple techniques. The data for complex cases is either unreliable or not available at all.

The research presented in the following addresses this problem. It does not aim at proposing solutions to the problem of hydrodynamics of damaged ships but it attempts to answer two fundamental questions. Firstly, it is the question of feasibility to perform simple, efficient and accurate measurements of hydrodynamic reaction in roll carried out on a floating body subjected to forced oscillations in calm water in intact and damaged conditions. Secondly, an attempt is made to reason on why contemporary 'theory' and experiments do not match up.

1.1 Research objectives

The primary objective of this research is to demonstrate and discuss the feasibility of accurate measurements of hydrodynamic reaction in roll motion performed on an unconstrained cylindrical model in the presence of an 'open-to-sea' compartment.

This entails the following specific tasks:

- Design and deployment of a gyroscopic roll generator
- Validation of measurements of hydrodynamic reaction on the model in intact condition
- Measurements of hydrodynamic reaction on the model in damaged condition
- Post-processing and analysis of the results

In the last stage, the data collected during the experiments is analysed and benchmarked against available experimental and numerical results.

It should be emphasised here that it was *not* an objective of the present research to investigate any particular theoretical model. The objective was to investigate – experimentally – a particular mechanical system (rigid body in forced roll - intact and damaged) and to discuss how the evidence collected during the measurements could be used to enhance knowledge of the hydrodynamic/dynamic properties of the system in question.

1.2 Organisation of the thesis

The thesis opens with a critical review of an available literature with particular attention paid to the experimental works on roll hydrodynamics. The review is presented in Chapter 2.

Some brief introduction to dynamics of a floating body is presented in Chapter 3.

In Chapter 4 some experimental works are discussed in some detail in order to 'set a stage' for presenting results of the current research.

Chapter 4 addresses the experiments undertaken. A general discussion on the work undertaken and the key contributions of this research follows in Chapter 6, leading to specific conclusions and recommendations in Chapter 7. Finally, bibliography and references are given in Chapter 8.

Chapter 2 Critical Review

While the matter of the research presented here is very specific and narrow, it inherits the complexity of several topics. In the most general terms, it can be encapsulated as interaction of a fluid and rigid body. Depending on a problem formulation, a variety of mathematical techniques can be employed to depict physics and study the nature of the interaction. The diversity of mathematical tools expands further when the interaction involves actions of not only external but also internal fluids. While physical representation becomes more detailed, the models develop into very complex compositions, which can seldom be solved without help of numerous assumptions. This in turn, results in a countless number of scientific treatises and engineering papers. For that reason the résumé of available references cannot be, by any manner of means, complete. Contrary, the selection of papers presented here, whilst being very specific, it is dictated mainly by availability of the source and on personal critique.

From the point of view of the research undertaken, those papers addressing physical tests are of key interest. Thus, it seems right to start with Froude and his experimental work on 'resistance' forces experienced by the rolling ship as reported for example in (Froude, 1861). Theoretically, the hydrodynamic reaction and the fluid-body interaction was investigated by many great researchers, e.g. as outlined in (Lamb, 1932), but it was not until the mid-twentieth century before first, simplified but complete, solutions to the problem were obtained (Ursell, 1949). This allowed developing various methods based on distribution of hydrodynamic singularities and conformal mapping, e.g. Frank's 2D source method (Frank, 1967), making use of the so-called 'strip theory' and evolving further into slender-body models, e.g.(Wehausen, 1969) or (Webster, 1975). Although based on an inviscid flow assumption, the models proved reasonably accurate, fast and very convenient to use, making them first-choice tools for many sea-keeping computer applications, see for instance (Ankudinov, 1991) or (Journee, 1992).

The numerical techniques for solving flow about ships advancing in waves have further evolved towards more complex tools allowing better handling of nonlinear phenomena, e.g. (Papanikolaou and Shellin, 1992), (Raven, 1997) or (Yasukawa, 2000).

The most advanced but requiring also significant computational power CFD techniques are not yet used in full extent in sea-keeping calculations or numerical survivability assessment. Instead, they are employed to address some very specific problems of hydrodynamics (Gao et al., 2011a) or coupled with other sea-keeping codes for better performance (Gao et al., 2011b).

Concerning physical experiments, it is impossible not to refer to impressive and highly appreciated experiments by Vugts, who investigated hydrodynamic reaction on cylinders swaying, heaving and rolling in free surface (Vugts, 1968). For more than half a century the experimental work of Vugts served as a yardstick for benchmarking numerous theoretical and experimental studies on roll hydrodynamics. The works of Vugts were followed by an extensive research carried out in Japan in 1970's, aiming at determining damping due to bilge keels and viscous effects. The research had been reported in a series of detailed reports, e.g. (Ikeda et al., 1978a, Ikeda et al., 1978b, Ikeda et al., 1979) and later outlined by Himeno (Himeno, 1981). These studies provided empirical formulae for estimating various components of roll damping (friction, lift, wave and eddy making as well as components due to bilge keels). Although the so-called Ikeda's method bears all disadvantages of statistical averaging and is applicable only to 'typical' ships, it has been in common use until today and has been incorporated into numerous computer codes.

Obviously, the research activities on roll damping continue in Japan, e.g. (Katayama et al., 2012), but the American researchers have also done some interesting work focusing on physical experiments and CFD techniques to mention only (Seah and Yeung, 2003, Yeung et al., 1998) or (Bassler et al., 2012, Bassler et al., 2010). Particularly the former papers by Yeung and Seah and Yeung are of special interest as they report on numerical and experimental studies on rolling cylinders subjected to forced oscillations in a free surface of a viscous fluid. As shown, the numerical results obtained by means of Free-surface Random Vortex Method (FRVM) match very well the authors own experimental data as well as results of experiments by Vugts. Specifically, it is discussed in there that the viscous flow prediction provides higher estimate for roll damping and lower for roll added inertia, in line with Vugts findings. The numerical results presented in the second paper are benchmarked

against the experiments by (Na et al., 2002) on the optimised configuration of bilge keels of FPSOs operating in high seas.

Interesting, although debatable, experiments on roll damping of unconventional mid-ship sections have been reported in (Yuck et al., 2003). The controversy derives from the fact that the centre of gravity of the model was varied in such a way that any given excitation frequency corresponded to the natural frequency of the ship in the amended configuration.

The nonlinear nature and aspects related to modelling of roll damping have attracted attention of researchers and scientists over decades, as summarised in (Cotton et al., 2000), (Spyrou and Thompson, 2000), (Spyrou, 2004) and recently in (Bassler et al., 2009). Generally, the driving factor for this research was interest in the stability of ships in intact and damaged condition, particularly in frequency ranges close to the roll natural frequency. In 1980 Cardo (Cardo et al., 1981) presented results of studies on sub- and ultra-harmonic resonances (where the response is dominated either by natural frequency lower or higher than excitation frequency) while taking into account nonlinearities in damping and restoring moments. It concluded that the ultra-harmonic resonance would not compromise safety whilst the results indicated a stability hazard from sub-harmonic resonance.

In the later paper, Cardo studied two distinct models of nonlinear damping (Cardo et al., 1982). The mixed linear-quadratic and linear-cubic formulae were discussed in a relation to predicting of roll response in free and forced motions. The meticulous investigation referred to many earlier research studies (including those by Froude) suggesting (linear or) quadratic dependency of the roll damping on a motion amplitude. In particular, the point was made after (Dalzell, 1978) that the cubic dependency was used mainly for the reason of simpler mathematical manipulation. The author highlighted also that significant discrepancies could be expected while deriving critical damping based on free- or forced- oscillations due to distinctions in the underlying mathematical models. The author concluded that a set of experiments were needed in order to explore the problem further - free roll on ship models of the variable inertial moment and determination of maximum amplitude, based on forced oscillations, as a function of the excitation intensity.

In 1990's Contento published a paper on the applicability of a constant coefficients roll equation for predicting large amplitude motions (Contento et al., 1996). The authors investigated also the impact of the number of degrees of freedom (DoF) considered. The work was supplemented by an extensive experimental campaign. Although not entirely concluded, the research highlighted the need for expressing of the hydrodynamic coefficients as functions of frequency, amplitude and effective wave steepness. The authors underlined the necessity of further, extensive, experimental studies in order to derive empirical or semi-empirical multivariate coefficients.

Some interesting studies were presented in (Taylan, 2000), where comparison of various models of nonlinear damping and restoring on roll response of a ship subjected to regular wave excitation was presented. Also in (Kuroda and Ikeda, 2003) there is an experimental study on intact ship behaviour in heavy beam seas in relation to coupling with heave and large drift.

More recently techniques for obtaining critical damping data were published in (Spyrou, 2004) and (Bulian, 2004).

It is noteworthy that customarily, the ship equations of motions are usually given in the vectorial notation, e.g. see (Pawłowski, 2001, Pawłowski, 1999) or any handbook on basic ship theory. There are relatively few references where the Euler-Lagrange formulation of the problem is used, e.g. Hamiltonian formulation by (van Daalen et al.), effect of forward speed by (Marshall et al., 1982) or dynamics of floating bodies by (Sadeghi, 2005).

One of the important nonlinear problems related to the stability of ships highlighted in (Spyrou and Thompson, 2000) is the presence of large free surfaces, e.g. on LNG carriers or other ship types. This inevitably leads to consideration of a sloshing phenomenon i.e. movements of liquid in containers, which are usually subjected to external excitation. In principle, even relatively small motions of the containers may lead to significant deformations of free surface and violent motions of the fluid. This may lead to significant dynamic loads on the structure of the container and have serious impact on ship motions, in particular roll and sway.

An example of the early studies on the stability of a free surface can be found in (Benjamin and Ursell, 1954), where the deformation of a plane free surface of an ideal fluid is treated analytically. In 1960's (Verhagen and Wijngaarden, 1965) studied hydraulic jumps forming in an oscillating open tank. Based on linearised equations (shallow water waves) the authors determined the resonant frequency at which (theoretically) the amplitude of oscillations would become infinite. Experiments showed good agreement with theory and observed wave formations (jumps) had profiles similar to those predicted, within expected accuracy. Furthermore, at the jump disappearance (at frequencies well beyond resonant frequency), a formation of a solitary wave (travelling across the tank) was observed.

It is noteworthy that damping properties of free-surface tanks on roll motion has been known for almost a century, and the passive anti-rolling tanks (ART) as we know them today, were studied already by Froude and his contemporaries. A comprehensive review on the development of anti-rolling devices can be found in (Moaleji and Greig, 2007). However, due to the complexity of the problem advances in theoretical and experimental studies have been of rather limited nature. In mid-sixties there was a remarkable experimental campaign run at the TU of Delft, Netherlands, where the damping properties of some type of free-surface tanks were investigated by (van den Bosch and Vugts, 1966).

In the research that followed, Chester investigated the theory describing the oscillations of a liquid in a tank near resonant frequency where linearised theory is invalid (Chester, 1968). It was shown by the author that although phenomena are described adequately by the classical wave equation the boundary conditions could not be satisfied unless nonlinear terms were included in the formulation. The nonlinear effects discussed comprised dissipation in boundary layer (only due to small amplitude) and dispersion, which introduced higher order harmonics. It was also shown there that the response spectrum became multivalued at some frequencies. The theoretical considerations by Chester were benchmarked against experiments reported in the latter publication (Chester and Bones, 1968). In principle, the theory proved to be qualitatively in good agreement with the experimental results. Some discrepancies were observed and explained by the insufficient dissipation in the boundary layer model

(where only sides of the tank were accounted for) and the fact that some calculated parameters diverged from the actual experimental values. Specifically, it was shown that the nonlinearities included in the mathematical model were well pronounced and the attained wave profiles were similar to those predicted. Furthermore, the response characteristics showed clearly the presence of several local maxima (where the response curve was multivalued). It was postulated by the authors that the fact that the maximum on the response characteristics was attained and the response curve was connected indicated influence of dissipative components.

Apart from purely theoretical studies there was some work carried out on full-scale ARTs, as for example trials addressing efficiency of anti-rolling tanks reported in (Plank et al., 1972), where an attempt had been made to determine a transfer function of ART fitted onboard of the research vessel R/V *Yaquina*.

The energy dissipation in sloshing was a subject to the series of papers by Demirbilek who studied energy dissipation in a rectangular tank undergoing roll motion about a fixed axis (Demirbilek, 1983a, Demirbilek, 1983b, Demirbilek, 1983c). The author derived the mathematical formulation to the problem and proposed a technique (based on a variant of Rayleigh dissipation function) for solving the equations.

.From the point of view of ship dynamics, a matter of prime importance is a coupling of sloshing with ship motions. Given the importance and complexity of the problem, there is a large volume of publications on the subject. This is partially due to the fact, that similar coupling effects are observed while studying the dynamics of a damaged ship. Indeed, the only formal difference between sloshing of liquid cargo and a hull-floodwater interaction derives from the absence of damage opening in the former case.

The principal difficulty in studying the coupling of sloshing with ship motions derives from the fact that the resultant system is closed, i.e. by analogy to control systems it can be said that a ship with a partially filled compartment forms a feedback system. Furthermore, since both the oscillating ship and the water sloshing in the compartment are nonlinear systems (with the latter characterised by a particularly strong nonlinear characteristics) modelling of the responses becomes a very complex

task. Firstly, the nonlinearity of the problem defines the limit of applicability of linearised approaches. Secondly, response analysis in a frequency domain is by definition inappropriate for the nonlinear systems. Instead, the analysis (particularly when the system is subjected to a random excitation and large amplitude motions) should be carried out in a time domain. For these reasons, a number of theoretical and experimental studies were performed in order to enhance the understanding of the coupling of sloshing with ship motions.

In their research (Ikeda and Yoshiyama, 1991) observed strong effect of a coupling of roll and sway and studied its impact on performance of ARTs. In principle, they suggested that sway decreases reduction of roll (effectiveness of ARTs) and lengthens the natural period of oscillations of the tank.

In another important paper authors investigated the effect of a liquid cargo on roll response (Francescutto and Contento, 1994). They compared experimental data with CFD results on the coupling of roll and sloshing. While considering a 'frozen' cargo they noticed a very similar behaviour to that observed during the present studies. Namely, they reported that a presence of a liquid mass caused a significant shift of the roll natural frequency towards lower frequencies compared to the 'frozen' mass. In the case of a compartment filled with the liquid cargo two peaks were observed on the roll response curve. The first dominated by hydrostatic effects and the second by sloshing. The measured roll motion was heavily damped.

Similar observations were made by (Francescutto et al., 1996), who presented a preliminary comparison between hydrostatic and 'fully' hydrodynamic models for sloshing in a 2D roll-sloshing coupling problem. The studies highlighted significant differences in the mathematical formulations- in the case of a hydrostatic model the roll response was characterised by a single fundamental mode whereas the hydrodynamic model implied two natural modes. The authors reported also a noticeable impact of sloshing on roll damping.

In their studies (Kambisseri et al., 1997) investigated damping effect of floodwater. The experiments were performed with the flooded compartment positioned below- and above the deck. In both cases, floodwater caused a significant increase in roll

damping. However, the authors concluded that more damping was experienced in the case of the flooded compartment positioned above the deck.

The chaotic response of a box-shaped barge with partially filled (closed) compartment oscillating in regular waves was investigated by (Murashige and Aihara, 1998). Their research originated from the observation made during the steady-state oscillations. Namely, during the steady-state oscillations the model was unintentionally impinged with a stick. As a result, the amplitude of roll increased significantly while the period lengthened from T to 2T. The subsequent tests on a simplified cylindrical model (3DOF - sway, heave and roll) confirmed the chaotic behaviour and existence of strange attractors (not present in case of "dry" hull). Further analysis indicated that the chaotic behaviour could be a result of the highly nonlinear restoring moment in the ship-floodwater system.

The complexity of transient behaviour in a closed system was also highlighted by (Rognebakke and Faltinsen, 2003). The authors studied the coupling of sway motion and sloshing, following a detailed experimental programme. They observed a harmonic steady-state response even in the presence of violent sloshing inside the compartment. They concluded that the harmonic response allows employing simplified models for analysing the steady state sloshing problems. However, an attempt to use of simplified models to describe transient phenomena was unsuccessful.

By late 1980s a simplified model of floodwater dynamics to be used in sea-keeping simulations was presented by Vassalos and Turan. The model was further improved by Letizia and Vassalos (Kaliningrad 1995) and (Papanikolaou and Spanos, 2002). This simple model proved sufficiently accurate for qualitative assessment of survivability of damaged ship.

Dedicated studies on the impact of floodwater dynamics on behaviour of a damaged ship have been carried out by many researches in the pursuit for better understanding of underlying physics and more accurate mathematical modelling, e.g. (Vassalos et al., 1998) or (Jasionowski, 2001a, Jasionowski et al., 2007, Jasionowski, 2010). In one of the attempts (Kong and Faltinsen, 2010) investigated the time-domain behaviour of a damaged ship with a large scale damage. They carried out physical tests and

performed numerical simulations in calm water and in regular waves. The simulated RAOs were checked against the ITTC benchmark study. The results showed that the unsatisfactory accuracy of the floodwater model and the authors concluded that the further theoretical studies should be supported by an extensive experimental campaign.

A comprehensive résumé on the impact of liquid cargo on ship dynamics can be found in (Journee, 2000). However, there have been very few attempts to derive an expression for a force of hydrodynamic reaction in the damaged condition in a way similar to the intact ship formulation. Customarily the models of a damaged ship hydrodynamics use a set of hydrodynamic coefficients derived for the intact vessel, e.g. (Letizia, 1996), (de Kat, 2000), (Dodworth, 2000) or (Jasionowski, 2001b). An attempt to derive experimentally hydrodynamic coefficients of a damaged ship was reported in (Jasionowski and Vassalos, 2002).

In case of a damaged ship, apart from the flooding model there is a need for modelling a flow through the shell openings. High accuracy (in terms of a flow rate prediction combined with floodwater dynamics) of the flooding process can only be achieved with use of CFD techniques. If the interest is mainly on the rate of flow, there are various models based on the Bernoulli equation such as presented in (Vassalos et al., 2000). The simplified inflow/outflow models are easy to integrate with ship motions calculators, see for example (Jasionowski, 2001b) and offer reasonable approximation of hydrostatic loads impressed by floodwater on the ship structure. An example of validation of the flooding modules based on Bernoulli equation can be found in (Ruponen, 2006).

The list compiled here would be incomplete without mentioning the PhD theses of those who carried out physical tests on roll hydrodynamics. The studies by (Turan, 1993) and (Chai, 2005) shall be discussed in a more detail in the following.

The preliminary results of experiments discussed in the following have already been presented in (Cichowicz et al., 2009), (Cichowicz et al., 2010). (Cichowicz et al., 2011). The content of these publications served as a starting point to the discussion presented in Chapter 4 and Chapter 6.

There is one publication that started it all - the report of forced roll experiments performed with use of gyro-based roll generator (Spouge et al., 1986). Without it, the thesis would look different.

Chapter 3 Dynamics of a floating body

3.1 Introductory remarks

The following chapter addresses a specific problem of a floating body. The body in question shall be considered rigid and its boundaries shall be impenetrable to particles of surrounding fluid. Furthermore, the body and a surrounding fluid shall be treated generally as *one dynamical system and thus the troublesome calculations of the effect of the fluid pressures on the surfaces of the solids is avoided* (Lamb, 1932). Unless specified otherwise, the fluid, by which the rigid body is surrounded either entirely or in part, is assumed incompressible and irrotational, characterised by single-valued velocity potential, ϕ, and motions of the fluid are due to those of the body. The fluid must satisfy continuity condition expressed by means of Laplace equation

$$\nabla^2\phi = 0 \tag{3.1}$$

Additionally, a component of the fluid velocity normal to the surface of the body at any given point must be equal to the normal component of the velocity of the surface. Finally, all components of the fluid velocity far from the body must vanish. This implies that a closed surface can be determined within the otherwise unbounded domain of the fluid surrounding the body, through which, on account of vanishing velocity, no flux of matter is observed.

From formal point of view, both the rigid body and the fluid domain are described by the same mathematical model of continuum. It should be noted, however, that the model of continuum is an abstraction – physical matter is discrete, composed of elementary particles (Aris, 1962) although in many physical applications the microscopic structure of matter is of secondary importance. Instead of looking into interactions between molecules, the attention is paid to interactions between small but finite dimensions *particles*. These particles are characterised by properties (e.g. energy, momentum, velocity, temperature) taken as an average of the properties of the individual molecules constituting the particle. The fundamental difference between a rigid body and a fluid is that it is assumed in the most physical applications that de-

formation of the former is assumed negligible. This property is a consequence of very strong forces of interactions between molecules. Such forces are much weaker within fluids; furthermore, fluid molecules perform frequent, chaotic, "jumps" between points of a space. Subsequently, the molecules can respond fast to external forces of relatively small magnitudes by rearranging or *deforming*. Since a structure of fluid adapts "fast", the deformation takes place with finite velocities, proportional to impressed forces. Such feature is called *liquidity*.

3.2 Hydrodynamic reaction due to motion of a solid body

In the most general case a force and moment of a hydrodynamic reaction can be expressed in the following form

$$\mathbf{f}_h = -\oint_{S_F} \mathbf{p}_n dS \tag{3.2}$$

$$\mathbf{M}_h = -\oint_{S_F} \mathbf{r} \times \mathbf{p}_n dS \tag{3.3}$$

These equations – the force of reaction and moment of it - portray interaction of some isolated fluid domain V_F with the rest of the surrounding fluid. However, in the case of a floating body the expressions could be reformulated; if the integration of took place over surface of the solid, S_B, these quantities would correspond to forces of interaction between the solid body and the surrounding fluid. Furthermore, since the body and the fluid constitute the same mechanical system they must, at any given point in time maintain the dynamical equilibrium. This also implies that it is irrelevant whether motions of fluid initiated motions of the solid or vice versa – the d'Alembert's principle requires all the forces to be balanced, regardless of their nature and origin. Thus, the problem can be formulated twofold – either as motions of the fluid in which the wetted surface of the body forms a part of the fluid boundary or as motions of the body in which the entire fluid domain reduces to the wetted surface of the body. In the following, the problem will be addressed from the fluid perspective at first and then it shall be reformulated in order to derive description coherent with the physical tests presented in the following chapters.

3.2.1 General formulation

The principles of mechanics imply that the rate of change of linear momentum of the fluid domain must be equal to all the forces acting on in. These forces consist of body, or mass forces, and surface forces acting on the fluid domain through the bounding surface. In a presence of the body immersed in the fluid, the surface of the fluid domain will be a sum of the "outside" surface of the fluid domain S_F and the surface of the body, S_B that is $S_\Sigma = S_F + S_B$. Hence, conservation of linear momentum takes the following form

$$\int_{V_F} \rho \frac{d\mathbf{v}}{dt} dV = \int_{V_F} \rho \mathbf{F} dV + \oint_{S_\Sigma} \mathbf{p}_n dS \tag{3.4}$$

Analogically, rate of change of angular momentum accommodates for a presence of the body immersed in the fluid domain, that is

$$\int_{V_F} \frac{d}{dt}\left[\mathbf{r} \times (\rho \mathbf{v})\right] dV = \int_{V_F} \mathbf{r} \times (\rho \mathbf{F}) dV + \oint_{S_\Sigma} \mathbf{r} \times \mathbf{p}_n dS \tag{3.5}$$

It should be noted that the differentiation operator could be applied to the integrand based on the assumption that the volume V_F corresponds to volume of fluid at initial time $t = 0$.

Bearing in mind that the normal stresses $\mathbf{p}_n$ can be expressed as $\mathbf{n} \cdot P_S$ the surface integrals of the above equations can be expanded by means of the body, S_B, and fluid, S_F surfaces with normal vectors $\mathbf{n}_F$ and $\mathbf{n}_B$, respectively. Thus, given that the $\mathbf{n}_F$ and $\mathbf{n}_B$ have opposite directions, it follows that

$$\oint_{S_\Sigma} \mathbf{p}_n dS = \oint_{S_F} \mathbf{n}_F \cdot P_S dS - \oint_{S_B} \mathbf{n}_B \cdot P_S dS = \oint_{S_F} \mathbf{n}_F \cdot P_S dS - \mathbf{f}_h \tag{3.6}$$

and

$$\oint_{S_\Sigma} \mathbf{r} \times \mathbf{p}_n dS = \oint_{S_F} \mathbf{r} \times (\mathbf{n}_F \cdot P_S) dS - \oint_{S_B} \mathbf{r} \times (\mathbf{n}_B \cdot P_S) dS = \oint_{S_F} \mathbf{r} \times (\mathbf{n}_F \cdot P_S) dS - \mathbf{M}_h \tag{3.7}$$

where P_S denotes the stress tensor and $\mathbf{f}_h$ and $\mathbf{M}_h$ are a force and a moment of force of hydrodynamic reaction, respectively.

Coming back to the linear momentum equation, the LHS of the expression can be rewritten by expanding the material derivative of the velocity, namely

$$\int_{V_F} \rho \frac{d\mathbf{v}}{dt} dV = \int_{V_F} \rho \frac{\partial \mathbf{v}}{\partial t} dV + \int_{V_F} \rho (\nabla \cdot \mathbf{v}) \mathbf{v} dV \tag{3.8}$$

The second integral on the RHS can be transposed into a surface integral by means of the Gauss's divergence theorem, that is

$$\int_{V_F} \rho (\nabla \cdot \mathbf{v}) \mathbf{v} dV = \int_{V_F} \rho \nabla \cdot (\mathbf{v} \otimes \mathbf{v}) dV = \oint_{S_\Sigma} \rho \mathbf{n}_F \cdot (\mathbf{v} \otimes \mathbf{v}) dS = \oint_{s_\Sigma} \rho (\mathbf{n}_F \cdot \mathbf{v}) \mathbf{v} dS = \oint_{S_\Sigma} \rho v_{nF} \mathbf{v} dS \tag{3.9}$$

where v_{nF} is magnitude of velocity $\mathbf{v}$ in direction normal to the fluid's surface S_F.

Clearly, the above integral can be expressed in terms of the fluid, S_F, and the body, S_B, surfaces, as in the following

$$\oint_{S_\Sigma} \rho v_{nF} \mathbf{v} dS = \oint_{S_F} \rho v_{nF} \mathbf{v} dS - \oint_{S_B} \rho v_{nB} \mathbf{v} dS \tag{3.10}$$

Combining these terms results in the following equality

$$\int_{V_F} \rho \frac{\partial \mathbf{v}}{\partial t} dV + \oint_{S_F} \rho v_{nF} \mathbf{v} dS - \oint_{S_B} \rho v_{nB} \mathbf{v} dS = \int_{V_F} \rho \mathbf{F} dV + \oint_{S_F} \mathbf{n}_F \cdot P_S dS - \mathbf{f}_h \tag{3.11}$$

Hence, the hydrodynamic reaction can be written as

$$\begin{aligned} \mathbf{f}_h &= -\int_{V_F} \rho \frac{\partial \mathbf{v}}{\partial t} dV - \oint_{S_F} \rho v_{nF} \mathbf{v} dS + \oint_{S_B} \rho v_{nB} \mathbf{v} dS + \int_{V_F} \rho \mathbf{F} dV + \oint_{S_F} \mathbf{n}_F \cdot P_S dS = \\ &= -\frac{d\mathbf{P}}{dt} + \int_{V_F} \rho \mathbf{F} dV + \oint_{S_F} \mathbf{n}_F \cdot P_S dS \end{aligned} \tag{3.12}$$

where $\mathbf{P}$ stands for the vector of linear momentum

Proceeding analogically with the equation of angular momentum, the moment of the hydrodynamic reaction with respect to a stationary frame of reference can be expressed as

$$\begin{aligned}
&\mathbf{M}_h = \mathbf{r}\times\mathbf{f}_h = \\
&= -\int_{V_F}\mathbf{r}\times\left(\rho\frac{\partial\mathbf{v}}{\partial t}\right)dV - \oint_{S_F}\mathbf{r}\times\left(\rho v_{nF}\mathbf{v}\right)dS + \oint_{S_B}\mathbf{r}\times\left(\rho v_{nB}\mathbf{v}\right)dS + \oint_{S}\mathbf{r}\times\mathbf{n}_F\cdot P_S dS + \int_{V_F}\mathbf{r}\times\left(\rho\mathbf{F}\right)dV = \\
&= -\frac{d\mathbf{L}}{dt} + \oint_{S}\mathbf{r}\times\mathbf{n}_F\cdot P_S dS + \int_{V_F}\mathbf{r}\times\left(\rho\mathbf{F}\right)dV
\end{aligned} \tag{3.13}$$

These equations are valid for any kind of fluid but they express the force and moment at the given point P of the fluid domain. Therefore, in order to obtain the resultant force of hydrodynamic reaction and resultant moment of that force it is necessary to calculate the force in every point of the fluid domain. The hydrodynamic force field can be obtained by means of CFD calculations but this is time consuming and requires a significant computational effort. Less accurate but much faster solution can be obtained if the velocity field is given as a potential field, i.e. the flow of the fluid caused by motions of the body can be determined as a gradient of some scalar function ϕ.

3.2.2 Hydrodynamic reaction in a potential flow

In the potential flow approach, it is assumed that the fluid is incompressible, $\nabla\cdot\mathbf{v} = 0$, and inviscid, $\mu = 0$. Specifically, assuming one of the axes of the global frame of reference aligned with a vector of the gravity acceleration (pointed from the centre of the Earth) the unit body forces become $\mathbf{F} = -\nabla U = -g\mathbf{k}$, where $U = gz$ and g stands for a magnitude of the gravitational acceleration and $\mathbf{k}$ is an unit vector in a direction of the axis. Furthermore, in the inviscid fluid the stress tensor P_S becomes a spherical tensor $-pI$, where I is a unit matrix and p stands for the hydrodynamic pressure. Thus, the product $\mathbf{n}_F\cdot P_S$ becomes $-p\mathbf{n}_F$ and the force of hydrodynamic reaction can be written as

$$\mathbf{f}_h = -\frac{d\mathbf{P}}{dt} - \int_{V_F}\rho\nabla U dV - \oint_{S_F} p\mathbf{n}_F dS = -\frac{d\mathbf{P}}{dt} - \rho\int_{V_F}\nabla U dV - \oint_{S_F} p\mathbf{n}_F dS \tag{3.14}$$

Bearing in mind that the fluid is incompressible and its velocity can be derived from a single scalar function, i.e. $\mathbf{v} = \nabla\phi$, where the velocity potential is given as a function of coordinates and time $\phi = \phi(x, y, z, t)$, the rate of change of linear momentum can be expressed as

$$\frac{d\mathbf{p}}{dt} = \int_{V_F} \rho \frac{\partial \mathbf{v}}{\partial t} dV + \oiint_{S_F} \rho v_{nF} \mathbf{v} dS - \oiint_{S_B} \rho v_{nB} \mathbf{v} dS = \rho \int_{V_F} \frac{\partial}{\partial t} \nabla \phi dV + \rho \oiint_{S_F} v_{nF} \mathbf{v} dS - \rho \oiint_{S_B} \rho v_{nB} \mathbf{v} dS \tag{3.15}$$

Based on the Gauss's divergence[1] theorem and on the fact that ϕ is continuous function, the first integral can be transposed to a surface integral, that is

$$\rho \int_{V_F} \frac{\partial}{\partial t} \nabla \phi dV = \rho \int_{V_F} \nabla \frac{\partial \phi}{\partial t} dV = \rho \oiint_{S_\Sigma} \frac{\partial \phi}{\partial t} \mathbf{n}_F dS = \rho \oiint_{S_F} \frac{\partial \phi}{\partial t} \mathbf{n}_F dS - \rho \oiint_{S_B} \frac{\partial \phi}{\partial t} \mathbf{n}_B dS \tag{3.16}$$

Following the same procedure, the volume integral of the body forces can be expressed by means of a surface integral as

$$\rho \int_{V_F} \nabla U dV = \rho \oiint_{S_F} U \mathbf{n}_F dS - \rho \oiint_{S_B} U \mathbf{n}_B dS \tag{3.17}$$

Therefore, substituting these relations into the expression for a hydrodynamic reaction and grouping similar terms yields

$$\mathbf{f}_h = -\oiint_{S_F} \left(\rho \frac{\partial \phi}{\partial t} + \rho U + p \right) \mathbf{n}_F dS - \oiint_{S_F} v_{nF} \mathbf{v} dS + \oiint_{S_B} \rho U dS + \rho \oiint_{S_B} \left(\frac{\partial \phi}{\partial t} \mathbf{n}_B + v_{nB} \mathbf{v} \right) dS \tag{3.18}$$

Since the flow is potential and viscosity is neglected, the first integral can be approached with help of the Cauchy-Lagrange's equation where a general solution to the equation of motion assumes the following form

$$\frac{\partial \phi}{\partial t} + \frac{v^2}{2} + U + \frac{p}{\rho} = C(t) \tag{3.19}$$

---

[1] Considering a scalar function f and an orthonormal basis (frame of reference), it is that $\int_V \nabla f dV = \mathbf{i}_1 \int_V \frac{\partial f}{\partial x_1} dV + \mathbf{i}_2 \int_V \frac{\partial f}{\partial x_2} dV + \mathbf{i}_3 \int_V \frac{\partial f}{\partial x_3} dV$.

Hence, the integrands can be expressed as $\nabla \cdot f \mathbf{i}_k$ and thus the Gauss's theorem reads $\mathbf{i}_k \int_V \nabla \cdot f \mathbf{i}_k = \mathbf{i}_k \int_S \mathbf{n} \cdot f \mathbf{i}_k dS$.

However, it is also that $\mathbf{n} \cdot \mathbf{i}_k = n_k$ and the surface integral becomes $\int_S f \left(n_1 \mathbf{i}_1 + n_2 \mathbf{i}_2 + n_3 \mathbf{i}_3 \right) dS = \int_S f \, \mathbf{n} dS$.

Thus, it is that $\int_V \nabla f dV = \int_V f \, \mathbf{n} dS$

Indeed, it can be assumed that if the fluid domain is sufficiently large, the fluid velocity v must vanish at the far-field boundary and the velocity potential and pressure will assume some constant values U_0 and p_0, respectively. Thus, the integration constant $C(t)$ in the Cauchy-Lagrange's equation can be derived from the following identity

$$C(t) = \frac{\partial \phi}{\partial t} + U_0 + \frac{p_0}{\rho} \tag{3.20}$$

From this, is it follows that the integral can be replaced with

$$\oiint_{S_F} \left(\rho \frac{\partial \phi}{\partial t} + \rho U + p \right) \mathbf{n}_F dS = \oiint_{S_F} \rho \frac{v^2}{2} \mathbf{n}_F dS + \oiint_{S_F} (\rho U_0 + p_0) \mathbf{n}_F dS \tag{3.21}$$

However, since the integrand of the second integral on the RHS is constant for an incompressible fluid the integral must vanish, because $\oiint_{S_F} \mathbf{n} dS = \mathbf{0}$. Thus, the hydrodynamic reaction becomes

$$\mathbf{f}_h = -\rho \oiint_{S_F} \frac{v^2}{2} \mathbf{n}_F dS - \rho \oiint_{S_F} v_{nF} \mathbf{v} dS + \rho \oiint_{S_B} U \mathbf{n}_B dS + \rho \oiint_{S_B} \left(\frac{\partial \phi}{\partial t} \mathbf{n}_B + v_{nB} \mathbf{v} \right) dS \tag{3.22}$$

Furthermore, the kinematical condition implies that the velocity of the fluid on the surface of the body must be equal to the velocity of the body's surface, i.e. $v_{nB} = v_{nF}$. From this[2], it follows that

$$\oiint_{S_B} \left(\frac{\partial \phi}{\partial t} \mathbf{n}_B + v_{nB} \mathbf{v} \right) dS = \oiint_{S_B} \left(\frac{\partial \phi}{\partial t} \mathbf{n}_B + (\mathbf{v} \otimes \mathbf{v}) \cdot \mathbf{n}_B \right) dS = \frac{d}{dt} \oiint_{S_B} \phi \mathbf{n}_B dS \tag{3.23}$$

Moreover, as the assumption of an unbounded fluid domain implies vanishing of the velocity at far-field boundaries, the sum of the first two terms in the expression for

---

[2] The surface integral can be transposed to volume integral of integrand $\nabla \cdot \left(\frac{\partial \phi}{\partial t} + \mathbf{v} \otimes \mathbf{v} \right)$. Then, making use of continuity of φ it can be rewritten as $\frac{\partial}{\partial t} \nabla \phi + \nabla \cdot (\nabla \phi \otimes \mathbf{v})$, which makes generalised Reynolds's transport theorem applicable to the integral.

the hydrodynamic reaction must vanish, which reduces the equation to the following form

$$\mathbf{f}_h = \rho \oint_{S_B} U \mathbf{n}_B dS + \rho \frac{d}{dt} \oint_{S_B} \phi \mathbf{n}_B dS = \rho \int_{V_B} \nabla U dV + \rho \frac{d}{dt} \oint_{S_B} \phi \mathbf{n}_B dS = \rho g V_B \mathbf{k} + \rho \frac{d}{dt} \oint_{S_B} \phi \mathbf{n}_B dS \tag{3.24}$$

It can be readily seen from the above equation, that if the body is completely submerged in the unbounded domain of the inviscid and incompressible fluid characterised by the velocity potential, the hydrodynamic reaction assumes very simple form. The first term on the RHS corresponds to the mass forces produced by the gravitational potential. The second, inertial, term corresponds simply to the rate of change of the linear momentum of the fluid.

When the body moves in the free surface, the boundary condition on the undisturbed free surface is following

$$\rho \frac{\partial \phi}{\partial t} + \rho \frac{v^2}{2} + \rho U + p = p_0 \tag{3.25}$$

Thus, the hydrodynamic reaction becomes

$$\mathbf{f}_h = -\int_{S_B} (p - p_0) \cdot \mathbf{n}_B dS = \rho \int_{S_B} \left(\frac{\partial \phi}{\partial t} + \frac{v^2}{2} + U \right) \cdot \mathbf{n}_B dS = \rho \int_{S_B} \frac{\partial \phi}{\partial t} \mathbf{n}_B dS + \rho \int_{SB} \left(\frac{v^2}{2} + U \right) \cdot \mathbf{n}_B dS \tag{3.26}$$

where S_B denotes the wetted surface of the body and ϕ is the velocity potential given in the local, body-fixed, coordinate system.

As shown in (Krężelewski, 1982) the first integral on the RHS can be expanded with help of a variant of the Reynolds's transport theorem,[3] and thus, the hydrodynamic reaction can be written as

---

[3] For an arbitrary vector $\mathbf{u}$ it is that $\frac{d}{dt} \int_{S(t)} \mathbf{u} \cdot d\mathbf{S} = \int_{S(t=t_0)} \frac{\partial \mathbf{u}}{\partial t} \cdot d\mathbf{S} + \int_{S(t=t_0)} \mathbf{v} (\nabla \cdot \mathbf{u}) \, d\mathbf{S} + \oint_{\partial S_0} (\mathbf{u} \times \mathbf{v}) \, d\mathbf{r}$. Where ∂S_0 is a boundary curve of a surface S at some initial time t_0, i.e. $S_0 = S(t = t_0)$. The line integral can also be written as $\oint_{\partial S_0} (\mathbf{v} \times d\mathbf{r}) \cdot \mathbf{u}$.

$$\mathbf{f}_h = \rho \frac{d}{dt} \int_{S_B} \phi \mathbf{n}_B dS - \rho \int_{S_B} \nabla\phi (\mathbf{v} \cdot \mathbf{n}_B) dS - \rho \oint_{\partial S_B} (\phi \mathbf{v} \times d\mathbf{r}) + \rho \int_{S_B} \left(\frac{v^2}{2} + U \right) \cdot \mathbf{n}_B dS \tag{3.27}$$

Therefore, after simple rearrangement, the equation can be rewritten as

$$\mathbf{f}_h = \rho \frac{d}{dt} \int_{S_B} \phi \mathbf{n}_B dS + \rho \int_{S_B} U \cdot \mathbf{n}_B dS + \rho \int_{S_B} \left(\frac{1}{2} (\nabla\phi)^2 \mathbf{n}_B - \frac{\partial \phi}{\partial n} \nabla\phi \right) dS + \rho \oint_{\partial S_B} (d\mathbf{r} \times \phi \mathbf{v}_S) \tag{3.28}$$

where, $v^2 = \mathbf{v} \cdot \mathbf{v} = \nabla\phi \cdot \nabla\phi = (\nabla\phi)^2$ and $\mathbf{v}_S \cdot \mathbf{n}_B = \mathbf{v} \cdot \mathbf{n}_B = \nabla\phi \, \mathbf{n}_B = \frac{\partial \phi}{\partial n}$, based on the assumption that the surface S_B is impenetrable to the fluid and there is no flow separation on the surface (and thus the condition of equal velocities holds).

Similar formula can be obtained for moment of the hydrodynamic reaction which, bearing in mind that $\mathbf{M}_h = -\rho \int_{S_W} (p - p_0) \mathbf{r}_S \times \mathbf{n}_B dS$, is given as

$$\begin{aligned} \mathbf{M}_h = {} & \rho \frac{d}{dt} \int_{S_B} \phi \mathbf{r}_S \times \mathbf{n}_B dS + \rho \int_{S_B} U \mathbf{r}_S \times \mathbf{n}_B dS + \rho \int_{S_B} \left(\frac{1}{2} (\nabla\phi)^2 \mathbf{r}_S \times \mathbf{n}_B - \mathbf{r}_S \times \frac{\partial \phi}{\partial n} \nabla\phi \right) dS + \\ & + \rho \oint_{\partial S_B} \mathbf{r}_S \times (d\mathbf{r} \times \phi \mathbf{v}_S) \end{aligned} \tag{3.29}$$

where $\mathbf{r}_S$ is a radius vector of the surface element dS in the global, fixed in space, reference system.

Comparing the above equations to that obtained for a solid moving through the unbounded fluid - equation (3.24) - shows clearly that the presence of the free surface introduces additional terms to the formulation of the hydrodynamic reaction. These, given as the last two terms on the RHS of the equation correspond to the system of waves generated by motions of the body in or in the proximity of the free surface of the fluid. It is noteworthy that even in the case of a submerged body ($\partial S_W = 0$) only the line integral vanishes while the third term on the RHS remains.

Although the above equation could be further transformed to reveal additional information about a nature of the hydrodynamic reaction, it shall be left in the current form – sufficient to withdraw general conclusions on a flow caused by motions of a body in proximity of the free surface of the inviscid, incompressible and irrotational fluid.

3.2.3 Free surface deformation – energy radiation

Motion of some hypothetical object, e.g. of an infinitely long circular cylinder or of a hydrodynamic singularity (e.g. infinitely long vortex filament), moving with constant velocity parallel to the undisturbed free surface at some small depth h below the surface induces a pressure field in the fluid domain. Assuming the depth h sufficiently small, the movement must cause deformation of the free surface. More precisely, far away in front of the object, the free surface would remain undisturbed but far behind the body it would become a two-dimensional regular wave. The wave would propagate away from the object with the group velocity equal to the velocity of the cylinder or the singularity. Generation of the wave is a consequence of transporting energy from the body to the free surface of the fluid. In the simple case, the amount of energy transferred from the body can be readily calculated.

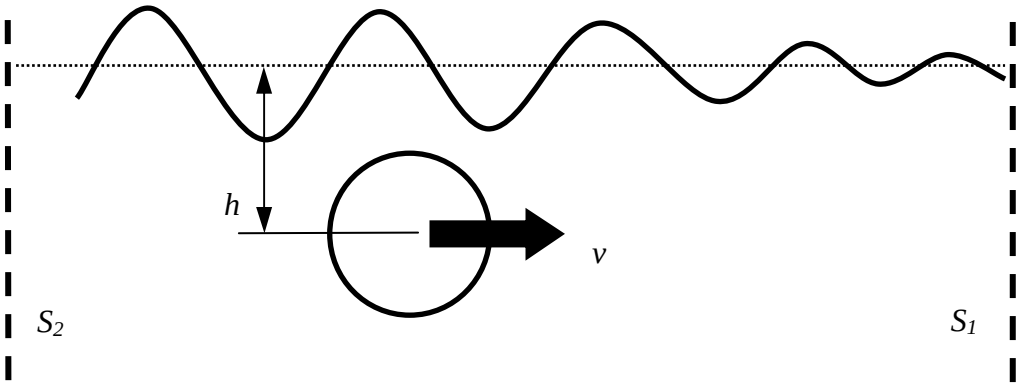

*Fig.**3.1**: The free surface deformation caused by motion of a hypothetical body*

Firstly, let a region of the fluid be contained between two flat surfaces of unit length, S_1 and S_2, parallel to the axis of the cylinder and perpendicular to the undisturbed free surface. The surface S_1 is located far in front of the object while the surface S_2 is located far behind it. Then, as shown in (Pawłowski, 2005), the increase of energy of the fluid within one second is given as $E_w v$, where E_w is an average, per period, total energy of the wave per unit area of the free surface and v stands for a magnitude of the velocity of the object. The energy increase equals to a sum of power of pressure $E_w u$ in the surface S_2 and power of the wave resistance force induced on the object, R_w, that is

$$E_w v = E_w u + R_w \tag{3.30}$$

where u is a group velocity of the wave. Note that the vector of the wave resistance force is parallel but opposite to the velocity vector $\mathbf{v}$.

Given that the average total energy E_w is given as $E_w = \frac{1}{2}\rho g \zeta_0$, where ζ_0 stands for the amplitude of the wave, the wave resistance force per unit length of the object is given as

$$R_w = \frac{1}{2}\rho g \zeta_0 \left(1 - \frac{u}{v}\right) = \frac{1}{2}\rho g \zeta_0 \left(1 - \frac{2kH}{\sinh 2kH}\right) \tag{3.31}$$

where k is the wave number $k = \frac{2\pi}{\lambda}$, λ stands for length of the wave and H is depth of the fluid domain.

It can be readily seen from the above that in the limiting case of $H \to 0$ the wave resistance would vanish, i.e. $R_w \to 0$. Furthermore, if the object in question were a vortex filament of intensity Γ, then it would be that

$$R_w = \frac{\rho g}{v}\Gamma^2 \exp\left(-\frac{2gh}{v}\right) \tag{3.32}$$

Hence, as shown in (Krężelewski, 1982) , for the singularity characterised by the depth Froude number 0.5, i.e. $F_h = \frac{v}{\sqrt{gh}} = 0.5$, the exponential term would be very small (0.0003) and the wave resistance would virtually vanish.

Before proceeding further to the case of oscillatory motion, it is noteworthy that, the assumptions made at the beginning of this chapter (i.e. inviscid and incompressible fluid) imply that the wave generated by the object would never decay – instead, in an unbounded fluid domain the radiated wave would propagate to infinity.

Furthermore, the energy needed to generate the radiation wave was not dissipated but merely transferred from the body to the free surface. That is because dissipative forces assume a form of an antisymmetric tensor but taking $\mu = 0$ causes vanishing of the antisymmetric part of the fluid stress tensor. In the case of a viscid fluid, the av-

erage power dissipated by the two dimensional surface wave, can be given after (Krężelewski, 1982), as follows

$$N_\mu = -2\mu g \zeta_0 k^2 = -2\pi^2 \frac{\mu}{\rho} g \left(\frac{2\zeta_0}{\lambda} \right)^2 \tag{3.33}$$

3.3 Added inertia and damping

It has been shown in the previous section that one component of the hydrodynamic reaction can be identified as rate of change of linear momentum of the fluid and as such can be accounted for as an inertial force. Assuming again unbounded domain of ideal (i.e. inviscid, incompressible and irrotational fluid) the momentum is given by means of integral over surface of the body

$$\mathbf{P}^I = -\rho \oiint_{S_B} \phi \mathbf{n}_B dS \tag{3.34}$$

where the superscript I is used to emphasise inertial character of the momentum.

3.3.1 Added inertia

In the linear formulation of the problem the velocity potential ϕ is often expressed (in the Cartesian frame of reference) as a sum of so-called unit potentials, that is

$$\phi(x_1, x_2, x_3, t) = \sum_{i=1}^{6} v_i(t) \phi_i(x_1, x_2, x_3) \tag{3.35}$$

The number of unit potentials and the terms $v_i(t)$ are derived from the kinematical condition on the body surface. Namely, since the velocity of the surface element is given as $\mathbf{v}_S = \mathbf{v}_O + \boldsymbol{\omega} \times \mathbf{r}_S$ the scalar product $\frac{\partial \phi}{\partial n} = \mathbf{v}_S \cdot \mathbf{n}_B$ has six components, i.e. $\mathbf{v}_S \cdot \mathbf{n}_B = \mathbf{v}_O \cdot \mathbf{n}_B + (\boldsymbol{\omega} \times \mathbf{r}_S) \mathbf{n}_B = \mathbf{v}_O \, \mathbf{n}_B + \boldsymbol{\omega} (\mathbf{r}_S \times \mathbf{n}_B)$. Furthermore, the components of the velocity vector $\mathbf{v}_O$ can be denoted by v_p where $p = 1,2,3$ while components of the angular velocity $\boldsymbol{\omega}$ can be substituted with v_q where $q = 4,5,6$. Similarly, components of normal vector $\mathbf{n}_B$ can be represented by n_1, n_2 and n_3 whereas n_4, n_5 and n_6 are given by appropriate components of the vector product $\mathbf{r}_S \times \mathbf{n}_B$, e.g. $n_4 = x_2 n_3 - x_3 n_2$. Bearing in mind that the terms $v_1, \ldots, v_6$ are independent on a location, the directional derivative of the veloc-

ity potential given by the equation above can be simply expressed as (summation over $k = 1, 2, ..., 6$)

$$\frac{\partial \phi}{\partial n} = v_k \frac{\partial \phi_k}{\partial n} = v_k n_k \tag{3.36}$$

The above implies that following identity holds: $n_k = \frac{\partial \phi_k}{\partial n}$.

The terms n_k are often referred to as generalised directional cosines.

Now, the linear momentum can be expressed in terms of components, as

$$\mathbf{P}^I = -\left(\rho \oiint_{S_B} \phi n_{B1} dS\, \mathbf{i}_1 + \rho \oiint_{S_B} \phi n_{B2} dS\, \mathbf{i}_2 + \rho \oiint_{S_B} \phi n_{B3} dS\, \mathbf{i}_3 \right) \tag{3.37}$$

Furthermore, given that $n_{Bj} = n_j = \frac{\partial \phi_j}{\partial n}$ for $j = 1, 2, 3$ and $\phi = \phi_k v_k$ for $k = 1, 2, ..., 6$ and bearing in mind that the terms v_k depend only on time not on a position, the momentum equation expands as

$$\mathbf{P}^I = -\left(\rho \oiint_{S_B} \phi_k v_k \frac{\partial \phi_1}{\partial n} dS\, \mathbf{i}_1 + \rho \oiint_{S_B} \phi_k v_k \frac{\partial \phi_2}{\partial n} dS\, \mathbf{i}_2 + \rho \oiint_{S_B} \phi_k v_k \frac{\partial \phi_3}{\partial n} dS\, \mathbf{i}_3 \right) = -v_k \rho \oiint_{S_B} \phi_k \frac{\partial \phi_j}{\partial n} dS \mathbf{i}_j \tag{3.38}$$

where $j = 1, 2, 3$ and $k = 1, 2, ..., 6$.

Hence, denoting components of the momentum as P_j^I allows expressing the momentum equation as

$$P_j^I = \left(-\rho \oiint_{S_B} \phi_k \frac{\partial \phi_j}{\partial n} dS \right) v_k = a_{kj} v_k \tag{3.39}$$

Similar procedure can be followed with respect to the moment of the hydrodynamic reaction, where the inertial angular momentum is given[4] as

$$\mathbf{L}^I = -\rho \oiint_{S_B} \phi \mathbf{r}_S \times \mathbf{n}_B dS \tag{3.40}$$

[4] See equation (3.29).

For example, component of the momentum along the axis $\mathbf{i}_1$ is given as

$$L_1^I = -\rho \oint_{S_B} \phi_k v_k \left(x_2 n_3 - x_3 n_2 \right) dS = v_k \left(-\rho \oint_{S_B} \phi_k n_4 dS \right) = v_k \left(-\rho \oint_{S_B} \phi_k \frac{\partial \phi_4}{\partial n} dS \right) \tag{3.41}$$

Hence, the term in parentheses can also be written shortly as a_{kl} where $k = 1,2,...,6$ and $l = 4,5,6$. It can be readily seen the terms a_{kj} and a_{kl} have the identical form hence, the components of the inertial momenta can be written a compact form, as in the following

$$F_j^I = a_{kj} v_k \tag{3.42}$$

where $j,k = 1,2,...,6$.

The components of the $[6 \times 6]$ matrix a_{kj} are called added mass or added inertia, as they have dimensions of a mass, static moments of mass and moments of inertia.

In the case of the flow considered here matrix a_{kj} is symmetrical, i.e. $a_{kj} = a_{jk}$ so in total there are 21 different components a_{kj} in the added inertia matrix.

Furthermore, if the body has planes or axes of symmetry, some terms in the added inertia matrix will vanish. This could be proved directly by application of the Green's theorem to integrals in the terms a_{kj} but it could also be deducted if the components a_{kj} are seen as coupling terms between different modes of motions.

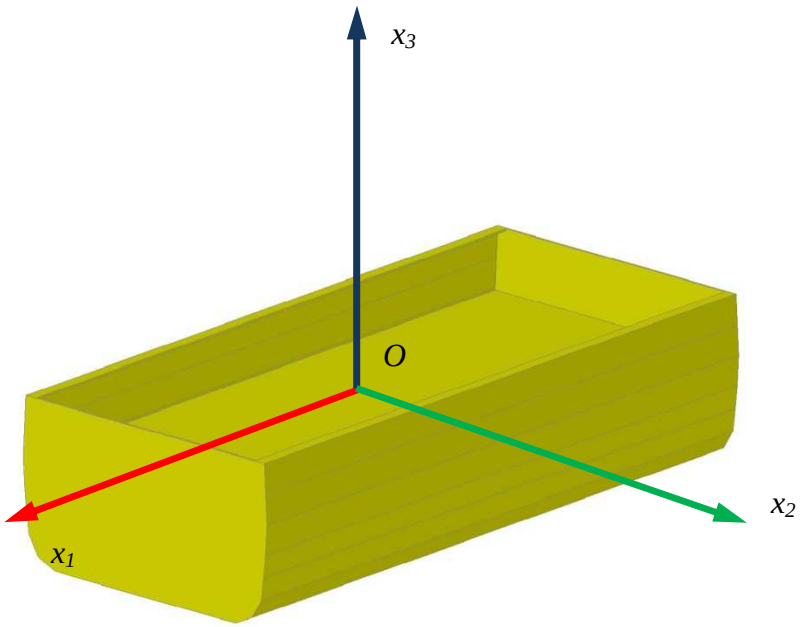

*Fig.**3.2**: The body fixed coordinate system*

In the case of a body symmetrical with respect to the plane Ox_1x_3 of the body-fixed coordinate system motion in a direction of the axis Ox_1 cannot, due to symmetry of the body, induce any motion (and thus any reaction force opposing the motion) in a direction of the axis Ox_2 or a rotation about other two axes. Hence[5], a_{21}, a_{41} and a_{61} must vanish. Similarly, rotations about an axis perpendicular to the plane of symmetry cannot produce any motions along the axis or a rotation about the axis Ox_1, therefore $a_{25} = a_{45} = 0$. Furthermore, pure rotations about the axis Ox_3 cannot induce motions along or rotations about the axis Ox_2, perpendicular to the plane of symmetry - $a_{36} = a_{56} = 0$. For the same reason translations about this axis cannot produce rotations about the axis Ox_1 which results in $a_{43} = 0$. Due to symmetry of the matrix the components with the transposed indices must vanish too, and thus, in total there are twelve non-zero components of the added inertia matrix.

The reasoning on symmetry of added inertia terms is particularly helpful in model tests when some of the assumptions made with respect to the *ideal* nature of the fluid are violated. In such a case, the inertial part of the hydrodynamic reaction force and

[5] The convention adopted here is that *j*-th mode of motion (i.e. second index) corresponds to "main" mode of motion whereas the *k*-th mode is induced motion.

moment must still be associated with momenta of the fluid but the components of the reaction force could not be subjected to such a meticulous analytical treatment. The concept of an added momentum due to the fluid motions induced by movements of the rigid body would hold *in principle* but its mathematical formulation would be either much complex or unavailable at all.

Before proceeding further to the case of motions in proximity of the free surface of the fluid it is noteworthy to show, that kinetic energy of the fluid can be conveniently expressed by components of the added inertia matrix, that is

$$T = \frac{\rho}{2}\int_V v^2 dV = \frac{\rho}{2}\oint_{S_F}\phi\frac{\partial\phi}{\partial n_F}dS = -\frac{\rho}{2}\oint_{S_B}\phi\frac{\partial\phi}{\partial n_B}dS = \frac{1}{2}v_j v_k a_{jk} \tag{3.43}$$

3.3.2 Oscillations in a free surface of an ideal fluid

In the case of motions in or proximity of the free surface, the problem of determining forces of the hydrodynamic reaction becomes more complex. This derives from the formulation of the boundary condition on the free surface accounting for its deformation. In the linear approach, the problem is usually tackled by a superposition of the potential flow corresponding to steady motions of the body with some velocity $\mathbf{v}_0$ and small oscillations of the body about its mean position. Furthermore, in problems addressing motions or responses of the body in waves, it is necessary to include wave and diffraction potentials – the former inducing a velocity field in the fluid domain (as without the body) and the latter describing disturbances introduced by steady motions of the body to the fluid's velocity field associated with waves. Hereafter, only problem of body oscillations in the otherwise undisturbed fluid domain will be briefly presented.

Analytically the problem of a body oscillating in proximity of the free surface is usually formulated as follows:

- The fluid is inviscid and incompressible and its flow irrotational.
- The effects of surface tensions can be neglected.

- The motion amplitudes are small so the generated waves are of small amplitudes and the boundary condition on free surface can be linearised.

It follows from these assumptions that the flow must satisfy continuity equation given by the Laplace's equation $\nabla^2\phi = 0$. Furthermore, if the origin of global frame of reference is located in the plane of undisturbed free surface and Ox_3 axis directed vertically down, the free surface condition takes the following form $\frac{\partial^2\phi}{\partial t^2} - v_O \frac{\partial^2\phi}{\partial x_1^2} - g\frac{\partial\phi}{\partial x_3} = 0$. The boundary condition accounts for the progressive velocity of the body of magnitude v_O in the direction of the body-fixed axis O_1x_1. Additionally, it is assumed that the fluid is deep, thus the velocity vanish at large depth, i.e. $\lim_{x_3\to\infty}|\nabla\phi| = 0$ and the fluid velocity on the surface of the body must be equal to normal velocity component of the surface, i.e. $\frac{\partial\phi}{\partial n} = \mathbf{v}_S \cdot \mathbf{n}_B$. The latter condition implies that the surface is impenetrable to the fluid and that the flow separation cannot occur. The final condition is that the wave generated by the oscillating body must have, in the far field, a form of a regular and progressive gravitational wave.

The linear problem can be solved by means of superposition of individual solutions. For instance, the Kirhoff's method of unit potentials can be employed in the same fashion as in solving the problem of the body moving through an unbounded fluid. The individual modes of motions could be considered separately, thus the velocity field in general motion of the body could be given by means of a sum of the potentials obtained for the individual modes of motions, i.e. $\phi = \sum_{i=1}^{6}\phi^{(i)}$. Obviously all the individual potentials must satisfy the specified boundary conditions. Furthermore, the excitation forces can be given by means of linear combination of harmonic components, e.g. in terms of Fourier series. However, the problem may be quite challenging in the case of an arbitrarily shaped body, even in the domain of the ideal fluid, particularly at the presence of a progressive velocity. Thus, quite often components of the hydrodynamic reaction are obtained for individual cross-sections of the body and integrated along the body. The technique, often referred to as the strip theory, origi-

nated in the mid-twentieth century[6] and it remains in common use to date. Details on the strip theory (or more general on application of potential flow to the problem of a body moving through an unbounded domain of the ideal fluid) can be found in many textbooks and scientific publications see for example (Journee, 1992) or (Dudziak, 2008). In the following, however, equations of motion shall be derived with use of a very simple technique based on a variant of the Lagrangian formulation, as described by (Sadeghi, 2005).

3.3.3 Equations of motions of a floating body in generalised coordinates

The equation (3.43) demonstrates clearly, how conveniently kinetic energy of the system can be expressed by means of the components of the added inertia matrix. The terms $v_1,...,v_6$ are nothing else than the time derivatives of the generalised coordinates $q^1,...,q^6$, thus, the equation (3.43) could be simply rewritten as

$$T = \frac{1}{2} a_{jk} \dot{q}^j \dot{q}^k \tag{3.43).a}$$

The fact of upmost importance is that although the system is infinitely large (due to the infinitely large fluid domain), kinetic energy of the entire fluid domain can be expressed in terms finite number of dimensions. In simple terms, it is that kinetic energy of the entire fluid domain can be associated with the wetted surface S_B of the body.

In the procedure detailed by Sadeghi a complex potential (usually employed in the free-surface problems) $\phi = \sum_{j=1}^{6} \left(\phi_j^c + i\phi_j^s \right)$ is replaced by a superposition of the real-valued potentials (in phase with generalised displacements and velocities, respectively)

$$\phi = \sum_{j=1}^{6} \left(\phi_j^c + i\phi_j^s \right) = \pi_j \dot{q}^j + \psi_j q^j \tag{3.44}$$

[6] Details can be found, for example, in (Ursell, 1949) or (Frank, 1967)

where the π_j and ψ_j are steady-state potentials, which satisfy all the necessary boundary conditions.

The dynamic pressure induced on the wetted surface of the body can be derived from the Bernoulli equation, hence

$$p_d = -\rho \frac{\partial \phi}{\partial t} = -\rho \left(\pi_j \ddot{q}^j + \psi_j \dot{q}^j \right) \tag{3.45}$$

From this, it follows that the generalised inertial/radiation force is given as

$$Q_j^R = -\rho \int_{S_B} n_j \pi_k dS \ddot{q}^k - \rho \int_{S_B} n_j \psi_k dS \dot{q}^k = -\rho \int_{S_B} \pi_k \frac{\partial \pi_j}{\partial n} dS \ddot{q}^k - \rho \int_{S_B} \psi_k \frac{\partial \pi_j}{\partial n} dS \dot{q}^k \tag{3.46}$$

Thus, making the following substitutions $a_{jk} = -\rho \int_{S_B} n_k \pi_j dS$ and $b_{jk} = -\rho \int_{S_B} n_k \psi_j dS$, results in the following

$$Q_j^R = a_{jk} \ddot{q}^k + b_{jk} \dot{q}^k \tag{3.47}$$

Hence, kinetic energy of the system is given as

$$T = -\frac{\rho}{2} \int_{S_B} \phi \frac{\partial \phi}{\partial n} dS \tag{3.48}$$

However, by analogy to the equation (3.36) it is that $\frac{\partial \phi}{\partial n} = \frac{\partial \pi_k}{\partial n} \dot{q}^k + \frac{\partial \psi_k}{\partial n} \dot{q}^k$ and from the boundary condition it follows that $\frac{\partial \psi_k}{\partial n}$ must vanish. Therefore, kinetic energy can be written as

$$T = -\frac{\rho}{2} \int_{S_B} \phi \frac{\partial \phi}{\partial n} dS = -\frac{\rho}{2} \int_{S_B} \left(\pi_j \dot{q}^j + \psi_j q^j \right) \frac{\partial \pi_k}{\partial n} \dot{q}^k dS = -\frac{\rho}{2} \int_{S_B} n_k \pi_j dS \dot{q}^j \dot{q}^k - \frac{\rho}{2} \int_{S_B} n_k \psi_j dS q^j \dot{q}^k \tag{3.49}$$

After substituting a_{jk} and b_{jk} in the place of the integrals, kinetic energy of the fluid can be expressed in a very compact way, as in the following

$$T = \frac{1}{2} a_{jk} \dot{q}^j \dot{q}^k + \frac{1}{2} b_{jk} q^j \dot{q}^k \tag{3.50}$$

It can be readily seen from the above equation, when the body oscillates in the free surface, kinetic energy is a quadratic form of generalised velocities and generalised displacements. Most importantly, the scalar quantity associated with the wetted surface of the body contains all the information about inertial and radiation components of the hydrodynamic reaction[7]. To see this, one can compute the Lagrangian of the above equation, which yields

$$\frac{d}{dt}\left(\frac{\partial T}{\partial \dot{q}^j}\right)-\frac{\partial T}{\partial q^j}=\frac{1}{2}a_{jk}\dot{q}^k-\frac{1}{2}b_{jk}\dot{q}^k=\frac{1}{2}\frac{d}{dt}\left(a_{jk}\dot{q}^k\right)-\frac{1}{2}b_{kj}\dot{q}^k \tag{3.51}$$

The first term in the above is nothing else than components of the rate of change of the momentum, where $P_j=\frac{\partial T}{\partial \dot{q}^j}$ as discussed in (Krężelewski, 1982) whereas the second term stands for a generalised *dissipative* force. In fact, the term $-\frac{1}{2}b_{jk}\dot{q}^k$ is simply partial derivative of the Rayleigh dissipation function with respect to $\dot{q}^j$, that is

$$\frac{\partial D}{\partial \dot{q}^j}=\frac{\partial}{\partial \dot{q}^j}\left(-\frac{1}{2}b_{jk}\dot{q}^j\dot{q}^k\right)=-\frac{1}{2}b_{jk}\dot{q}^k=Q_j^D \tag{3.52}$$

where $-Q_j^D$ is generalised dissipative force, as asserted[8].

The remaining part of derivation of the equations of motion involves the hydrostatic reaction forces (restoring forces). These forces can be expressed in a matrix form as $c_{jk}q^k$ where the nonzero components c_{jk} are given as (Dudziak, 2008)

$$\begin{aligned} c_{33}&=\rho g A_W & c_{44}&=\rho g h_0 V_B \\ c_{35}&=-\rho g A_W \bar{x}_{1F} & c_{53}&=\rho g H_0 V_B \end{aligned} \tag{3.53}$$

where A_W is the area enclosed by the contour ∂S_B, $\bar{x}_{1F}$ stands for the abscissa of the centre of floatation, h_0 is the transverse metacentric height, H_0 is the longitudinal metacentric height, and V_B stands for the volume of the submerged part of the body. All the quantities correspond to the upright position of the body in the undisturbed free surface.

---

[7] It should be noted that in his thesis Sadeghi came to quite different conclusion.

[8] More details can be found in (Skalmierski, 1994)

It is assumed, that the generalised external force Q_j^E is applied directly to the body and not to the fluid and therefore motions of the fluid are induced by the body. Thus, action of the external force is opposed by:

- rate of change of generalised momentum of the rigid body alone, given as $M_{jk}\ddot{q}^k$
- generalised hydrodynamic reaction associated with the rate of change of the generalised momentum of the fluid $a_{jk}\ddot{q}^k$ and the generalised radiation force $b_{jk}\dot{q}^k$
- generalised hydrostatic reaction $c_{jk}q^k$

Given that no wave-induced forces act on the body, the generalised diffraction forces as well as the generalised Froude-Krylov forces can be ignored. Thus, the equation of motion has the following matrix form

$$\left(M_{jk}+a_{jk}\right)\ddot{q}^k + b_{jk}\dot{q}^k + c_{jk}q^k = Q_j^E \tag{3.54}$$

where components of the generalised external force Q_j^E are harmonic functions of time.

This equation constitutes starting point for analysing results of experiments on forced oscillations of a floating body, detailed in the following chapter.

3.4 Summary

One of the most important implications of the d'Alembert's principle is that a particle or a system of material particles can be replaced with an inertial force. In case of a floating body oscillating in an unbounded domain of an ideal fluid, the entire fluid domain is replaced with a force of hydrodynamic reaction. It has been show that kinetic energy of the entire fluid domain can be associated with kinetic energy of the wetted surface. This scalar quantity contains all the information about momenta of the fluid and about the energy radiated through the free surface deformation.

Chapter 4 Some physical experiments on roll hydrodynamics

There have been many physical experiments addressing roll hydrodynamics but most of them have been performed solely to provide experimental data for benchmarking of the particular case. There are very few systematic studies involving comprehensive test matrices and the most important of them are very briefly discussed in the following.

4.1 Vugts (1968)

The objective of Vugts's work was to benchmark the prediction of roll hydrodynamics (based on potential theory) with measurements. The experiments were carried out on cylindrical bodies subjected to forced oscillations in a free surface. Vugts investigated three modes of motion – sway, heave and roll, and the measurements were conducted on the cylinders of different cross-sections: circle, rectangle (with three different beam-to-draught ratios, B/T: 2, 4 and 8), triangle and two Lewis forms (the Lewis sections were not tested in sway and roll). In roll, the cylinders were oscillated about a fixed axis of rotation passing through the sections' centre of gravity. Apart from the rectangular sections of B/T-ratio 4 and 8 the sections' centre of gravity was lying in the calm-water plane.

In his paper, Vugts presented a detailed account of the experiments with particular attention paid to the accuracy of the measurements. The heave and sway experiments proved very reliable and matched closely the theoretical prediction. The roll measurements, however, were less reliable. The measured characteristics deviated substantially from the prediction and the results were affected by significant uncertainties. In particular, Vugts pointed out to the problems in an accurate assessment of the sections' inertia in air causing substantial uncertainty in the added inertia estimates. An additional difficulty derived from the fact that cylinders of B/T-ratio 4 and 8 were oscillated about an elevated axis of rotation.

The results obtained for the rectangle of B/T-ratio 2 showed good agreement with the prediction. The coupling terms followed closely theoretical curves. The roll added

inertia and damping terms deviated slightly from the predicted characteristics. An influence of viscosity was observed in the damping estimates resulting in differences increasing almost linearly with the roll amplitude.

The measurements for the sections rolling about the elevated axis of rotation showed much larger discrepancies. For example, the estimated roll damping at the 0.05 rad roll amplitude was much higher that the estimates at 0.1 and 0.2 radians. The measured added inertia in turn exhibited an anticipated dependency on the roll amplitude but its magnitude was much smaller than predicted. Vugts reasoned that these results are overall highly unreliable. He accounted the discrepancies mainly for the inaccurate estimates of the inertia in air and the fact that the roll motion was about the elevated axis of rotation, but it he also pointed out that these explanations were rather speculative. In particular, he concluded that the B/T-ratio influences strongly the measured quantities with the roll damping almost vanishing in the practical range of draughts. Furthermore, he pointed out to the complex relationship between of the coupling terms (sway-into-roll and roll-into-sway) and the vertical position of the centre of gravity.

The results for the rectangular cylinders of B/T-ratio 2 and 4 are presented in the figures below.

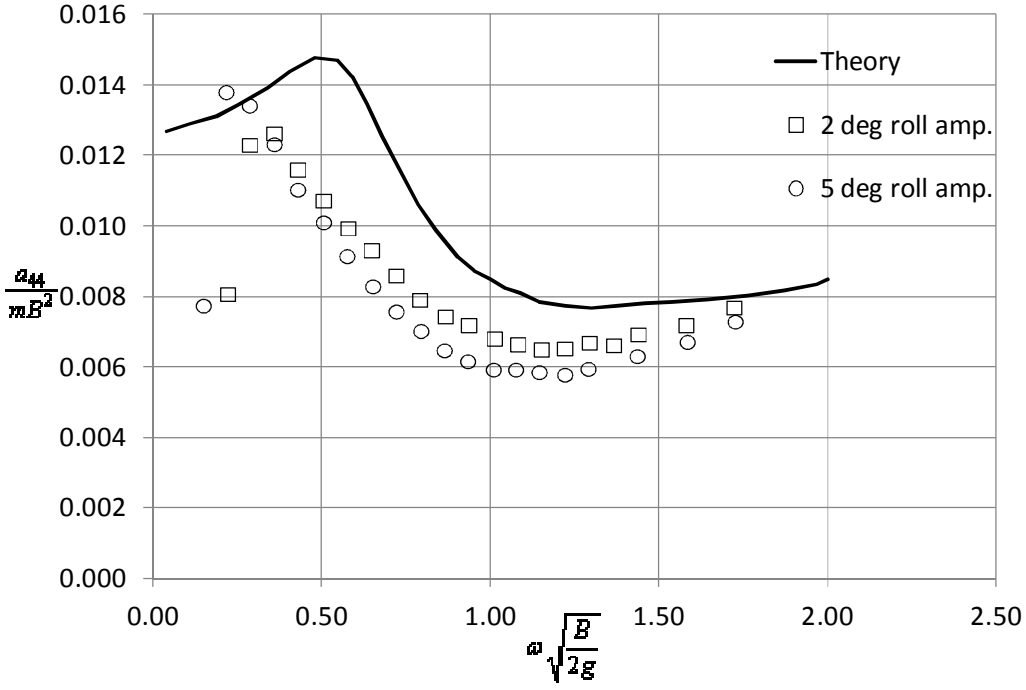

*Fig.**4.1**: Added inertia coefficient (B/T=2)*

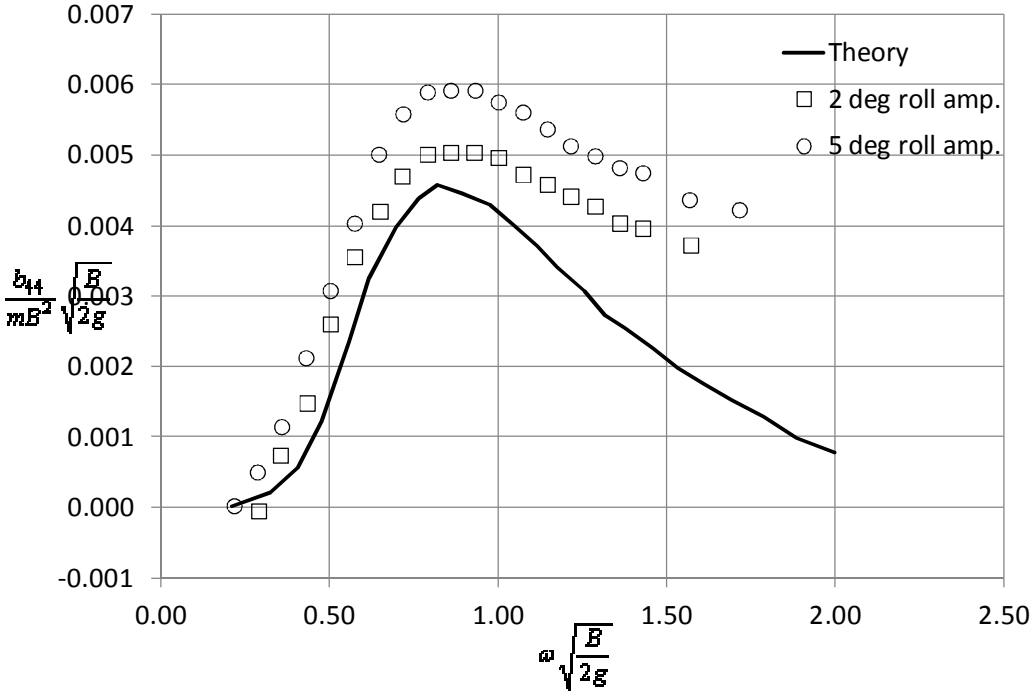

*Fig.**4.2**: Roll damping coefficient (B/T=2)*

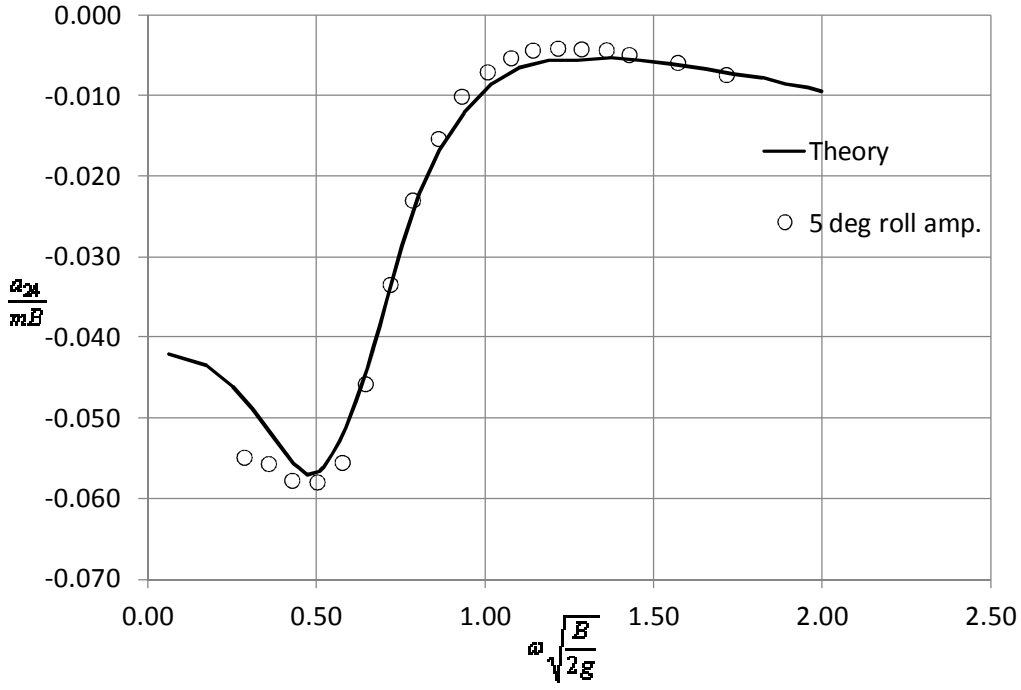

*Fig.**4.3**: Added inertia coefficient in coupling of roll into sway (B/T=2)*

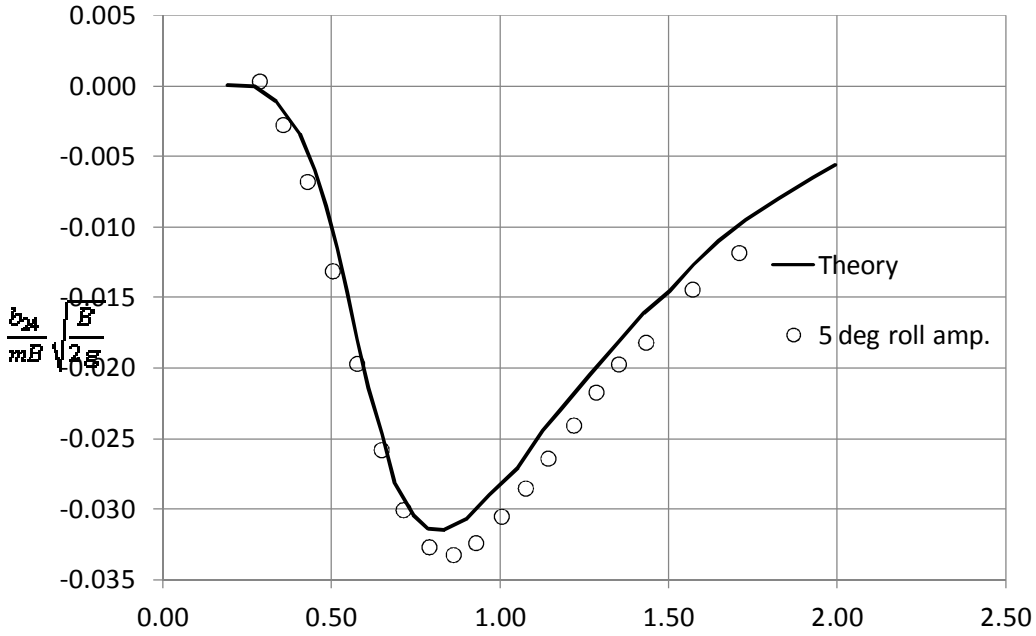

*Fig.**4.4**: Damping coefficient in coupling of roll into sway (B/T=2)*

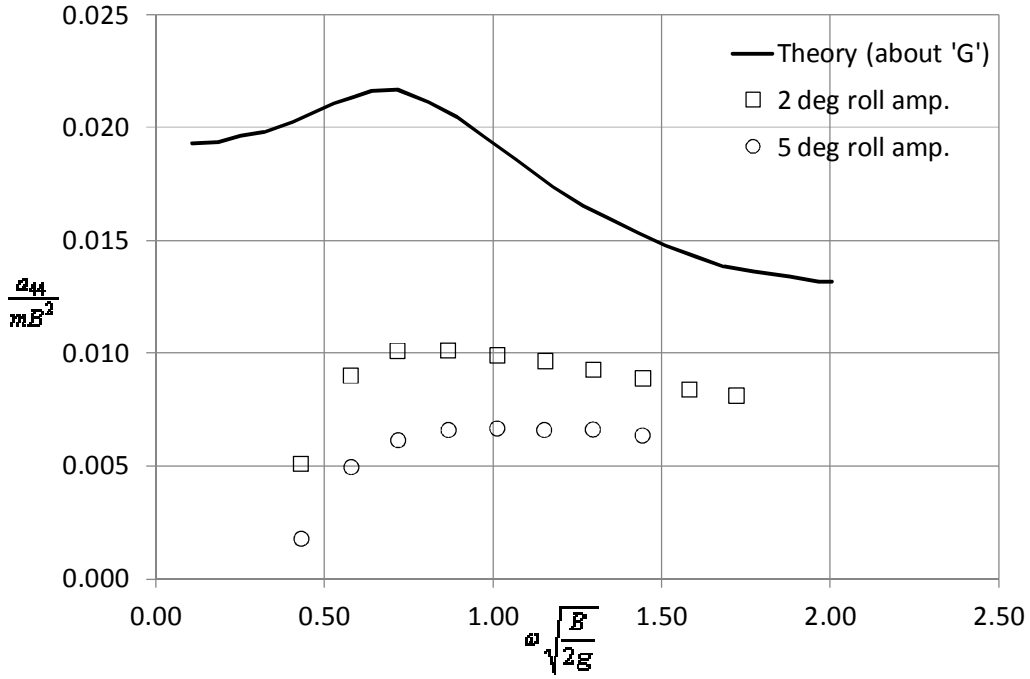

*Fig.**4.5**: Added inertia coefficient (B/T=4). Axis of rotation passes through centre of gravity lying B/4=0.1m above calm water-plane.*

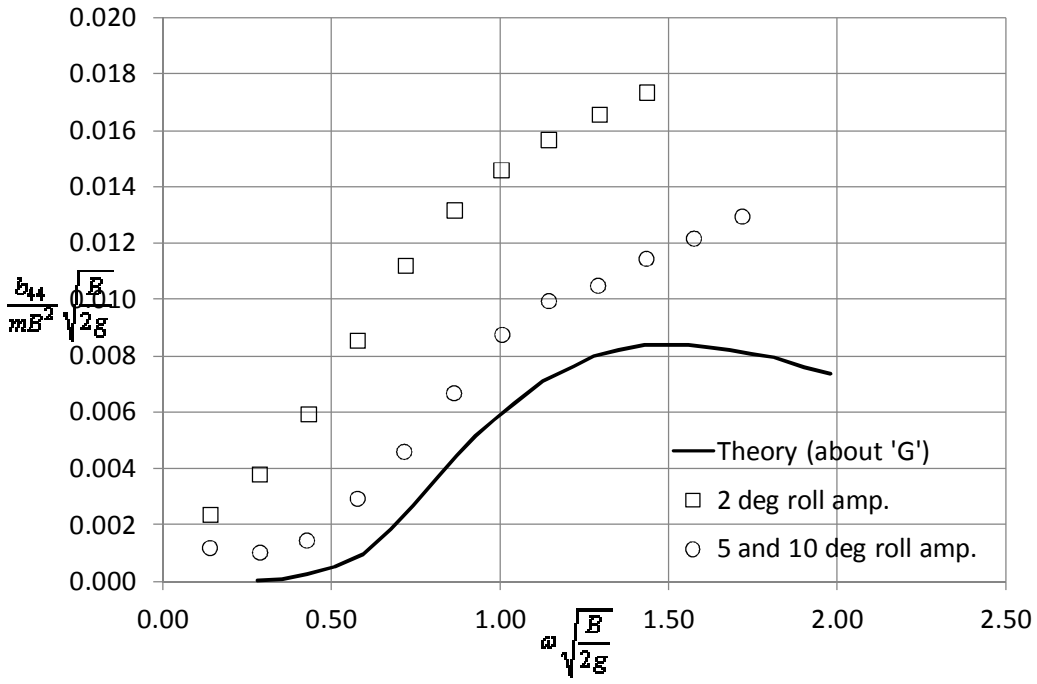

*Fig.**4.6**: Roll damping coefficient (B/T=4)*

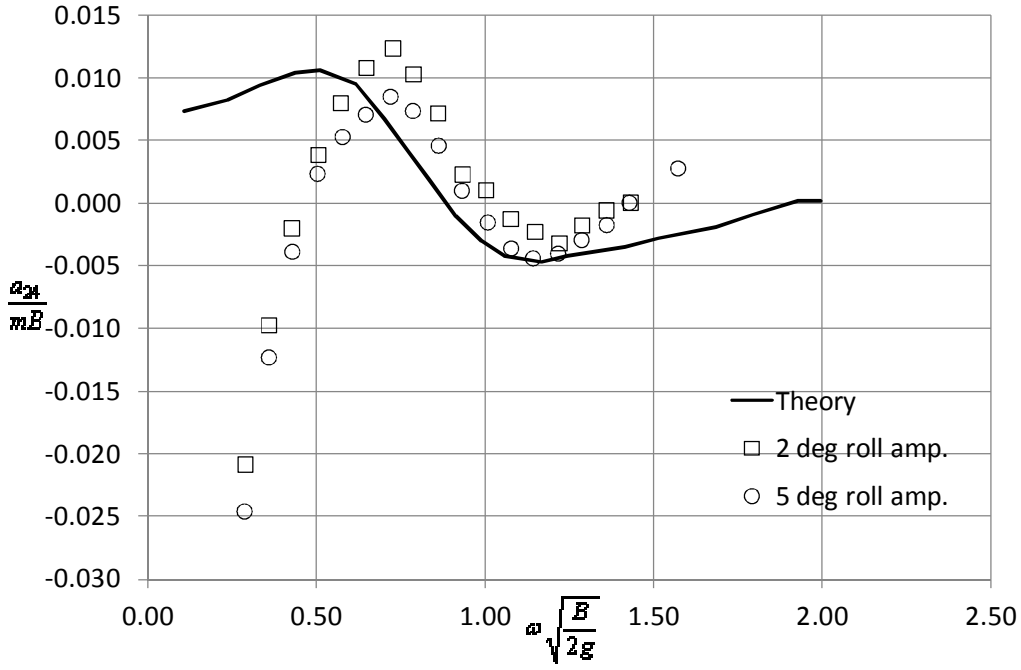

*Fig.**4.7**: Added inertia coefficient in coupling of roll into sway (B/T=4)*

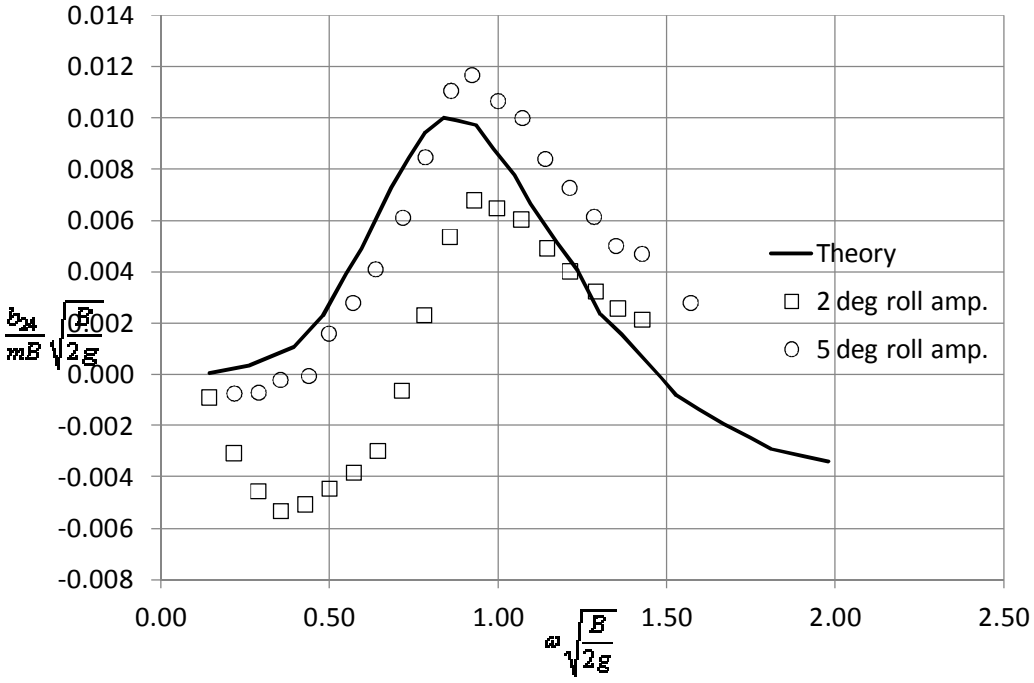

*Fig.**4.8**: Damping coefficient in coupling of roll into sway (B/T=4)*

4.2 Ikeda (1970s)

The research carried out in Japan in the 1970s aimed at developing empirical formulae for individual damping components[9], that is: radiation, skin friction, lift, eddy making as well as the components associated with bilge keels. The study involved considerable experimental programme, where not only two-dimensional but also three-dimensional models were tested. As a result, the empirical formulae were developed for individual damping components. The expressions, valid for "typical" ship geometries, are in use to date in many sea-keeping computer codes[10] based otherwise on the linear theory. These formulae allow estimating corrections terms accounting for viscous effects and supplementing potential damping prediction (the formulae and even the original Fortran code developed by Ikeda can be found in (Himeno, 1981)).

It is noteworthy that the Ikeda's method was not used in the present research to estimate relevant damping components (i.e. eddy making and friction). The reason for this is that the additional damping components predicted by the Ikeda's method need to be added to the predicted potential damping. However, the prediction presented in the following is used solely to provide reference for qualitative judgment of the experimental estimates. Therefore, given the substantial discrepancies between the prediction and the experiments there is no point of adding corrective terms to the calculated damping. On the other hand, the comprehensive research carried out by Ikeda provides valuable information on the scale of the individual damping components and may help to understand the results of the present experiment.

As mentioned above, from the results presented by Himeno, it follows that in the absence of forward speed and bilge keels the equivalent linear damping is a sum of the friction (B_F), wave-(B_W) and eddy-making (B_E) components. It can be concluded from the figures below (reproduced from Himeno and based on the experimental data) that for a "typical" ship-like shape the eddy-making components is a linear

[9] Based on the assumption that equivalent linear damping can be given as a combination of several components.

[10] This includes the Proteus 3 mentioned earlier.

function of frequency of oscillation while the friction component is almost linear. The wave-making component is present only at higher frequencies and is strongly nonlinear.

Considering the dependency on roll amplitude, it can be concluded that the friction and wave-making components are amplitude independent while the eddy-making component is almost linear function of the amplitude. This implies combined linear-quadratic damping model, e.g. $B_1\dot{\varphi} + B_2|\dot{\varphi}|\dot{\varphi}$ where B_1 contains friction and wave-making components while B_2 includes the amplitude-dependent eddy-making component. Furthermore, a rough estimate can be made, that implies that the skin-friction damping is much smaller (order of magnitude) than the wave damping. The amplitude-dependent eddy-making component reaches similar amplitude to the friction component at about 5 degrees roll angle. This indicates that B_F, B_W and B_E contributions to the total damping (given $F_n = 0.0$ and no bilge keels) are approximately 10, 75 and 15%. Obviously, these figures are only indicative and must be approached with due reserve.

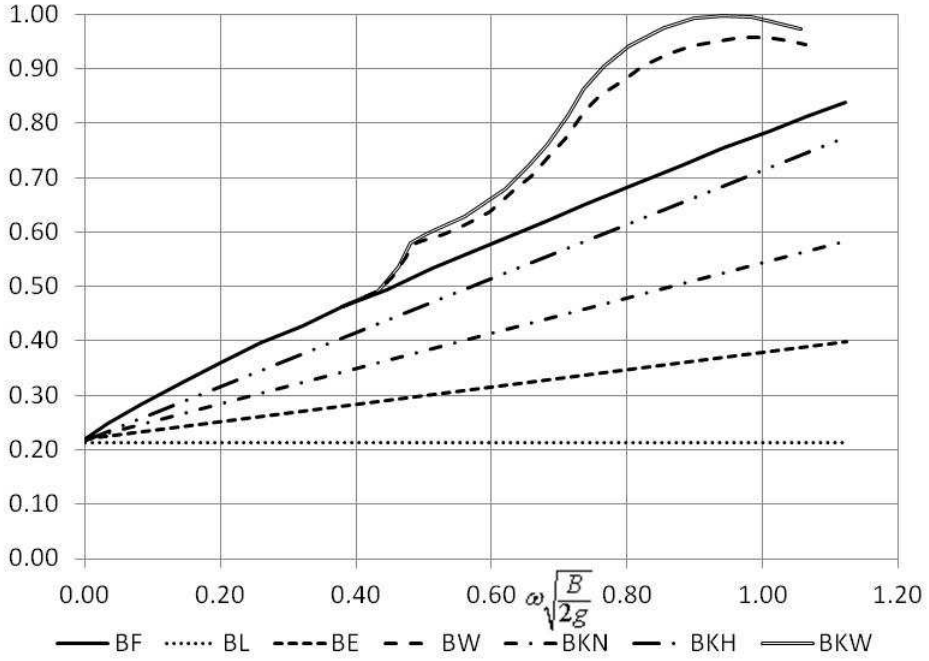

*Fig.**4.9**: Components of total (effective) roll damping coefficient in function of frequency of oscillations*

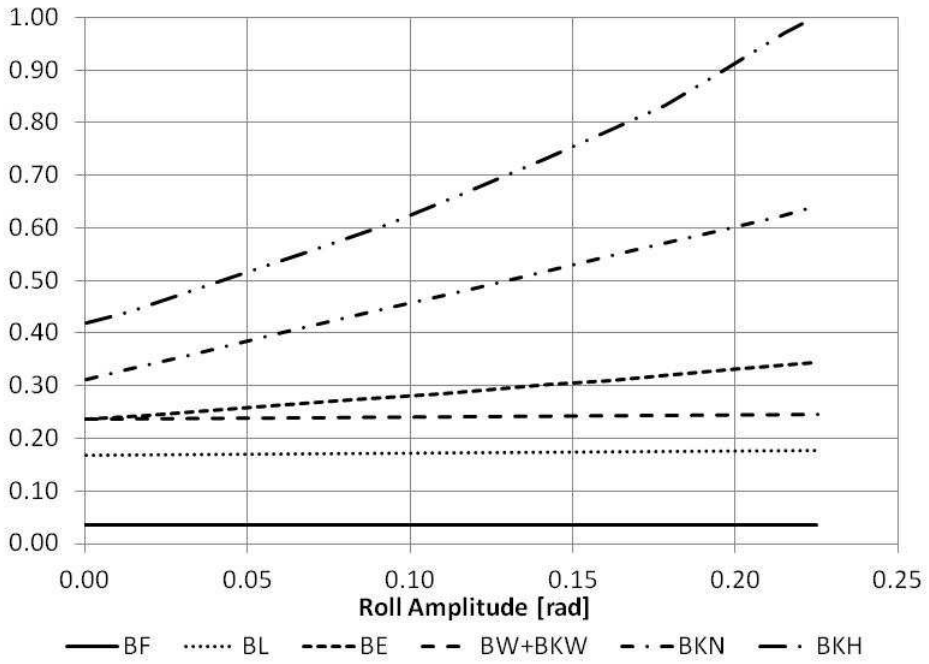

*Fig.**4.10**: Components of total (effective) roll damping coefficient in function of roll amplitude*

4.3 Standing (1992)

The test performed by the BMT Fluid Mechanics Ltd. involved the 1:50 scale models of the cylindrical sections of a typical ocean-going barge used in the offshore and oil industry. The tests were carried out with three draughts: shallow (B/T=15), medium (B/T=10) and deep of B/T-ratio 5. The sections were fitted with 0, 10 and 20 mm bilge keels. Furthermore, the sections were made with different bilge (corner) curvature of 0, 10 and 30mm. Additional tests were performed with bare hull sections at high rolling centre of 0.3 m. Breadth of all models was 0.6 m and their length chosen to allow 5-10 mm clearance each side of the tank (of 1.2 m width). The test matrix covered significant number of configurations.

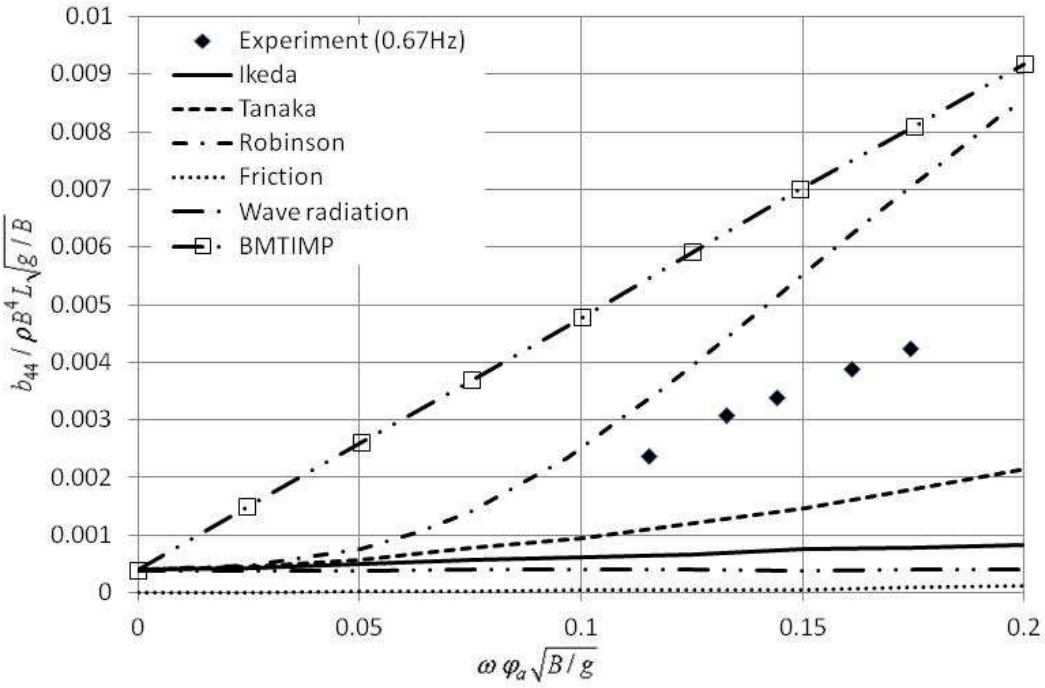

*Fig.**4.11**: Measured and predicted damping for section with the high roll centre, rounded corner and no bilge keels.*

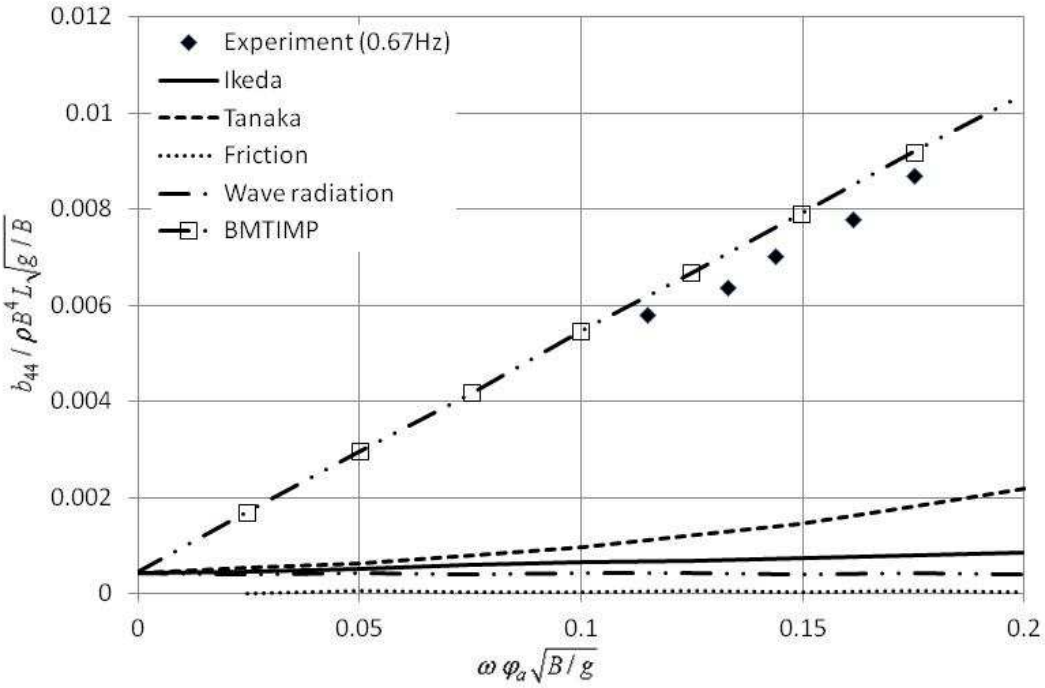

*Fig.**4.12**: Measured and predicted damping for section with the high roll centre, sharp corners and no bilge keels.*

As reported in (Standing et al., 1992) the forced roll experiments (with the fixed axis of rotation) tended to give lower damping estimates (at the roll natural frequency of 0.67 Hz) than a free roll.

The prediction by the discrete vortex method was very satisfactory for the sharp-cornered sections and the sections fitted with bilge keels but seriously overestimated damping for the round-cornered sections.

The experiments and predictions both showed linear or almost linear increase in damping with roll velocity amplitude. That is, the measured and predicted damping remained in agreement with the combined liner and quadratic terms of damping moment of the form: $B_L\dot{\phi} + B_Q\dot{\phi}\left|\dot{\phi}\right|$

In all the cases tested the friction damping was negligible and, as expected, the wave radiation independent of the velocity amplitude.

4.4 Chai (2005)

Results of the experiment were presented first in (Jasionowski and Vassalos, 2002) and elaborated further in (Chai, 2005). The measurements were performed on a 1:40 scale model of RoPax ferry[11]. The tests comprised measurements in intact as well as damaged condition in heave and roll modes of motion but without considering coupling between the modes in damaged condition. The motions were induced by external forced mechanism, as shown in the figure below. In roll, the oscillations took place about a fixed axis passing through centre of gravity of the model. The extensive test matrix covered frequencies[12]in range of 0.2-1.3 rad/s (with low frequency tests to determine restoring characteristics at 0.05 rad/s), 0, 10 and 20 degrees heel angles. The measurements were performed with two amplitudes of oscillations: 0.4 and 1.0m in heave and 5 and 10 degrees in roll.

[11] The model, known as the PRR01, was extensively tested in many survivability studies, including EU project HARDER and ITTC benchmark studies. The cylinder tested during the research presented herein is a midship-section of the model tested by Chai.

[12] All data in full scale

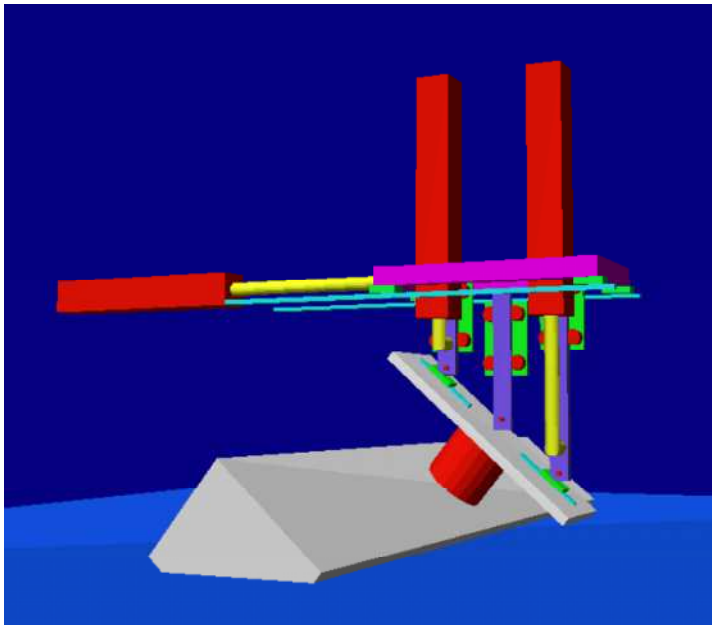

*Fig.**4.13**: Forcing mechanism in experiments by Chai*

In spite of the robust instrumentation, the experiment proved very difficult not only in damaged but also in intact condition. One of the reasons for this was that the tests were performed on a 3D ship model and this must have introduced complex interactions between various modes of motion. As such situation had been anticipated, forces were measured with use of state-of-the-art 6DoF load-cell. However, as it was learnt later, due to its large inertia and complex construction, the load-cell was source of the significant time lags. In addition to this, the measurements in higher frequencies might have been affected by large and heavy construction of the forcing mechanism.

Nevertheless, although the experiments lacked in accuracy they provided very valuable insight, particularly into hull-floodwater interaction. Specifically, the following observations were made (Jasionowski and Vassalos, 2002)

- The floodwater free surface undergoes oscillations of different amplitude than that of the roll motion and vary significantly with frequency of excitation.
- The amplitude of floodwater free surface varies with the direction of roll, i.e. it depends on whether the ship rolls towards the damage side or away from it.
- The phase angle between roll motion and floodwater free surface oscillation varies with frequency and amplitude of excitation.

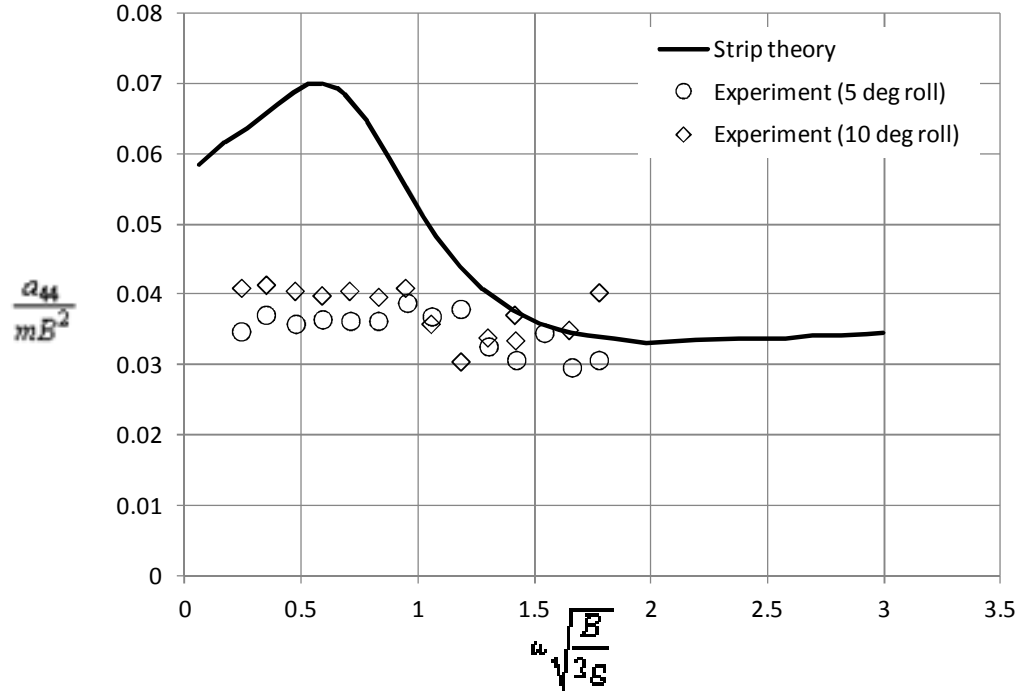

*Fig.**4.14**: Roll added inertia coefficient (intact condition, upright ship)*

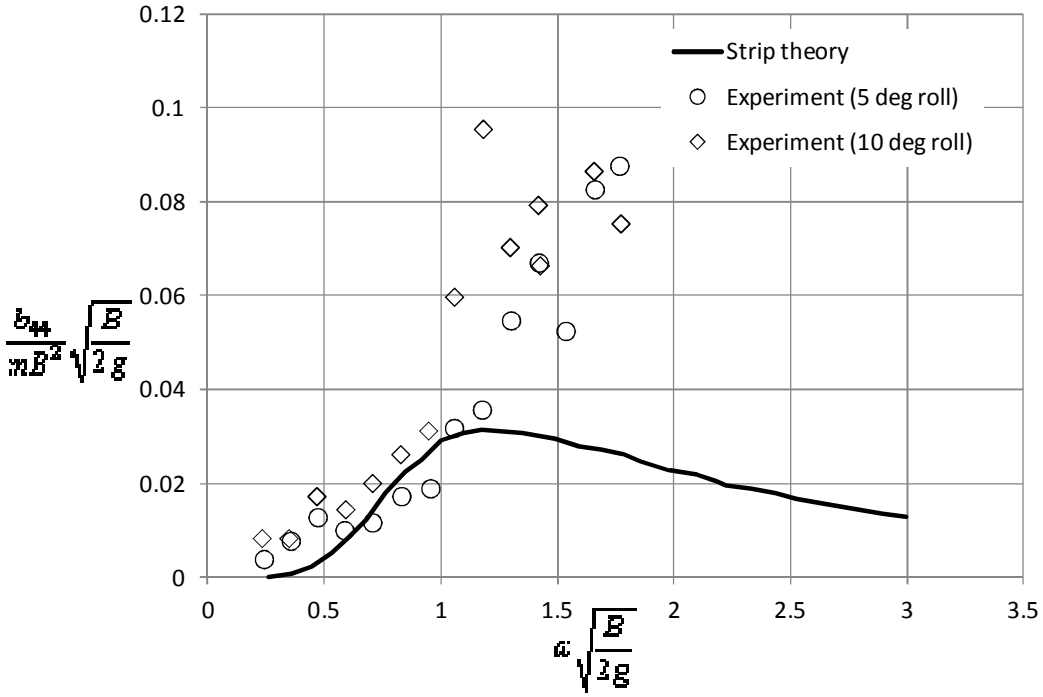

*Fig.**4.15**: Roll damping coefficient (intact condition, upright ship)*

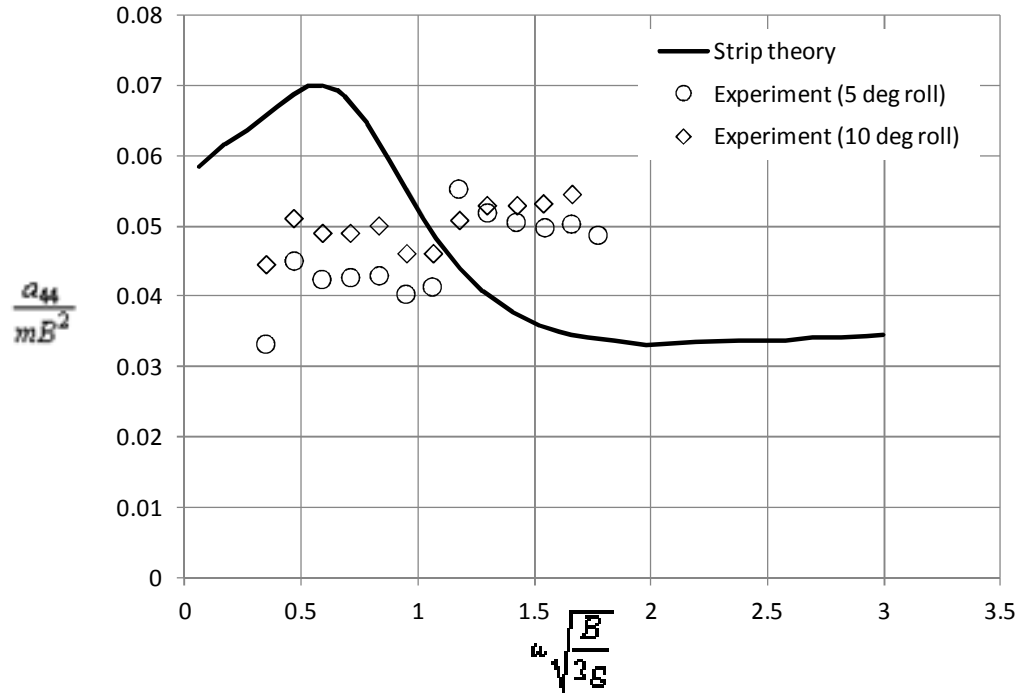

*Fig.**4.16**: Roll added inertia coefficient (damaged condition, upright ship)*

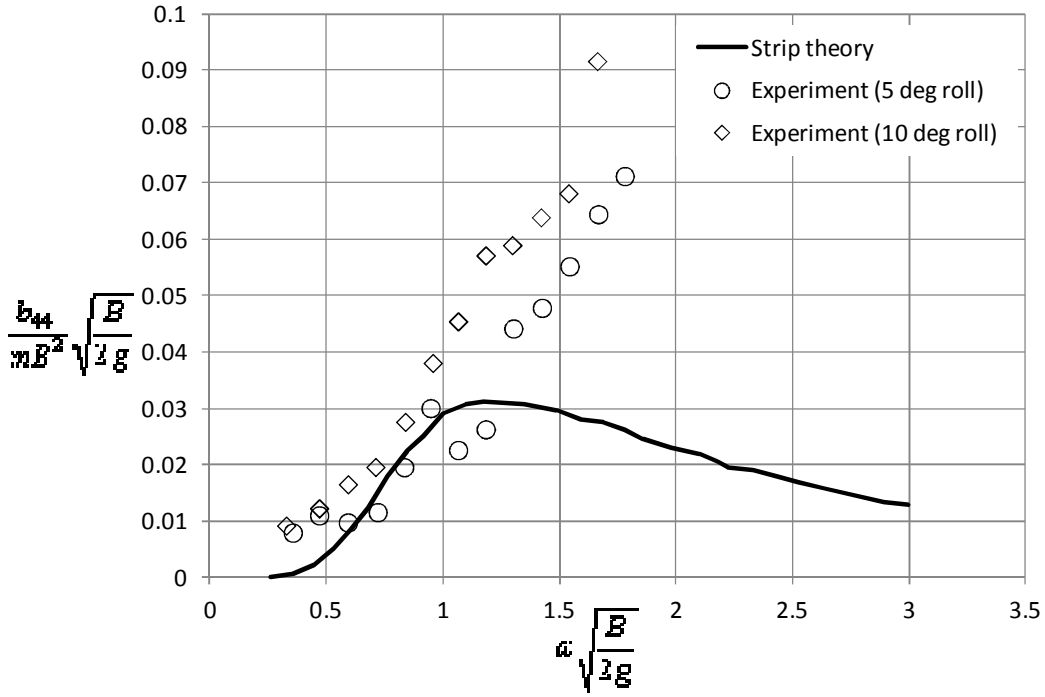

*Fig.**4.17**: Roll damping coefficient (damaged condition, upright ship)*

Chapter 5 Experiments on a floating body

5.1 Introductory remarks

The methodology for forced oscillations of an unconstrained cylindrical body as well as its validation for intact ship measurements have been already presented[13] in the series of conference papers (Cichowicz et al., 2009, 2010, 2011). In the following, the matter will be discussed in a detail with particular attention paid to the interpretation of results.

Undoubtedly, the measurements on a floating body have certain disadvantages, such as limitation in imposed modes of oscillation, but on the other hand, they offer a unique possibility to study complex, multi-modal response of the vessel without imposing extra constraints on the system. This aspect is of a particular importance in measurements in a damaged condition where ship-floodwater interaction may assume very complex form.

5.2 Experimental set-up and the test programme

The experiments reported in the ensuing were conducted at the Kelvin Hydrodynamics Laboratory (KHM), testing facilities of the University of Strathclyde[14]. Main dimensions of the towing tank at the KHM are (length, breadth and depth respectively): 76.0×4.6×2.5 m. The tank is equipped with a modern four-paddle wave maker and on opposite end of the tank there is an adjustable beach allowing tests at variable water depths. Additionally, for the purpose of the tests reported herein, two sets of pool booms (swimming pool line-markers) were fitted alongside of the tank.

---

[13] Some sections in the following are largely based on these publications. Contents of the first paper, comprised mainly mathematical model and design principles of the forcing apparatus, and this is detailed in the Appendix A The paper presented in 2010 reported the first successful measurements in intact conditions (details on these are given in the section 5.8). The last paper, presented in 2011, discussed preliminary results of the measurements carried out on the flooded model as elaborated further in the section 5.9.

[14] http://www.strath.ac.uk/na-me/facilities/cmh/

The reason for fitting the line-markers was to diffract radiation waves from the side-walls of the tank when the model was not positioned accurately across the tank. In fact, given that the wave-damping beach was fitted on one end of the tank only, it has been observed that positioning the model "diagonally" had a positive impact on re-peatability of measurements, particularly while testing at low frequencies.

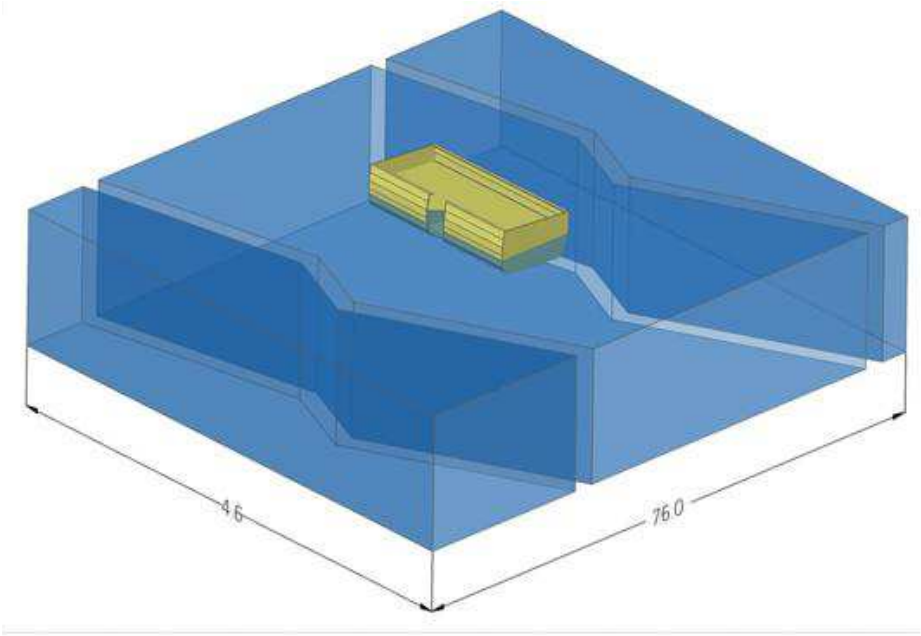

*Fig.**5.1**: The model and main dimensions of the tank (meters)*

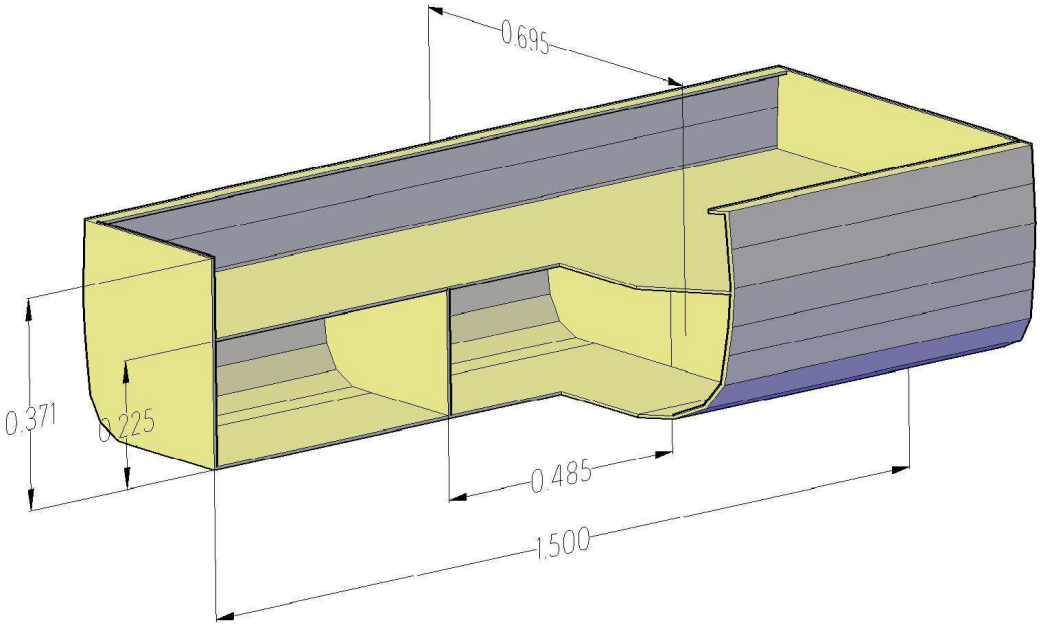

*Fig.**5.2**: Main dimensions and the internal arrangement of the model*

The model was manufactured of fibreglass about 5mm thick and fitted with the acrylic-glass bulkhead deck. Below the deck, two transverse bulkheads divided the internal space into three watertight compartments. The midship compartment was floodable through the prismatic (SOLAS-type) opening, penetrating the shell and the deck up to B/5. The width of the opening was 0.203 m, which corresponded to 8.1m full scale. During the measurements in the intact condition, the opening was sealed with a detachable piece of the hull shell.

Particular dimensions of the model are presented in the table below:

Table 1 *Particular dimensions of the model*

	Dim.	Intact	Dam.
L	m	1.500	1.500
B	m	0.695	0.695
T	m	0.158	0.157
KMT	m	0.343	0.344
KG (dry)	m	0.220	0.297
KG (flooded)	m	-	0.232
GM	m	0.123	0.047
Mass	kg	156.8	116.7
kxx	Nm/rad	189.2	53.79
Roll inertia (air)	$kg \cdot m^2$	10.4	4.8
Radius of in. (i_{xx})	m	0.258	0.251
i_{xx}/B	-	0.370	0.36
Scale	-	40	40

The unconstrained, freely floating, model was forced to roll in calm water by an internal gyroscopic device (see Appendix A for details). The device was pivoted (an axis of pivoting is schematically represented in the figure below by the point *P*) on a stiff frame attached to the steel structure reinforcing uppermost part of the model. The supporting frame comprised of three longitudinal and two transverse Bosch profiles of considerable stiffness. The rolling moment generated by the forcing apparatus was impressed upon the model through a torque arm (the L-shaped plate attached

to the side of the mechanism) through a 500lb load-cell fixed to one of the longitudinal beams of the supporting frame (positioned 0.212m off the centre of the model). The apparatus was intentionally pivoted with a minimal clearance above the deck in order to maintain position of the centre of gravity of the model close to the waterplane.

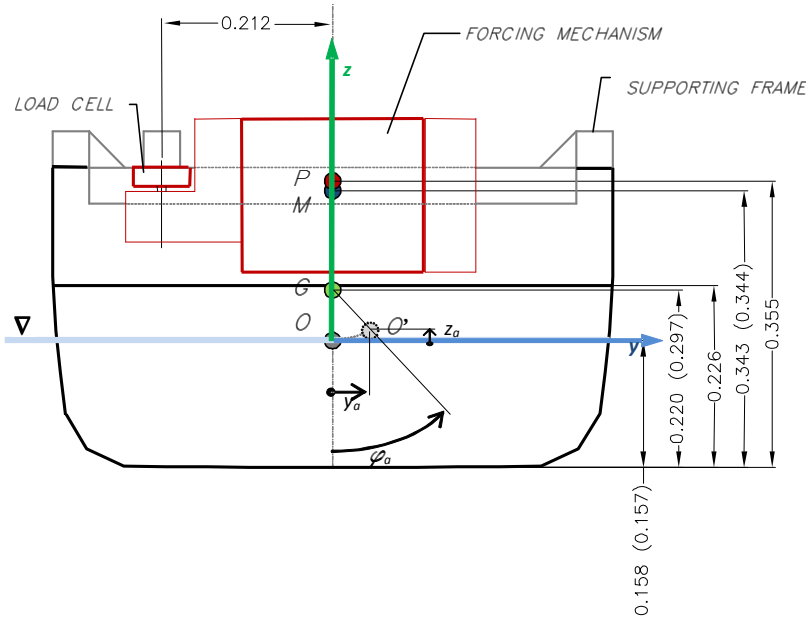

*Fig.**5.3**: The configuration of the system (values in parentheses as in damaged condition, all dimensions in millimetres). In the upright position, stationary and body-fixed frames of reference overlap.*

Motions of the model were recorded with use of an optical motion capture system (Qualisys ^{TM}). In order to monitor possible deflection of the forcing mechanism two "rigid bodies" were defined (with use of reflective markers) in the optical tracker – one associated with the model and one "attached" to the forcing mechanism. Motions of the markers were recorded by a set of four, high-speed, infrared cameras. Motions of the individual markers were combined into translations and rotations of the "rigid bodies" resulting in 6DoF recordings. For the reference estimate of the phase lag (between excitation and response), a single axis accelerometer was also fitted to the model.

The model was ballasted to the draught marks with ballast weights located in the "forward" and "aft" compartments. Some small weights were placed on the deck to allow correcting trim and heel of the model. The weights were secured in their positions with use of silicon adhesive. Additionally, for tests in the intact condition, some weights were placed in the middle compartment. These weights were used to make up for amount of floodwater inside of the compartment (in static equilibrium) while testing in the damaged condition. Tests were carried out at virtually the same draught in both conditions (dry and flooded hull). However, due to some inaccuracy in positioning of the replacement masses (i.e. weights placed inside the floodable compartments) the estimated position of the centre of gravity of the flooded system was 0.012 m (0.48 m full scale) higher than in the case of the intact ship. Freeboard in the flooded condition was 0.071 m (2.82 m full scale) – sufficient to realise roll motions of an amplitude of about 10 degrees without submerging of the bulkhead deck.

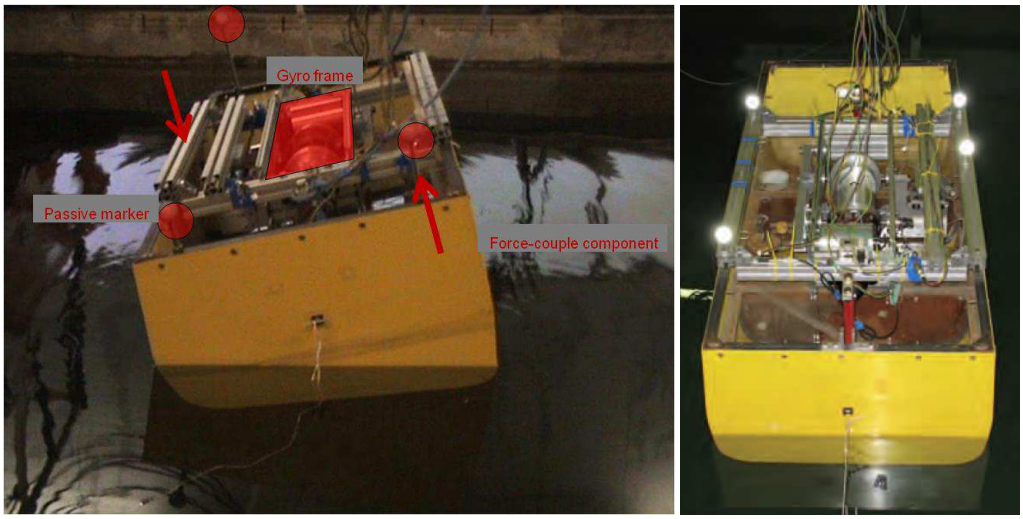

*Fig.**5.4**: The arrangement of the forcing apparatus*

5.3 Calibration, data acquisition and data processing

The motion capture system was calibrated in two stages as described in the system's manual (Qualisys, 2009). At the first stage, the measurement volume was specified by placing a calibration frame (an L-shaped reference structure) in the calm-water plane in such a way that one of the arms of the reference frame was aligned with the longitudinal axis of the tank. The static calibration aimed at determining axes of the

global (Earth-fixed) coordinate system. In the second stage, dynamic calibration was performed with use of a calibration wand moved within the measurement volume in some random way. Once the calibration was completed, the aforementioned “rigid bodies” were defined by identifying appropriate markers on the model.

The model was weighted with use of a standard industrial scale with +/- 0.050 kg accuracy. Estimates of the model’s centre of gravity were based on a standard inclining test.

The final stage of model preparation involved estimating of the model’s inertia in air. This was carried out by swinging the model on a purpose-built platform and measuring a period of natural oscillations. The platform was suspended from a frame with use of a “knife-edge” support. Bearings were not used in the suspension.

The load-cell measuring a component of the moment to sustain motion was calibrated before and after each series of measurements. The calibration involved placing the forcing apparatus (along with its supporting frame) “upside-down” on a rigid horizontal surface (a table of a CNC router was used for this purpose). Once the supporting frame of the forcing mechanism was fastened to the table the calibration weights were placed on a steel rod fitted to the torque arm. The load-cell was calibrated up to 150% of an anticipated load. The procedure involved up- and downloading and a characteristics obtained this way did not indicate any substantial hysteresis error. The load-cell output was amplified so maximum and minimum loads corresponded to +/- 5V analogue output. The amplifier settings were held fixed between the calibrations.

In total, there were thirteen signals recorded:

- the moment to sustain motion (channel 1);
- six components of the model motions (i.e. surge, sway, heave, roll, pitch and yaw; channels 2-7);
- the roll component of the gyro frame (in order to monitor possible system deflection at large loads; channel 8);

- the inclinometer output (channel 9);
- spin velocities of the gyros (channels 10 and 11);
- the reference signal of the frequency of the excitation (channel 12);
- the output of the MEM single axis gyro (channel 13).

All the channels were sampled with the Cambridge Electronic Design (Power1401 mk II), 16-bit ADC (Analogue to Digital Converter) at the sampling rate of 150.08 Hz. The analogue input signals were sampled sequentially but, according to the manufacturer's data, ADC's chip holds a built-in "sample-and-hold" circuit. Therefore, it is expected[15] that the time latency of the sampling could be considered negligible.

Sampled signals were exported to the text files and processed in the Matlab environment. The process was carried out in few steps:

- filtering with a digital, low-pass filter (Butterworth) of cut-off frequency 5Hz;
- manual selection of the steady-state part of the waveforms;
- least-square fitting of the steady-state signals to determine frequency, amplitudes and phases of the signals;
- correcting of the phases of motion signals based on the inclinometer's phase estimate.

5.4 Equations of equilibrium

As shown in the previous chapter, the equation of a body oscillating in undisturbed free surface of the fluid can be expressed in terms of generalised coordinates as follows

[15] The latency in the ADC sampling was also investigated at the early stage of the research. It was verified that the ADC does not introduce any significant lags.

$$\left(M_{jk}+a_{jk}\right)\ddot{q}^{k}+b_{jk}\dot{q}^{k}+c_{jk}q^{k}=Q_{j}^{E} \tag{3.54}$$

where $(.)_{jk}$ are 6×6 matrices and $(.)^{j}$ are 6×1 column vectors.

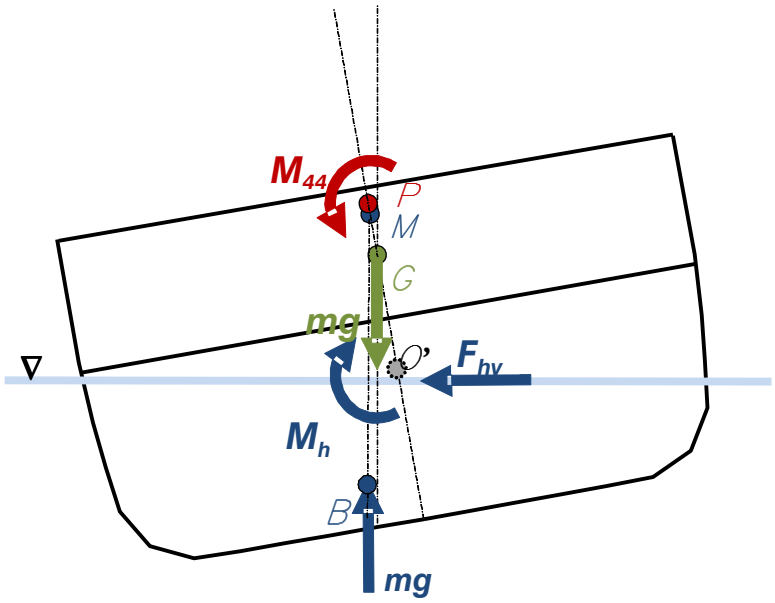

*Fig.**5.5**: Free-body diagram of the cylinder during forced roll. In the sketch the assumed rotation takes place about the axis passing through the point* G *and therefore it is that* $\overline{OA}=\overline{OG}$

In the case of a cylindrical body rolling about an axis perpendicular to the cylinder's cross-section, the above equation can be re-written with help of 3×3 matrices and 3×1 vectors

$$\begin{bmatrix} m+a_{22} & a_{23} & a_{24} \\ a_{32} & m+a_{33} & a_{34} \\ a_{42} & a_{43} & I_{44}+a_{44} \end{bmatrix}\begin{bmatrix} \ddot{y} \\ \ddot{z} \\ \ddot{\varphi} \end{bmatrix}+\begin{bmatrix} b_{22} & b_{23} & b_{24} \\ b_{32} & b_{33} & b_{34} \\ b_{42} & b_{43} & b_{44} \end{bmatrix}\begin{bmatrix} \dot{y} \\ \dot{z} \\ \dot{\varphi} \end{bmatrix}+\begin{bmatrix} c_{22} & c_{23} & c_{24} \\ c_{32} & c_{33} & c_{34} \\ c_{42} & c_{43} & c_{44} \end{bmatrix}\begin{bmatrix} y \\ z \\ \varphi \end{bmatrix}=\begin{bmatrix} F_2 \\ F_3 \\ M_{44} \end{bmatrix} \tag{5.1}$$

where m stands for the mass of the model (dry hull), whereas displacements (and their time derivatives) y,z,φ and external forces F_2,F_3,M_{44} are harmonic functions of the form

$$
\begin{aligned}
y &= y_a \sin\left(\omega t + \varepsilon_y\right) \\
z &= z_a \sin\left(\omega t + \varepsilon_z\right) \\
\varphi &= \varphi_a \sin\left(\omega t + \varepsilon_\varphi\right) \\
F_2 &= F_{2a} \sin\left(\omega t + \varepsilon_{F_2}\right) \\
F_3 &= F_{3a} \sin\left(\omega t + \varepsilon_{F_3}\right) \\
M_{44} &= M_{44a} \sin\left(\omega t + \varepsilon_M\right)
\end{aligned}
\tag{5.2}
$$

The subscript a denotes amplitude, ω stands for circular frequency and ε is a phase of the waveform. All the coordinates are expressed in the inertial (or simply stationary in this case) frame of reference, as shown in the *Fig.**5.3***.

Given that the tested model has two planes of symmetry, Ox_1x_3 and Ox_2x_3, it can be reasoned that the vertical displacements induce a symmetric pressure field, and therefore a_{23}, a_{43}, b_{23} and b_{43} should vanish. On the other hand, while flooded, the model was no longer symmetrical with respect to the Ox_1x_3 plane so the coupling of heave into roll and sway might have taken place, due to the presence of the opening. However, this contribution could be expected small compared to the other modes of motion and therefore, it has been neglected. Furthermore, sinkage and heel are opposed by non-zero hydrostatic forces. In the case of two coupled displacements, i.e. c_{34} and c_{43}, it is apparent that the latter should not generate any restoring moment, due to symmetry of the model, however static heel may generate a non-zero restoring force along the Oz axis. Thus, in the case of oscillations about the axis passing through the point *O*, the equations take the following form

$$
\begin{bmatrix} m+a_{22} & 0 & a_{24} \\ a_{32} & m+a_{33} & a_{34} \\ a_{42} & 0 & I_{44}+a_{44} \end{bmatrix} \begin{bmatrix} \ddot{y} \\ \ddot{z} \\ \ddot{\varphi} \end{bmatrix} + \begin{bmatrix} b_{22} & 0 & b_{24} \\ b_{32} & b_{33} & b_{34} \\ b_{42} & 0 & b_{44} \end{bmatrix} \begin{bmatrix} \dot{y} \\ \dot{z} \\ \dot{\varphi} \end{bmatrix} + \begin{bmatrix} 0 & 0 & 0 \\ 0 & c_{33} & c_{34} \\ 0 & 0 & c_{44} \end{bmatrix} \begin{bmatrix} y \\ z \\ \varphi \end{bmatrix} = \begin{bmatrix} 0 \\ 0 \\ M_{44} \end{bmatrix}
\tag{5.3}
$$

It is noteworthy, that the above equation implies that the external forces impressed on a body do not have any vertical or lateral components. This assumption is based on the mathematical model of the forcing apparatus, as discussed in detail in the appendix A.1.

Furthermore, no assumption is being made on the symmetry of added inertia and damping matrices, hence, the equation contains fifteen unknowns (fourteen compo-

nents of added inertia and damping matrices and one component of the restoring matrix) while the c_{33} and c_{44} are approximated by the formulae presented in the previous chapter.

The above equation has been derived for the case of oscillation about the axis passing through the point O. However, an unconstrained body experiences rotations about the so-called natural axis of rotation (Balcer, 2004). In fact, the natural axis is associated with instantaneous rotation, which, in principle, can change direction and location during the motion. However, in the case investigated here, the pitch angle observed during the motion was at least one order of magnitude smaller than roll and could be considered negligible (see the graph below). Similarly, when the forcing apparatus was properly set the model did not experienced any significant yaw motion, thus it could be safely assumed that the instantaneous axis of rotation lies on a cylindrical surface with an axis parallel to the longitudinal axis of the model.

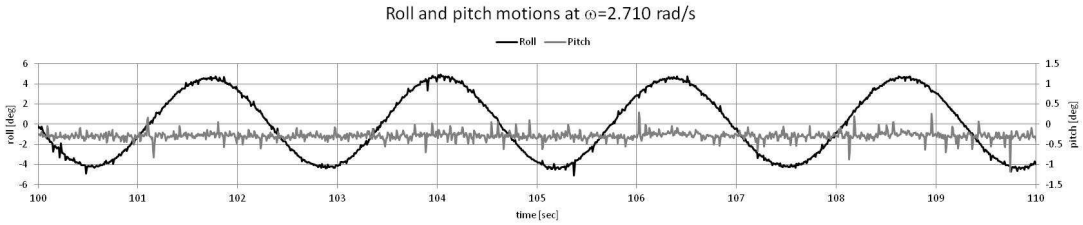

*Fig.**5.6**: Roll and pitch time histories for low-frequency oscillations of intact model.*

In his paper, Balcer has shown that the location of the natural rolling axis could be quite easily determined based on the homogeneous sway equation. This procedure requires however, prior knowledge of the added mass a_{22} and the coupling term of added inertia of roll into sway a_{24}. This makes the procedure inapplicable for mathematical modelling presented in this section (the formula derived by Balcer shall be discussed later).

At this stage, it has been decided that an average (per cycle) elevation of the axis of rotation above the calm-water plane can be approximated as

$$\overline{OA} = \frac{y_a}{\sin(\varphi_a)} \tag{5.4}$$

It is expected, that the above relation should hold for small amplitudes and small phase difference between roll and sway.

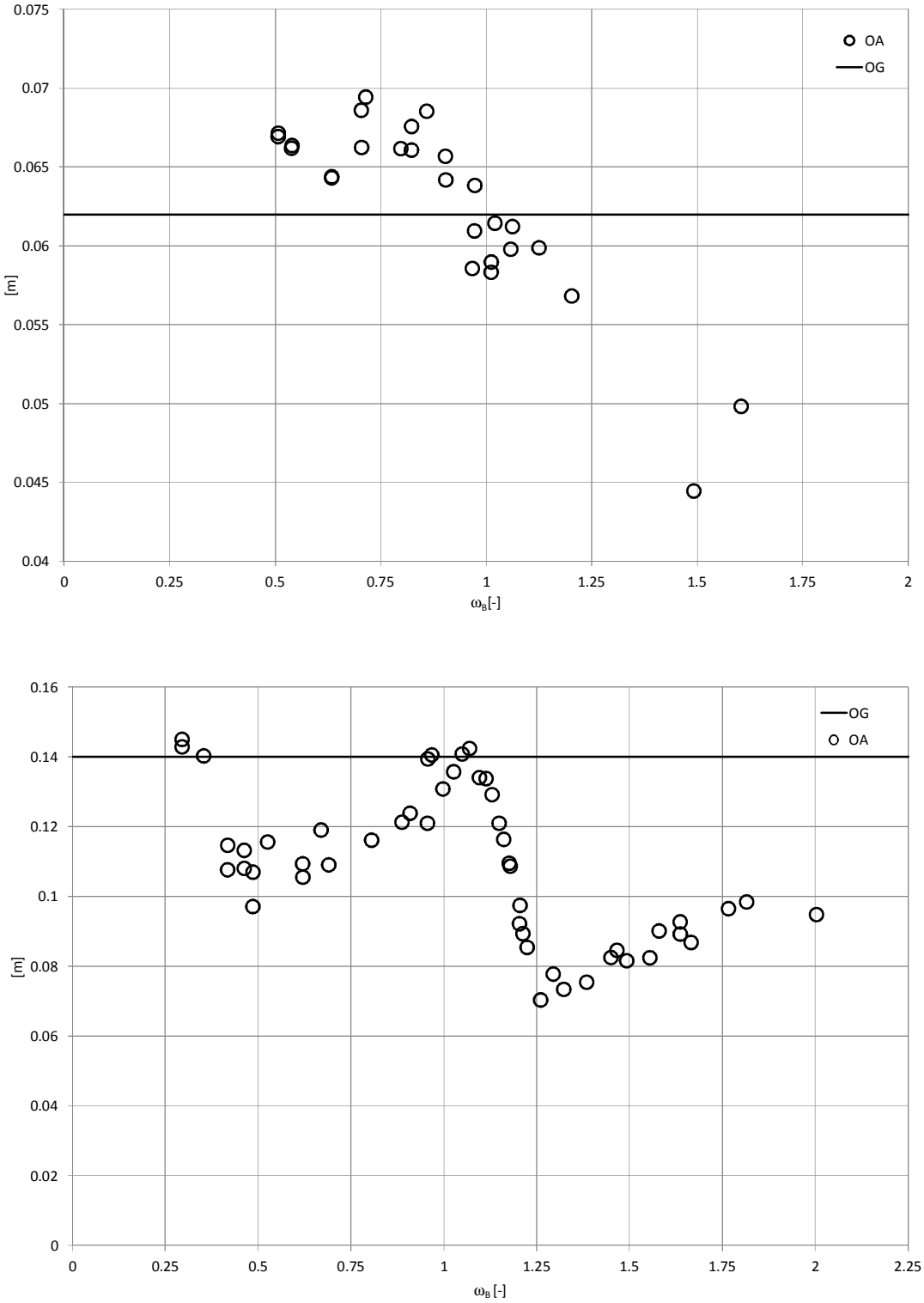

Fig.5.7: Approximated elevation of the rolling axis above the calm-water plane – intact (left) and flooded model (right). Solid line represents elevation of centre of gravity in upright position of floating model.

The hydrodynamic forces (see *Fig.5.5*) are assumed to act at the fixed in space location, corresponding to the origin O of the stationary frame of reference, and therefore components of added inertia and damping matrices should be expressed in this coordinates system. The rigid body equations of motions are, on the other hand, most conveniently expressed as translations of and rotations about the body's centre of gravity, G. However, following the assumptions made with respect to the elevation of the axis of rotation and the fact that the moment to sustain motion was measured about the point P, it seems reasonable to treat the point A as an effective centre of gravity of the system. This allows expressing the following relationships between coordinates

$$\begin{aligned} y_A(t) &= y(t) - \varphi(t)\cdot\overline{OA} \\ z_A(t) &= z(t) \\ \varphi_A(t) &= \varphi(t) \end{aligned} \tag{5.5}$$

It should be noted that if roll motion were about fixed axis of rotation the first equation in the above would read that $y_A = 0$.

If the magnitude of roll is small (i.e. $\sin(\varphi) \approx \varphi$ and $\cos(\varphi) \approx 1$) the dynamic equilibrium condition could be expressed by means of three scalar equations

$$\begin{aligned} F_{hy} &= m\ddot{y}_A \\ F_{hz} &= -\left(m\ddot{z}_A + c_{33}z_A\right) \\ M_h + F_{hy}\overline{OP} &+ I'_{44}\ddot{\varphi}_A + c_{44}\varphi_A + m\ddot{y}_A\overline{AP} = M_{44} \end{aligned} \tag{5.6}$$

where $mg\left(\overline{GP} - \overline{MP}\right) = mg\overline{GM} = c_{44}$, I'_{44} stands for the inertia of the body about the axis passing through A, F_{hy} are F_{hz} are components of the hydrodynamic force along the appropriate axes of the global coordinate system and M_h is a moment of the hydrodynamic force about the point O.

Based on the equation (5.3) hydrodynamic forces can be expanded in terms of components of added inertia and damping matrices, that is

$$\begin{aligned} F_{hy} &= a_{22}\ddot{y} + a_{24}\ddot{\varphi} + b_{22}\dot{y} + b_{24}\dot{\varphi} \\ F_{hz} &= a_{32}\ddot{y} + a_{33}\ddot{z} + a_{34}\ddot{\varphi} + b_{32}\dot{y} + b_{33}\dot{z} + b_{34}\dot{\varphi} \\ M_h &= a_{42}\ddot{y} + a_{44}\ddot{\varphi} + b_{42}\dot{y} + b_{44}\dot{\varphi} \end{aligned} \tag{5.7}$$

Substituting these identities into the equation (5.6) leads to the set of governing equations

$$a_{22}\ddot{y}+a_{24}\ddot{\varphi}+b_{22}\dot{y}+b_{24}\dot{\varphi}=m\left(\ddot{y}-\ddot{\varphi}\overline{OA}\right)$$

$$\begin{aligned}&a_{22}\ddot{y}\overline{OP}+a_{24}\ddot{\varphi}\overline{OP}+a_{42}\ddot{y}+a_{44}\ddot{\varphi}+b_{22}\dot{y}\overline{OP}+b_{24}\dot{\varphi}\overline{OP}+b_{42}\dot{y}+b_{44}\dot{\varphi}=\\&=M_{44}-\left(I_{44}+m\overline{AG}^2\right)\ddot{\varphi}-c_{44}\varphi-m\left(\ddot{y}-\ddot{\varphi}\overline{OA}\right)\overline{AP}\end{aligned}\qquad(5.8)$$

$$a_{32}\ddot{y}+a_{33}\ddot{z}+a_{34}\ddot{\varphi}+b_{32}\dot{y}+b_{33}\dot{z}+b_{34}\dot{\varphi}=-\left(m\ddot{z}+c_{33}z\right)$$

5.5 Estimates of added inertia and damping

The first two expressions in the set given by the equation (5.8) are coupled roll-sway equations containing eight unknown coefficients (added inertia and damping terms). The third, heave equation, contains seven unknown coefficients but it is not coupled with the other two. With the help of orthogonal decomposition, the coupled roll-sway equation can be expanded into a system of four linearly independent equations with eight unknowns, while the heave equation results in the system of two equations with seven unknowns. Denoting by $(.)_1$ displacements, velocities, accelerations and forces at the time $t=0$, and by $(.)_2$ the values corresponding to $t=\frac{\pi}{2\omega}$, the roll-sway system can be written simply as a matrix equation $A\mathbf{B}=\mathbf{C}$, where the matrices are

$$A=\begin{bmatrix}\ddot{y}_1 & \ddot{\varphi}_1 & 0 & 0 & \dot{y}_1 & \dot{\varphi}_1 & 0 & 0\\ \ddot{y}_2 & \ddot{\varphi}_2 & 0 & 0 & \dot{y}_2 & \dot{\varphi}_2 & 0 & 0\\ \ddot{y}_1\overline{OP} & \ddot{\varphi}_1\overline{OP} & \ddot{y}_1 & \ddot{\varphi}_1 & \dot{y}_1\overline{OP} & \dot{\varphi}_1\overline{OP} & \dot{y}_1 & \dot{\varphi}_1\\ \ddot{y}_2\overline{OP} & \ddot{\varphi}_2\overline{OP} & \ddot{y}_2 & \ddot{\varphi}_2 & \dot{y}_2\overline{OP} & \dot{\varphi}_2\overline{OP} & \dot{y}_2 & \dot{\varphi}_2\end{bmatrix}$$

$$\mathbf{B}=\begin{bmatrix}a_{22} & a_{24} & a_{42} & a_{44} & b_{22} & b_{24} & b_{42} & b_{44}\end{bmatrix}^T$$

$$\mathbf{C}=\begin{bmatrix}-m\left(\ddot{y}_1-\ddot{\varphi}_1\overline{AG}\right)\\ -m\left(\ddot{y}_2-\ddot{\varphi}_2\overline{AG}\right)\\ M_{44}\left(t=0\right)-\left(I_{44}+m\overline{AG}^2\right)\ddot{\varphi}_1-c_{44}\varphi_1-m\left(\ddot{y}_1-\ddot{\varphi}_1\overline{OA}\right)\overline{AP}\\ M_{44}\left(t=\frac{\pi}{2\omega}\right)-\left(I_{44}+m\overline{AG}^2\right)\ddot{\varphi}_1-c_{44}\varphi_1-m\left(\ddot{y}_1-\ddot{\varphi}_1\overline{OA}\right)\overline{AP}\end{bmatrix}\qquad(5.9)$$

where $M_{44}(t=0) = M\sin(\varepsilon_M)$ and $M_{44}\left(t=\frac{\pi}{2\omega}\right) = M\sin\left(\frac{\pi}{2}+\varepsilon_M\right)$, M stands for an amplitude of the measured moment and ε_M is a phase angle of the excitation. All other derivatives are computed in the similar fashion.

Proceeding analogically with the heave equation, it is possible to express it in matrix form as: $D\mathbf{E} = G$, where

$$
\begin{aligned}
D &= \begin{bmatrix} \ddot{y}_1 & \ddot{z}_1 & \ddot{\varphi}_1 & \dot{y}_1 & \dot{z}_1 & \dot{\varphi}_1 \\ \ddot{y}_2 & \ddot{z}_2 & \ddot{\varphi}_2 & \dot{y}_2 & \dot{z}_2 & \dot{\varphi}_2 \end{bmatrix} \\
\mathbf{E} &= \begin{bmatrix} a_{32} & a_{33} & a_{34} & b_{32} & b_{33} & b_{34} \end{bmatrix}^T \\
\mathbf{G} &= \begin{bmatrix} -\left(m\ddot{z}_1 + c_{33}z_1\right) \\ -\left(m\ddot{z}_2 + c_{33}z_2\right) \end{bmatrix}
\end{aligned}
\tag{5.10}
$$

The systems of equations are under-determined and cannot be solved analytically. Numerically, the problem could by attacked from various directions. One of the strategies would be to employ a method based on the least-squares fitting methodology and apply it directly to the scalar equations (5.8) to minimise error in fits. However, the problem with the least-squares estimations is that some of the unknown added inertia and damping terms are in phase with each other e.g. a_{22} and a_{42} in the moment equation. Obviously, the coupling term a_{42} could be determined from the sway equation, which does not contain waveforms exactly in phase, but this imposes an assumption of symmetry of the added inertia and damping matrices, i.e. $a_{42} = a_{24}$, etc. Clearly, the symmetry assumption is acceptable in the case of intact measurements but does not have to remain valid in the case of the flooded cylinder. This is one of the main reasons, for which it had been decided to derive estimates of added inertia and damping terms with use of the Lagrange's multipliers method. The method will be discussed from more formal perspective later, when the results will be analysed. At this point, it should suffice to state that applying the Lagrange's multiplier method to the present problem would result in finding such components of the vectors $\mathbf{B}$ and $\mathbf{E}$ which would minimise length of the vectors. The equations of motion are given as a constraint to the problem. Namely, taking for instance the coupled roll-

sway equation, the constraint is given as $A\mathbf{B}=\mathbf{C}$ and components of the vector $\mathbf{B}$ must minimise its magnitude[16]

$$|\mathbf{B}| = \mathbf{B}\cdot\mathbf{B} = \mathbf{B}^T\mathbf{B} = min \tag{5.11}$$

The corresponding Lagrangian function $\Lambda(\mathbf{b},\boldsymbol{\lambda})$ is given as

$$\Lambda(\mathbf{B},\boldsymbol{\lambda}) = \mathbf{B}^T\mathbf{B} + \boldsymbol{\lambda}^T(\mathbf{C} - A\mathbf{B}) \tag{5.12}$$

where $\boldsymbol{\lambda}$ is a vector of Lagrange multipliers.

The multipliers $\boldsymbol{\lambda}$ corresponding to the minimal[17] solution can be determined by finding the stationary value of the Lagrangian function, i.e. by solving the following equation

$$\frac{\partial}{\partial\mathbf{B}}\Lambda(\mathbf{B},\boldsymbol{\lambda}) = \frac{\partial}{\partial\mathbf{B}}\left(\mathbf{B}^T\mathbf{B} + \boldsymbol{\lambda}^T(\mathbf{C} - A\mathbf{B})\right) = \mathbf{0} \tag{5.13}$$

From this, it follows that

$$2\mathbf{B} - \boldsymbol{\lambda}^T A = 2\mathbf{B} - A^T\boldsymbol{\lambda} = 2A\mathbf{B} - AA^T\boldsymbol{\lambda} = 2\mathbf{C} - AA^T\boldsymbol{\lambda} = \mathbf{0} \tag{5.14}$$

Hence, assuming that the matrix AA^T is not singular, the required multipliers $\boldsymbol{\lambda}$ can be given as

$$\boldsymbol{\lambda} = 2\left(AA^T\right)^{-1}\mathbf{C} \tag{5.15}$$

However, it is also that $A^T\boldsymbol{\lambda} = 2\mathbf{B}$ and therefore after multiplying both sides of the above equation by A^T and dividing by 2 leads to the solution vector $\mathbf{B}$

$$\mathbf{B} = A^T\left(AA^T\right)^{-1}\mathbf{C} \tag{5.16}$$

where $A^T\left(AA^T\right)^{-1}$ is a pseudo-inverse of the matrix A.

---

[16] The procedure found here follows an (unnamed) article found on the website: http://people.csail.mit.edu/bkph/articles/Pseudo_Inverse.pdf

[17] Strictly speaking, the solution obtained with use of the Lagrange's multiplier method corresponds to an extremum, i.e. the vector may be of either minimum or maximum length. The exact nature of the solution could be determined by an additional tests (McQuarrie, 2003).

It needs to be emphasised that the components of the vectors **B** and **E** are *not* added inertia or damping terms. They are just *some* coefficients, which happen to satisfy the equations of motion. However, the estimates are likely to be closely related to their hydrodynamic counterparts and to emphasise that relationship they will be printed in square brackets, i.e. $[a]_{22}$ denotes the estimate of the sway added inertia a_{22}.

5.6 Dissipation of energy

It has been already shown that damping matrix contains information on dissipative forces. More specifically, the radiation force can be expressed by means of the Rayleigh dissipation function, which in turn can be constructed with use of the symmetrical part of the damping matrix. It has been stated in the foregoing that symmetry of the added inertia and damping matrices should not be assumed thus, for the purpose of the energy dissipation the damping matrix could be decomposed into symmetrical h_{jk} and anti-symmetrical $\bar{h}_{jk}$ (parts) matrices. As shown in (Skalmierski, 1994) the antisymmetric matrix $\bar{h}_{jk}$ is associated with the gyroscopic forces, which are not dissipative (their work vanish). Hence, the dissipative forces are associated only the symmetrical matrix h_{jk}. The matrix h_{jk} is given as

$$h_{jk} = \frac{1}{2}\left([b]_{jk} + [b]_{kj}\right) = \begin{bmatrix} [b]_{22} & \frac{1}{2}\left([b]_{23} + [b]_{32}\right) & \frac{1}{2}\left([b]_{24} + [b]_{42}\right) \\ \frac{1}{2}\left([b]_{23} + [b]_{32}\right) & [b]_{33} & \frac{1}{2}\left([b]_{34} + [b]_{43}\right) \\ \frac{1}{2}\left([b]_{24} + [b]_{42}\right) & \frac{1}{2}\left([b]_{34} + [b]_{43}\right) & [b]_{44} \end{bmatrix} \tag{5.17}$$

The rate of work done by the dissipative force can be expressed (in terms of generalised velocities) as $\frac{d\bar{w}}{dt} = -h_{jk}\dot{q}^j\dot{q}^k$ and thus the work over one period of oscillation T_0 is given as

$$W_0 = -h_{jk}\int_{\tau}^{\tau+T_0} \dot{q}^j\dot{q}^k dt \tag{5.18}$$

In the case discussed here the generalised velocities are harmonic functions of the form $\dot{q}^j = q_a^j\omega\cos\left(\omega t + \varepsilon_j\right)$ where q_a^j is amplitude of the *j*-th mode of motion and ε_j is the corresponding phase angle, the above equation can be rewritten in the following form

$$W_0 = -h_{jk}\int_{\tau}^{\tau+T_0} \dot{q}^j \dot{q}^k dt = \sum_{j,k=2}^{4}\left[-\omega^2 h_{jk} q_a^j q_a^k \int_{\tau}^{\tau+T_0} \cos\left(\omega t+\varepsilon_j\right)\cos\left(\omega t+\varepsilon_k\right) dt\right] \tag{5.19}$$

where no summation over a takes place.

Based on the trigonometric identities the above integral can be rewritten as

$$\int_{\tau}^{\tau+T_0} \cos\left(\omega t+\varepsilon_j\right)\cos\left(\omega t+\varepsilon_k\right) dt = \frac{1}{2}\int_{\tau}^{\tau+T_0} \cos\left(2\omega t+\varepsilon_j+\varepsilon_k\right) dt + \frac{1}{2}\int_{\tau}^{\tau+T_0} \cos\left(\varepsilon_j-\varepsilon_k\right) dt = \\ = \frac{1}{2} T_0 \cos\left(\varepsilon_j-\varepsilon_k\right) \tag{5.20}$$

Hence, the amount of work dissipated over one period of oscillations can be simply expressed as

$$W_0 = -\frac{T_0}{2}\omega^2 \sum_{j,k=2}^{4}\left[h_{jk} q_a^j q_a^k \cos\left(\varepsilon_j-\varepsilon_k\right)\right] = -\pi\omega \sum_{j,k=2}^{4}\left[h_{jk} q_a^j q_a^k \cos\left(\varepsilon_j-\varepsilon_k\right)\right] \tag{5.21}$$

Making use of the symmetry of the h_{jk} matrix, the sum can be expanded as follows

$$W_0 = -\pi\omega\left[h_{22}\left(q_a^2\right)^2 + h_{33}\left(q_a^3\right)^2 + h_{44}\left(q_a^4\right)^2\right] + \\ -\pi\omega\left[2h_{23} q_a^2 q_a^3 \cos\left(\varepsilon_2-\varepsilon_3\right) + 2h_{24} q_a^2 q_a^4 \cos\left(\varepsilon_2-\varepsilon_4\right) + 2h_{34} q_a^3 q_a^4 \cos\left(\varepsilon_3-\varepsilon_4\right)\right] \tag{5.22}$$

Interestingly, as the rate of change of work is a scalar quantity (zero-order tensor) of the form given by $\frac{d\bar{w}}{dt} = -h_{jk}\dot{q}^j\dot{q}^k$ this implies[18] that h_{jk} must be a second-order tensor in the case of the system of 3DoF (sway-heave-roll), as investigated herein.

5.7 Non-dimensional forms of added mass and damping

In the ensuing, the estimates (as well as theoretically or numerically derived components) of added inertia and damping matrices will be given in the form of non-dimensional hydrodynamic coefficients, plotted against the non-dimensional circular frequency ω_B. These coefficients, are obtained by multiplying appropriate terms by the normalising factors as shown below

[18] By means of the quotient rule (Borisenko and Tarapow, 1976)

$$\omega_B = \omega\sqrt{\frac{B}{2g}}$$

$$\widehat{a_{22}} = \frac{a_{22}}{m} \qquad \widehat{b_{22}} = \frac{b_{22}}{m}\sqrt{\frac{B}{2g}}$$

$$\widehat{a_{24}} = \frac{a_{24}}{mB} \qquad \widehat{a_{42}} = \frac{a_{42}}{mB} \qquad \widehat{b_{24}} = \frac{b_{24}}{mB}\sqrt{\frac{B}{2g}} \qquad \widehat{b_{42}} = \frac{b_{42}}{mB}\sqrt{\frac{B}{2g}}$$

$$\widehat{a_{44}} = \frac{a_{44}}{mB^2} \qquad \widehat{b_{44}} = \frac{b_{44}}{mB^2}\sqrt{\frac{B}{2g}}$$

5.8 Intact ship measurements

The measurements in the intact condition were performed mainly in order to provide data for validation against the theoretical prediction and other experimental data. It is clear that the quantitative judgment is difficult in both cases, as neither the prediction nor the available experimental data maintain one-to-one correspondence with the present measurements. Both – the theory and the previous experiments - deal with oscillations about the fixed axis. In the case of floating body, the axis of rotation is instantaneous and even its "average" elevation varies with the frequency. Furthermore, as indicated already, the estimates of added inertia and damping are merely related to their analytical counterparts by the fact that they are components of the hydrodynamic reaction. Mainly for these reasons, the theoretical prediction is given here simply as a guidance, in order to verify whether the data collected follow expected trends.

5.8.1 Summary

The measurements were performed at about[19] 2 and 5 degrees roll amplitudes. However, due to very small magnitude of the hydrodynamic force, the results for 2 degrees roll should not be considered reliable, particularly at the low-frequency part of

[19] The inaccuracy in roll amplitude may be significant at some points. However, the results indicate that estimates of added inertia and damping are relatively insensitive to the errors in the attained roll amplitude (see section 5.10 for details). For this reason, it was decided to carry out measurements in a wide range of frequencies on the expense of an absolute accuracy.

the spectrum. Indeed, some 10% of the measurements had to be disregarded due to observed irregularities in motion caused by the imprecise setting of the forcing apparatus.

The roll RAO and phase lag characteristics[20] indicate clearly that the system is lightly damped – the near resonance amplitude is very high and the phase lag transition very rapid. Outside the 0.75-1.25 frequency band the roll damping is very low.

The elevation $\overline{OA}$ of the axis of rotation above the waterplane suggests that the vertical position of the centre of gravity of the model has been slightly underestimated. The less likely but still possible explanation for rotations about the axis lying above the estimated *KG* is that at the low frequencies the body might have undergone some sidewise translations resulting in higher than expected amplitudes of sway.

Roll and sway motions are generally out of phase, practically over the entire range of frequencies. In fact, the phase lag of sway becomes quite significant at frequencies where the largest damping occurs.

The vertical motions induced by roll were, where present at all, so small, that it virtually prohibited any realistic estimates of heave coefficients. Therefore, at the further stages, the heave motion has been disregarded and the entire attention focused on the coupled roll-sway motion. There, the main question was whether the added inertia and damping matrices should be considered symmetrical. In order to compare the estimates it has been assumed at first that the symmetry assumption holds, and the results were obtained for that case with slightly modified equations (5.8). Then the analysis was performed without assuming symmetry of the matrices. As anticipated, the results produced by either of method are different.

Firstly, both methods failed to give realistic estimates of sway coefficients $[\hat{.}]_{22}$. The estimates are not random (they follow clear trends) but are about two orders of magnitude smaller than predicted by the theory. The coupling term $[\hat{b}]_{24}$ is practically unaffected by the choice of the method. Remaining quantities, i.e. roll added inertia and

[20] Graphs illustrating the results can be found at the end of the section.

damping as well as coupling added inertia coefficient of roll into sway, are strongly influenced by the assumed symmetry of the matrices. In the case when the assumption is dropped, not only sway coefficients but also the coupling terms of sway into roll virtually vanish. This results in the slightly higher roll damping and in the significantly lower added inertia. The coupling added inertia, $[\widehat{a}]_{24}$, has similar distribution but much lower magnitude than in the case of the "unconstrained" equations.

Although results of the exercise do not provide any definitive answer as to which method is "better" they do offer some "hints". The first indication is that the sway added mass and damping vanish by both methods. Furthermore, if the symmetry of the matrices is not imposed the coupling terms of sway into roll vanish as well. In this case only the roll and roll-into-sway quantities remain, all in phase with roll velocity and displacement (acceleration). It is an important observation, because unlike in the case of the fixed-axis oscillations, here sway and roll are generally, out of phase and yet, the contribution of hydrodynamic forces associated with sway and sway into roll is negligible.

Those "hints" lead to the conclusion that there is no evidence supporting the assumption of the symmetrical matrices. This is so, not because those matrices are not symmetrical but because such information is not present in the measured moment. This is a direct consequence of yet another "hint", already formulated in the previous section. Namely, it has been stated there that there is an assumed functional relationship between roll and sway, in the form of the identity $y_A(t) = y(t) - \overline{OA}\varphi(t)$. However, if the phase difference between roll and sway is small the relation reduces to $y(t) = \overline{OA}\varphi(t)$ and this implies that sway is completely determined by roll. More formally, the last identity is a geometrical constraint. The functional relation between coordinates is finite (holonomic) and as such reduces number of degrees of freedom of the system. Initially, the analysed system had three degrees of freedom – sway, heave and roll. Heave motion was disregarded as the observed heave amplitude was practically zero and thus, only two degrees of freedom remain – sway and roll. However, the number of degrees of freedom has been further reduced by introducing the

constraint $y(t) = \overline{OA}\varphi(t)$. Hence, the analysed system is a single degree of freedom oscillator.

5.8.2 Applicability of the multipliers method

The conclusion on number of degrees of freedom brings the discussion back to the method chosen for deriving the estimates of added inertia and damping. In analytical mechanics the Lagrange's multiplayer method is usually employed for handling systems with constraints (Lanczos, 1986). Formally, the equilibrium conditions combined with kinematical constraints form an over-determined system of equations. In a simple case of holonomic constraints, i.e. given by the finite relationships between coordinates, the constraints can be used to eliminate some variables but the arbitrary process of reduction may violate symmetry of the variables. The multipliers method works even if the constraints are non-holonomic, so the variables cannot be eliminated arbitrarily but far more important is their physical interpretation – they give a force of reaction necessary to maintain the constraint.

In the problem of determining added inertia and damping components, the constraints are given in the form of equilibrium equations. The system *is* in dynamic equilibrium and the multipliers method is employed to derive the force of reaction necessary to maintain the equilibrium at any given time. There is however one important question, namely whether the assumed kinematical condition given as $y_A(t) = y(t) - \overline{OA}\varphi(t)$ could be maintained in the equilibrium or not? If the constraint is not violated, the number of degrees of freedom should be reduced. Indeed, in the case discussed here the multipliers method resulted in vanishing of the components associated with sway. Only quantities associated with roll remain and hence it was stated that the system is a single degree of freedom oscillator, as reasoned earlier. The fact of upmost importance is that the results were obtained without imposing any partiality – roll was not underscored as a main or preferred mode of motion. Based on this it has been concluded that the Lagrange's multipliers method is an appropriate technique for estimating added inertia and damping in the case studied here. Furthermore, fact that the system has single degree of freedom implies that the measured

moment does not contain information on the hydrodynamic quantities associated with sway.

5.8.3 Experimental estimates vs. prediction

The added mass and potential damping components have been calculated with use of in-house developed sea-keeping code *Proteus 3* (details on the development can be found in (Jasionowski, 2001b)).

The prediction of hydrodynamic quantities produced by the software is based on the strip theory discussed already in the section 3.3. The 2D pressure field induced by harmonic oscillations of a body is calculated on a basis of linearised momentum equation with the velocity potentials derived from the boundary element method (BEM). The viscous effects can be accounted for by means of the Ikeda method but they were not included in the prediction.

The added mass and the potential damping in roll are derived for oscillations about the axis passing through the centre of gravity. Hence, system's configuration in theory and during the experiments was very similar, at least in the low-frequency part of the spectrum. Yet, the experimental estimates depart significantly from the predicted components of the hydrodynamic reaction. Although all hydrodynamic coefficients preserve (to some extent) trends of the theoretical distribution, quantitatively the results are completely different. Specifically, the roll damping $[b]_{44}$ is much larger and the added inertia $[a]_{24}$ much smaller than predicted. Noticeably, the discrepancies are large irrespective of whether the assumed symmetry of the added inertia and damping matrices was investigated.

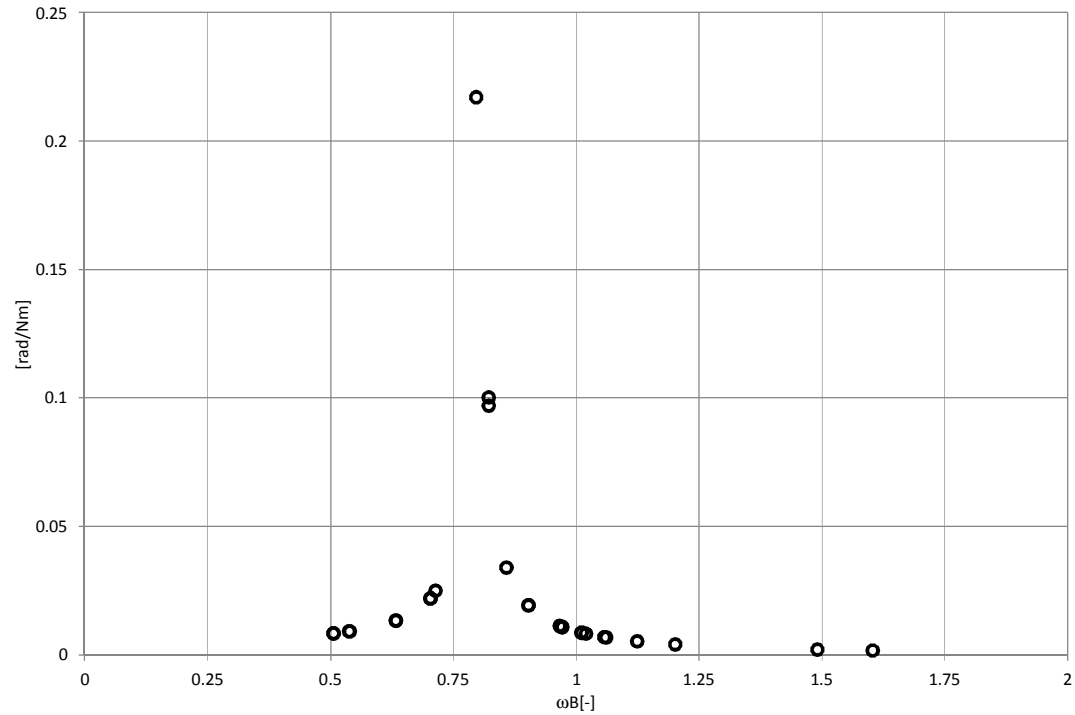

*Fig.**5.8**: Roll RAO. Intact condition, amplitude 5 degrees*

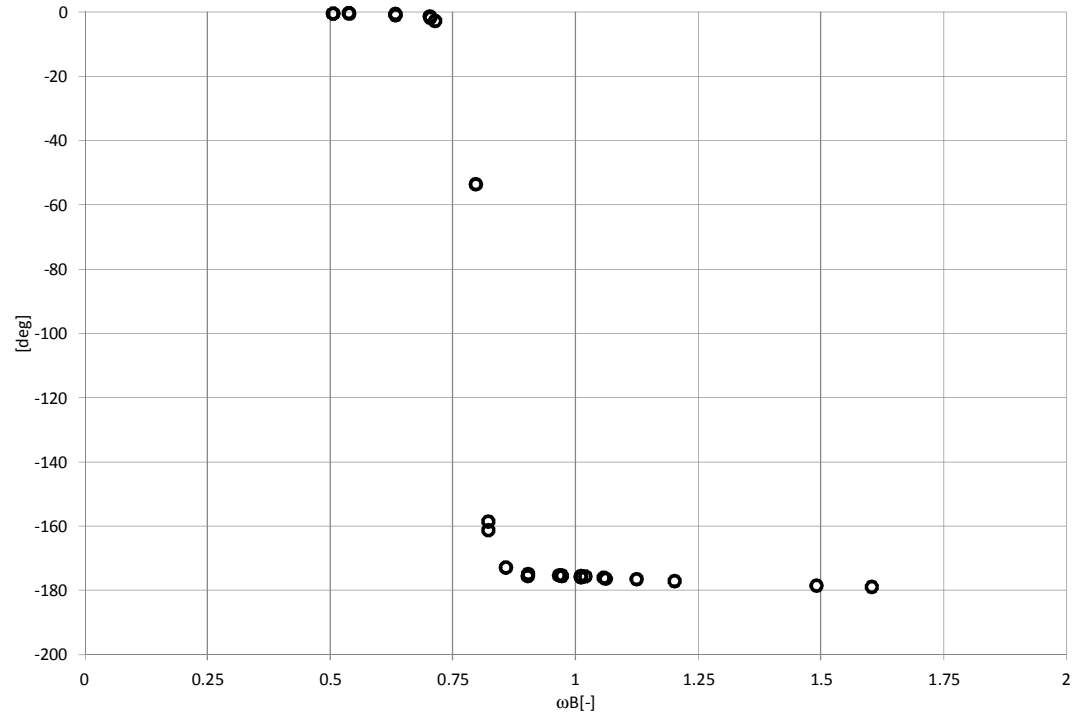

*Fig.**5.9**: Roll phase lag, amplitude 5 degrees*

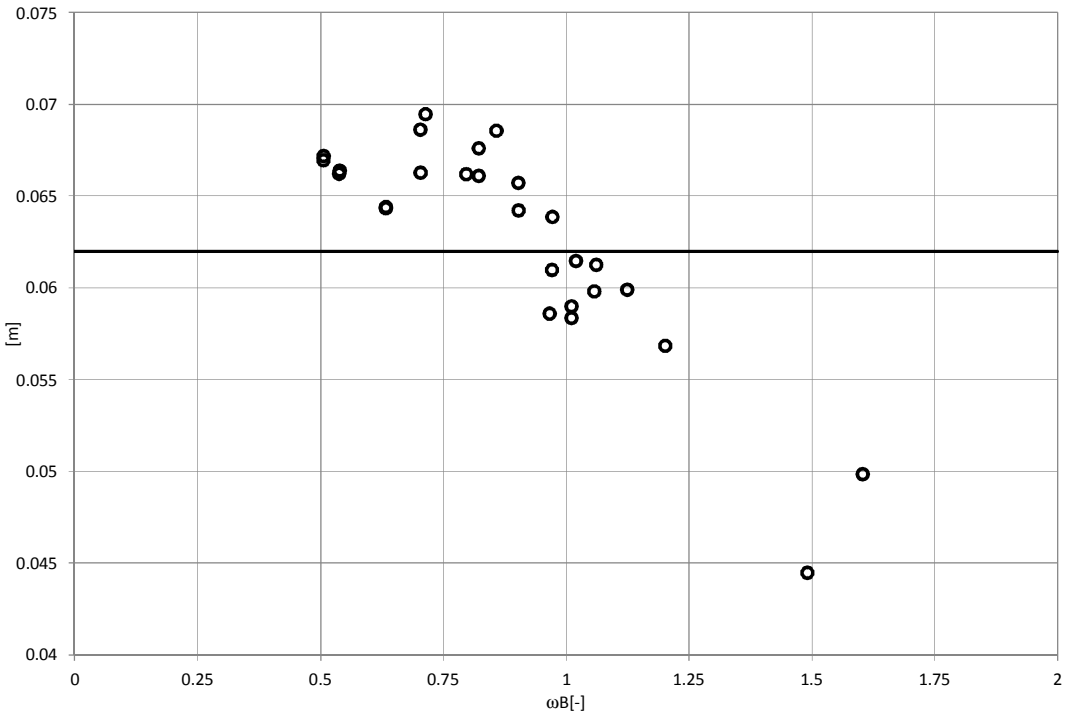

*Fig.**5.10**: Elevation of the axis of rotation above waterplane (solid line represents elevation of the centre of gravity in the upright position); amplitude 5 degrees.*

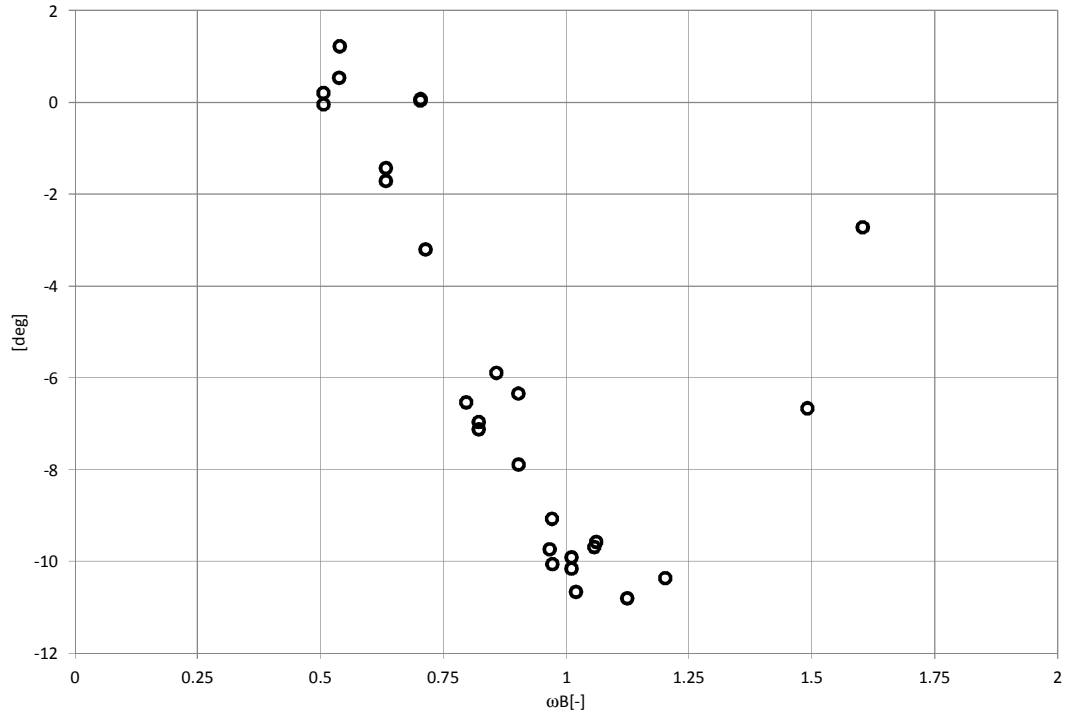

*Fig.**5.11**: Phase difference between sway and roll, amplitude 5 degrees*

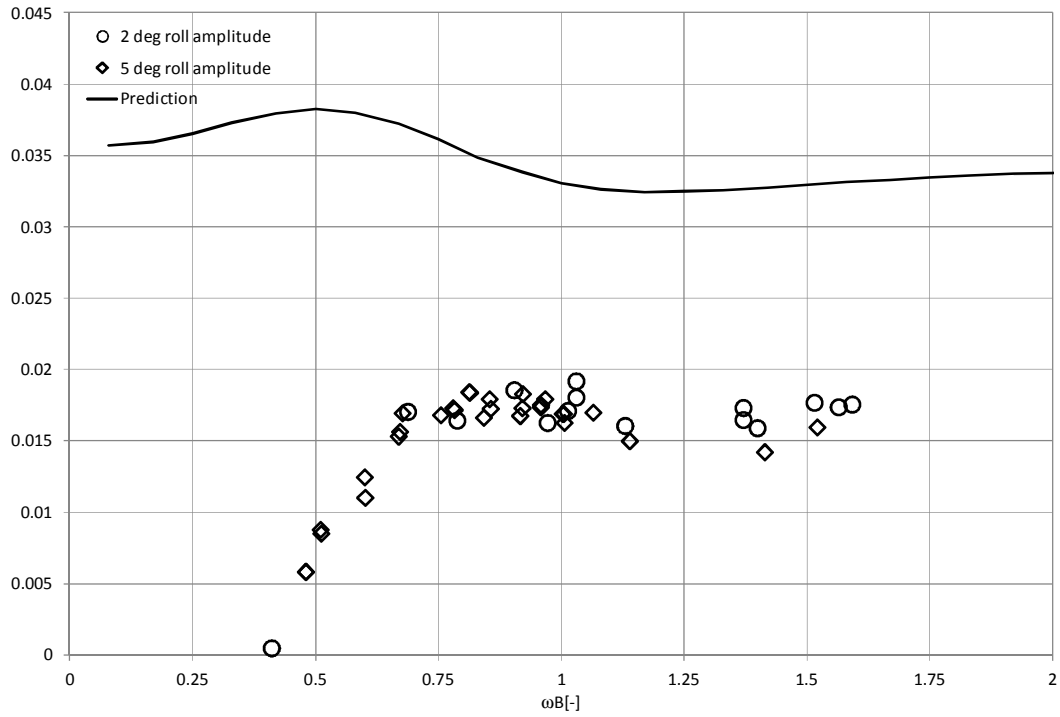

*Fig.**5.12**: Roll added inertia coefficient* $[a_{44}]$

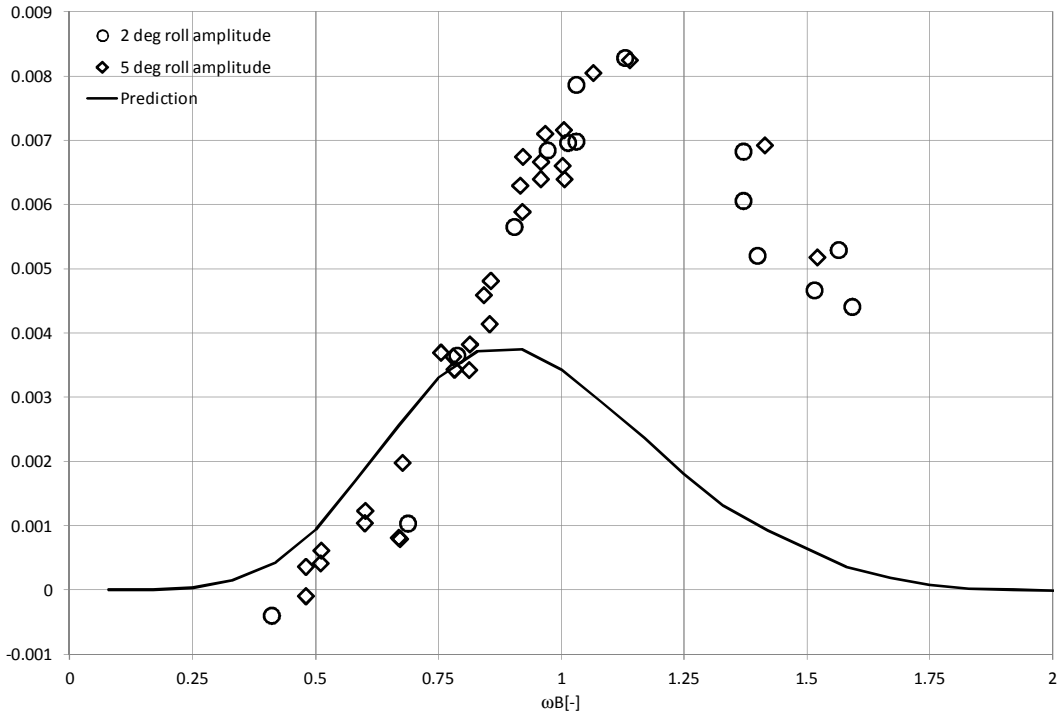

*Fig.**5.13**: Roll damping coefficient* $[b_{44}]$

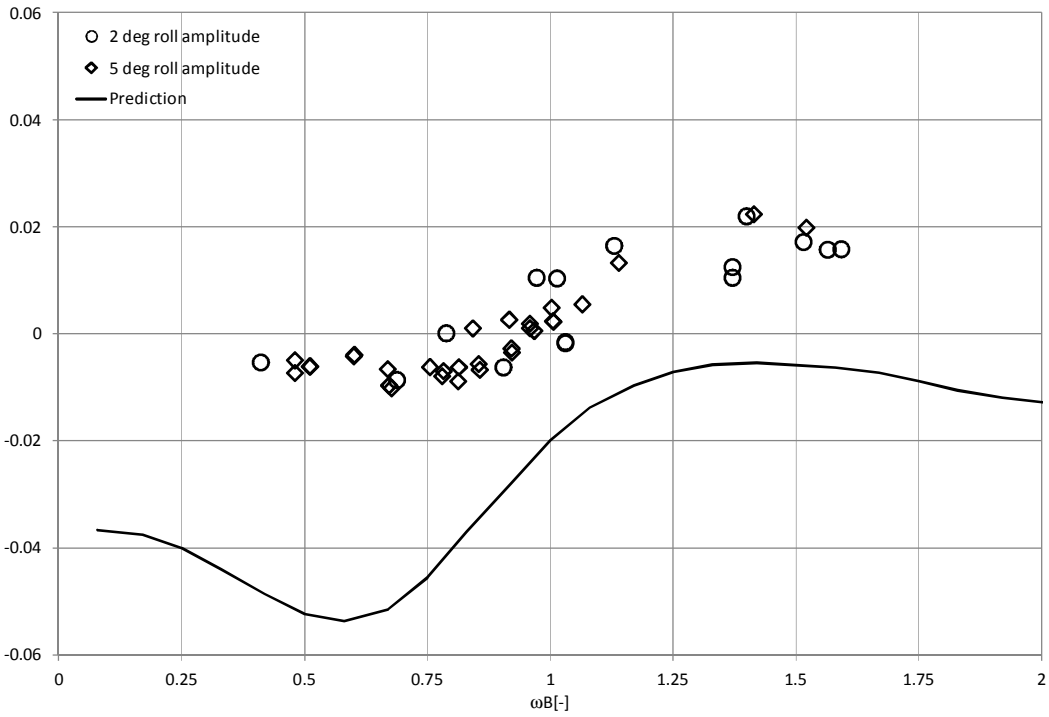

*Fig.**5.14**: Roll into sway coupling coefficient* $[a_{24}]$

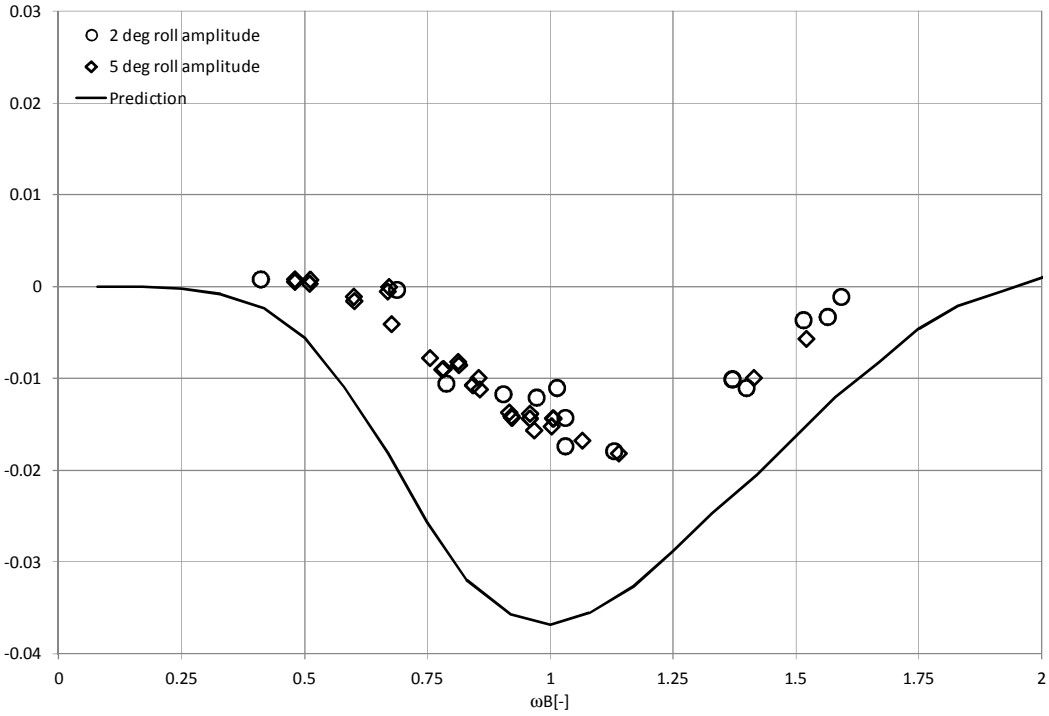

*Fig.**5.15**: Roll into sway coupling coefficient* $[b_{24}]$

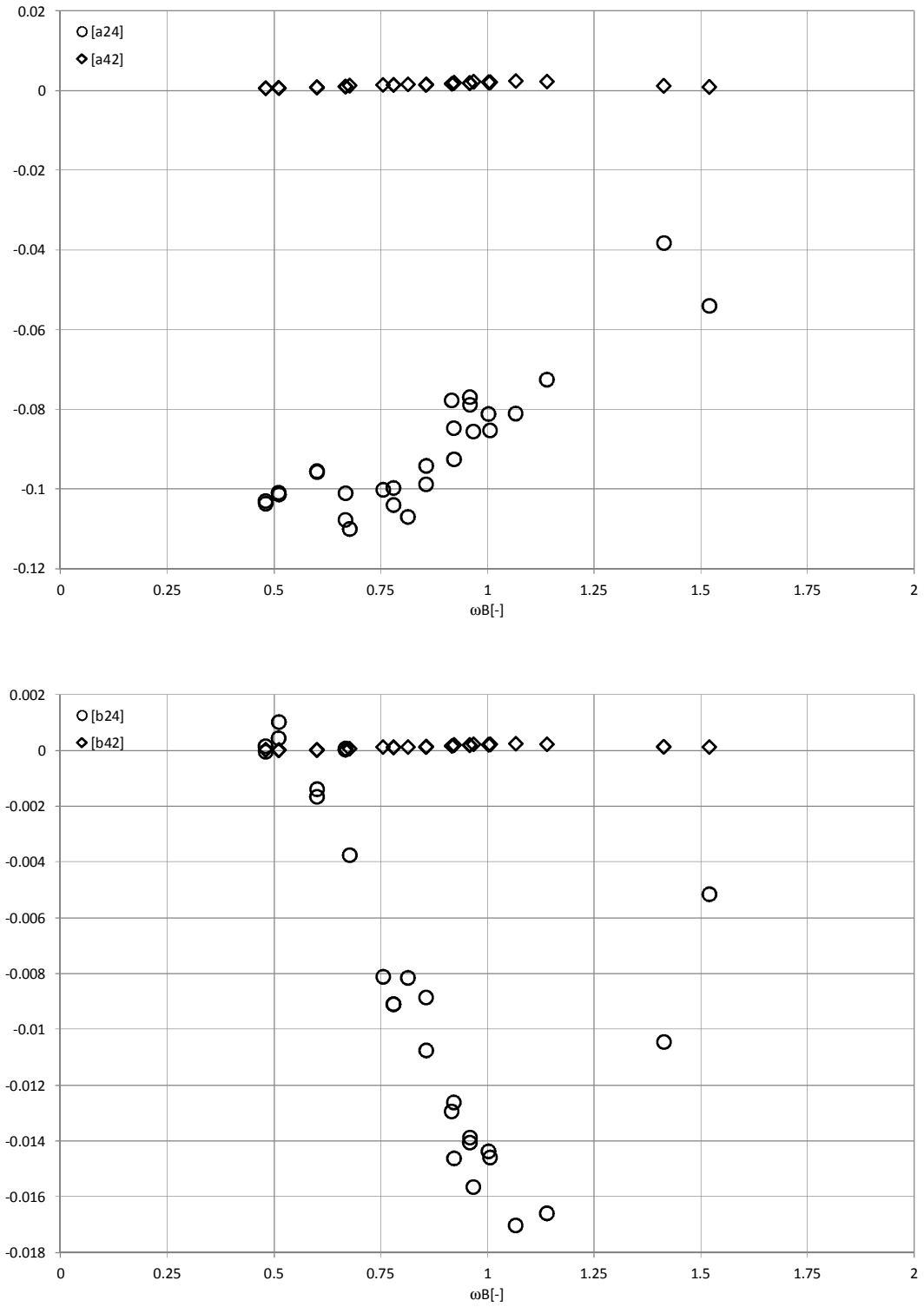

*Fig.**5.16**: The* $[.]_{24}$ *and* $[.]_{42}$ *coefficients as derived while allowing asymmetry of the added inertia and the damping matrices. Similar results were obtained for the (virtually) vanishing* $[.]_{22}$ *coefficients, i.e. the coefficients were much smaller but preserved theoretical distributions (although might be of opposite sign as in the case of the* $[b_{24}]$ *above.*

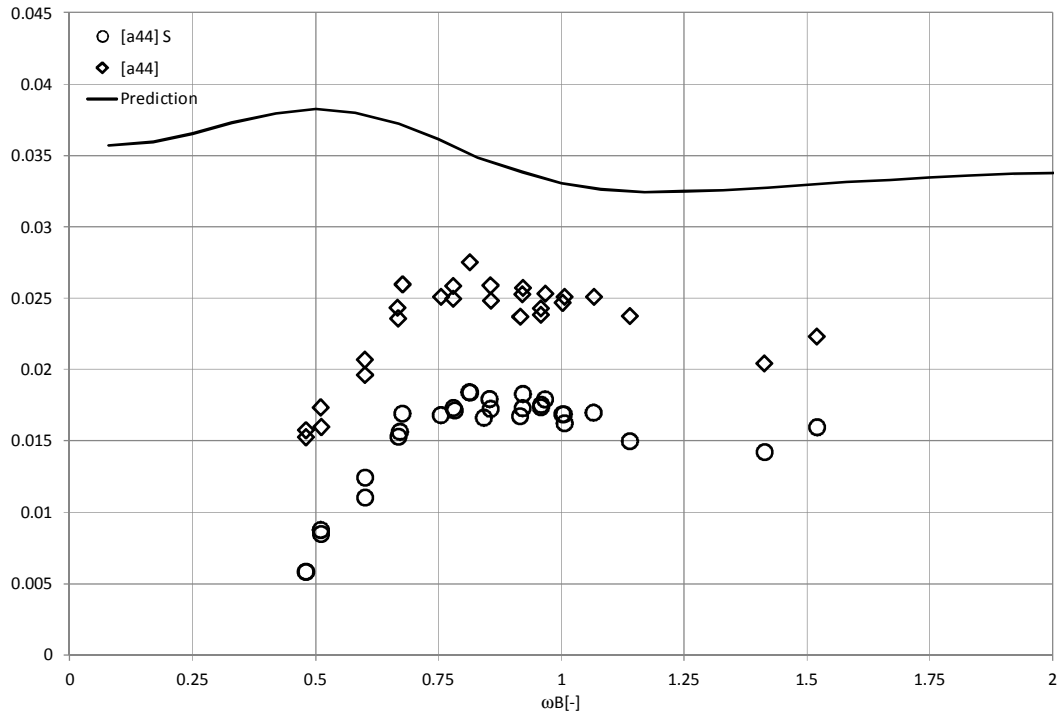

*Fig.**5.17**: The $[a_{44}]$ coefficients obtained with, (S), and without assumption on the symmetry of added inertia and damping matrices.*

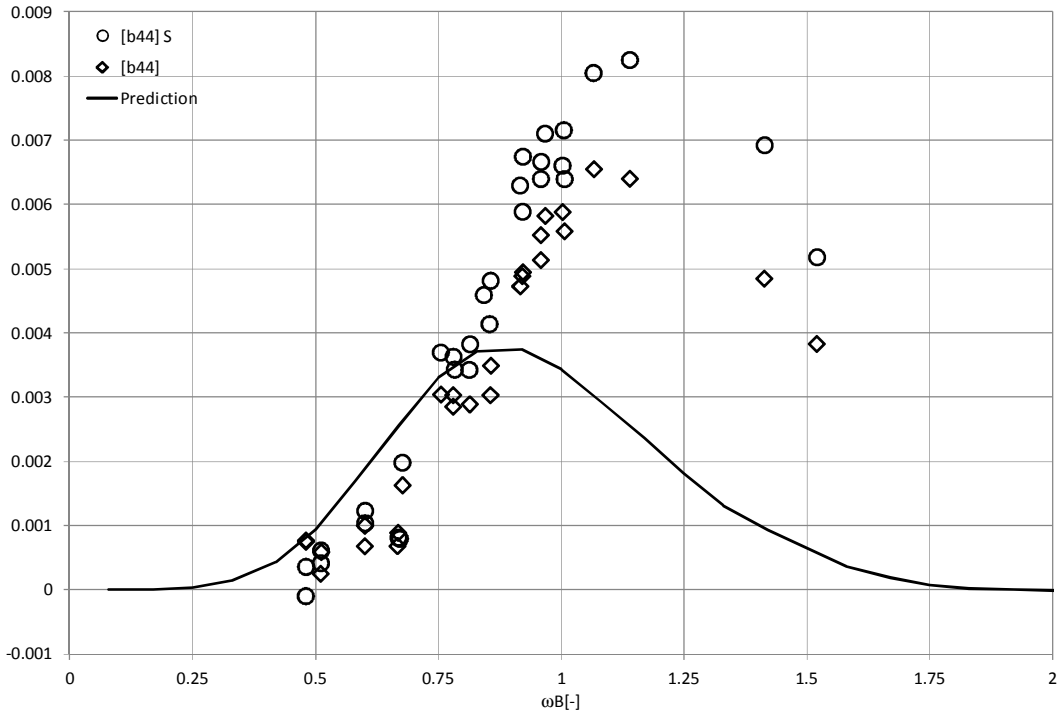

*Fig.**5.18**: Roll damping coefficient $[b_{44}]$ calculated with and without symmetry assumption.*

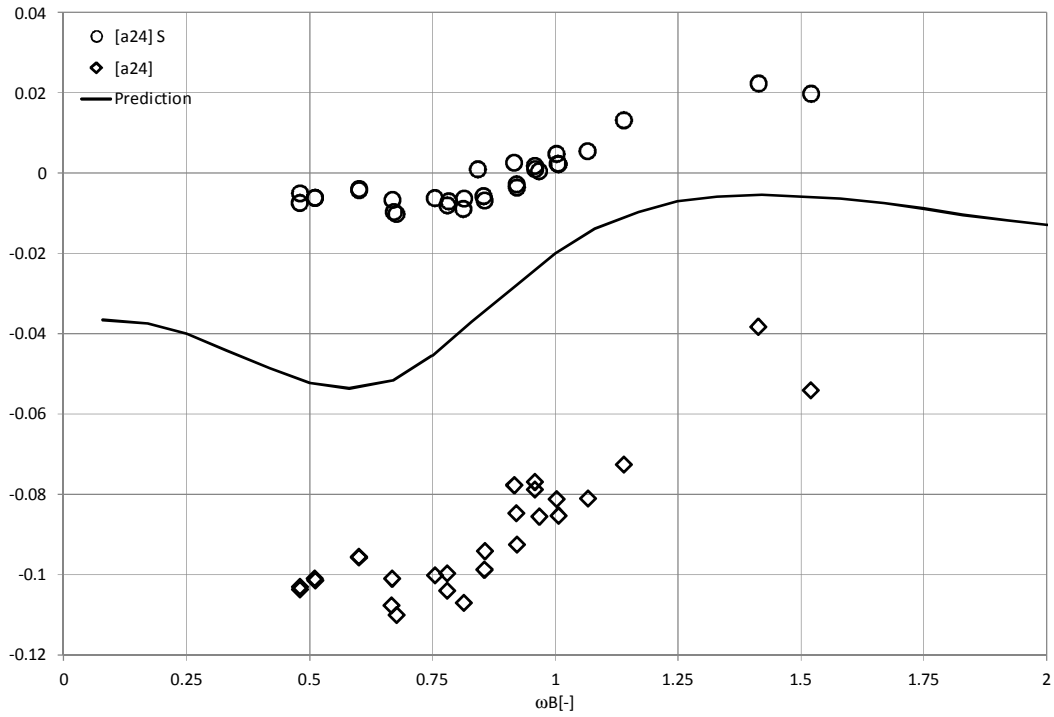

*Fig.**5.19**: Coupling coefficient* $[a_{24}]$ *calculated with and without symmetry assumption.*

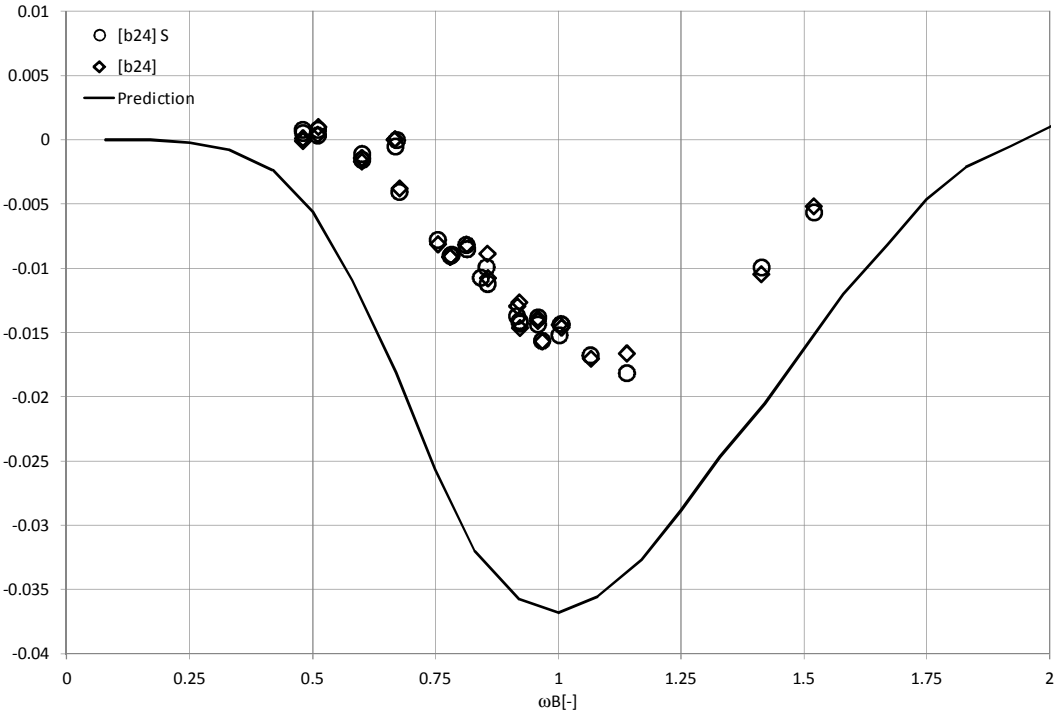

*Fig.**5.20**: Coupling coefficient* $[b_{24}]$ *calculated with and without symmetry assumption.*

5.9 Damaged ship measurements

The estimates of added inertia and damping in the flooded conditions have been derived with use of the same technique as in the case of the intact hull. The only difference derives from the fact that the mathematical model accounts for the drift resulting from the asymmetric pressure distribution due to sloshing.

5.9.1 Summary

The amplitude-phase characteristics show clearly that although the effective mass of the system (i.e. the resultant mass of the hull and the floodwater) did not change the hull natural frequency shifted from about $\omega_B \approx 0.5$ to $\omega_B \approx 0.5$. However, the maximum measured RAO (at the hull natural frequency) indicates similar (to the case of intact hull) amount of critical damping.

Impact of the floodwater and sloshing is more pronounced in the phase characteristics. Firstly, a large decrease (in absolute terms) of the phase lag can be observed in the frequency range of $\omega_B = (1;1.25)$. Furthermore, at the frequencies exceeding $\omega_B = 1.6$ there is a phase jump in the characteristics. In the graph, the phase angle is wrapped to the $\langle -180;180 \rangle$ degrees but in fact, the response phase angle at these frequencies simply exceeds -180 degrees. Generally, at frequencies over $\omega_B > 0.75$ the response is dominated by the floodwater dynamics.

The phase difference between sway and roll in the range of frequencies dominated by the hull dynamics $(\omega_B < 0.75)$, has similar characteristics to that of the dry hull. At higher frequencies, where the sloshing starts to play a dominant role the difference undergoes rapid changes from the significant lag to the noticeable phase advance. The observed difference is much higher there than observed for the intact hull and this indicates relatively high damping in the coupled mode.

Basic characteristics of the system in with flooded compartment indicate clearly that its hydrodynamic properties must be completely different to those associated with the intact hull, particularly at the frequencies where motions of the body are significantly

affected by sloshing and the intensive flow through the opening occurs. Inside the flooded compartment, fluid pressure acts on both sides of the shell and this, combined with the presence of the opening, must results in a very complex flow. Waves are not only radiated from the body but also diffracted while passing the opening. This makes the direct comparison of intact and damaged measurements difficult even in qualitative terms.

At low frequencies, where impact of slosh dynamics is much smaller, the response can be affected by the asymmetry in the restoring moment caused by the presence of the opening. The asymmetry undermines adequacy of the single harmonic model of the response. This is particularly important at small-amplitude motions where the error in the fitting model may result in the relatively large uncertainties.

5.9.2 Estimates of added inertia and damping

Although the estimates of the sway added mass and damping (in particular) are generally smaller than the intact ship prediction, the results indicate that in the flooded case sway plays more important role than during the oscillations of the intact hull. Specifically, there is a visible dip on the added mass characteristics at the sloshing resonance. On the other hand, this region corresponds to the observed maximum drift velocity and it could be that the sway added mass "contribution" might be due to the drift forces, which are not accounted for in the mathematical model. In any case, simplicity of the model is a certain drawback. Although the overall performance of the model is satisfactory, it is incapable of accounting for more complex phenomena occurring at the range of significant sloshing or at very high frequencies. Thus, since the drift forces[21] are not accounted for in the equations of motions it can only be assumed that any sway or sway-into-roll contribution is not genuine but comes from the fact that the equations of motion are incomplete.

Similar comments apply to the coupling terms $[a]_{42}$ and $[b]_{42}$ where damping is virtually unaffected by sloshing but impact of sloshing is clearly visible on the added

[21] A comprehensive briefing to the mathematical modelling of drift forces can be found in (Journee and Massie, 2001)

mass characteristics. Here again it is assumed that the effect is caused by the incompleteness of the mathematical model.

The roll-into-sway $[.]_{24}$ characteristics comprise of three distinct regions. At low frequencies, below $\omega_B = 0.5$ added inertia and damping are determined by motions of the body. In the higher, relatively broad range of frequencies, the quantities are affected by sloshing and undergo dramatic changes. Added inertia and damping both vanish at about $\omega_B = 1.35$. In the range of the highest frequencies (beyond the $\omega_B = 1.35$) damping becomes positive and the magnitude of added inertia begins to increase.

The roll added inertia, $[a]_{44}$ is much higher than in the case of the intact hull. It undergoes changes similar to the coupling term $[a]_{24}$.

In the roll damping characteristic there are also three regions worth attention. At the lowest frequency range ($\omega_B < 0.5$) the damping magnitude is similar to that of the intact ship. Above the $\omega_B = 0.5$ the roll damping decreases gradually but rises again at frequencies $\omega_B > 0.6$. At the frequencies below the $\omega_B = 0.6$, damping is comparable to that of the intact hull. At higher frequencies, dominated by the sloshing phenomena up to almost $\omega_B = 1.5$ the damping is very large. At its peak, it is almost tenfold higher than maximum damping corresponding to the dry hull. At $\omega_B > 1.5$ the roll damping becomes negative. The phase lag characteristics shows clearly that in that range of frequencies there is a phase jump in the response – the roll lag exceeds -180 degrees. This may indicate instability of the system and such possibility cannot be disregarded as the recorded time series were not tested against any stability criteria. However, the phase jump can occur due to changes in the vortex shedding formations. Such phenomena has been reported by some authors, particularly those investigating the vortex-induced vibrations of the offshore structures, see for example (Bearman and Currie, 1979) or (Ongoren and Rockwell, 1988).

At the high frequency range ($\omega_B > 1.6$), work of the dissipative forces becomes positive and this fact is a serious indication that the dissipation model based on the

Rayleigh dissipation function is not sufficient to describe the phenomena observed at the high-frequency oscillations.

The results obtained for the flooded model show much stronger dependency of the hydrodynamic quantities on the roll amplitude.

The coupling added inertia term, $[a]_{24}$, is most sensitive to changes in the roll amplitude at the frequencies below sloshing resonance and the dependency on the motion amplitude diminishes gradually at higher frequencies.

In the case of the coupling term in damping, there is an indication of small nonlinearities in the sloshing region but more pronounced deviations could be observed in the very high frequency range, where presumed change in the vortex shedding formation takes place.

Roll added inertia is affected by the change in the motion amplitude over the entire frequency range except the relatively narrow band around the sloshing resonance. The roll damping coefficient, $[b]_{44}$, is most notably influenced by the magnitude of motion in the region between the hull natural frequency and sloshing resonance. In the remaining part of the spectrum, impact of the amplitude on roll damping is rather insignificant.

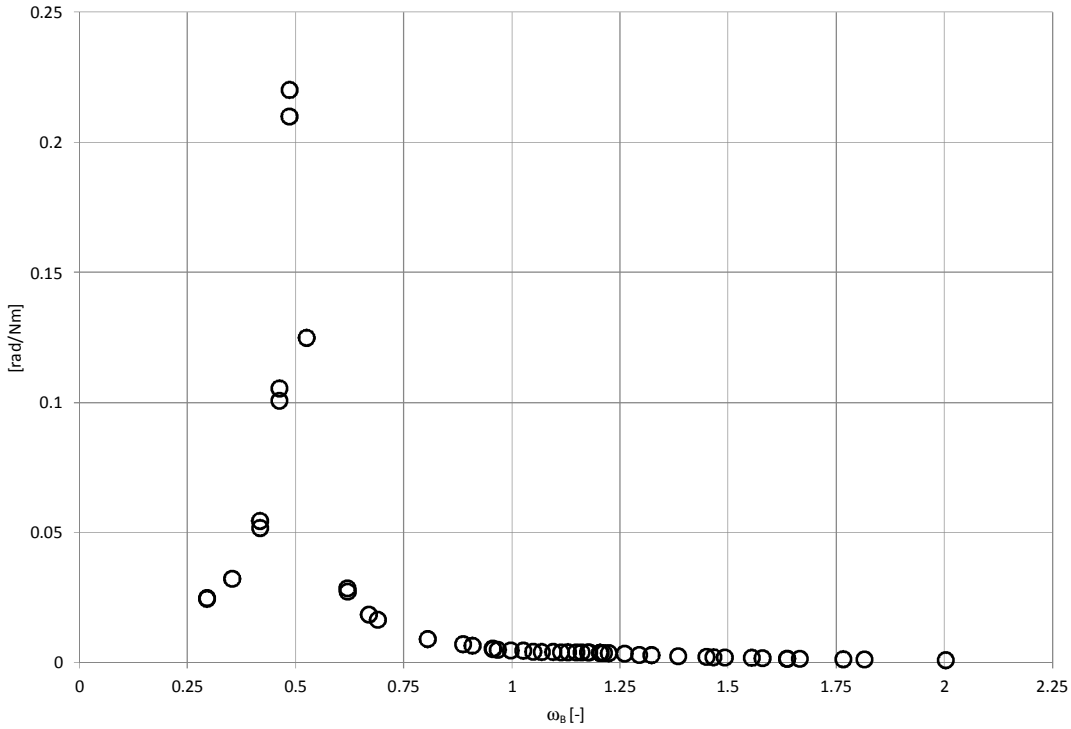

*Fig.**5.21**: Roll RAO- damaged condition, amplitude 5 degrees*

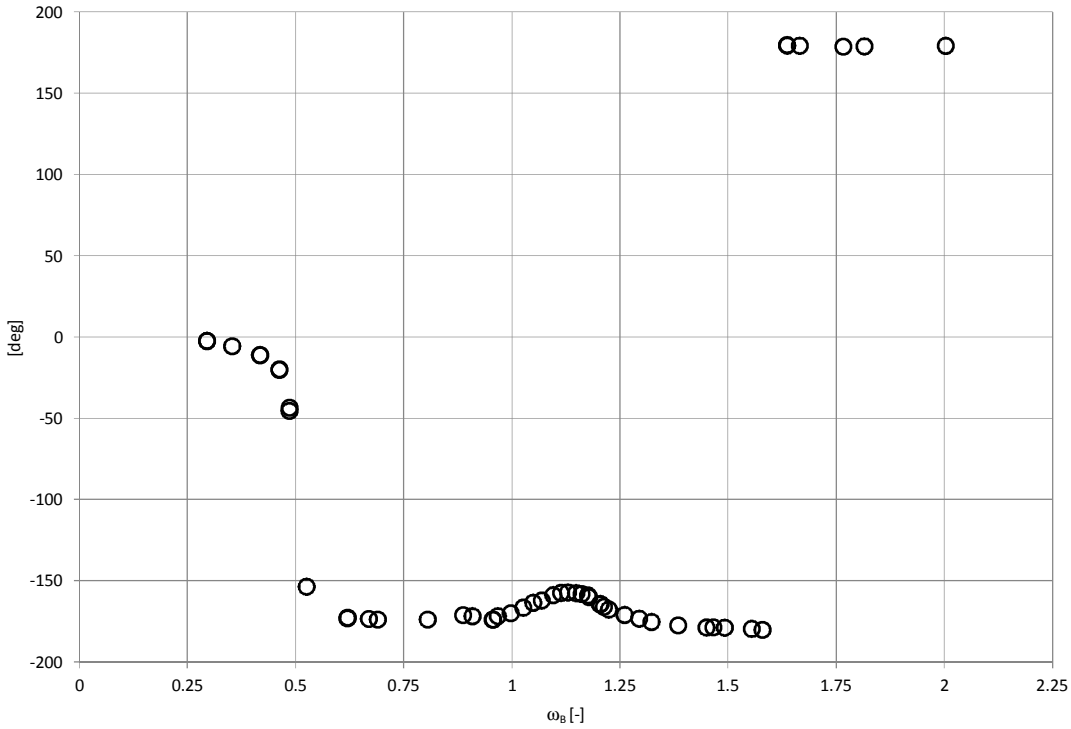

*Fig.**5.22**: Roll phase lag, damaged condition, amplitude 5 degrees*

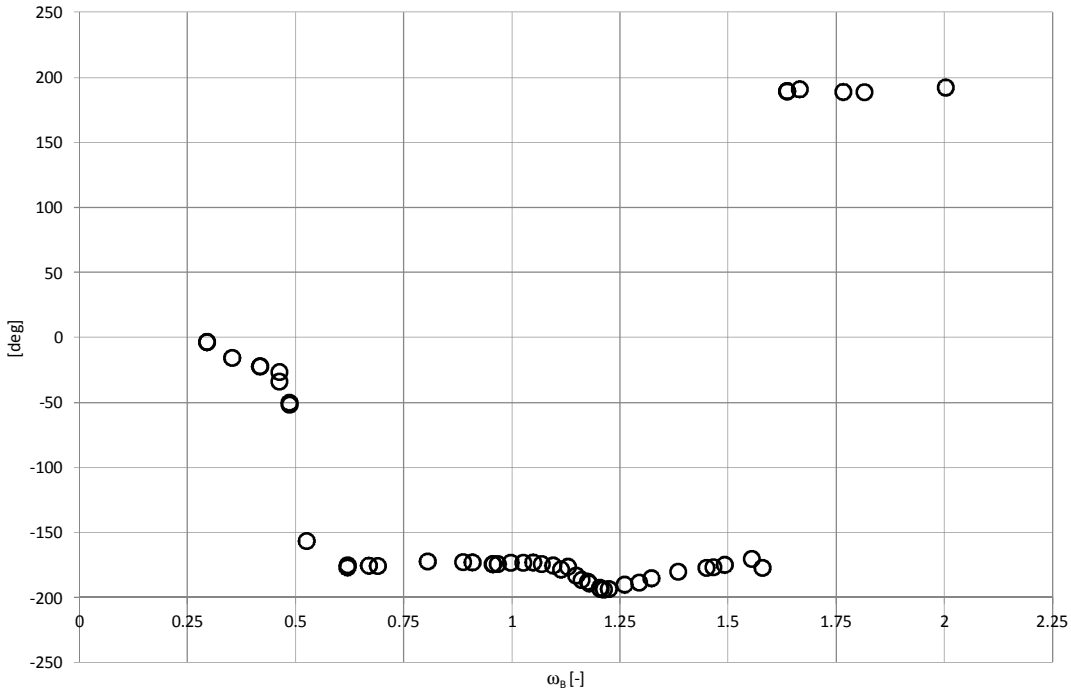

*Fig.**5.23**: Sway phase with respect to the excitation, damaged condition, amplitude 5 degrees*

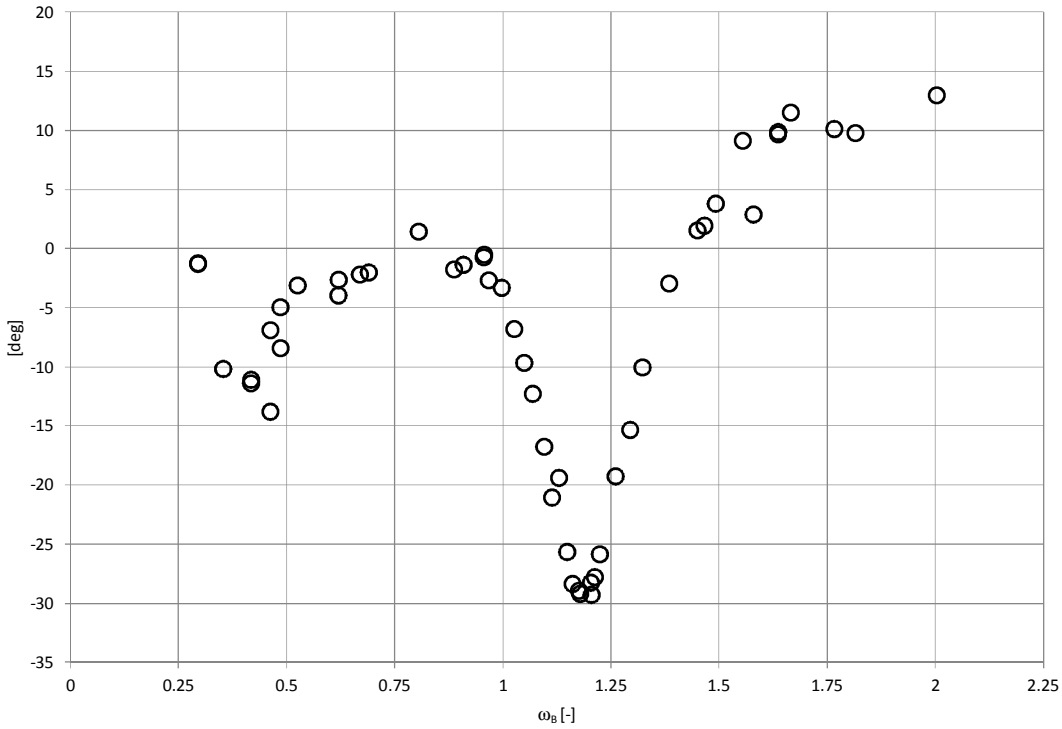

*Fig.**5.24**: Phase difference between sway and roll, damaged condition, amplitude 5 degrees*

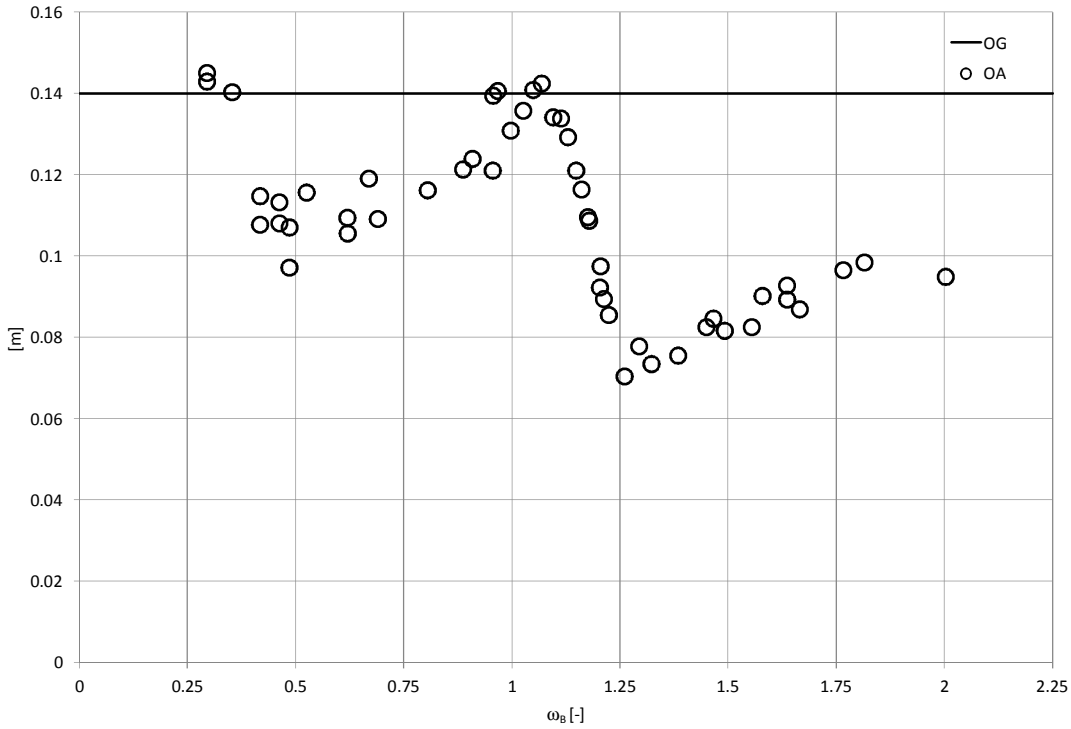

*Fig.**5.25**: Elevation of axis of rotation above waterplane (solid line represents elevation of centre of gravity in upright position), damaged condition, amplitude 5 degrees*

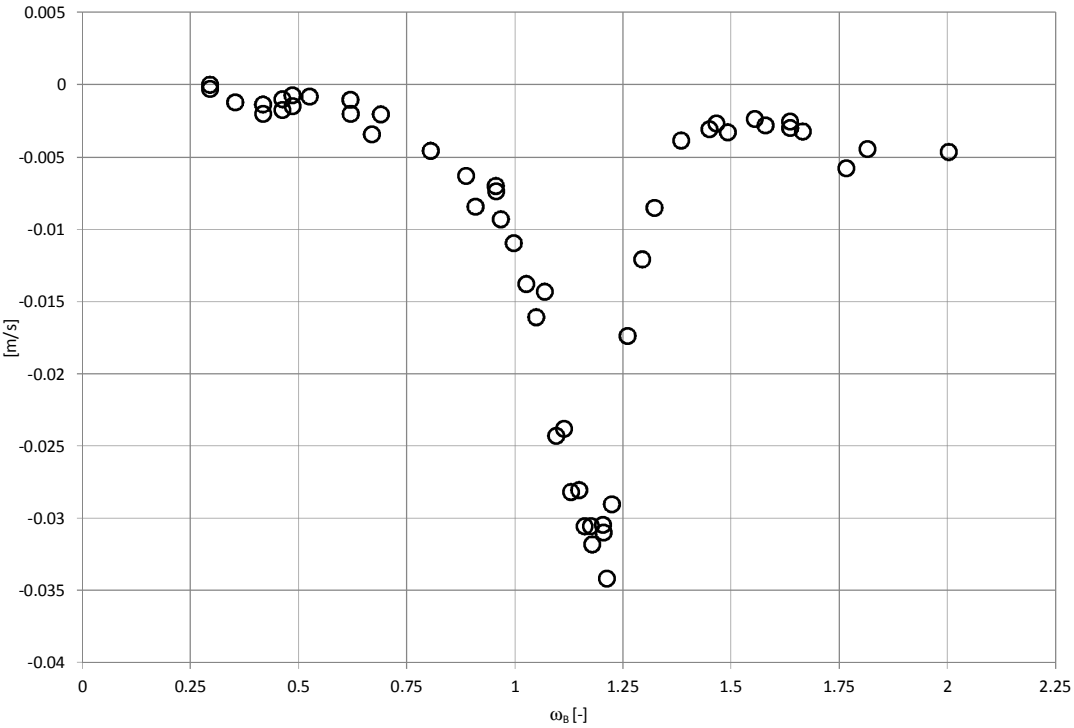

*Fig.**5.26**: Drift velocity, damaged condition, amplitude 5 degrees*

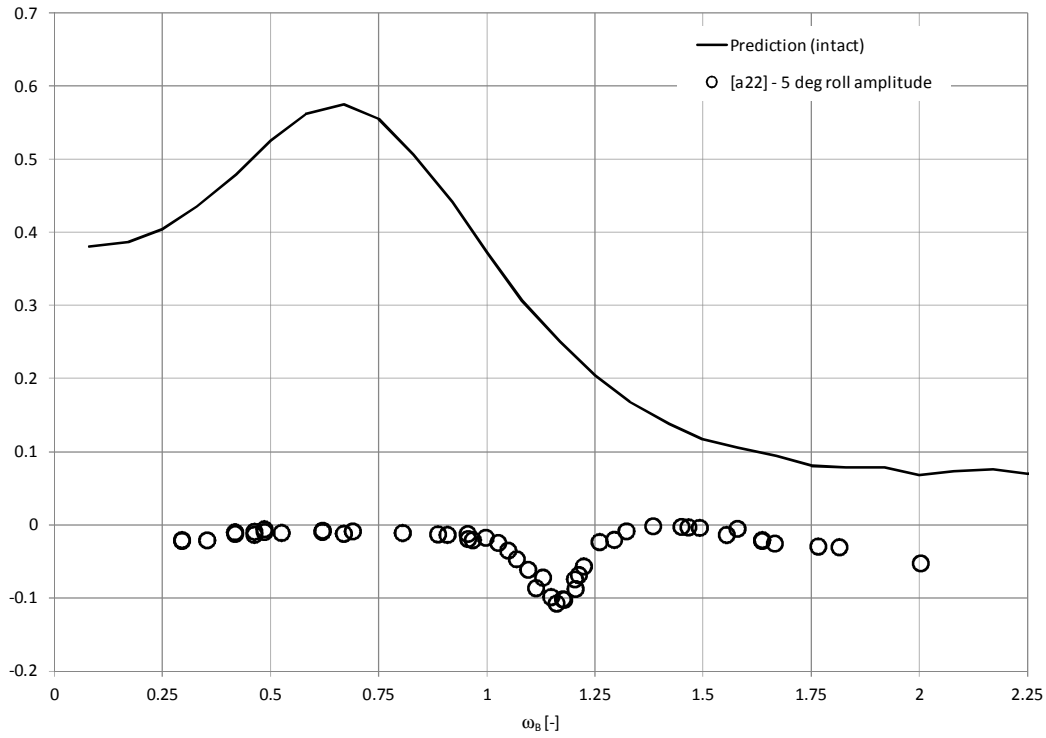

*Fig.**5.27**: Sway added mass* $[a]_{22}$ *, 5 degrees roll, damaged condition. The solid curve represents the theoretical prediction (intact ship).*

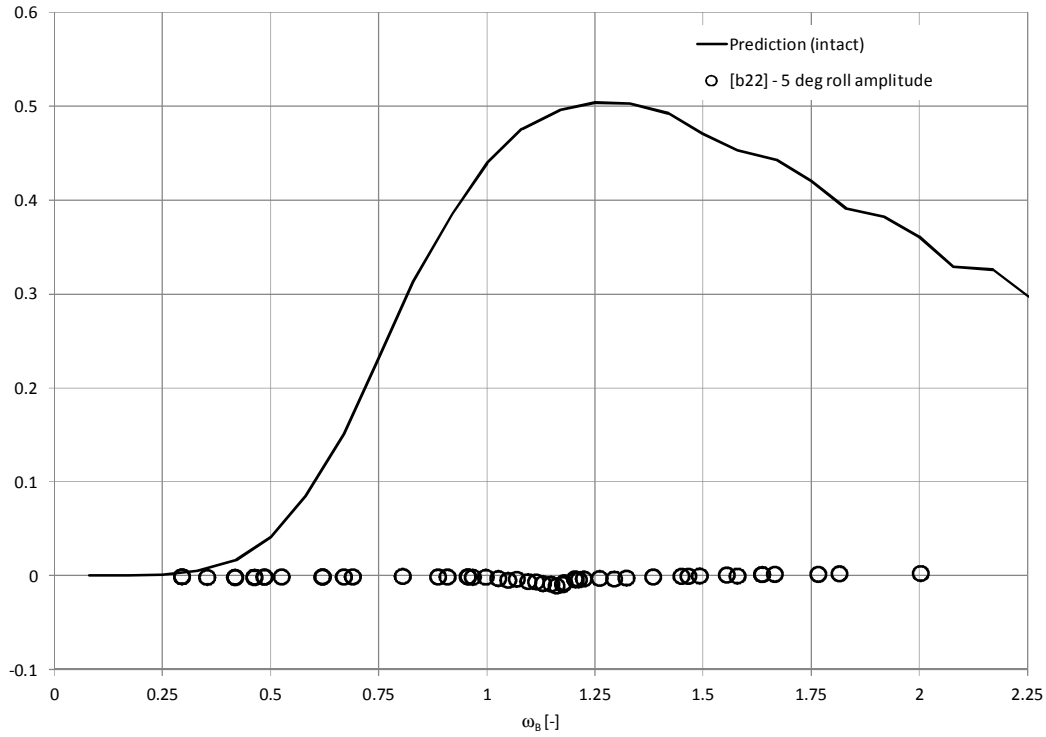

*Fig.**5.28**: Damping coefficient* $[b]_{22}$ *, 5 degrees roll, damaged condition*

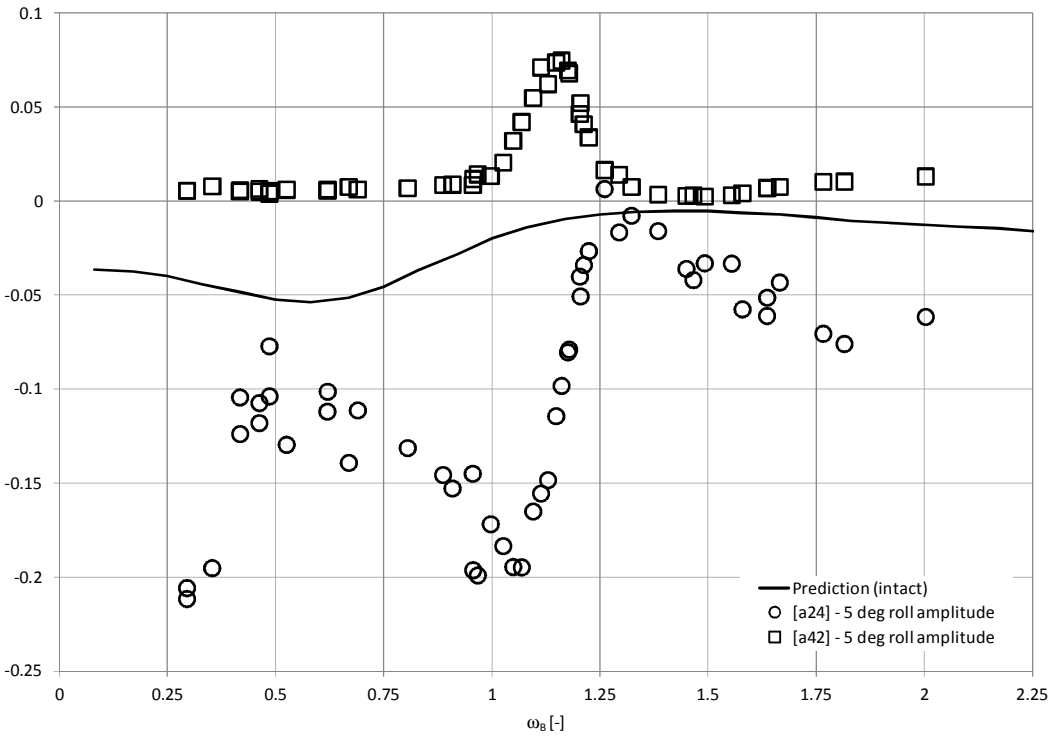

*Fig.**5.29**: Coupling added inertia coefficients* $[a]_{24}$ *and* $[a]_{42}$ *, 5 degrees roll, damaged condition*

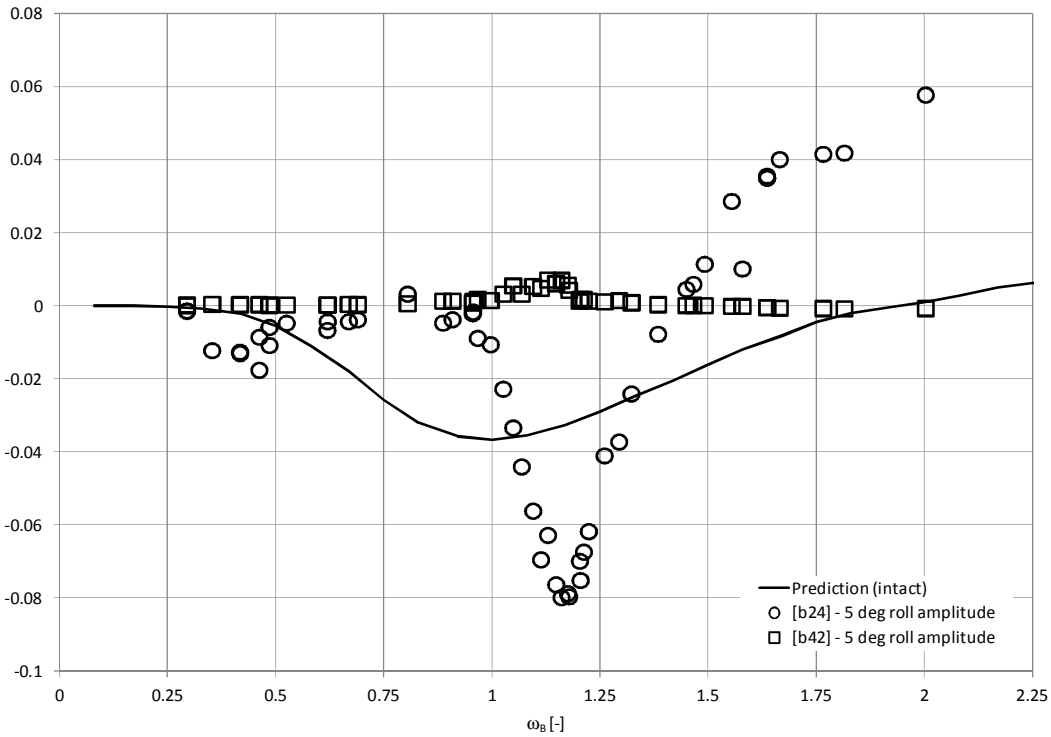

*Fig.**5.30**: Coupling damping coefficients* $[b]_{24}$ *and* $[b]_{42}$ *, 5 degrees roll, damaged condition*

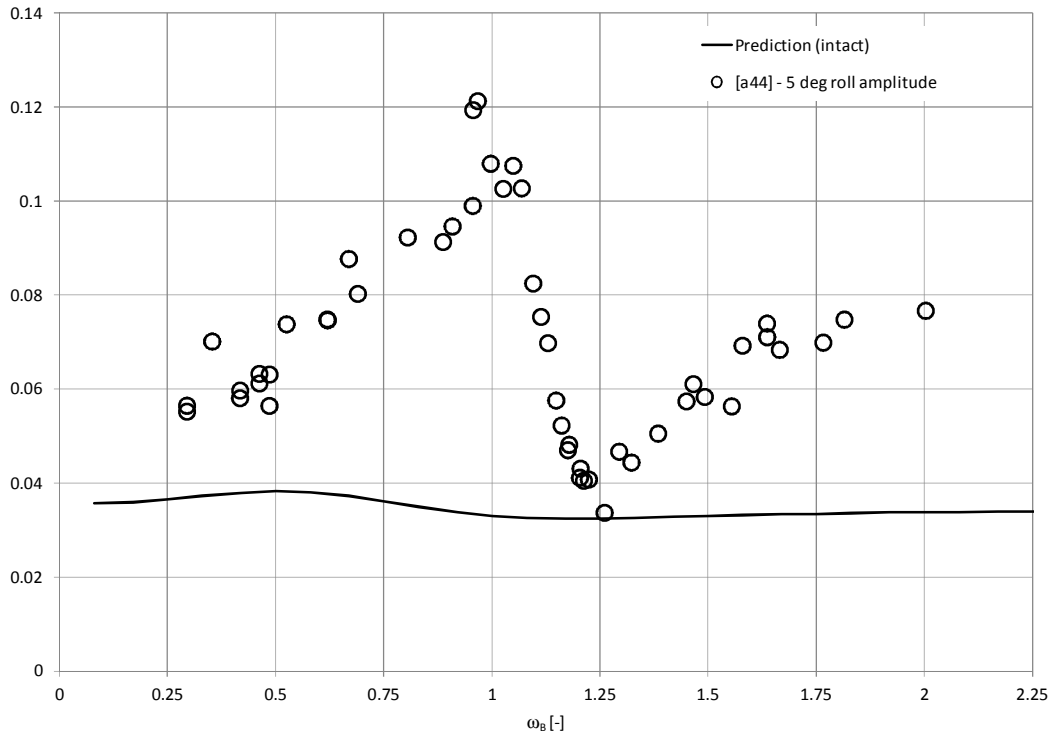

*Fig.**5.31**: Added inertia coefficient* $[a]_{44}$*, 5 degrees roll, damaged condition*

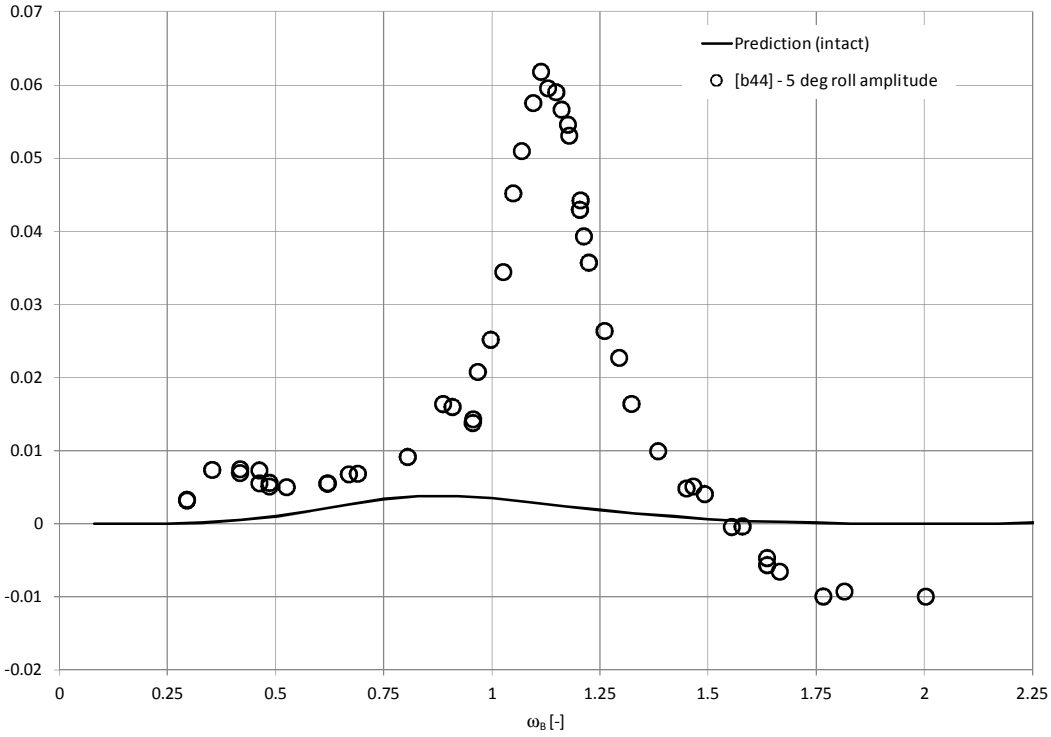

*Fig.**5.32**: Damping coefficient* $[b]_{44}$*, 5 degrees roll, damaged condition*

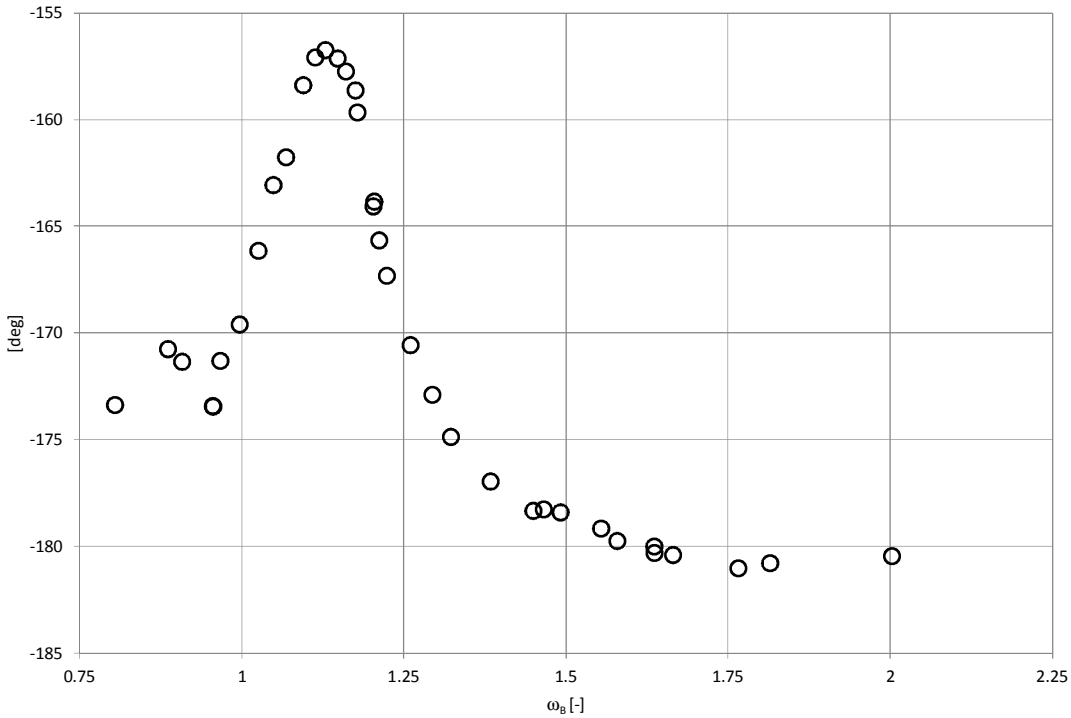

*Fig.**5.33**: Roll phase (unwrapped) in the region of significant sloshing*

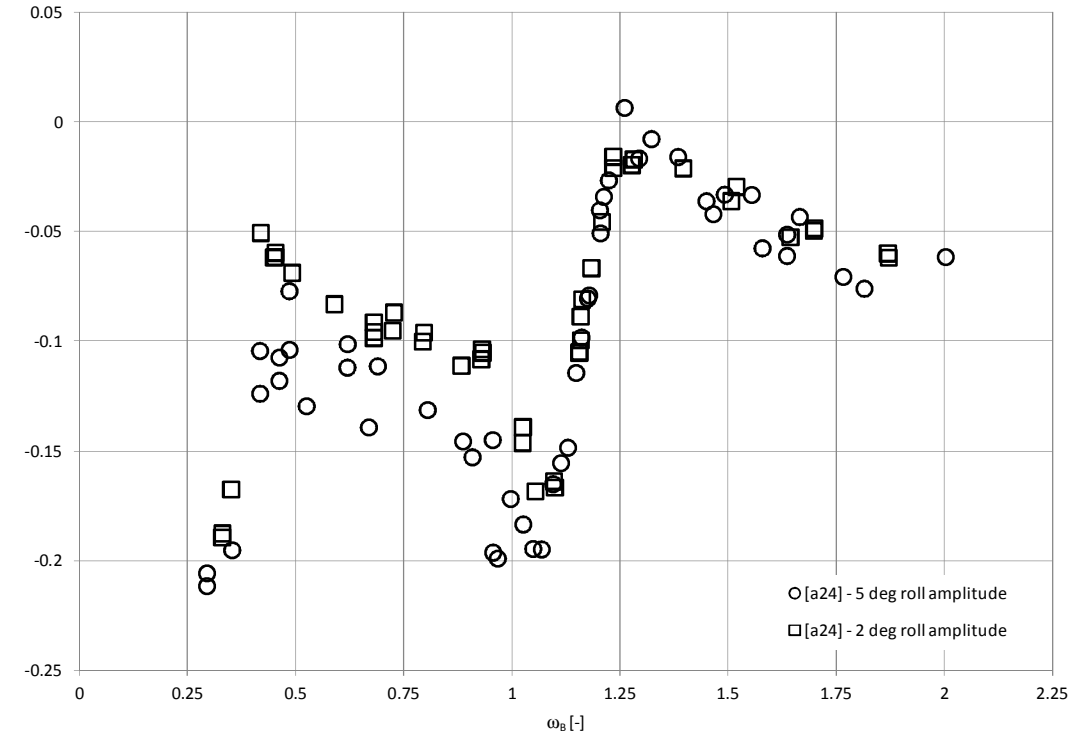

*Fig.**5.34**: Impact of roll amplitude on* $[a]_{24}$

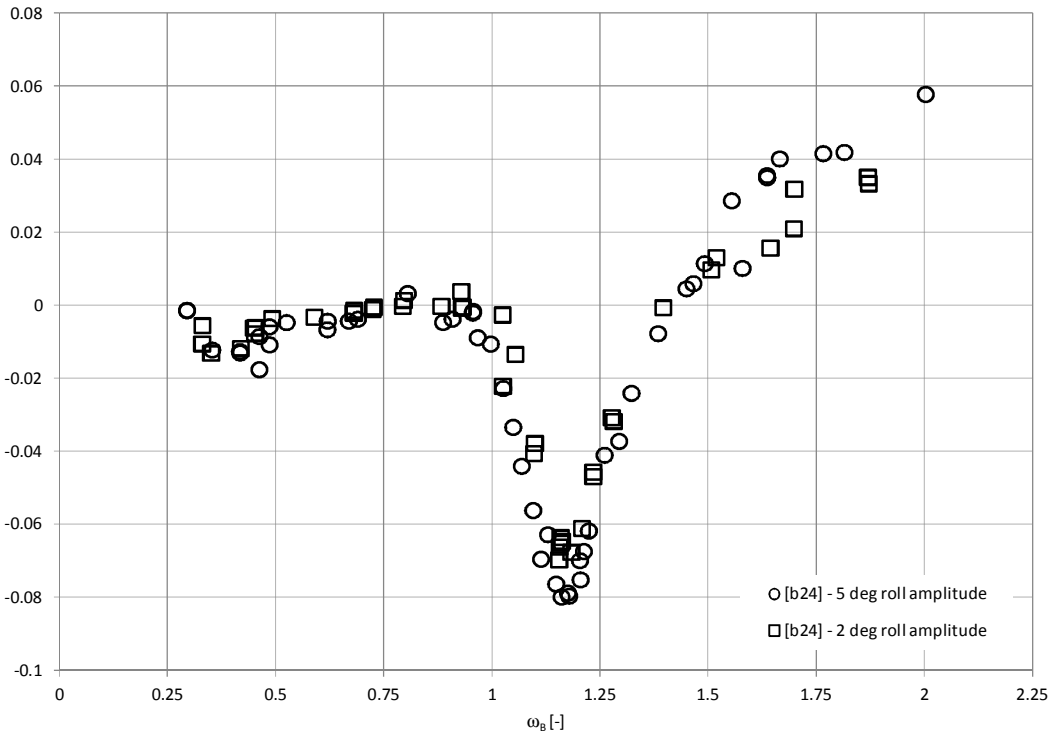

*Fig.**5.35**: Impact of roll amplitude on* $[b]_{24}$

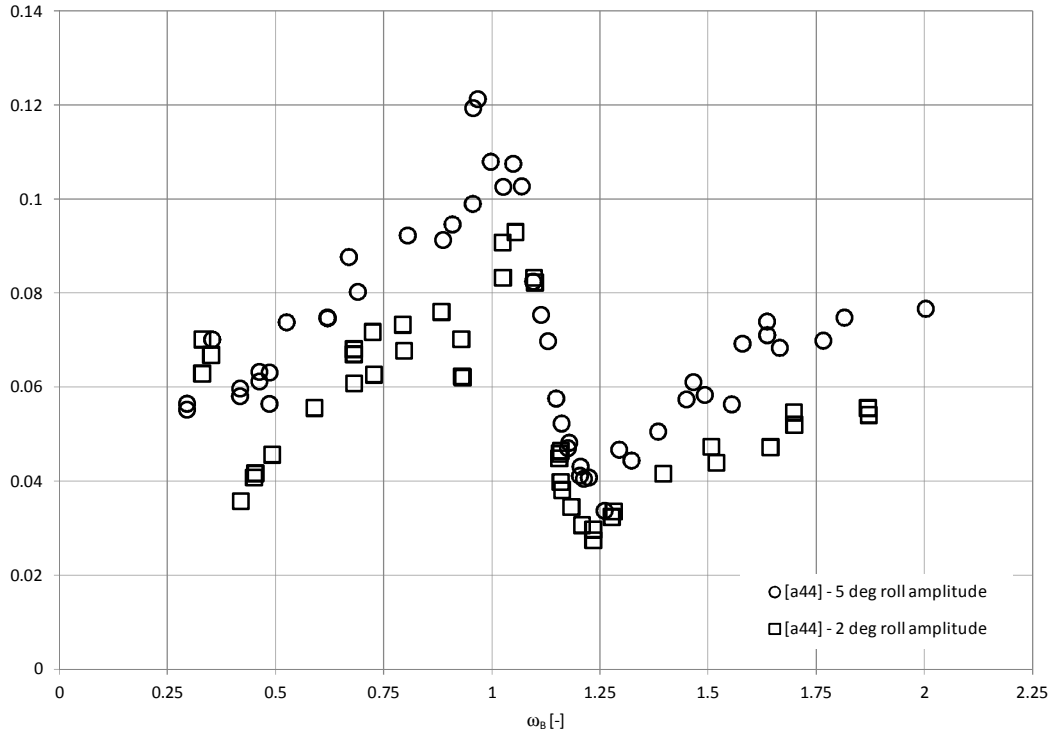

*Fig.**5.36**: Impact of roll amplitude on* $[a]_{44}$

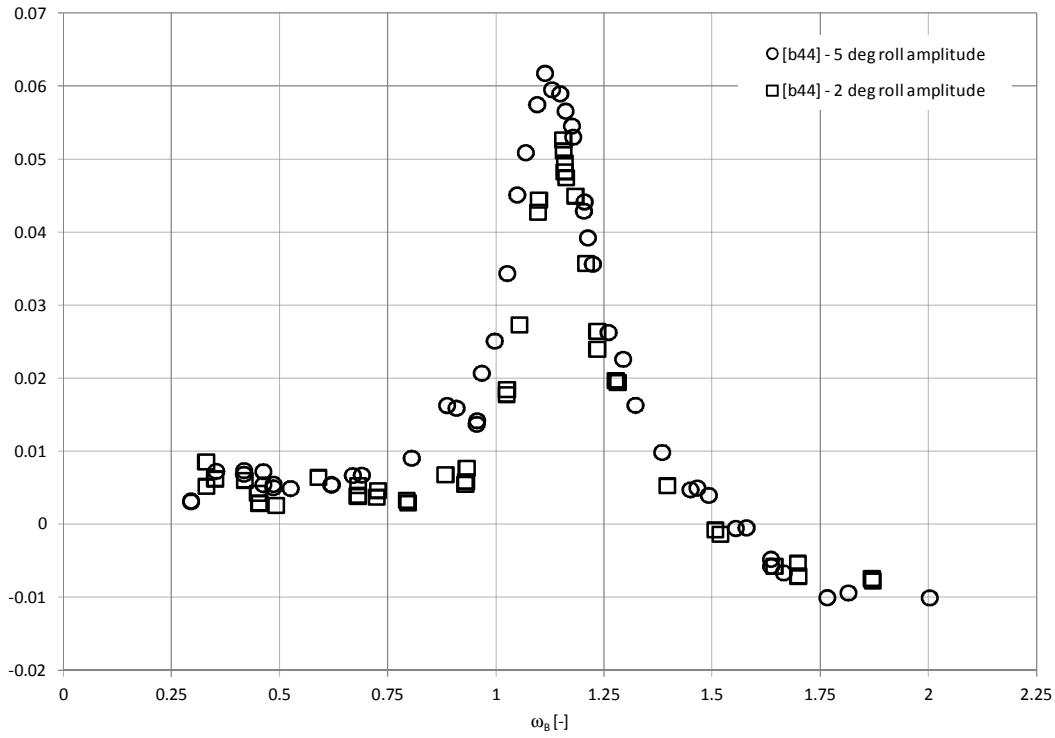

*Fig.**5.37**: Impact of roll amplitude on* $[b]_{44}$

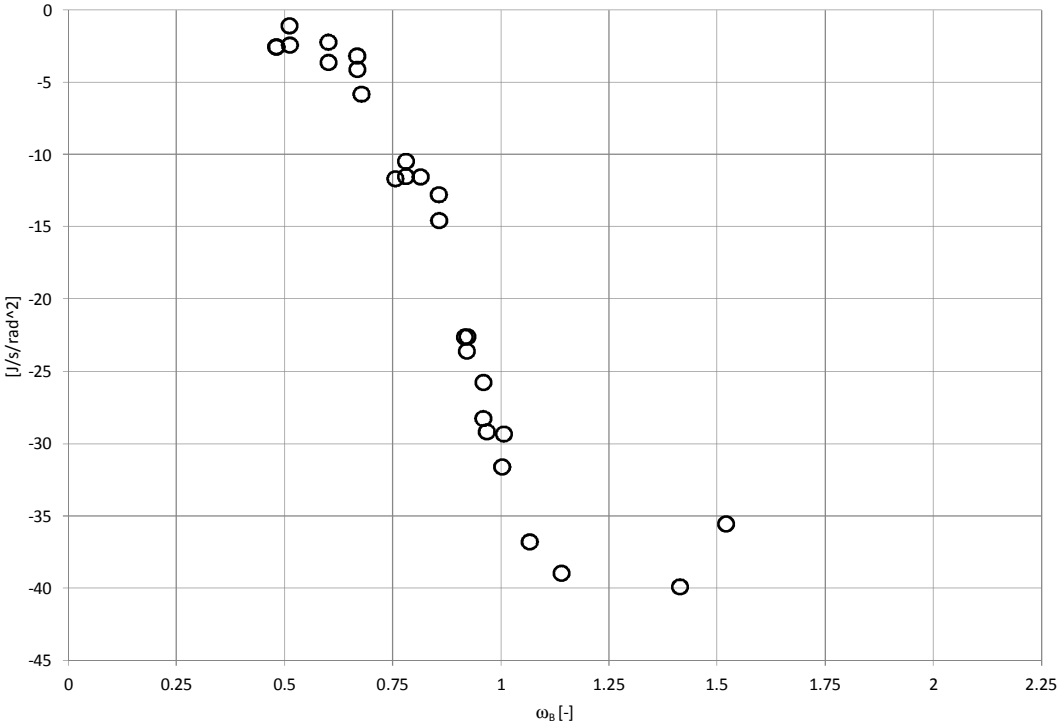

*Fig.**5.38**: Work of dissipative forces per period per squared roll amplitude – intact hull, 5 degrees roll*

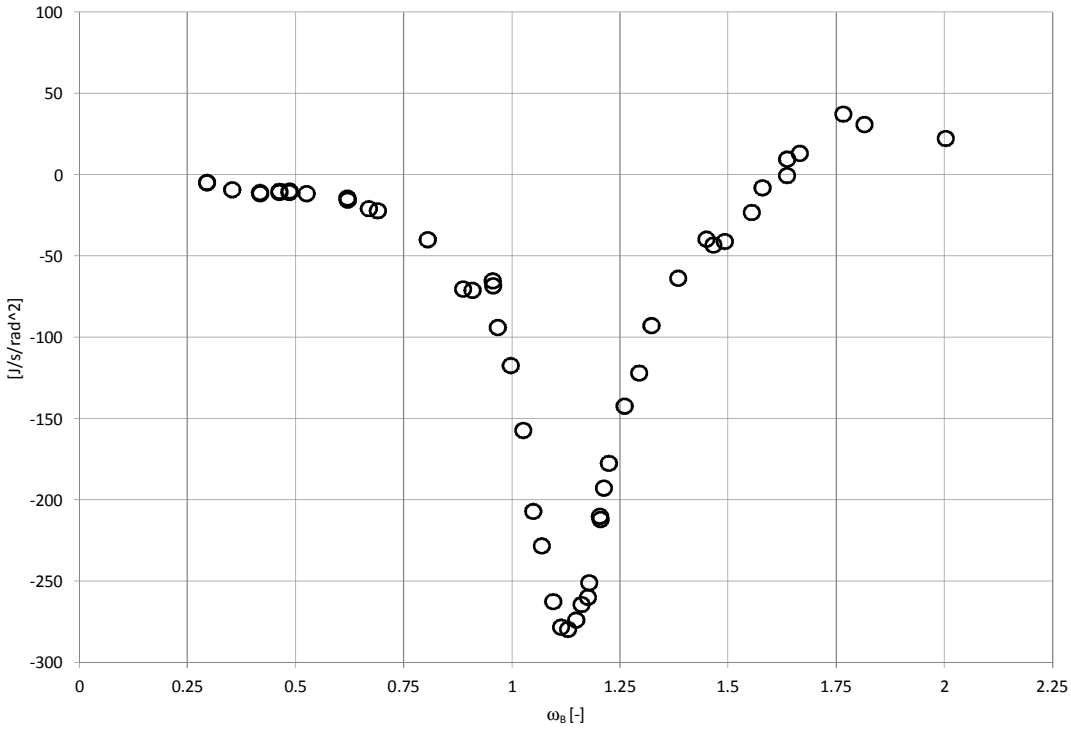

*Fig.**5.39**: Work of dissipative forces per period per squared roll amplitude – flooded hull*

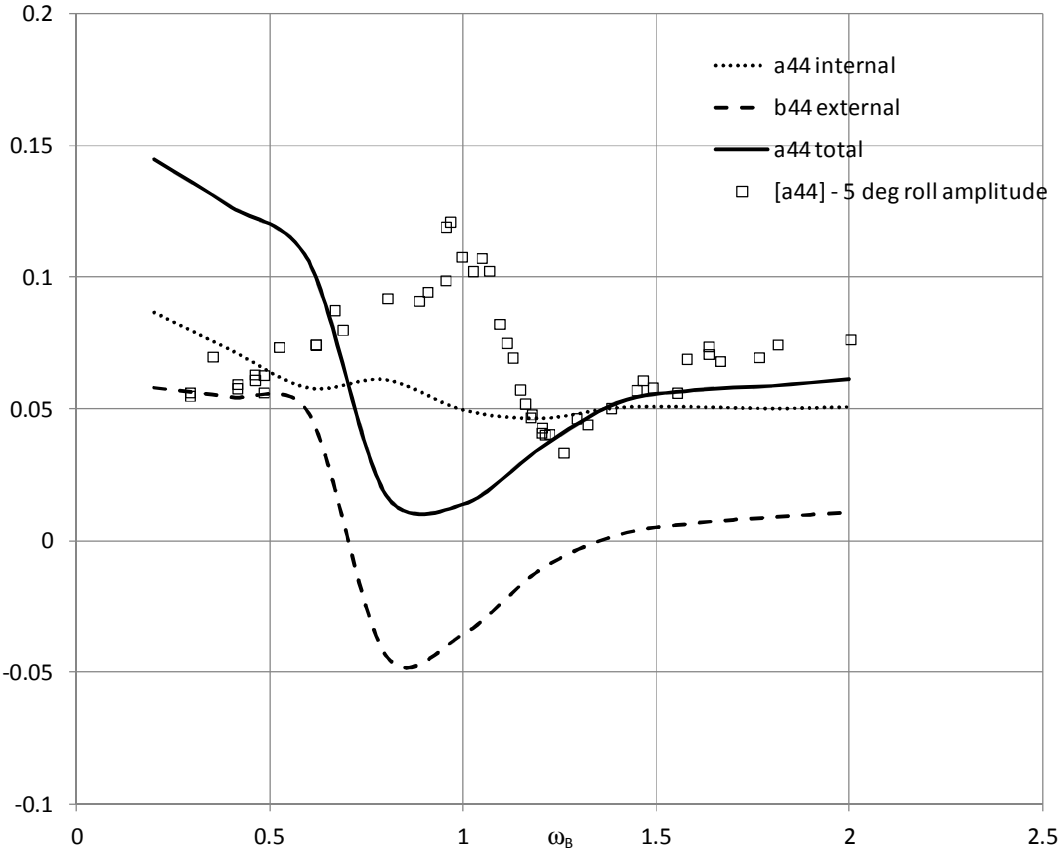

*Fig.**5.40**: Added inertia of the flooded hull – CFD and measured. Direct comparison to CFD is impossible because of the different configurations. Qualitatively the results demonstrate similar trends and scale. Dashed lines correspond to components of added inertia associated with the hull (external) and internal compartment.*

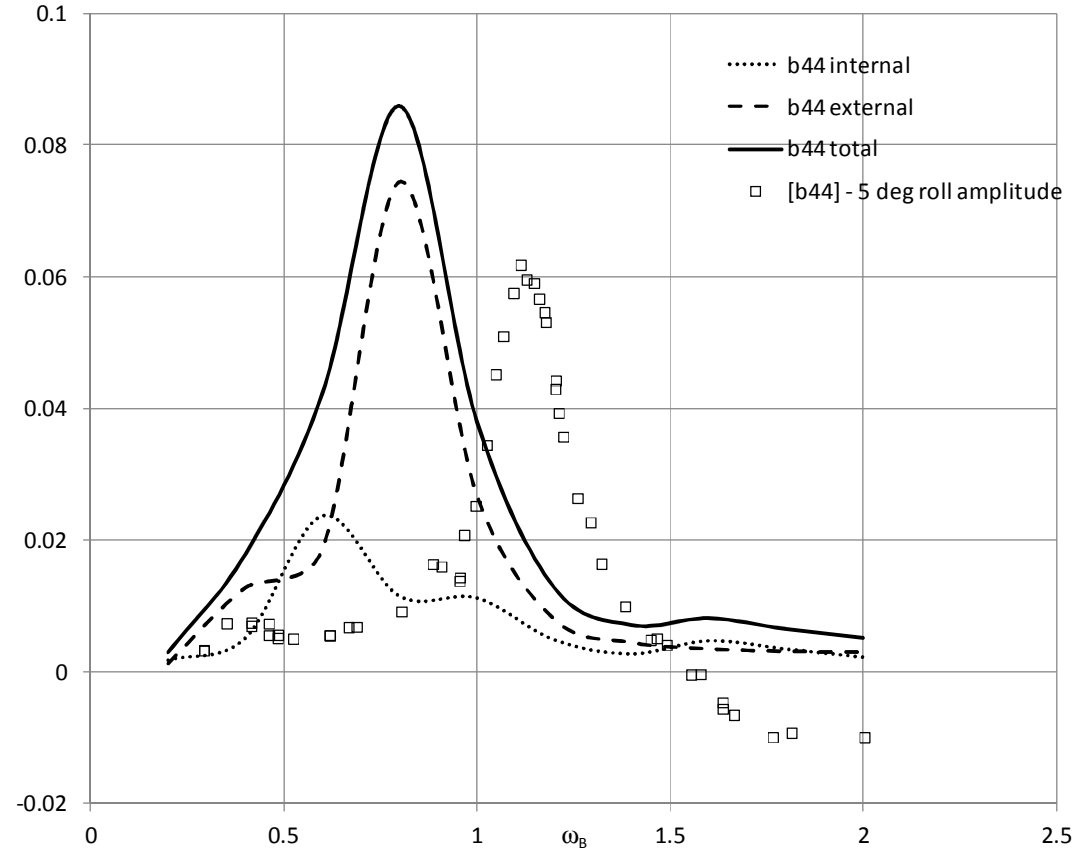

*Fig.**5.41**: Roll damping of the flooded hull – CFD and measured.*

#1

#2

#4

#3

#5

#6

*Fig.**5.42:** Sequence of video frames (numbered) showing pattern of the waves created by the flow through the opening at 1.69 Hz roll frequency (approximately 1 cycle)*

5.10 Notes on uncertainty

The studies on uncertainty in the coupled roll-sway model have been presented in (Cichowicz et al., 2010). Similar assessment has been performed for the mathematical model derived in this thesis. However, due to the time-consuming symbolic op-

erations[22] the analysis was carried out only for several points. Nevertheless, since the both methods resulted in comparable error estimates the uncertainty assessment will be demonstrated with use of the simpler, 2DoF, model.

The 2DoF mathematical model comprise coupled roll-sway equations with the assumed symmetry in coupling terms, as shown below

$$\begin{aligned}&\left(m+a_{22}\right)\ddot{y}+a_{24}\ddot{\varphi}+b_{22}\dot{y}+b_{24}\dot{\varphi}=0\\&a_{42}\ddot{y}+\left(I_{44}+a_{44}\right)\ddot{\varphi}+b_{42}\dot{y}+b_{44}\dot{\varphi}+c_{\phi\phi}\varphi=M_{44}\end{aligned} \tag{5.23}$$

The added mass and damping components were derived for oscillations about the natural axis of rotation with help of the following identities

$$\begin{aligned}&y=\overline{OA}\sin\varphi\\&\dot{y}=\overline{OA}\dot{\varphi}\cos\varphi\\&\ddot{y}=\overline{OA}\left(\ddot{\varphi}\cos\varphi-\dot{\varphi}\sin\varphi\right)\end{aligned} \tag{5.24}$$

The roll added inertia and damping have been derived with use of the orthogonal decomposition, where sway coefficients were assumed known quantities, that is

$$\begin{aligned}&\left[a_{44}\right]=\frac{c_{44}}{\omega^2}-\frac{M_0\cos\varepsilon}{\varphi_0\omega^2}-I+\overline{OA}^2\left(m\left(1-\cos^2\varphi_0\right)+a_{22}\cos^2\varphi_0\right)\\&\left[b_{44}\right]=-\frac{M_0\sin\varepsilon}{\varphi_0\omega}+\overline{OA}^2\cdot b_{22}\end{aligned} \tag{5.25}$$

where the superscript *0* denotes amplitude of the appropriate harmonic function, I is hull inertia about axis passing through A and ε stands for the phase lag of roll with respect to excitation.

The assessment aimed at the systematic uncertainties only and it was assumed that the measured variables are not correlated and therefore the total systematic error can be estimated with use of the following scheme (Coleman and Steele, 1999)

[22] The $[.]_{jk}$ obtained by means of Lagrange's multipliers method are functions of several variables derived from the pseudo-inverse matrix $A^T\left(AA^T\right)^{-1}$. In order to compute errors the components of the total differentials of these functions had to be calculated.

$$u_S(f)^2 = \sum_{i=1}^{n}\left(\frac{\partial f}{\partial x_i} u_S(x_i)\right)^2 \tag{5.26}$$

where f is a functional relation between measured variables x_i , $u_S(.)$ denote systematic errors in derived quantities and measured variables; *n* stands for number of variables. Partial derivatives in the above formula are referred to as sensitivity coefficients.

The results based on the errors in the measured variables obtained for roll added inertia and damping are presented in the figures below

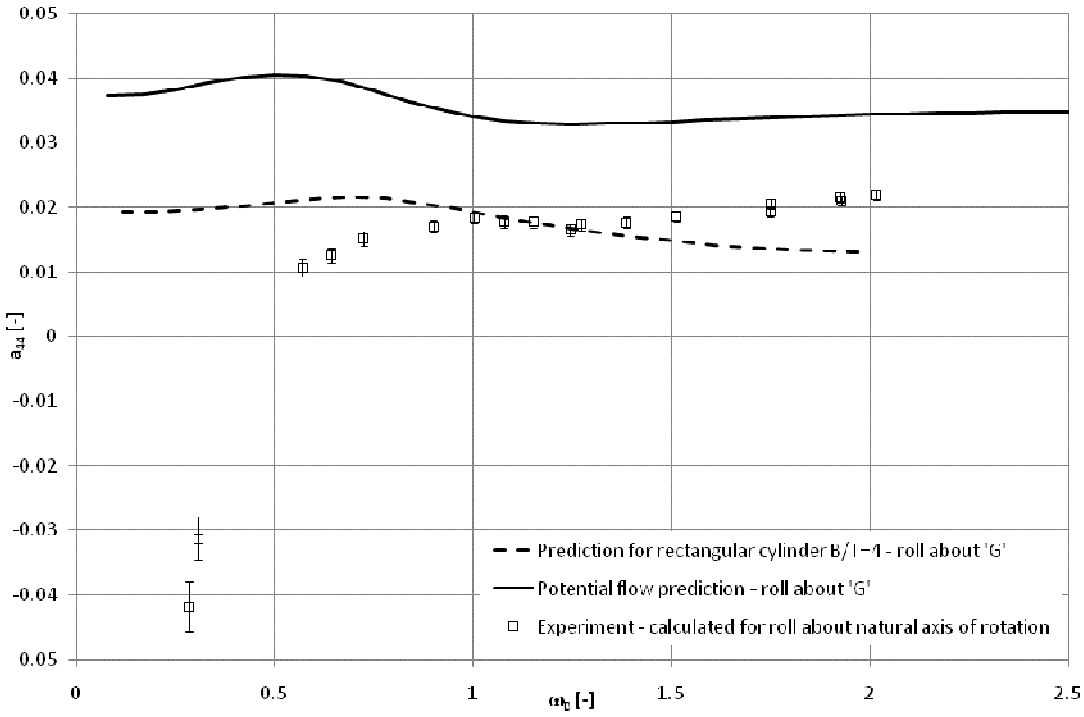

*Fig.**5.43**: Systematic errors in roll added inertia estimate*

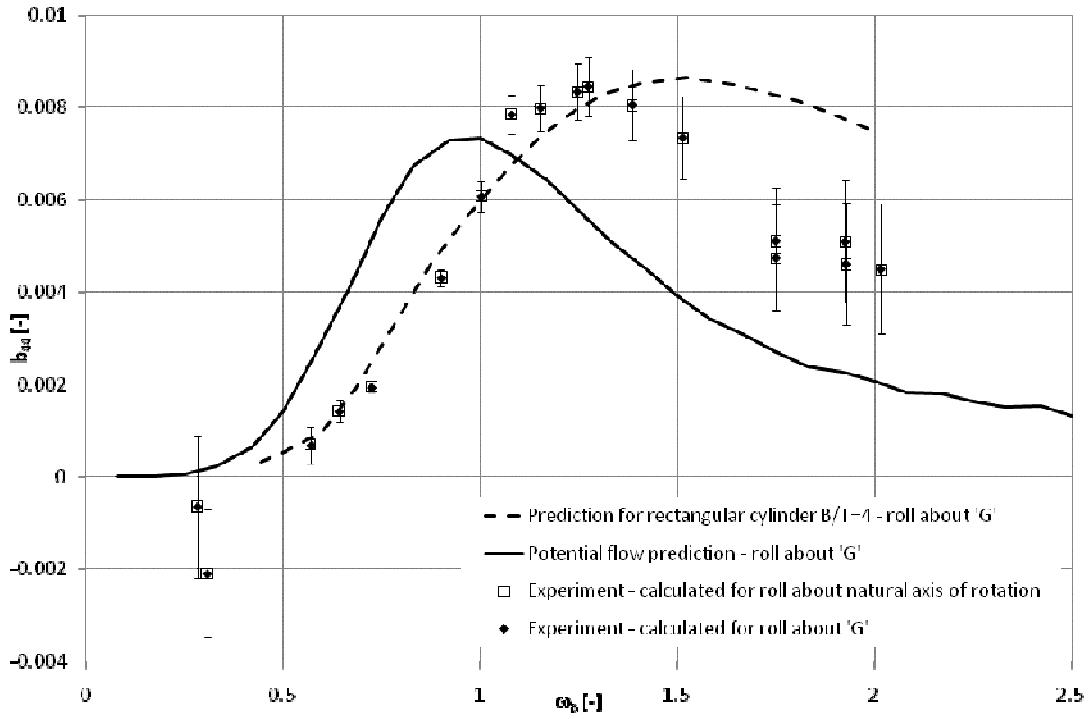

*Fig.**5.44**: Systematic errors in roll damping estimate*

It can be readily seen in the above graphs that the biggest uncertainties can be expected at the very low and the very high frequencies. In particular, the two points at the lowest frequency should be disregarded as unreliable. In this case the negative added inertia derives from the fact that the moment of inertia of the hull was not corrected to account for the location of the axis of rotation. Negative damping, in turn, is a consequence of the uncertainty in phase lag assessment.

The contribution of individual components to the total error can be more systematically analysed with use of the following ratio

$$\frac{\left(\frac{\partial f}{\partial x_i} u_S(x_i)\right)^2}{u_S(f)^2} = \frac{\left(\frac{\partial f}{\partial x_i} u_S(x_i)\right)^2}{\sum_{i=1}^{n}\left(\frac{\partial f}{\partial x_i} u_S(x_i)\right)^2} \tag{5.27}$$

Individual contributions, expressed in terms of percentage, are presented in the following figures

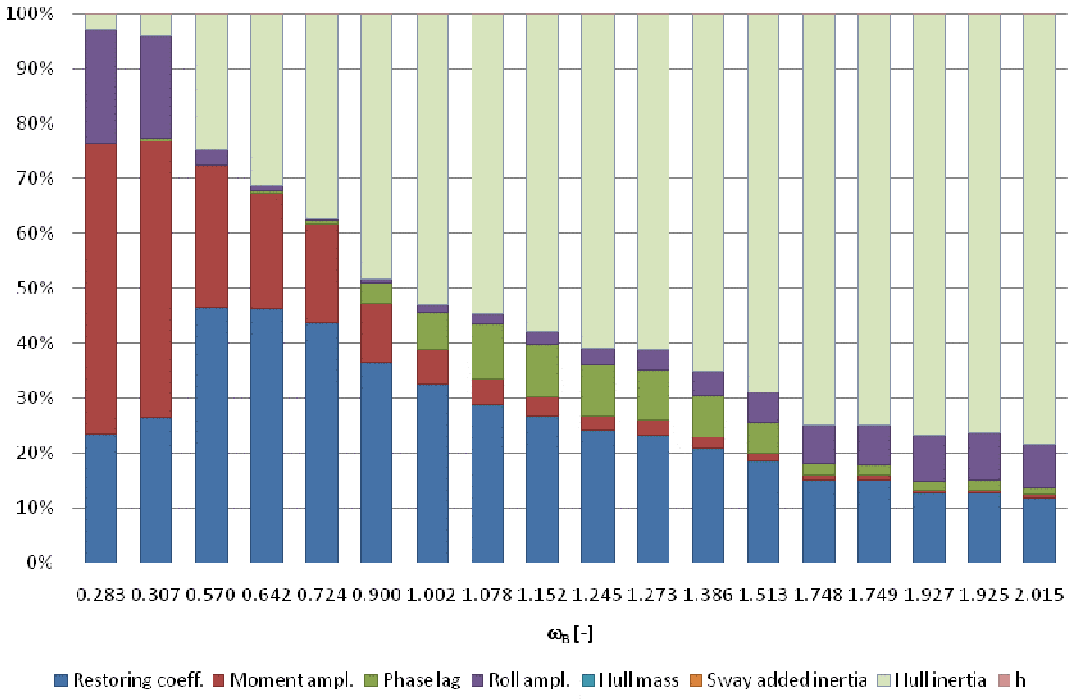

*Fig.**5.45**: Contributions of individual components in total bias error estimated for roll added inertia coefficient*

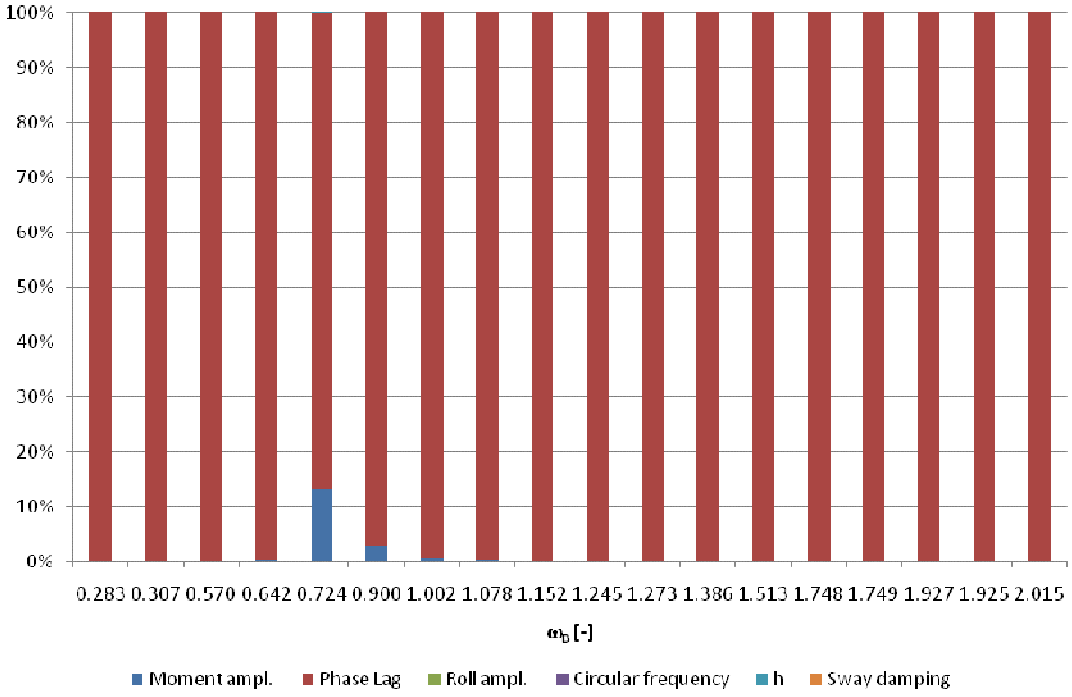

*Fig.**5.46**: Contributions of individual components in total bias error estimated for roll damping coefficient*

There are four major contributors to the error in added inertia estimate, namely: restoring coefficient, external moment amplitude, roll amplitude and hull inertia. Furthermore, the influence of coefficients (except the restoring coefficient) varies significantly with the frequency. At the low-frequency range, major contributors are the

quantities derived from the recorded time series – the moment amplitude and the roll amplitude. At the high-frequency range, the error is mostly dominated by the dry hull inertia.

In the case of roll damping, the picture is monochromatic – the entire error is caused virtually by one quantity – the phase lag, with the exception of near resonance frequencies, where the moment amplitude error is playing some role (i.e. where the measured moment is very small and the corresponding errors large).

As stated before, the analysis performed on several points estimated with use of the Lagrange's multipliers method resulted in comparable (in terms of magnitude and distribution) systematic errors. However, one has to bear in mind that the matter is more complex when it comes to the flooded hull where the mathematical model is incomplete. Therefore, the error estimates based on the simple model are underestimated.

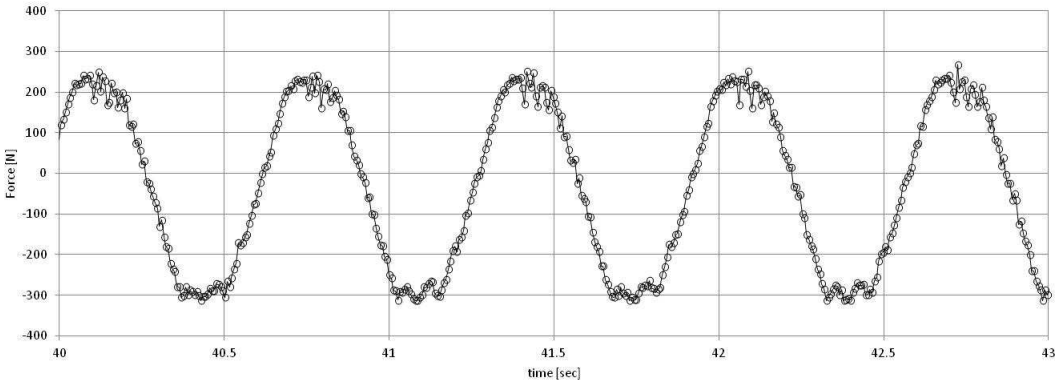

*Fig.**5.47**: Time history of force measured by load cell, run 217, damaged condition, 5 degrees roll,* $\omega = 9.6379\left[rad/s\right]$

For instance, the time history in the graph above shows that the signal (the measured moment to sustain motion) is not harmonic. It is a periodic function and the simple sinusoidal fit removes the information carried by the higher order harmonics. On the other hand, it is clear from the graph that when the body starts to roll away from the damage (just beyond the maximum of the load curve) there is some substantial (although short-lasting) change in the flow characteristics. Similarly, when the hull approaches maximum roll, away from the damage (the minimum on the load curve) there is symmetrical variation in the induced flow. Unfortunately, although the in-

formation is there, it cannot be easily extracted due to sampling rate insufficient for use of the spectral techniques. On the other hand, the sinusoidal fitting is an averaging process and therefore the data carried with higher harmonics is not completely lost– it results in the local trend's variations or residuals. Obviously, such incomplete information is of limited use but it indicates order of magnitude of the higher-order effects.

Chapter 6 Analysis of Results

6.1 Introductory remarks

As discussed in the foregoing, the problem of deriving forces of hydrodynamic reaction acting on a body moving in or below the free surface of the fluid is often addressed by means of the linear theory. In a consequence, motions of the body are required to be small in order to allow neglecting higher order velocity-terms. Furthermore, the linearised free-surface condition requires the radiated wave to be of small steepness (small amplitude to wave-length ratio). Undoubtedly, the linear models have many advantages – they are computationally efficient, relatively simple and reasonably accurate in predicting the hydrodynamic reaction of *typical* ship-like objects. Moreover, linearity of the models allows employing the superposition principle – the usual complexity of the time-domain analysis can be eased by approaching the problem in the frequency domain.

Clearly, the notion of *small-amplitude motions* bears all the drawbacks of arbitrariness. For instance, in the original Frank's paper (Frank, 1967) it is stated that

"[...] *the motion amplitudes and velocities are all small enough that all but the linear terms of the free surface condition, the kinematic boundary condition on the cylinder, and the Bernoulli equation may be neglected.*"

Although not particularly specific, such definition is sufficient in analytical formulation, where arbitrariness can indeed be an advantage (e.g. customary assumption of the infinitesimal motion amplitudes). However, when it comes to physical experiments the perception of smallness is different. It is not dictated by the boundary condition or a conformance with relevant mathematical formulae but determined by the ability to measure the requisite physical entity. It is always desirable to maintain one-to-one correspondence between the theory and the experiment but this seldom can be achieved. Even if most physical constraints could be overcome, there always are parameters that could not be controlled and the quantities, which could not be directly measured. Finally, there is a question concerning the mathematical modelling and

data processing - the question of uncertainty assessment and the inherent necessity for reasoning on the errors that cannot be formally quantified.

6.2 Dealing with errors - intact ship

In the theoretical approach, the rigid body is modelled as an impenetrable to the fluid boundary, a surface upon which certain kinematical constraints have to hold. Hence, the body is a massless entity subjected to prescribed motions in the fluid domain. Furthermore, the velocity field resulting from the motion of the wetted surface is induced in the fluid instantaneously as a series of pressure impulses, which in the limit become a continuous function of time. In such a configuration, neither inertia nor hydrostatic forces have to be accounted for, as the hydrodynamic reaction is obtained by means of surface integration of the hydrodynamic pressure impressed by the fluid upon the wetted surface of the body. In a case of harmonic motions, the derived forces are usually expressed by means of orthogonal components in phase with acceleration and in phase with velocity in the coordinate system corresponding to the mean position of the wetted surface.

Similarly, in the ‘classical’ experiment, the forces of hydrodynamic reaction are derived from measurements performed on a model undergoing prescribed motions but the measured forces and moments to sustain the motion include the body’s inertia as well as hydrostatic forces, which need to be subtracted from the total load recorded. As the motions of the body are prescribed, the experiments on constrained body resemble well the configuration of the mathematical model. However, some theoretical assumptions *must* be violated during the physical tests. Firstly, the real fluid is viscous and therefore energy is not only radiated from the system but it is also dissipated through friction and eddy making components. It is often assumed that effects of water viscosity *are* small for small velocities of the body but again, the notion of "smallness" is inconveniently arbitrary. In fact, the significant deviation of the hydrodynamic forces derived experimentally from prediction is rather a rule than an exception. As demonstrated by Seah and Yeung accounting for viscosity brings the theoretical prediction closer to the measured values (Seah and Yeung, 2003). Similar results were reported by Standing in (Standing et al., 1992).

Nevertheless, although *in principle* impact of the fluid viscosity on the hydrodynamic quantities is obvious, the question of the accuracy of the prediction is still open particularly in the case of smooth bodies. Specifically, the experiments by Vugts indicate relatively strong dependency of roll hydrodynamic coefficients on the amplitude of motion whereas the present measurements show much lesser sensitivity to increase in the motion amplitude, at least in the case of the intact ship. Similarly, experiments by Ikeda and Standing show that the viscous roll damping can be accurately predicted for sections fitted with bilge keels or sharp corners but Standing's prediction fails in case of the round-cornered sections without bilge keels. It is unlikely that a simple and straightforward explanation could be given to these discrepancies but it is possible that in the case of smooth, lightly damped bodies, the viscous effects are strongly influenced by the system configuration, i.e. presence of physical constraints.

In forced sway, the model is allowed to move only in the calm-water plane with the roll constrained. In such configuration, the measurements of the lateral force and the moment to maintain the constraint are sufficient for deriving sway coefficients $(.)_{22}$ and coupling coefficients of sway into roll $(.)_{42}$.

In forced roll, the model undergoes prescribed rotations about a fixed axis – in this case, sway is the constrained motion. This configurations allows deriving roll, $(.)_{44}$, and roll into sway, $(.)_{24}$ coefficients. Intuitively, if the body is a symmetrical cylinder the symmetry in coupling terms should also be maintained. Furthermore, in both cases the presence of the constraint results single degree of freedom oscillations.

In the case of the measurements on the floating cylinder, the oscillations take place about the natural, variable, axis of rotation. There is no physical constraint present in the system and apparently the body has two (if heave can be neglected) degrees of freedom. Yet, as shown in the foregoing, effectively the system is also a single degree of freedom oscillator. That is because in the investigated case sway and roll could be linked by means of the identity $y = \overline{OA}\varphi$. The finite relationship between the coordinates forms a holonomic constraint and therefore it reduces number of degrees of freedom. However, during the forced roll about the fixed axis the constraint is no

longer $y = \overline{OA}\varphi$ but $y = 0$. These two systems are not mechanically equivalent, as maintaining of the different constraints requires different forces.

Furthermore, there is a principal difference between numerical and physical experiments. Namely, in the former case, the system comprises of a fluid domain bounded (entirely or partially) by a set of surfaces and the wetted surface of the body is just one of the boundaries. The velocity field inside the fluid domain is determined by the physical properties of the fluid and the kinematical conditions imposed upon boundaries. The resultant hydrodynamic reaction must fulfil not only the boundary condition on the wetted surface but also the "global" condition that $y = 0$. In the linear theory approach, where the flow separation cannot occur but the amplitudes are finite, the constraint may lead to local singularities in the boundary condition on the wetted surface. In fact the integrability issues are inherent to the linear approach and a variant of such the problem was addressed by Frank[23], who discussed the presence of discrete 'eigenfrequencies' in certain formulations of 2D and 3D potential problems, for which Green's equations would fail to provide unique solutions. Although such the problem did not have to be caused by the boundary condition on the free surface alone, one can speculate that in some cases the constraint, or rather the forces to maintain the constraint may be a factor determining the flow around the wetted surface. Subsequently, the constraint may cause significant "deformations" in the predicted hydrodynamic quantities.

In the physical system the flow separation can occur hence, maintaining of the constraint may lead to the local flow conditions resulting in the flow separation, which might not happen if the constraint *were* different. Noticeably, the fixed-axis experiments discussed in the Chapter 4 show clearly that measurements are in good agreement with the theory where the system characteristics is "bold", i.e. for small B/T ratios, for sharp-rounded hulls or for the models fitted with bilge keels. In virtually all other configurations, large discrepancies occur and these differences are not only due to an inaccuracy of the measurements.

---

[23] Frank reported the problem after (John, 1950). He concluded that in case of slender bodies the problem is practically irrelevant.

In experiments on the floating body there are no constraints imposed on the system. The system has six degrees of freedom, but only three of these need to be considered. That is, the excitation – a pure moment - does not produce surge, pitch and yaw of the cylinder. Furthermore, sinkage resulting from small roll angles did not exceed 1 mm and the heave motion could be neglected. The sway motion is a consequence of rolling about the axis lying above the calm-water plane. However, as shown earlier there is a *conceptual* constraint imposed on the system, apparently identical to that of rolling about a fixed axis of rotation: $y = \varphi\overline{OA}$. The constraint is not physical – we simply assume that since there is no excitation in the lateral plane sway is caused by the roll motion. Therefore, since the coupling into heave can be neglected, the system can be considered as having two degrees of freedom – sway and roll. However, establishing functional relation between sway and roll makes the system a single-degree-of-freedom oscillator. The constraint is not violated by large amount because it would require large forces although it does not hold *exactly* - when the phase difference between the roll and sway motion increases the sway motion becomes more "independent" and the sway coefficients start to play some role. The system still has single degree of freedom but the condition $y = \varphi\overline{OA}$ describes the relationship between roll and sway inaccurately.

The amplitude of sway varies with the frequency of oscillations and it is that the identity $\overline{OA} = \overline{OG}$ holds at low frequencies. However, maintaining that condition would require an additional force as it changes the *natural* path along which the motion would be realised in the configuration space. Instead, the elevation of the axis of rotation changes – a striking example of the principle of least action.

There can be another constraint imposed on the system – the assumed symmetry of $(.)_{24}$ and $(.)_{42}$ coefficients. The first question is whether such information can be acquired from the forced roll experiments performed on the floating body. The question is valid as it determines the form of equations of motion. The second question is whether assuming the symmetry is appropriate to describe the mechanical system in question. Eventually, the constraint has been dropped – it has been postulated that such information cannot be derived without performing additional sway experiments. It has been reasoned – based on comparison of roll added inertia and damping coeffi-

cients – that the symmetry assumption resulted in an unrealistic prediction of these two coefficients.

In any case, there is a certain ambiguity in experimentally derived hydrodynamic. This derives directly from the fact that the axis of rotation does not lie in the calm-water plane. From the point of view of the rigid-body configuration, it does not really matter how we describe the motion – whether it is translation of the body-fixed origin followed by a rotation about that point, or whether it is pure rotation about some elevated axis of rotation. However, since sway motion *results* from roll and both motions are practically in phase - how to distinguish between components in phase with lateral and angular accelerations?

In his report, Vugts provided the equations he employed for deriving the estimates of hydrodynamic coefficients for rolling about a fixed axis passing through the centre of gravity of the model - $\overline{OG}$. In particular the a_{22} and a_{24} were given as

$$\begin{aligned} a_{22} &= -\frac{Y_{osc}\cos(\varepsilon_Y)}{\omega^2 y} - m \\ a_{24} &= -\frac{Y_{osc}\cos(\varepsilon_Y)}{\omega^2 \varphi} - \overline{OG}\cdot a_{22} \end{aligned} \tag{6.1}$$

where Y_{osca} stands for amplitude of the horizontal force, ε_Y is phase angle between the force and sway, y and φ_a denote amplitude of sway and roll, respectively.

Resolving both equations for $-\frac{Y_{osca}\cos(\varepsilon_Y)}{\omega^2}$ and combining the expressions yields in the following

$$a_{22}\left(\frac{y}{\varphi} - \overline{OG}\right) - a_{24} = \frac{y}{\varphi} m \tag{6.2}$$

However, when the cylinder oscillates about the fixed axis of rotation the expression $\left(\frac{y}{\varphi} - \overline{OG}\right)$ vanishes and hence the coupling term cannot depend on the a_{22} coefficient.

Regarding the axis of rotation, Balcer showed in his paper (Balcer, 2004) that the vertical position of the axis of rotation above the calm-water surface is in the case of two degrees of freedom given as

$$\overline{OA} = \frac{m\overline{OG} - a_{24}}{m + a_{22}} \tag{6.3}$$

However, taking the experimental results for $\overline{OA}$ and $[a]_{24}$, and solving the equation for a_{22} resulted approximately in $a_{22} \approx m$. Therefore, it is proposed to modify the formula, so the following holds (for a cylinder rolling in undisturbed free surface)

$$\overline{OA} = \frac{m\overline{OG} - [a]_{24}}{2m} = \frac{1}{2}\left(\overline{OG} - \frac{[a]_{24}}{m}\right) \tag{6.4}$$

In this case, the following should hold, at least for small roll angles

$$[a]_{24} = m\left(\overline{OG} - 2\overline{OA}\right) = m\left(\overline{OG} - 2\frac{y}{\varphi}\right) \tag{6.5}$$

Obviously, the modification to the Balcer's equation was arbitrary and should not be generalised but it shows the physical significance of the $[a]_{24}$. That is, it shows that the axis of rotation was completely determined by the coupling term $[a]_{24}$ and the model's mass distribution.

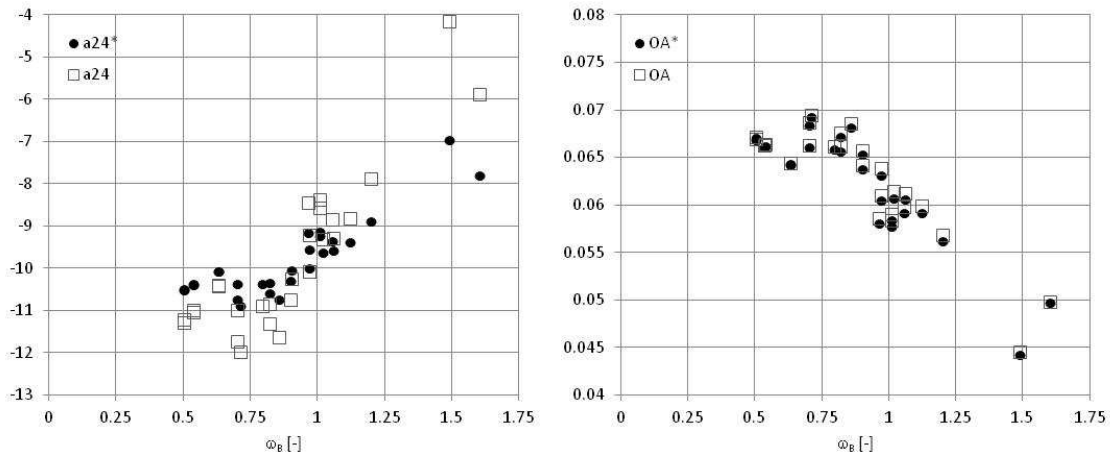

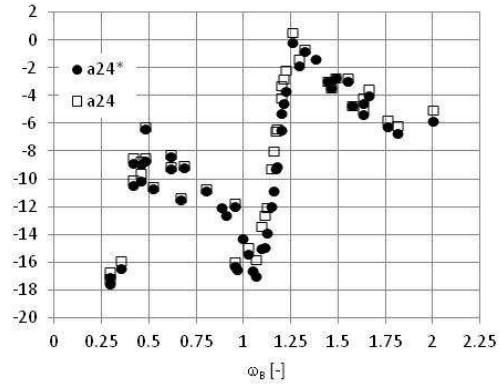

*Fig.**6.1**: Coupling term a_{24} estimated by Lagrange's multipliers method and derived from* (6.5) *– denoted by asterix (*). Intact condition-top, damaged-bottom, 5 degrees roll.*

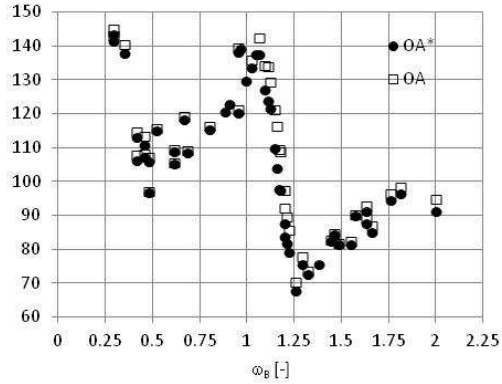

*Fig.**6.2**: Observed elevation of axis of rotation and derived from* (6.4) *– denoted by asterix (*). Intact condition-top, damaged-bottom, 5 degrees roll.*

Interestingly, the original formula presented by Balcer gives the correct prediction when applied to the results obtained with the presumed symmetry in coupling coefficients but with $[a_{22}]$ zero.

6.3 Key findings

The key findings (valid in the particular case tested) could be summarised as follows:

- The system, i.e. the unconstrained cylindrical body forced to roll in the undisturbed free surface, is a single degree of freedom oscillator. This is a consequence of the holonomic constraint $y = \varphi\overline{OA}$.
- The roll motion is practically unaffected by sway coefficients $(.)_{22}$ and $(.)_{42}$.
- The cylinder is rolling about the *natural* axis of rotation lying in distance $\overline{OA}$ above the calm-water plane.
- Elevation of natural the axis of rotation, $\overline{OA}$, is completely determined by the coupling term of added inertia, $[a]_{24}$, mass of the cylinder and vertical position of its centre of gravity $\overline{OG}$. There is no indication that damping has any impact on the roll axis, although this may not necessarily hold in principle. Elevation of the axis is a function of frequency. It may be dependent on motion

amplitude (although there is no such evidence) if dependency on amplitude is observed in $[a]_{24}$.

- The damping term in coupling of roll-into-sway, $[b]_{24}$ determines the phase difference between roll and sway. When the damping is low, the lateral component of the hydrodynamic reaction is completely determined by terms in phase with roll acceleration and velocity. As damping increases, correction terms appear in phase with sway acceleration and velocity. These corrective terms are of much smaller magnitude than the predicted $(.)_{22}$ and $(.)_{42}$ terms.
- The question of symmetry of coupling terms cannot be answered without dedicated sway experiments

6.4 Dealing with Errors - Damaged Ship

It is apparent that the above conclusions should, in principle, hold also in the case of the flooded cylinder. Nevertheless, the measurements on the flooded cylinder provided some interesting observations, as briefed below.

Firstly, the asymmetry in a pressure distribution due to the presence of the damage opening causes significant drift at some, relatively broad, frequency range.

The damping characteristics become bimodal. At the lower frequency range, it is dominated by the 'hull dynamics'. As the frequency increases towards the first natural frequency of sloshing the damping increases dramatically – its magnitude is about ten-fold larger than the maximum observed at low frequencies. Subsequently, the increase in motion amplitude (RAO) is almost negligible. Furthermore, the hydrodynamic coefficients exhibit a slight nonlinearity although the nonlinear behaviour is somehow smaller than expected.

As in the intact condition, the system has a single degree of freedom, but the impact of sway is much more pronounced, particularly at sloshing resonance and higher frequencies. This is a consequence of a much larger coupling term in damping and corresponding phase difference between roll and sway.

Most importantly, the flow viscosity starts to play significant role, particularly during the high-frequency oscillations. At $\omega_B > 1.5$ work of dissipative forces is positive – energy in the system increases. This is because damping in the principal mode of motion – roll – becomes negative and the increase in the coupling term is insufficient to maintain the balance. The mathematical model used to derive the coefficients assumed that the dissipative force is a linear form of velocity (Rayleigh's dissipation function in mechanical system or the symmetric part of the velocity gradient tensor in viscous flow formulation). Clearly, such a description is insufficient – the energy dissipation function must involve higher order terms. Furthermore, the phase jump in both roll and sway observed at this frequency indicates that an abrupt change in the mechanism of vortex shedding must have taken place.

However, it has been concluded that this complex phenomena cannot be fully investigated by the adopted research methodology. Some information, although present in the recordings, could not be retrieved from the recorded signals because of the insufficient sampling rate but some quantities were not measured at all (e.g. waves patterns). On the other hand, the complexity of observed phenomena requires much more systematic studies, where scale of individual facts could be properly assessed. In the case of the damaged ship, there are many factors to be taken into account – such as shape, size and configuration of the opening and the flooded compartment, an effect of end conditions or mass properties of the model. Furthermore, some fundamental questions cannot be answered without performing of a dedicated forced sway experiment.

It has been anticipated that behaviour of a damaged ship must deviate significantly from that observed in the intact condition. This has been confirmed by the measurements but on the other hand, there is very little overlap in what was expected and what was observed. In particular, the observed scale of nonlinearity did not meet the anticipation – before commencing the experiments, it was thought that sloshing might have some very significant impact on the roll response. It clearly has but it appears that the impact of higher-order effects was diminished to some extent by the sloshing-induced drift.

Furthermore, it had been expected that the asymmetry of the model (e.g. large opening) would result in a strong non-harmonic response. Indeed, as discussed in the previous chapter, the measured moment to sustain motion was periodic but not harmonic at some frequencies but the deviations from the single-frequency response assumption were relatively small. Nevertheless, the time histories *contain* valuable information about instantaneous changes in the flow pattern. In the course of data post-processing, the information is lost but if the sampling frequency were higher, the data could provide high-quality figures for studying the complex nature of the flow. This could be particularly useful while comparing the experimental results with CFD prediction and therefore the issue of sampling frequency should be taken into account in future studies.

Chapter 7 Conclusions and future work

7.1 Summary

The present research shows significant discrepancies between the linear theory prediction and measurements in roll hydrodynamics but similar discrepancies are demonstrated by another experimental works. An attempt could be made to calculate the viscous corrections but it is unlikely that corrective terms, would bridge the gap. Obviously, there is a possibility that neglecting the viscous effects combined with the measurements error results in these substantial differences. However, the results are very consistent and therefore the differences would have to occur due to some systematic error. On the other hand, similar discrepancies are experienced in the most experimental works on roll hydrodynamics, thus it might be that the linear theory is deficient. Alternatively, it could be that the theoretical and experimental problems are different, or, as put by professor Pawłowski in private discussion

"[...] *in my opinion, the linear approach is consistent with reality as long as we do not make conceptual errors in its application*"

Hence, assuming that the linear theory is consistent with reality what are those *conceptual* errors?

The research behind this thesis cannot provide answer to this question. It can only indicate possible sources of discrepancies.

Firstly, in the analytical approach, we consider individual modes of motion separately – the wetted surface is subjected to a single mode oscillations. Such configuration is usually reproduced during the fixed-axis oscillations. Nevertheless, from the perspective of a floating body the configuration is artificial. A cylinder (to stay in the realm of two dimensions) of an arbitrary cross-section and an arbitrary centre of gravity will not realise the single mode oscillations. In the case studied here there were two modes of oscillations – sway and roll. It was demonstrated that from the mechanical perspective the oscillations were of single degree of freedom as the sway motion was completely determined by roll. The system was *kinematically* con-

strained and it was stated that the forces necessary to maintain the constraint are strong. In the investigated system, the only strong forces are inertia and restoring, both dependent on the mass distribution. The present research and the CFD studies (Gao et al., 2011a) indicate that in the unconstrained motion the hydrodynamic effects have different scale than in oscillations about the fixed axis. It would be speculative to judge to what extent these discrepancies are caused by the viscous effects but it is worth considering whether the strong nonlinearities reported in some experiments are not caused by the physical constraints resulting from the fixed axis of rotation. In fact, Ikeda carried out some of its experiments on vertical cylinders to minimise the impact of restoring and buoyancy on measurements.

Finally there is an interesting question concerning the tensor character of the added inertia and damping matrices as discussed in (Sadeghi and Incecik, 2005). Sadeghi and Incecik considered the 6×6 added inertia and damping matrices as partitioned matrices comprising of 3×3 block. They tested characters of the these blocks and concluded that some of them transformed like tensors, some like pseudotensors and some were just matrices. However, when the problem is reduced to the natural configuration of the sway-heave-roll (as in the present research) the 3×3 matrices in the equation of motion are second-order tensors. This follows directly from the quotient rule. Therefore, in the natural configuration the equations of motion are invariant under coordinate transformation. They hold in any frame of reference. It is noteworthy that after the heave motion was neglected, the system became a single degree of freedom oscillator. The single equation of motion was again expressed terms of tensor quantities. These simple facts are additional indication that the configuration of a system is very important. Irrespective of whether the system is subjected to the physical tests or to the analytical treatment, departing from the natural configuration introduce a risk that the measurements and the theory will diverge. The research presented here was also an adventure that started in a strong desire to find similarities in the experiment and the theoretical prediction but it happened that:

"[...] *he expected to find Piglet warming his toes in front of his fire, but to his surprise he saw that the door was open, and the more he looked inside the more Piglet wasn't there.*" (A.A. Milne: *The House at Pooh Corner*)

7.2 Conclusions

All the objectives have been met. In particular:

- The gyroscopic roll generator proved to be readily controllable device producing pure, virtually harmonic, roll moment. The initial problems with stiffness of the apparatus required only minor amendments following which the device performed very well within entire range of loads.
- The measurements were very difficult with particular problems concerning uncertainty in the phase angle estimation (caused by a random time latency of the motion capture system). This has been resolved by employing of an accelerometer as a reference for phase lag derivation.

Results of the final stage of measurements can be summarised as follows

- In the tested configuration, the measured hydrodynamic reaction (particularly damping) was very small which resulted in the relatively large uncertainties.
- Although it was anticipated that viscous effects might play significant role the experimentally derived coefficients exhibit weak dependency on roll amplitude (within the tested range).
- Results obtained for the flooded cylinder indicate rapid change in the vortex-shedding pattern observed at high frequencies where the phase jump occurs and the mathematical model inappropriately points to the negative work of dissipative forces.
- During the damaged ship measurements, significant drift of the model is observed at frequencies in proximity of the sloshing resonance. Impact of the drift on the hydrodynamic reaction cannot be easily assessed but it is presumed that it might be significant if tests are performed on a constrained model.
- The differences between theory and experiment are not easily explainable but there is an indication that the difference may be due to the system configuration in theoretical treatment and during the experiments. In principle, during physical tests a floating body oscillates about the ‘natural’ axis of rotation. Elevation of the axis varies with frequency and is determined by the position

of the centre of gravity of the body and coupling term (roll into sway) in the added inertia. Therefore, in 'natural' configuration body cannot oscillate about 'theoretical' axis lying in the calm-water plane without imposing additional constraints.

- Results show clearly that the tested model was a single degree of freedom oscillator. Entire sway contribution is rendered by the coupling coefficients of roll-into-sway.

7.3 Future work

The systematic research involving both CFD and experimental techniques is needed to address points raised in this thesis. In particular:

- Experiments should be performed on constrained and unconstrained model
- Roll experiments should be supplemented with forced sway measurements
- Experiments should be performed on cylinders of distinct shapes
- Study on viscous effects require broader range of roll amplitudes
- Effect of bilge keels should be investigated on an unconstrained body
- Experiments in flooded condition should allow testing in various configurations (geometries) of the flooded compartments and should involve variations in opening size
- Direct comparison with theory is possible only when configuration of the system is preserved by both methods. For that reason the vertical centre of gravity of the model should be adjusted in order to perform oscillations about axis lying in the calm-water plane

Chapter 8 References

ANKUDINOV, V. 1991. HYDRODYNAMIC HULL DAMPING (PHASE I). WASHINGTON D.C.: SHIP STRUCTURE COMITEE.

ARIS, R. 1962. *VECTORS, TENSORS AND THE BASIC EQUATIONS OF FLUID MECHANICS,* NEW YORK, DOVER PUBLICATIONS, INC.

BALCER, L. 2004. LOCATION OF SHIP ROLLING AXIS. *POLISH MARITIME RESEARCH.*

BASSLER, C. C., BELENKY, V., BULIAN, G., FRNACESCUTTO, A., SPYROU, K. J. & UMEDA, N. YEAR. A REVIEW OF AVAILABLE METHODS FOR APPLICATION TO SECOND LEVEL VULNERABILITY CRITERIA. *IN:* 10TH INTERNATIONAL CONFERECE ON STABILITY OF SHIPS AND OCEAN VEHICLES, 2009 SANKT PETERSBURG.

BASSLER, C. C., MILLER, R. & REED, A. M. 2012. CONSIDERATIONS FOR BILGE KEEL FORCE MODELS IN POTENTIAL FLOW SIMULATIONS OF SHIP MANOEUVRING IN WAVES. *12TH INTERNATIONAL SHIP STABILITY WORKSHOP.* WASINGTON D.C.

BASSLER, C. C., REED, A. M. & BROWN, A. J. 2010. A METHOD TO MODEL LARGE AMPLITUDE SHIP ROLL DAMPING. *11TH INTERNATIONAL SHIP STABILITY WORKSHOP.* WAGENINGEN, NETHERLANDS.

BEARMAN, P. W. & CURRIE, I. G. 1979. PRESSURE-FLUCTUATION MEASUREMENTS ON AN OSCILLATING CIRCULAR CYLINDER. *JOURNAL OF FLUID MECHANICS,* 91**,** 661-667.

BENJAMIN, T. B. & URSELL, F. 1954. THE STABILITY OF THE PLANE FREE SURFACE OF A LIQUID IN VERTICAL PERIODIC MOTION. *PROCEEDINGS OF THE ROYAL SOCIETY,* A255.

BORISENKO, A. I. & TARAPOW, I. E. 1976. *VECTOR AND TENSOR ANALYSIS WITH APPLICATIONS,* NEW YORK, DOVER PUBLICATIONS, INC.

BULIAN, G. 2004. ESTIMATION OF NONLINEAR ROLL DECAY PARAMETERS USING AN ANALYTICAL APPROXIMATE SOLUTION OF THE DECAY HISTORY. *INTERNATIONAL SHIPBUILDING PROGRESS,* 51**,** 5-32.

CANNON, R. H. J. 1967. *DYNAMICS OF PHYSICAL SYSTEMS,* MCGRAW-HILL BOOK COMPANY.

CARDO, A., FRANCESCUTTO, A. & NABERGOJ, R. 1981. ULTRAHARMONICS AND SUBHARMONICS IN THE ROLLING MOTION OF A SHIP: STEADY-STATE SOLUTION. *INTERNATIONAL SHIPBUILDING PROGRESS,* 28**,** 17.

CARDO, A., FRANCESCUTTO, A. & NABERGOJ, R. 1982. ON DAMPING MODELS IN FREE AND FORCED ROLLING MOTION. *OCEAN ENGINEERING,* 9**,** 171-179.

CHAI, S. 2005. *EXPERIMENTAL AND THEORETICAL INVESTIGATION OF THE HYDRODYNAMIC PROPERTIES OF DAMAGED SHIPS.* PHD, UNIVERSITY OF STRATHCLYDE.

CHESTER, W. 1968. RESONANT OSCILLATIONS OF WATER WAVES. I. THEORY. *PROCEEDINGS OF THE ROYAL SOCIETY OF LONDON,* 306**,** 17.

CHESTER, W. & BONES, J. A. 1968. RESONANT OSCILLATIONS OF WATER WAVES. II. EXPERIMENT. *PROCEEDINGS OF THE ROYAL SOCIETY OF LONDON,* 306**,** 16.

CICHOWICZ, J., JASIONOWSKI, A. & VASSALOS, D. 2010. UNCERTAINTY ASSESSMENT IN EXPERIMENTS ON A FLOATING BODY IN FORCED ROLL MOTION IN CALM WATER. *11TH INTERNATIONAL SHIP STABILITY WORKSHOP.* WAGENINGEN.

CICHOWICZ, J., VASSALOS, D. & JASIONOWSKI, A. YEAR. HYDRODYNAMICS OF DAMAGED SHIP IN ROLL MODE OF MOTION – AN EXPERIMENTAL APPROACH. *IN:* PROCEEDING OF THE 1ST INTERNATIONAL CONFERENCE ON ADVANCED MODEL MEASUREMENT TECHNOLOGY FOR THE EU MARITIME INDUSTRY, 2009 NANTES, FRANCE. 68-82.

CICHOWICZ, J., VASSALOS, D. & JASIONOWSKI, A. YEAR. EXPERIMENTS ON A FLOATING BODY SUBJECTED TO FORCED OSCILLATION IN CALM WATER AT THE PRESENCE OF AN OPEN-TO-SEA COMPARTMENT. *IN:* 12TH INTERNATIONAL SHIP STABILITY WORKSHOP, 2011 WASHINGTON D.C.

COLEMAN, H. W. & STEELE, W. G. 1999. *EXPERIMENTATION AND UNCERTAINTY ANALYSIS FOR ENGINEERS,* JOHN WILEY & SONS, INC.

CONTENTO, G., FRANCESCUTTO, A. & PICIULLO, M. 1996. ON THE EFFECTIVENESS OF CONSTANT COEFFICIENTS ROLL MOTION EQUATION. *OCEAN ENGINEERING,* 23**,** 597-618.

COTTON, B., THOMPSON, J. M. T. & SPYROU, K. J. 2000. *SOME RECENT ADVANCES IN THE ANALYSIS OF SHIP ROLL MOTION,* ELSEVIER.

DALZELL, J. F. 1978. A NOTE ON THE FORM OF SHIP ROLL DAMPING. *JOURNAL OF SHIP RESEARCH,* 22.

DE KAT, J. O. 2000. *DYNAMICS OF A SHIP WITH PARTIALLY FLOODED COMPARTMENT*.

DEMIRBILEK, Z. 1983A. ENERGY DISSIPATION IN SLOSHING WAVES IN A ROLLING RECTANGULAR TANK - I. MATHEMATICAL THEORY. *OCEAN ENGINEERING,* 10**,** 347-358.

DEMIRBILEK, Z. 1983B. ENERGY DISSIPATION IN SLOSHING WAVES IN A ROLLING RECTANGULAR TANK - II. SOLUTION METHOD AND ANALYSIS OF NUMERICAL TECHNIQUE. *OCEAN ENGINEERING,* 10.

DEMIRBILEK, Z. 1983C. ENERGY DISSPIATION IN SLOSHING WAVES IN A ROLLING RECTANGULAR TANK - III. RESULTS AND APPLICATIONS. *OCEAN ENGINEERING,* 10**,** 375-382.

DODWORTH, J. 2000. *THE APPLICATION OF POTENTIAL FLOW THEORY TO DAMAGED HULL DYNAMICS.* PHD, UNIVERISTY OF STRATHCLYDE.

DUDZIAK, J. 2008. *TEORIA OKRĘTU,* GDAŃSK, FUNDACJA PROMOCJI PRZEMYSŁU OKRĘTOWEGO I GOSPODARKI MORSKIEJ.

FRANCESCUTTO, A. & CONTENTO, G. 1994. AN EXPERIMENTAL STUDY OF THE COUPLING BETWEEN ROLL MOTION AND SLOSHING IN A COMPARTMENT. *ISOPE.* OSAKA.

FRANCESCUTTO, A., CONTENTO, G. & ARMENIO, V. 1996. A FULLY HYDRODYNAMIC APPROACH TO THE MOTION IN WAVES OF SHIPS WITH FREE SURFACE LIQUIDS ON BOARD. *11TH WORKSHOP ON WATER WAVES AND FLOATING BODIES.* HAMBURG.

FRANK, W. 1967. OSCILLATION OF CYLINDERS IN OR BELOW FREE SURFACE OF DEEP FLUIDS. WASHINGTON D.C.: NAVAL SHIP RESEARCH AND DEVELOPMENT CENTER.

FROUDE, W. 1861. ON ROLLING OF SHIPS. *PROCEEDINGS OF ROYAL INSTITUTION OF NAVAL ARCHITECTS.* LONDON: RINA.

GAO, Q., VASSALOS, D. & JASIONOWSKI, A. 2011A. NUMERICAL STUDY OF THE ROLL DECAY OF INTACT AND DAMAGED SHIPS. *12TH INTERNATIONAL SHIP STABILITY WORKSHOP.* WASHINGTON D.C.

GAO, Z., GAO, Q., JASIONOWSKI, A. & VASSALOS, D. 2011B. NUMERICAL STUDY OF DAMAGED SHIP MOTION IN WAVES. *12TH INTERNATIONAL SHIP STABILITY WORKSHOP.* WASHINGTON D.C.

HIMENO, Y. 1981. PREDICTION OF SHIP ROLLING DAMPING. A STATE OF THE ART. MICHIGAN UNIVERSITY.

IKEDA, Y., HIMENO, Y. & TANAKA, N. 1978A. COMPONENTS OF ROLL DAMPING OF SHIP AT FORWARD SPEED. OSAKA: UNIVERSITY OF OSAKA PREFECTURE.

IKEDA, Y., HIMENO, Y. & TANAKA, N. 1978B. ON EDDY MAKING COMPONENT OF ROLL DAMPING FORCE ON NAKED HULL. OSAKA: UNIVERSITY OF OSAKA PREFECTURE.

IKEDA, Y., KOMATSU, K., HIMENO, Y. & TANAKA, N. 1979. ON ROLL DAMPING FORCE OF SHIP - EFFECT OF HULL SURFACE PRESSURE CREATED BY BILGE KEELS. OSAKA: UNIVERSITY OF OSAKA PREFECTURE.

IKEDA, Y. & YOSHIYAMA, T. 1991. A STUDY ON FLUME-TYPE ANTIROLLING TANK. *JOURNAL OF KANSAI SOCIETY OF NAVAL ARCHITECTS.*

JASIONOWSKI, A. 2001A. ELEMENTS OF LIMIT STATE PERFORMANCE ASSESSMENT. GLASGOW: UNIVERSITY OF STRATHCLYDE.

JASIONOWSKI, A. 2001B. *AN INTEGRATED APPROACH TO DAMAGE SHIP SURVIVABILITY ASSESSMENT.* PHD, UNIVERSITY OF STRATHCLYDE.

JASIONOWSKI, A. 2010. STUDY OF THE SPECIFIC DAMAGE STABILITY PARAMETERS OF RO-RO PASSENGER VESSELS ACCORDING TO SOLAS 2009 INCLUDING WATER ON DECK CALCULATION. GLASGOW: THE SHIP STABILITY RESEARCH CENTRE.

JASIONOWSKI, A. & VASSALOS, D. 2002. DAMAGED SHIP HYDRODYNAMICS. *6TH INTERNATIONAL SHIP STABILITY WORKSHOP.* WEBB INSTITUTE, NY.

JASIONOWSKI, A., VASSALOS, D. & SCOTT, A. 2007. SHIP VULNERABILITY TO FLOODING. BERKELEY, CALIFORNIA: 3RD INTERNATIONAL CONFERENCE ON DESIGN FOR SAFETY.

JOHN, F. 1950. ON THE MOTION OF FLOATING BODIES II. *COMMUNICATIONS ON PURE AND APPLIED MATHEMATICS,* 3.

JOURNEE, J. M. J. 1992. QUICK STRIP THEORY CALCULATIONS IN SHIP DESIGN. *PRADS'92 CONFERENCE ON PRACTICAL DESIGN OF SHIPS AND MOBILE STRUCTURES.* NEWCASTLE UPON TIME, UK.

JOURNEE, J. M. J. 2000. FLUID TANKS AND SHIP MOTIONS. DELFT: DELFT UNIVERSITY OF TECHNOLOGY.

JOURNEE, J. M. J. & MASSIE, W. W. 2001. *OFFSHORE HYDROMECHANICS,* DELFT, DELFT UNIVERISTY OF TECHNOLOGY.

KAMBISSERI, R., HAMANO, T. & IKEDA, Y. 1997. EFFECT OF WATER INSIDE A SHIP ON ITS DAMAGE STABILITY. *7TH INTERNATIONAL OFFSHORE AND POLAR ENGINEERING CONFERENCE.* HONOLULU: THE INTERNATIONAL SOCIETY OF OFFSHORE AND POLAR ENGINEERS.

KATAYAMA, T., YOSHIOKA, Y. & KAKINOKI, T. 2012. A STUDY ON BILGE-KEEL COMPONENT OF ROLL DAMPING FOR TIME DOMAIN SIMULATION. *12TH INTERNATIONAL SHIP STABILITY WORKSHOP.* WASHINGTON D.C.

KONG, X. J. & FALTINSEN, O. M. YEAR. COUPLING BETWEEN SHIP MOTIONS AND FLOODING OF A DAMAGED SHIP IN

WAVES. *IN:* 9TH INTERNATIONAL CONFERENCE ON HYDRODYNAMICS, 2010 SHANGHAI.

KRĘŻELEWSKI, M. 1982. *HYDROMECHANIKA OGÓLNA I OKRĘTOWA,* GDAŃSK, POLITECHNIKA GDAŃSKA.

KURODA, T. & IKEDA, Y. 2003. EXTREME ROLL MOTION IN WIDE FREQUENCY RANGE DUE TO RAPID DRIFT MOTION. OSAKA: OSAKA PREFECTURE UNIVERSITY.

LAMB, S. H. 1932. *HYDRODYNAMICS,* NEW YORK, DOVER PUBLICATIONS.

LANCZOS, C. 1986. *THE VARIATIONAL PRINCIPLES OF MECHANICS,* NEW YORK, DOVER PUBLICATIONS, INC.

LETIZIA, L. 1996. *DAMAGE SURVIVABILITY OF PASSENGER SHIPS IN SEAWAY.* PHD, UNIVERSITY OF STRATHCLYDE.

MARSHALL, L. R., NAYFEH, A. H. & MOOK, D. T. 1982. FORWARD SPEED EFFECTS IN THE EQUATIONS OF SHIP MOTION. *JOURNAL OF SOUND AND VIBRATION,* 85.

MCQUARRIE, D. A. 2003. *MATHEMATICAL METHODS FOR SCIENTISTS AND ENGINEERS,* SAUSALITO, CALIFORNIA, UNIVERSITY SCIENCE BOOKS.

MOALEJI, R. & GREIG, A. R. 2007. ON THE DEVELOPMENT OF SHIP ANTI-ROLL TANKS. *OCEAN ENGINEERING***,** 18.

MURASHIGE, S. & AIHARA, K. 1998. EXPERIMENTAL STUDY ON CHAOTIC MOTION OF A FLOODED SHIP IN WAVES. *PROCEEDINGS OF THE ROYAL SOCIETY OF LONDON,* A**,** 16.

NA, J. H., LEE, W. C., SHIN, H. S. & PARK, I. K. YEAR. A DESIGN OF BILGE KEELS FOR HARSH ENVIRONMENT FPSO'S. *IN:* PROCEEDINGS OF THE 12TH INTERNATIONAL OFFSHORE AND POLAR ENGINEERING CONFERENCE, 2002 KITAKYUSHU, JAPAN. THE INTERNATIONAL SOCIETY OF OFFSHORE AND POLAR ENGINEERS.

ONGOREN, A. & ROCKWELL, D. 1988. FLOW STRUCTURE FROM AN OSCILLATING CYLINDER. PART1. MECHANISM OF PHASE SHIFT AND RECOVERY IN THE NEAR WAKE. *JOURNAL OF FLUID MECHANICS,* 191**,** 197-223.

PAPANIKOLAOU, A. & SHELLIN, T. 1992. A THREE-DIMENSIONAL PANEL METHOD FOR MOTIONS AND LOADS OF SHIPS WITH FORWARD SPEED. *SHIP TECHNOLOGY RESEARCH,* 39.

PAPANIKOLAOU, A. & SPANOS, D. 2002. ON THE MODELLING OF FLOODWATER DYNAMICS AND ITS EFFECTS ON SHIP MOTION. *6TH INTERNATIONAL SHIP STABILITY WORKSHOP.* NEW YORK.

PAWŁOWSKI, M. 1999. NONLINEAR MODEL OF SHIP ROLLING IN IRREGULAR WAVES. GDANSK: POLISH REGISTER OF SHIPPING.

PAWŁOWSKI, M. 2001. EQUATIONS OF SHIP MOTIONS. GDANSK: POLISH REGISTER OF SHIPPING.

PAWŁOWSKI, M. 2005. FALOWANIE MORSKIE. GDAŃSK: POLSKI REJESTR STATKÓW.

PLANK, W. S., BEARDSLEY, G. F., JR. & BURT, W. V. 1972. AN EXPERIMENTAL EVALUATION OF A PASSIVE ANTI-ROLL TANK SYSTEM. *OCEAN ENGINEERING,* 2**,** 131-139.

QUALISYS 2009. QUALISYS TRACK MANAGER. USER MANUAL. SWEDEN: QUALISYS AB.

RAVEN, H. C. 1997. THE NATURE OF NONLINEAR EFFECTS IN SHIP WAVE MAKING. *SHIP TECHNOLOGY RESEARCH,* 44.

ROGNEBAKKE, O. F. & FALTINSEN, O. M. 2003. COUPLING OF SLOSHING AND SHIP MOTIONS. *JOURNAL OF SHIP RESEARCH,* 47**,** 208-221.

RUPONEN, P. 2006. MODEL TESTS FOR PROGRESSIVE FLOODING OF A BOX-SHAPED BARGE. HELSINKI: HELSINKI UNIVERSITY OF TECHNOLOGY.

SADEGHI, K. 2005. *CLASSICAL AND APPROXIMATE METHODS IN THE DYNAMIC RESPONSE ANALYSIS OF A TRUSS SPAR IN WAVES.* PHD, UNIVERSITY OF NEWCASTLE UPON TYNE.

SADEGHI, K. & INCECIK, A. 2005. TENSOR PROPERTIES OF ADDED-MASS AND DAMPING COEFFICIENTS. *JOURNAL OF ENGINEERING MATHEMATICS*.

SEAH, R. K. M. & YEUNG, R. W. 2003. SWAY AND ROLL HYDRODYNAMICS OF CYLINDRICAL SECTIONS. *PROCEEDINGS OF THE 13TH INTERNATIONAL OFFSHORE AND POLAR ENGINEERING CONFERENCE.* HONOLULU.

SKALMIERSKI, B. 1994. *MECHANICS,* WARSZAWA, WYDAWNICTWO NAUKOWE PWN.

SPOUGE, J. R., IRELAND, N. & COLLINS, J. P. YEAR. LARGE AMPLITUDE ROLLING EXPERIMENT TECHNIQUES. *IN:* 3RD INTERNATIONAL CONFERENCE ON STABILITY OF SHIPS AND OCEAN VEHICLES, 1986 GDAŃSK.

SPYROU, K. J. 2004. NON-LINEAR DAMPING COEFFICIENTS FROM AN ASYMETRIC ROLL DECAY TIMESERIES. *PROCEEDINGS OF IMECHE*.

SPYROU, K. J. & THOMPSON, J. M. T. 2000. THE NONLINEAR DYNAMICS OF SHIP MOTIONS: A FIELD OVERVIEW AND SOME RECENT DEVELOPMENTS.

PHILOSOPHICAL TRANSACTIONS OF THE ROYAL SOCIETY OF LONDON. SERIES A, CONTAINING PAPERS OF A MATHEMATICAL OR PHYSICAL CHARACTER, 358**,** 1735-1760.

STANDING, R. G., JACKSON, G. E. & BROOK, A. K. 1992. EXPERIMENTAL AND THEORETICAL INVESTIGATION INTO THE ROLL DAMPING OF A SYSTEMATIC SERIES OF TWO-DIMENSIONAL BARGE SECTIONS. *BEHAVIOUR OF OFFSHORE STRUCTURES.* LONDON.

TAYLAN, M. 2000. THE EFFECT OF NONLINEAR DAMPING AND RESTORING IN SHIP ROLLING. *OCEAN ENGINEERING,* 27.

TURAN, O. 1993. *DYNAMIC STABILITY ASSESSMENT OF DAMAGED PASSENGER SHIPS USING A TIME SIMULATION APPROACH.* PHD, UNIVERSITY OF STRATHCLYDE.

URSELL, F. 1949. ON THE HEAVING MOTION OF A CIRCULAR CYLINDER ON THE SURFACE OF A FLUID. *QUARTERLY JOURNAL OF MECHANICS AND APPLIED MATHEMATICS,* 2.

VAN DAALEN, E. F. G., VAN GROESEN, E. & ZANDBERGEN, P. J. A HAMILTONIAN FORMULATION FOR NONLINEAR WAVE-BODY INTERACTIONS. ENSCHEDE: UNIVERISTY OF TWENTE, FACULTY OF APPLIED MATHEMATICS.

VAN DEN BOSCH, J. J. & VUGTS, J. H. 1966. SOME NOTES ON THE PERFORMANCE OF FREE SURFACE TANKS AS PASSIVE ANTI-ROLLING DEVICES. DELFT: TECHNOLOGICAL UNIVERSITY.

VASSALOS, D., HAMAMOTO, H., KAT, J. D., MOLYNEUX, D. & PAPANIKOLAOU, A. 1998. THE STATE OF THE ART IN MODELLING SHIP STABILITY IN WAVES. *25TH ATTC (AMERICAN TOWING TANK CONFERENCE).* IOWA.

VASSALOS, D., TURAN, O. & LETIZIA, L. 2000. *MODELLING THE ACCUMULATION OF WATER ON THE VEHICLE DECK OF A DAMAGED RO-RO VESSEL AND PROPOSAL OF SURVIVAL CRITERIA*, ELESVIER.

VERHAGEN, J. H. G. & WIJNGAARDEN, L. V. 1965. NON-LINEAR OSCILLATIONS OF FLUID IN A CONTAINER. *JOURNAL OF FLUID MECHANICS,* 22**,** 14.

VUGTS, J. H. 1968. THE HYDRODYNAMIC COEFFICIENTS FOR SWAYING, HEAVING AND ROLLING CYLLINDERS IN A FREE SURFACE. NETHERLANDS SHIP RESEARCH CENTRE TNO.

WEBSTER, W. C. 1975. THE FLOW ABOUT ARBITRARY, THREE-DIMENSIONAL SMOOTH BODIES. *JOURNAL OF SHIP RESEARCH,* 19**,** 206-218.

WEHAUSEN, J. V. 1969. USE OF LAGRANGIAN COORDINATES FOR SHIP WAVE RESISTANCE (FIRST- AND SECOND-ORDER THIN-SHIP THEORY). *JOURNAL OF SHIP RESEARCH*.

YASUKAWA, H. 2000. NONLINEAR TIME DOMAIN ANALYSIS OF HYDRODYNAMIC FORCES ON A SHIP ADVANCING IN WAVES. *4TH OSAKA COLLOQUIUM ON SEAKEEPING PERFORMANCE OF SHIPS.* OSAKA, JAPAN.

YEUNG, R. W., LIAO, S.-W. & RODDIER, D. 1998. HYDRODYNAMIC COEFFICIENTS OF ROLLING RECTANGULAR CYLLINDERS. *INTERNATIONAL JOURNAL OF OFFSHORE AND POLAR ENGINEERING,* 8**,** 9.

YUCK, R. H., LEE, D. H. & CHOI, H. S. 2003. ESTIMATION OF ROLL DAMPING COEFFICIENTS FOR NON-CONVENTIONAL MID-SHIP SECTIONS. *THE THIRTEENTH INTERNATIONAL OFFSHORE AND POLAR ENGINEERING CONFERENCE.* HONOLULU, HAWAII.

Appendix A Forcing mechanism

A.1 Design

An idea of using gyroscope to generate (or to counteract to) rolling moment is not entirely new. Such a device was built and successfully run at British Maritime Technology Ltd. during 1980's (Spouge et al., 1986) to carry out the experiments with large amplitude roll in calm water. The gyroscopic devices are also in use at the Vienna Model Basin (SVA) in Austria and at the MARIN in Netherlands.

A principal advantage of using gyroscopic roll generators for calm water tests is that the model can be oscillated by an internal device. Among the others, this feature allows the model to oscillate around "natural" (determined by hull geometry and its hydrodynamic characteristic) axis of rotation[24] (Balcer, 2004), which is of utmost importance if unsteady states or dynamics of systems with time-varying configuration (e.g. ship subjected to progressive flooding) are to be investigated.

Major downside of gyro-based forcing apparatus is that it, principally, allows generating only single degree of freedom angular oscillations. Furthermore, setting desired amplitude of motions involves usually "trial and error" approach. Nevertheless, performing measurements on freely floating body offers great opportunity to study dynamics of rolling motion of damaged ship in the most natural conditions and this seem to overrule other drawbacks of the approach.

A.1.1 Mechanical principles

The mechanical principles of the gyroscopic roll generator are very simple. They are based on a well-known fact that if the direction of the spin axis (of an axially- symmetrical body) is being changed (so-called torque induced precession) a reaction

[24] It is thought that constraining the model may introduce various changes to the flow around the body of difficult to assess impact on hydrodynamics. This is particularly important during large amplitude motions or in a case of a flooded body.

force (moment) will be induced. The reaction is proportional to the rate of change of the angular momentum (caused by the angular displacement of the spin axis).

Schematic picture of the two-axis gyro is presented in the figure *A.1.1*.

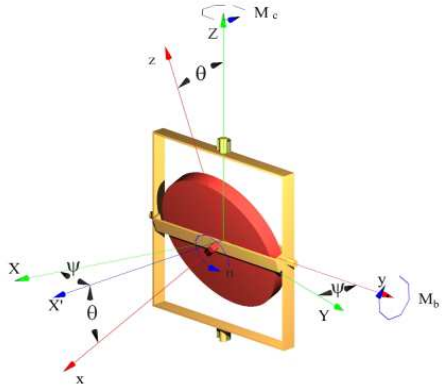

Fig. ***A.1.1****: Coordinate frames used to derive equations of motion.*

A rotor of the gyroscope is pivoted in the inner gimbal, which in turn is allowed for an angular displacement within the outer gimbal. For convenience, equations of motion of the system are usually expressed with use of three distinct co-ordinate frames, as shown in the figure *A.1.1*.

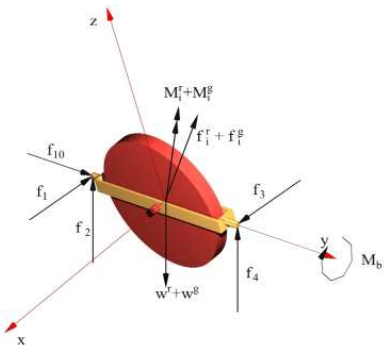

Fig. ***A.1.2:*** *Free-body diagram for system r(otor)+[inner]g(imbal).*

The system can be decomposed on two subsystems: first comprising the rotor and the inner gimbal and the second made up of the rotor and both gimbals[25]. Free-body diagrams of these sub-systems are shown below

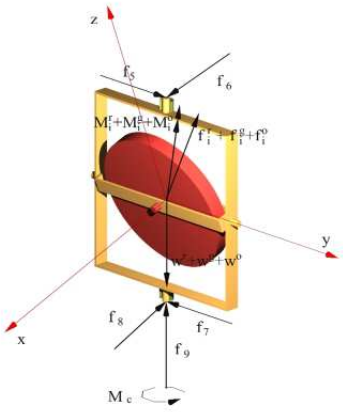

*Fig. **A.1.3:** Free-body diagram of the system r+g+o(uter gimbal).*

Angular velocities of the gimbals can be conveniently expressed as

$$\begin{aligned}\boldsymbol{\Omega}^{\beta} &= \dot{\psi}\mathbf{e}_Z \\ \boldsymbol{\Omega}^{\alpha} &= \boldsymbol{\Omega}^{\alpha/\beta} + \boldsymbol{\Omega}^{\beta} = \dot{\theta}\mathbf{e}_y + \dot{\psi}\mathbf{e}_Z\end{aligned} \tag{A.1.1}$$

where α denotes inner subsystem (rotor+inner gimbal), r denotes rotor, and β refers to the outer frame.

Inertial forces of the system components can be expressed by means of a vector equations

$$\begin{aligned}-\mathbf{M}_i{}^{r} &= \frac{d}{dt}\left(\mathbf{L}^{r}\right) = \overset{\alpha}{\mathbf{L}}{}^{r} + \boldsymbol{\Omega}^{\alpha}\times\mathbf{H}^{r} \\ -\mathbf{M}_i{}^{g} &= \frac{d}{dt}\left(\mathbf{L}^{g}\right) = \overset{\alpha}{\mathbf{L}}{}^{g} + \boldsymbol{\Omega}^{\alpha}\times\mathbf{L}^{g} \\ -\mathbf{M}_i{}^{o} &= \frac{d}{dt}\left(\mathbf{L}^{o}\right) = \overset{\beta}{\mathbf{L}}{}^{o} + \boldsymbol{\Omega}^{\beta}\times\mathbf{L}^{o}\end{aligned} \tag{A.1.2}$$

where $\mathbf{M}_i$ denote inertial moments, $\mathbf{L}$ stands for angular momentum, r, g and o denote rotor, inner system (rotor+inner gimbal) and outer (r+g+o) system respectively.

[25] More detailed derivation of the mathematical model can be found in (Cannon, 1967).

Greek indices above the symbols of angular momentum ($\mathbf{L}$) indicate time derivatives computed with respect to appropriate reference frames.

With the help of figure *A.1.1* equations of equilibrium for the inner and outer gimbals can be defined as

$$\begin{aligned}
&\textit{for system } r+g: \\
&\left(\sum \mathbf{M}\right)_y = 0 = \left(\mathbf{M}_i{}^r + \mathbf{M}_i{}^g\right)_y + \mathbf{M}_b \\
&\textit{for system } r+g+o: \\
&\left(\sum \mathbf{M}\right)_Z = 0 = \left(\mathbf{M}_i{}^r + \mathbf{M}_i{}^g + \mathbf{M}_i{}^o\right)_Z + \mathbf{M}_c
\end{aligned} \tag{A.1.3}$$

Time derivatives of the angular momentum in the rotating frames of refernce are given as

$$\begin{aligned}
&\overset{\alpha}{\mathbf{L}}{}^r = J_x{}^r\left(-\ddot{\psi}\sin\theta - \dot{\psi}\dot{\theta}\cos\theta\right)\mathbf{e}_x + J_y{}^r\ddot{\theta}\mathbf{e}_y + J_z{}^r\left(\ddot{\psi}\cos\theta - \dot{\psi}\dot{\theta}\sin\theta\right)\mathbf{e}_z \\
&\overset{\alpha}{\mathbf{L}}{}^g = J_x{}^g\left(-\ddot{\psi}\sin\theta - \dot{\psi}\dot{\theta}\cos\theta\right)\mathbf{e}_x + J_y{}^g\ddot{\theta}\mathbf{e}_y + J_z{}^g\left(\ddot{\psi}\cos\theta - \dot{\psi}\dot{\theta}\sin\theta\right)\mathbf{e}_z \\
&\overset{\beta}{\mathbf{L}}{}^o = J_Z{}^o\ddot{\psi}\mathbf{e}_Z
\end{aligned} \tag{A.1.4}$$

The vector products can be expanded as

$$\begin{aligned}
&\boldsymbol{\Omega}^\alpha \times \mathbf{L}^r = \dot{\psi}\dot{\theta}\left(J_z{}^r - J_y{}^r\right)\cos\theta\mathbf{e}_x + \left(\dot{\psi}^2\left(J_z{}^r - J_x{}^r\right)\sin\theta\cos\theta + J_x{}^r\dot{\psi}n\cos\theta\right)\mathbf{e}_y + \\
&+\left(\dot{\psi}\dot{\theta}\left(J_x{}^r - J_y{}^r\right)\sin\theta - J_x{}^r\dot{\theta}n\right)\mathbf{e}_z \\
&\boldsymbol{\Omega}^\alpha \times \mathbf{L}^g = \dot{\psi}\dot{\theta}\left(J_z{}^g - J_y{}^g\right)\cos\theta\mathbf{e}_x + \dot{\psi}^2\left(J_z{}^g - J_x{}^g\right)\sin\theta\cos\theta\mathbf{e}_y + \dot{\psi}\dot{\theta}\left(J_x{}^g - J_y{}^g\right)\sin\theta\mathbf{e}_z \\
&\boldsymbol{\Omega}^\beta \times \mathbf{L}^o = \mathbf{0}
\end{aligned} \tag{A.1.5}$$

where *J* denotes mass moment of inertia of the rotor (*r*), inner gimbal (*g*) and outer gimbal (hull) (*o*) with respect to appropriate axes (subscript indices).

The above equations can be further simplified with help of the following identities

$$J_x{}^r + J_x{}^g \overset{D}{=} J_x \quad J_y{}^r + J_y{}^g \overset{D}{=} J_x \quad J_z{}^r + J_z{}^g \overset{D}{=} J_z \quad J_x{}^r \cdot n \overset{D}{=} h \tag{A.1.6}$$

where *h* stands for constant “spin” momentum of the rotor.

Equations (A.1.4), (A.1.5) and (A.1.6) can be substituted into (A.1.3), which leads to the set of two scalar equations

$$\begin{aligned} &\ddot{\theta} J_y + \dot{\psi}^2 \left(J_z - J_x \right) \sin\theta \cos\theta + \dot{\psi} h \cos\theta = M_b \\ &\ddot{\psi} \left(J_z \cos^2\theta + J_x \sin^2\theta + J_Z{}^o \right) - \dot{\theta} h \cos\theta + 2 \left(J_x - J_z \right) \dot{\psi} \dot{\theta} \sin\theta \cos\theta = M_c \end{aligned} \tag{A.1.7}$$

The above equations determine configuration of the gyroscopic mechanism for forced roll experiments. That is, the gyroscope should be fitted to the hull model with the *OZ* axis parallel to the roll axis. The outer gimbal should be rigidly connected to the model while the inner gimbal should be displaced with the torque M_b (about *OY* axis). Thus, given that there is no external moment applied about axis *OZ* (M_c=0), the second equation of the (A.1.7) could be rewritten in the form

$$\ddot{\psi} \left(J_z \cos^2\theta + J_x \sin^2\theta + J_Z{}^o \right) + 2 \left(J_x - J_z \right) \dot{\psi} \dot{\theta} \sin\theta \cos\theta = \dot{\theta} h \cos\theta \tag{A.1.8}$$

The RHS of the above equation represents the ("external") rolling moment and the LHS corresponds to hull response[26].

However, careful investigation of the equations (A.1.4) and (A.1.5) reveals that single gyroscope would also produce a moment component about the *OX* axis. In order to cancel this undesired coupling second gyroscope of the same inertia parameters has to be fitted to the model – its rotor's precession and spin equal in magnitude but opposite in direction to the precession and spin of the first gyroscope. The rolling moment produced by the coupled gyroscopes with kinematical constrain in ψ is given as

$$M_{coupled} \left(t, \psi(t) = 0 \right) = 2 \dot{\theta} h \cos\theta \tag{A.1.9}$$

The kinematic constrain imposed on the system is valid only for conditions of stationary calibration, and therefore during actual rolling the quadratic and double[27] an-

[26] This equation describes motion of the pivoted hull rolling about *OZ* axis. In the case of single DoF oscillations of a floating body it should be supplemented with corresponding added inertia, damping and restoring forces.

[27] Products $\sin\theta \cos\theta$

gle harmonic terms in the equation (A.1.7) would be present. Their impact on actual forcing moment can be assessed as shown in the following section.

A.1.2 Design

The design objectives had been primarily pre-defined by the fact that the existing model was to be used in the experiment. Total displacement of the model was about 150 kg at the hull mass of about 50 kg. This limited maximum mass of the device to about 50 kg (the reserve of 50kg was necessary to accommodate for the floodwater inside the flooded compartment). The mechanism was required to generate the rolling moment (at roll amplitude 2 degrees) within 0.1-5 Hz[28] frequency range. The maximum rotors' speed should not exceed 10 000 rpm.

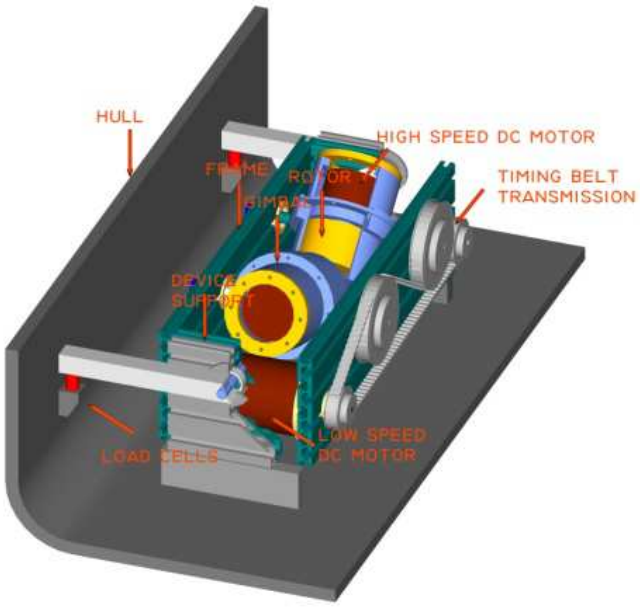

*Fig. **A.1.4:** Design concept*

The calculations based on the predicted hydrodynamic and hydrostatic properties of the model indicated that two rotors of mass 5kg each and spinning at rate of 7 000 rpm should generate sufficient momentum to maintain the required roll amplitude at

[28] Upper boundary used for strength calculations not for an actual rolling experiment.

the lowest frequency. For safety reasons rotors it was decided to enclose rotors in the thick-walled aluminium casings.

In order to maintain equal precession of the gimbals a synchronous belt transmission driven by one DC motor was used. In order to reduce mass of the device it was decided not to use any additional reduction gearbox at the motor shaft and therefore gear ratio had been determined by the size of timing pulleys (~1:4)[29].

The rotors were directly driven by small, high speed (7000 rpm at 100V), DC motors. Power feed and control signals were transmitted to motors through the low-noise slip rings with gold-on-gold contacts.

Transmission and gimbals bearing housings were fitted to the side plates of the bolted aluminium case (frame).

The assembled device had maximum dimensions of 680x340x220 mm (these include transmission and slip rings). Mass of the generator did not exceed 50 kg.

Special attention was paid to the fitting of the device to the model – in order to minimise possibility of lateral loads on the load-cell the gyro was pivoted on a separate frame (with bearings axis lying in the centre-plane of the model) with rotation about the pivoting axis constrained by the transducer. The frame was then fixed to the top of the model. Another advantage of the pivoting was that it allowed for some adjustments in the vertical position of centre of gravity of the model – the mechanism could be fixed to either side of the frame and therefore about 1/3 of the model mass can be easily moved by about 60 mm in a vertical direction.

Gimbals and rotors were design in a way ensuring negligible contribution of quadratic and double angle harmonic terms to the generated moment (see equation (A.1.7)). The estimates show that the magnitude of the periodic inertia variations was about 0.006 and 0.013 kgm^2 for the quadratic and double-angle terms respectively

[29] At later stages, the low-speed DC motor has been replaced with digitally controlled AC motor fitted with 1:10 mechanical gearbox.

(calculated about the axes of precession)[30]. This corresponds to about 0.06 and 0.12% of the dry hull inertia. Therefore, it can be assumed that impact of the instantaneous changes of inertia is negligible.

A.1.3 Operational aspects

The first runs of the mechanism showed that the device was easy to set and controllable. Nevertheless, the deployment phase exposed number of problems that could be split into two categories: mechanical and control-related. Mechanically, the gyroscope's case proved to be insufficiently stiff and its twisting could be observed even at moderate loads. Furthermore, use of single torque arm fitted on the pivoting shaft led to a damage of the keyway connection. The problems were resolved by reinforcing middle part of the case frame and fitting a torque arm made of thick L-shaped plate fixed to the side of the case at the reinforcing rib.

The control related problems had serious operational implications. Most importantly, the drives for the high speed motors recommended by the motors' manufacturer allowed for running them with only 70% of nominal speed (4900 instead of 7000 rpm) reducing output moment at the lowest (and most crucial) frequencies from expected 7.4 to 5.2 Nm.

Furthermore, the controllers did not perform well at higher gain settings. It was very difficult to tune (synchronise) the gyroscopes (in terms of gain-current couple settings needed to attain the same acceleration-deceleration pattern at dynamic load changes). Eventually it was decided to use the maximum safe settings for gain but "by-pass" the controllers and use the power supplies[31] in order to set the voltage and to control the speed adjustment dynamics.

---

[30] Although gyroscopes are balanced, during gimbals' rotation (precession) the mass distribution of the hull with fitted gyroscopes changes. This produces time variations of the total inertia about roll axis.

[31] The drives kept tripping the motors while accelerating at the high gain/current settings. This often led to some potentially dangerous situations with model suddenly forced to conical motion (roll in-phase with yaw).

Another difficulty related to high-speed motors was the lack of control dynamics in the feedback loop observable particularly at lower speeds. This can be solely endorsed to the fact that Hall sensors instead of digital encoders were used for speed feedback.

Low-speed motor (driving synchronous transmission) worked generally very well, except predictable difficulties while running at very low speeds. However, bearing in mind that target minimal roll frequency corresponds to 0.1 Hz, it requires, at gear ratio 1:4, the motor to run with 24 rpm. During high frequency runs, the only observed issue was acoustic noise of the transmission. Nevertheless, due to winding damage, the low-speed motor had to be replaced with an AC motor fitted with the 1:10 mechanical gearbox (the results presented here are obtained with use of this motor). This undesired change in the configuration resulted in much better operability of the device over the whole frequency range.

The single point force measurement proved to be one of the most reliable components. The force measurements were performed with use of a simple 500lb strain transducer calibrated over entire range. It is assumed that due to plain construction of the gauge the readings were satisfactorily precise and unaffected by transducer's own inertia and damping.

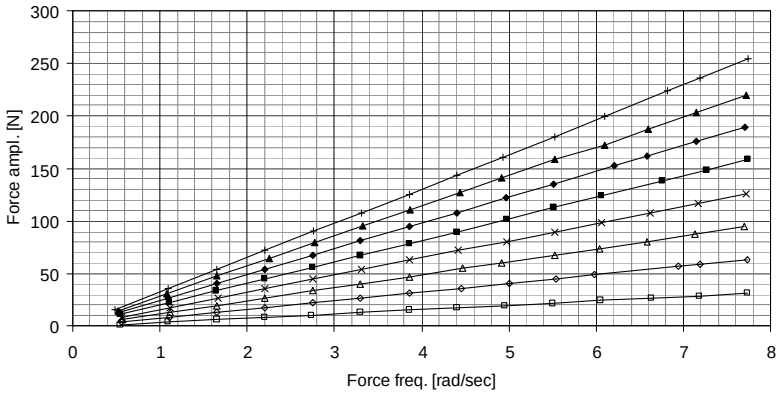

Fig. ***A.1.5:*** *Characteristics of the forcing mechanism obtained for rotors' spin within range 500-4000 rpm with 500 rpm step.*

The by-passing (the term is used here colloquially) of controllers means that drives' output current was limited by the supply output. This temporary solution worked well and such arrangement prevented accidental overloads and subsequent unintentional tripping of the motors.

A.2 Construction

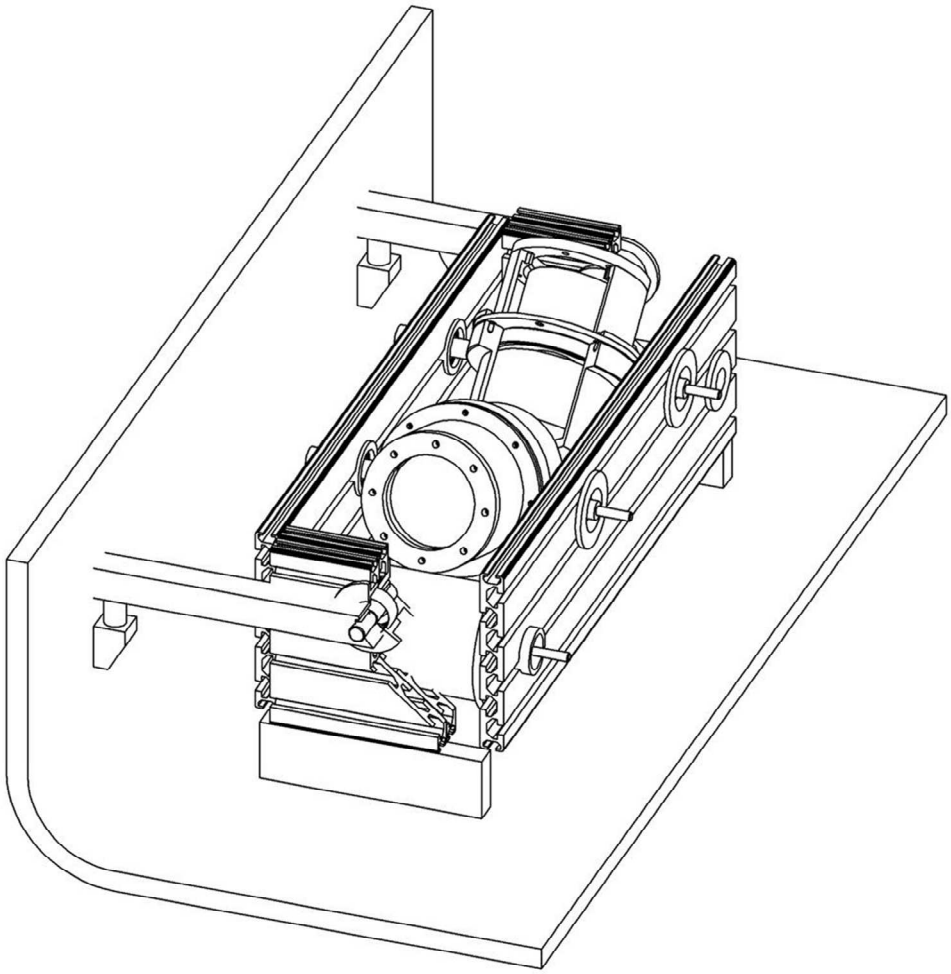

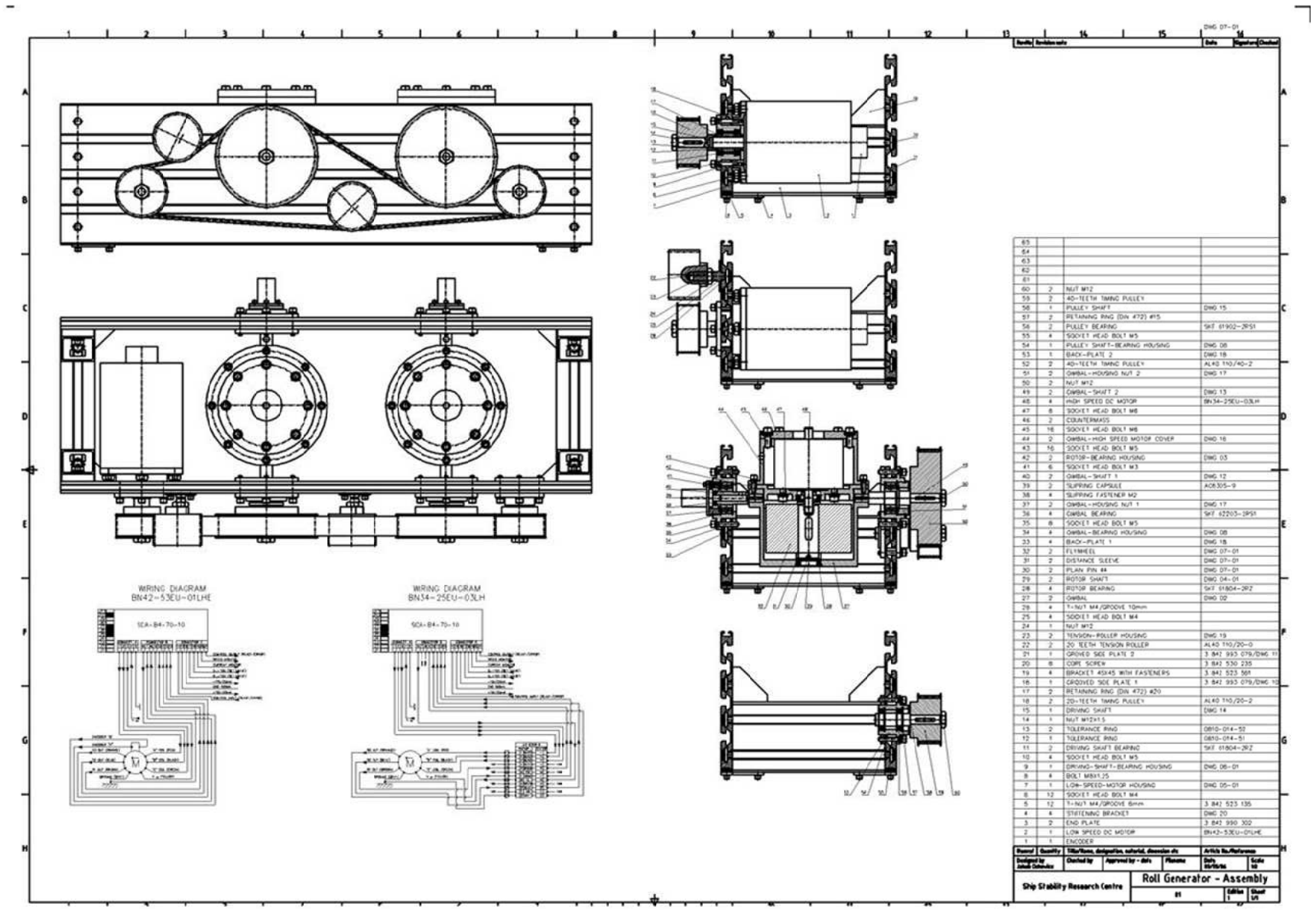

65			
64			
63			
62			
61			
60	2	NUT M12	
59	2	40-TEETH TIMING PULLEY	
58	1	PULLEY SHAFT	DWG 15
57	2	RETAINING RING (DIN 472) #15	
56	2	PULLEY BEARING	SKF 61902-2RS1
55	4	SOCKET HEAD BOLT M5	
54	1	PULLEY SHAFT-BEARING HOUSING	DWG 08
53	1	BACK-PLATE 2	DWG 18
52	2	40-TEETH TIMING PULLEY	ALAS 110/40-2
51	2	GIMBAL-HOUSING NUT 2	DWG 17
50	2	NUT M12	
49	2	GIMBAL-SHAFT 2	DWG 13
48	4	HIGH SPEED DC MOTOR	BN34-25EU-03LH
47	8	SOCKET HEAD BOLT M6	
46	2	COUNTERMASS	
45	16	SOCKET HEAD BOLT M6	
44	2	GIMBAL-HIGH SPEED MOTOR COVER	DWG 16
43	16	SOCKET HEAD BOLT M5	
42	2	ROTOR-BEARING HOUSING	DWG 03
41	6	SOCKET HEAD BOLT M3	
40	2	GIMBAL-SHAFT 1	DWG 12
39	2	SLIPPING CAPSULE	AOR305-9
38	4	SLIPPING FASTENER M2	
37	2	GIMBAL-HOUSING NUT 1	DWG 17
36	4	GIMBAL BEARING	SKF 62203-2RS1
35	8	SOCKET HEAD BOLT M5	
34	4	GIMBAL-BEARING HOUSING	DWG 08
33	4	BACK-PLATE 1	DWG 18
32	2	FLYWHEEL	DWG 07-01
31	2	DISTANCE SLEEVE	DWG 07-01
30	2	PLAIN PIN #4	DWG 07-01
29	2	ROTOR SHAFT	DWG 04-01
28	4	ROTOR BEARING	SKF 61804-2RZ
27	2	GIMBAL	DWG 02
26	4	T-NUT M4/GROOVE 10mm	
25	4	SOCKET HEAD BOLT M4	
24	1	NUT M12	
23	2	TENSION-ROLLER HOUSING	DWG 19
22	2	20 TEETH TENSION ROLLER	ALAS 110/20-0
21	1	GROVED SIDE PLATE 2	3 842 993 079/DWG 11
20	8	CORE SCREW	3 842 530 235
19	4	BRACKET 45X45 WITH FASTENERS	3 842 523 361
18	1	GROOVED SIDE PLATE 1	3 842 993 079/DWG 10
17	2	RETAINING RING (DIN 472) #20	
16	2	20-TEETH TIMING PULLEY	ALAS 110/20-2
15	1	DRIVING SHAFT	DWG 14
14	1	NUT M12X1.5	
13	2	TOLERANCE RING	0810-014-52
12	1	TOLERANCE RING	0810-014-51
11	2	DRIVING SHAFT BEARING	SKF 61804-2RZ
10	4	SOCKET HEAD BOLT M5	
9	1	DRIVING-SHAFT-BEARING HOUSING	DWG 06-01
8	8	BOLT M8X1.25	
7	1	LOW-SPEED-MOTOR HOUSING	DWG 05-01
6	12	SOCKET HEAD BOLT M4	
5	12	T-NUT M4/GROOVE 8mm	3 842 523 135
4	4	STIFENING BRACKET	DWG 20
3	2	END PLATE	3 842 990 302
2	1	LOW SPEED DC MOTOR	BN42-53EU-01LHE
1	1	ENCODER	

Name/	Quantity	Title/Name, designation, material, dimension etc.	Article No./Reference
Designed by: Jakub Dobrokes	Checked by:	Approved by - date:	Filename:
Date: 05/05/06	Scale: 1:2		
Ship Stability Research Centre	Roll Generator - Assembly		
	01	Edition: 1	Sheet: 1/1

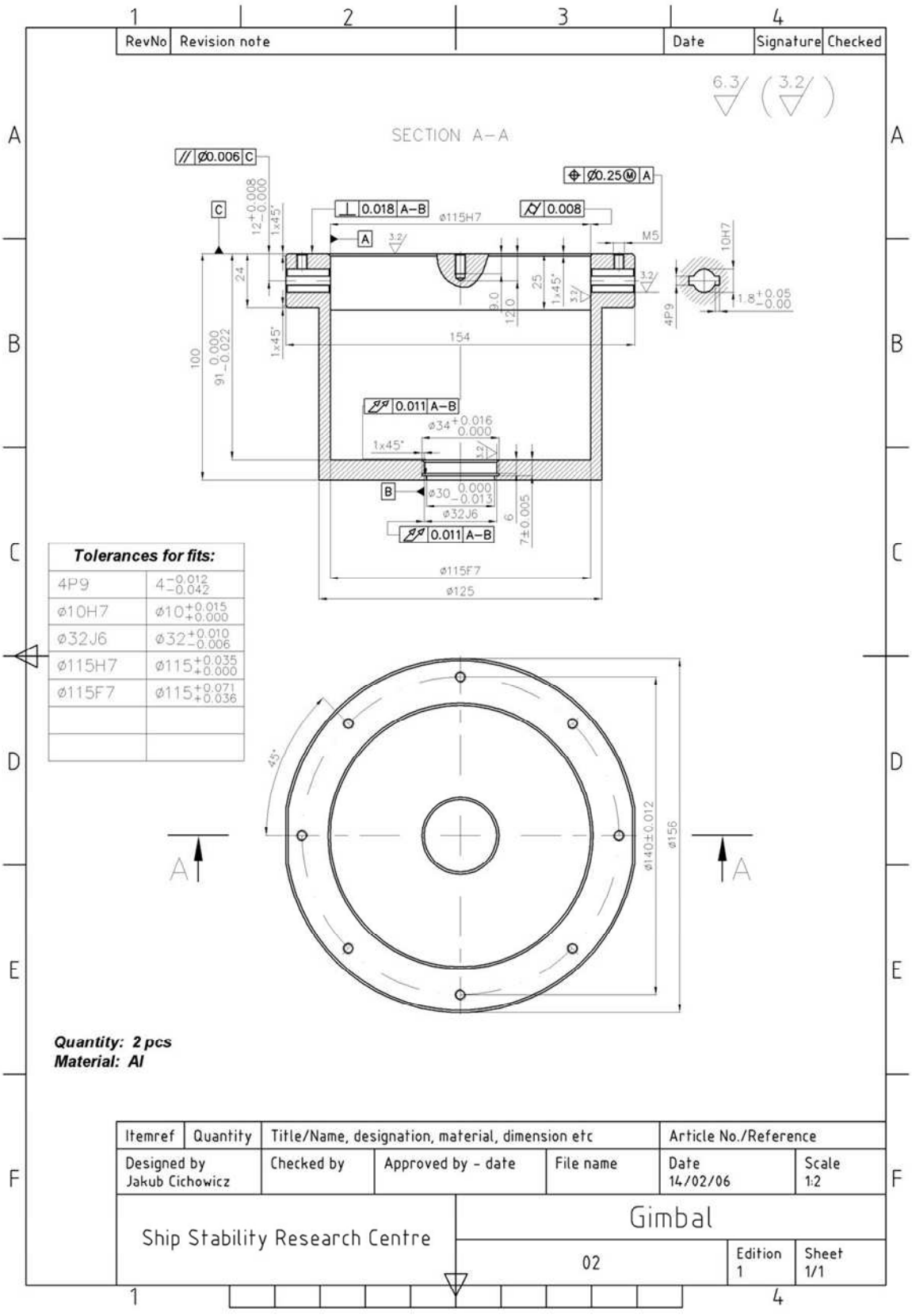
RevNo
Revision note
Date
Signature
Checked
SECTION A–A
Tolerances for fits:
4P9
ø10H7
ø32J6
ø115H7
ø115F7
Quantity: 2 pcs
Material: Al
Itemref
Quantity
Title/Name, designation, material, dimension etc
Article No./Reference
Designed by Jakub Cichowicz
Checked by
Approved by - date
File name
Date 14/02/06
Scale 1:2
Ship Stability Research Centre
Gimbal
02
Edition 1
Sheet 1/1

Note: the part manufactured of brass not aluminium as in the drawing.

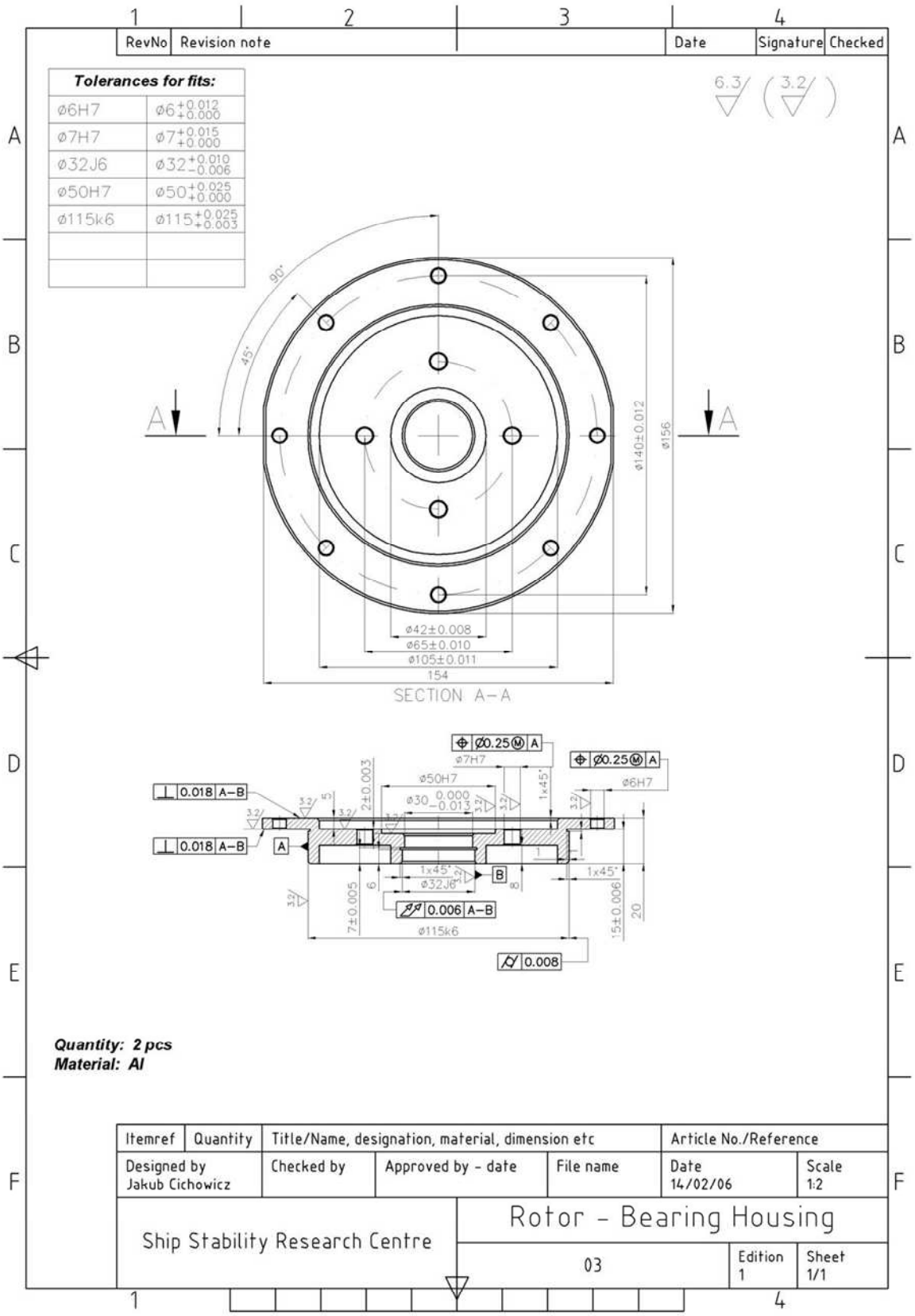

RevNo	Revision note	Date	Signature	Checked
1	Corr. bearing journal diameters	06/03/06		

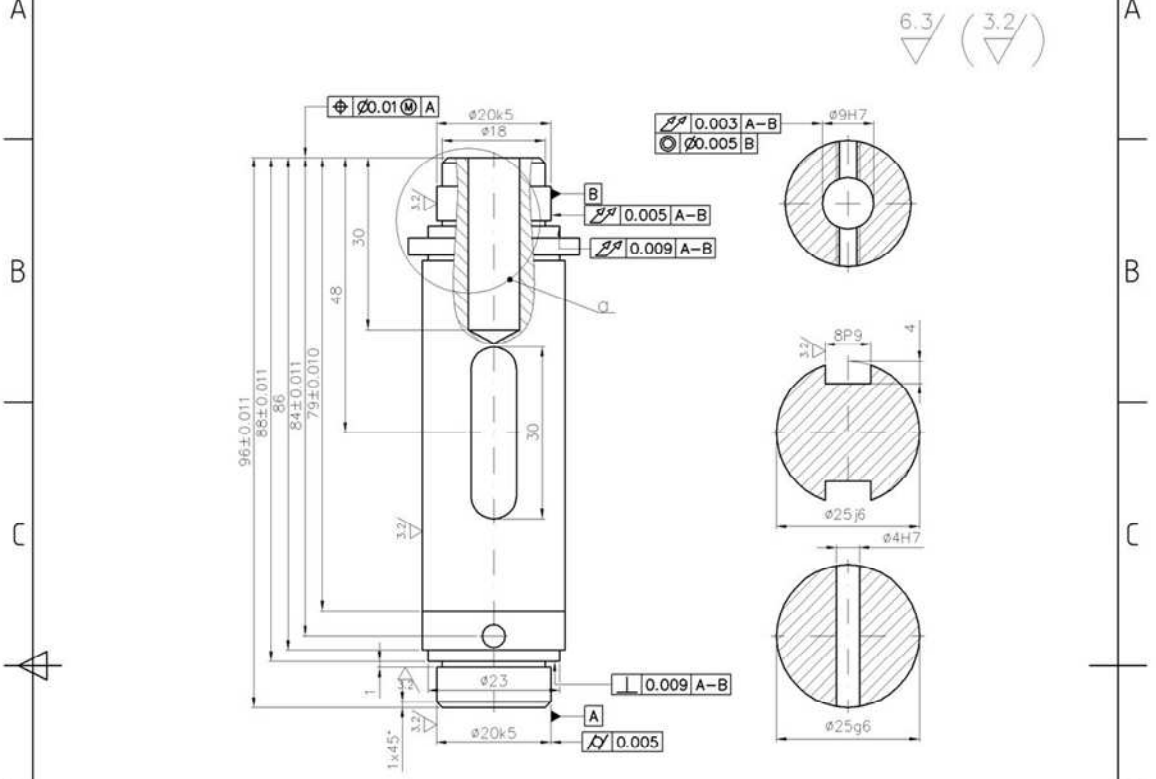

Tolerances for fits:	
ø4H7	$\varnothing 4^{+0.012}_{+0.000}$
8P9	$8^{-0.015}_{-0.051}$
ø9H7	$\varnothing 9^{+0.015}_{+0.000}$
ø20k5	$\varnothing 20^{+0.011}_{+0.002}$
ø25g6	$\varnothing 25^{-0.004}_{-0.017}$
ø25j6	$\varnothing 25^{+0.009}_{-0.004}$

Quantity: 2 pcs
Material: Steel

Itemref	Quantity	Title/Name, designation, material, dimension etc			Article No./Reference	
Designed by Jakub Cichowicz		Checked by	Approved by - date	File name	Date 17/02/06	Scale 1:1
Ship Stability Research Centre					Rotor - Shaft	
					04-01	Edition 1 / Sheet 1/1

RevNo	Revision note	Date	Signature	Checked
1	Corr. hole positions and key	10/03/06		

Tolerances for fits:	
ø9H7	$ø9^{+0.015}_{+0.000}$
10H7	$10^{+0.015}_{+0.000}$
ø45H7	$ø45^{+0.025}_{+0.000}$
ø70H7	$ø70^{+0.030}_{+0.000}$

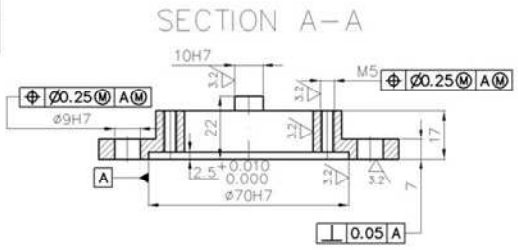

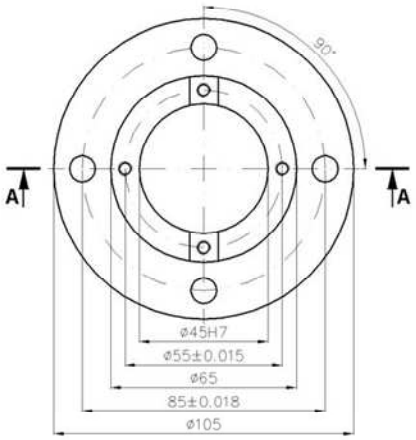

Quantity: 1 pc
Material: Al

Itemref	Quantity	Title/Name, designation, material, dimension etc			Article No./Reference	
Designed by Jakub Cichowicz		Checked by	Approved by - date	File name	Date 23/02/06	Scale 1:2
Ship Stability Research Centre					Low-Speed Motor Housing	
					05-01	Edition 1 / Sheet 1/1

RevNo	Revision note	Date	Signature	Checked
1	Corrected hole positions	10/03/06		

6.3 (3.2)

SECTION A–A

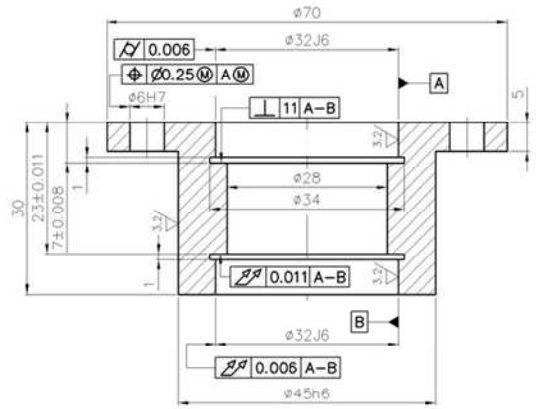

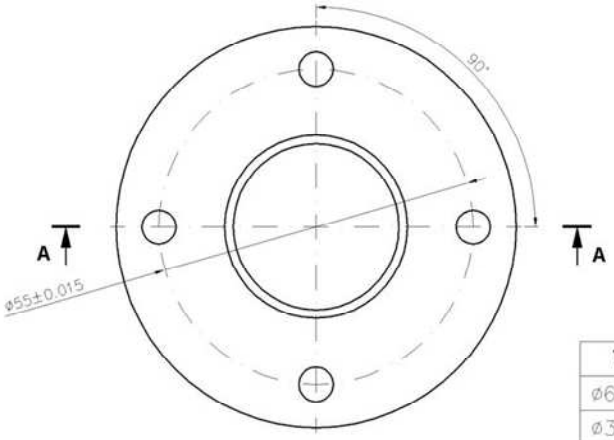

Tolerances for fits:	
ø6H7	$ø6^{+0.012}_{+0.000}$
ø32J6	$ø32^{+0.010}_{-0.006}$
ø45h6	$ø45^{+0.000}_{-0.016}$

Quantity: 1 pc
Material: Al

Itemref	Quantity	Title/Name, designation, material, dimension etc			Article No./Reference	
Designed by Jakub Cichowicz		Checked by	Approved by - date	File name	Date 23/02/06	Scale 1:1
Ship Stability Research Centre			Driving Shaft Housing			
			06-01		Edition 1	Sheet 1/1

RevNo	Revision note	Date	Signature	Checked
1	Corrected distance sleeve	06/03/06		

ROTOR

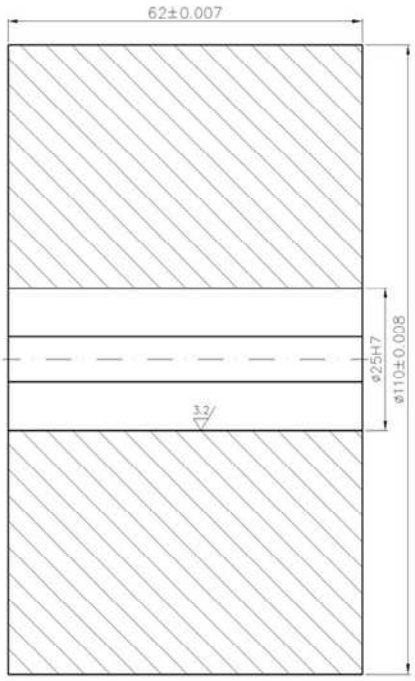

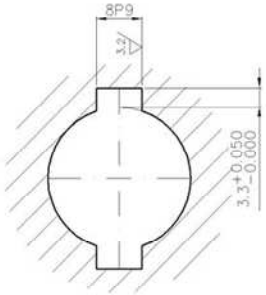

DISTANCE SLEEVE

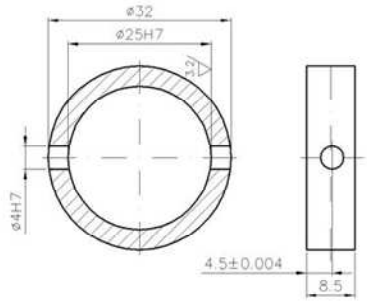

PLAIN PIN

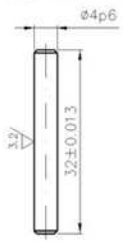

Tolerances for fits:	
ø4H7	$ø4^{+0.012}_{+0.000}$
ø4p6	$ø4^{+0.020}_{+0.012}$
ø25H7	$ø25^{+0.021}_{+0.000}$

Quantity: 2 pcs (each part)
Material: Brass (rotor), Steel (sleeve and pin)

Itemref	Quantity	Title/Name, designation, material, dimension etc			Article No./Reference	
Designed by Jakub Cichowicz		Checked by	Approved by - date	File name	Date 23/02/06	Scale 1:1
Ship Stability Research Centre			Rotor and Assemblies		07-01	Edition 1 / Sheet 1/1

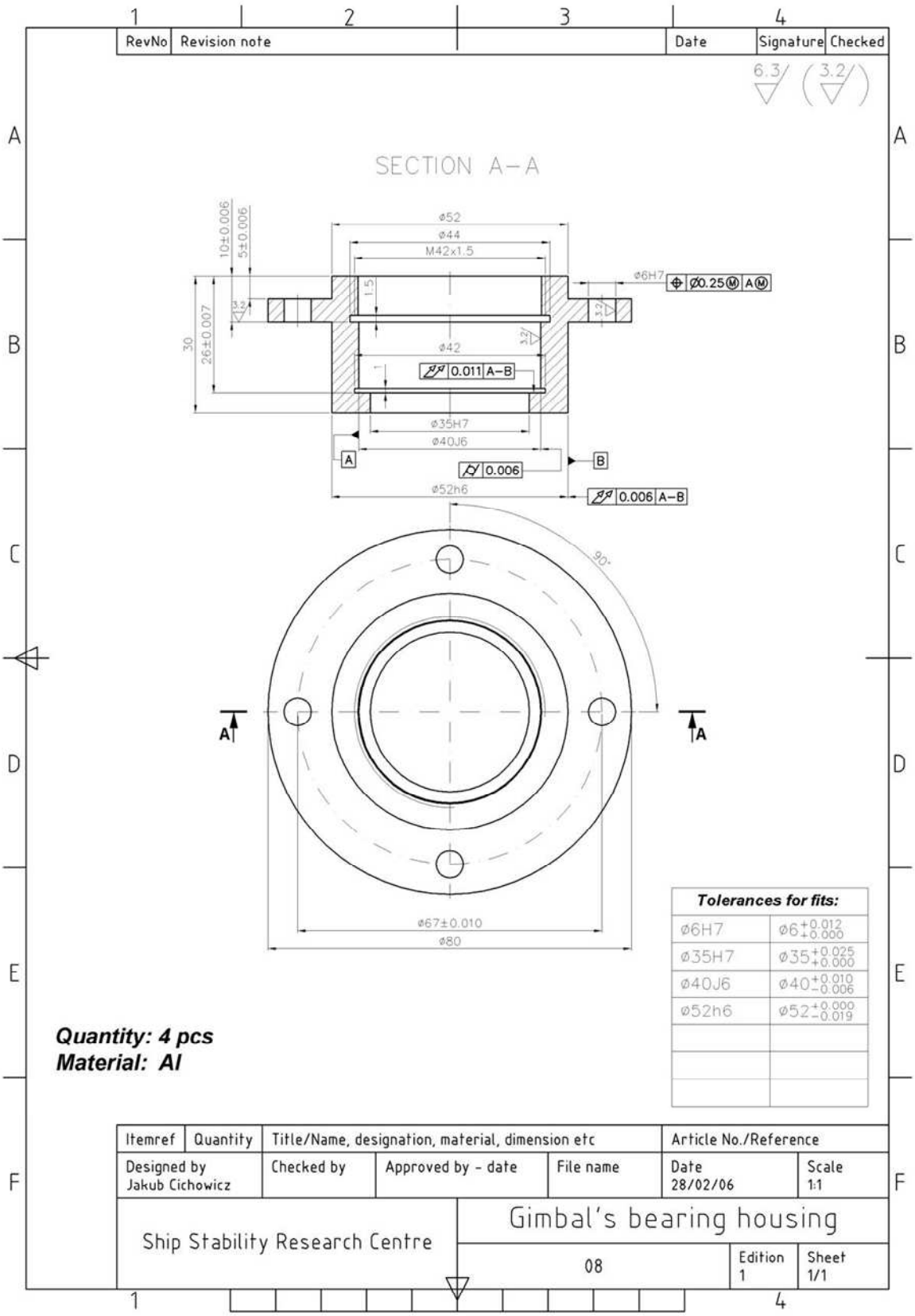
RevNo
Revision note
Date
Signature
Checked
6.3
3.2
SECTION A–A
ø52
ø44
M42x1.5
10±0.006
5±0.006
ø6H7
Ø0.25 M A M
1.5
3.2
30
26±0.007
ø42
0.011 A–B
ø35H7
ø40J6
A
B
0.006
ø52h6
0.006 A–B
90°
A
A
ø67±0.010
ø80
Quantity: 4 pcs
Material: Al
Tolerances for fits:
ø6H7
ø6 +0.012 +0.000
ø35H7
ø35 +0.025 +0.000
ø40J6
ø40 +0.010 −0.006
ø52h6
ø52 +0.000 −0.019
Itemref
Quantity
Title/Name, designation, material, dimension etc
Article No./Reference
Designed by
Jakub Cichowicz
Checked by
Approved by - date
File name
Date
28/02/06
Scale
1:1
Ship Stability Research Centre
Gimbal's bearing housing
08
Edition
1
Sheet
1/1

RevNo	Revision note	Date	Signature	Checked

6.3 (3.2)

SECTION A–A

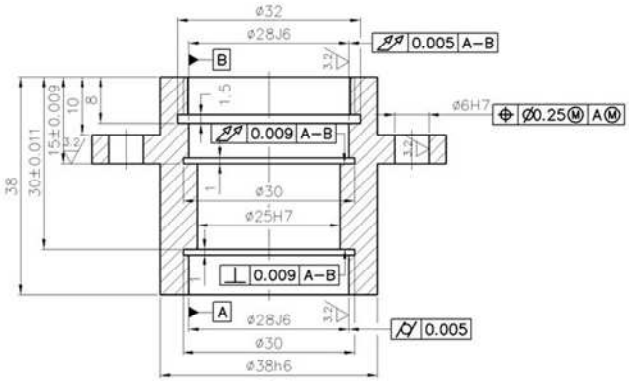

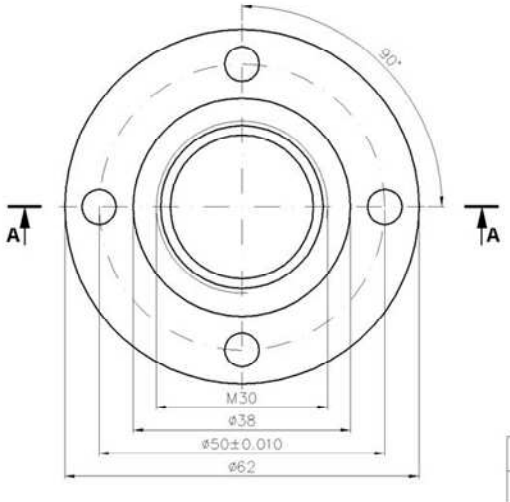

Tolerances for fits:	
ø6H7	$ø6^{+0.012}_{+0.000}$
ø25H7	$ø25^{+0.021}_{+0.000}$
ø28J6	$ø28^{+0.008}_{-0.005}$
ø38h6	$ø38^{+0.000}_{-0.016}$

Quantity: 1 pc
Material: Al

Itemref	Quantity	Title/Name, designation, material, dimension etc			Article No./Reference	
Designed by Jakub Cichowicz		Checked by	Approved by - date	File name	Date 06/03/06	Scale 1:1
Ship Stability Research Centre			Pulley's shaft housing			
			09		Edition 1	Sheet 1/1

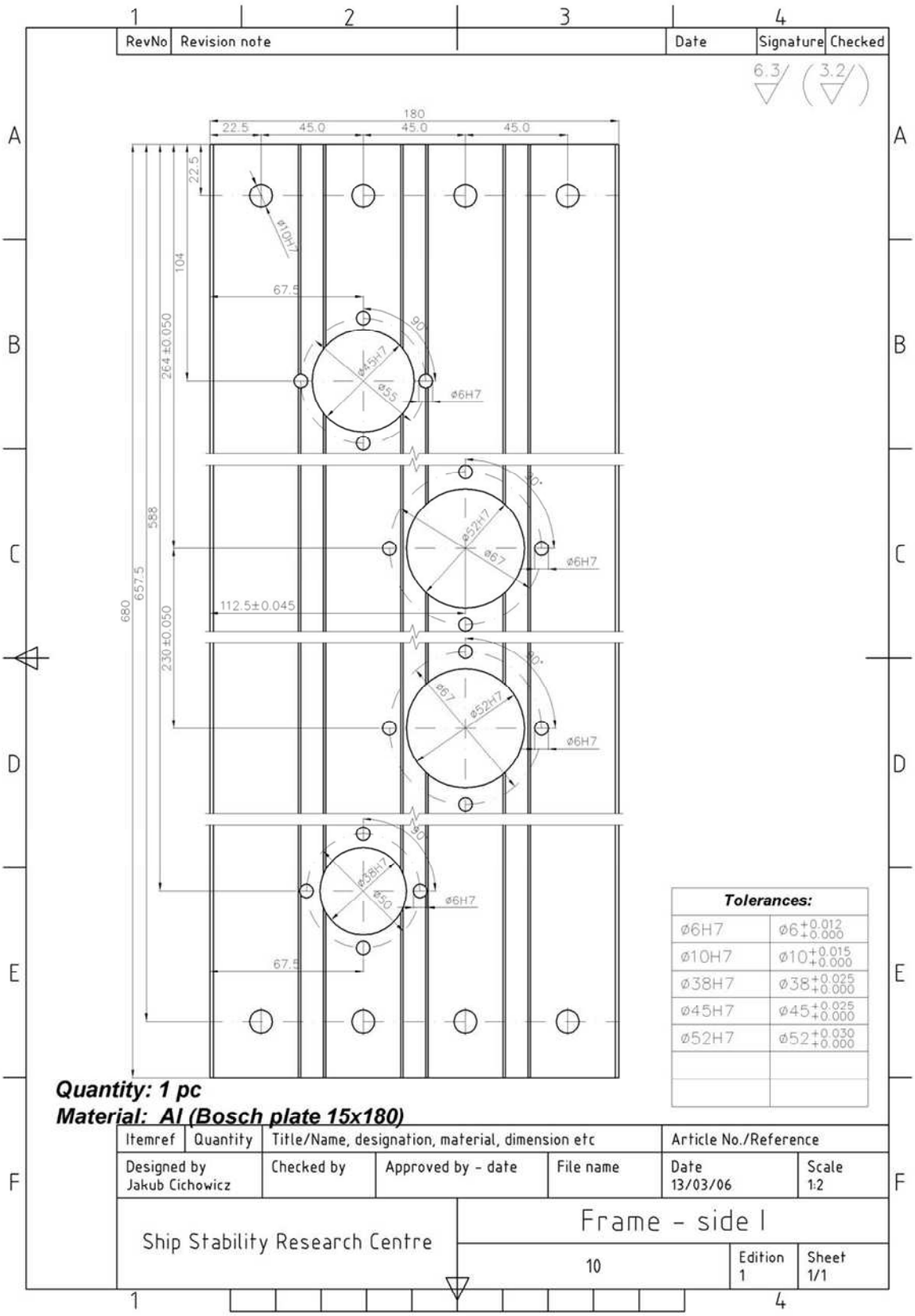
RevNo
Revision note
Date
Signature
Checked
6.3
3.2
180
22.5
45.0
45.0
45.0
22.5
104
67.5
264 ±0.050
588
657.5
680
112.5±0.045
230 ±0.050
ø10H7
ø45H7
ø55
ø6H7
90°
ø52H7
ø67
ø38H7
ø50
Tolerances:
ø6H7 ø6 +0.012 +0.000
ø10H7 ø10 +0.015 +0.000
ø38H7 ø38 +0.025 +0.000
ø45H7 ø45 +0.025 +0.000
ø52H7 ø52 +0.030 +0.000
Quantity: 1 pc
Material: Al (Bosch plate 15x180)
Itemref
Quantity
Title/Name, designation, material, dimension etc
Article No./Reference
Designed by
Jakub Cichowicz
Checked by
Approved by - date
File name
Date
13/03/06
Scale
1:2
Ship Stability Research Centre
Frame - side I
10
Edition
1
Sheet
1/1

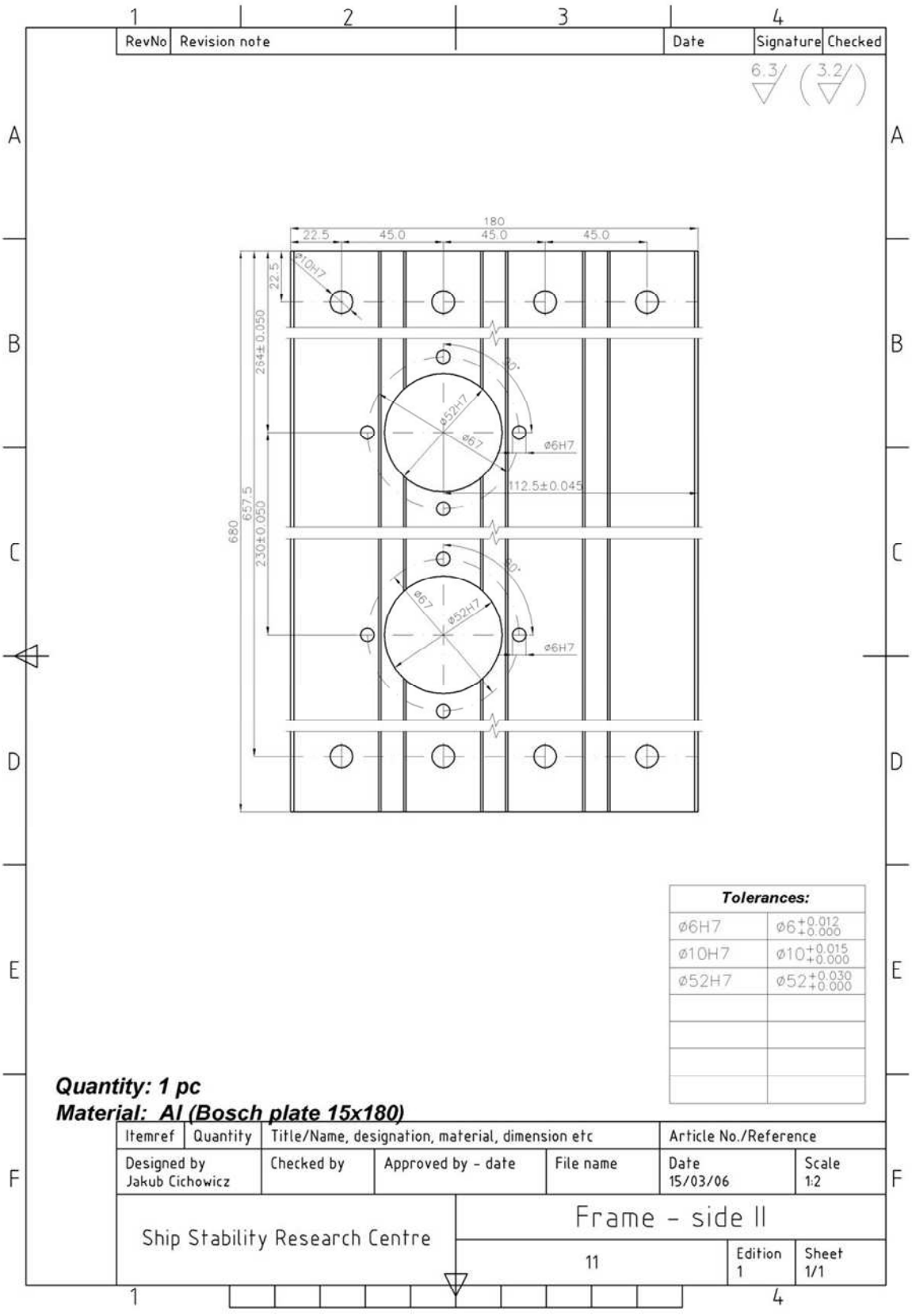
1
2
3
4
RevNo
Revision note
Date
Signature
Checked
6.3
3.2
A
B
C
D
E
F
180
22.5
45.0
45.0
45.0
ø10H7
22.5
264± 0.050
680
657.5
230±0.050
ø52H7
ø67
ø6H7
112.5±0.045
30°
Tolerances:
ø6H7
ø6 +0.012 +0.000
ø10H7
ø10 +0.015 +0.000
ø52H7
ø52 +0.030 +0.000
Quantity: 1 pc
Material: Al (Bosch plate 15x180)
Itemref
Quantity
Title/Name, designation, material, dimension etc
Article No./Reference
Designed by
Jakub Cichowicz
Checked by
Approved by - date
File name
Date
15/03/06
Scale
1:2
Ship Stability Research Centre
Frame - side II
11
Edition
1
Sheet
1/1

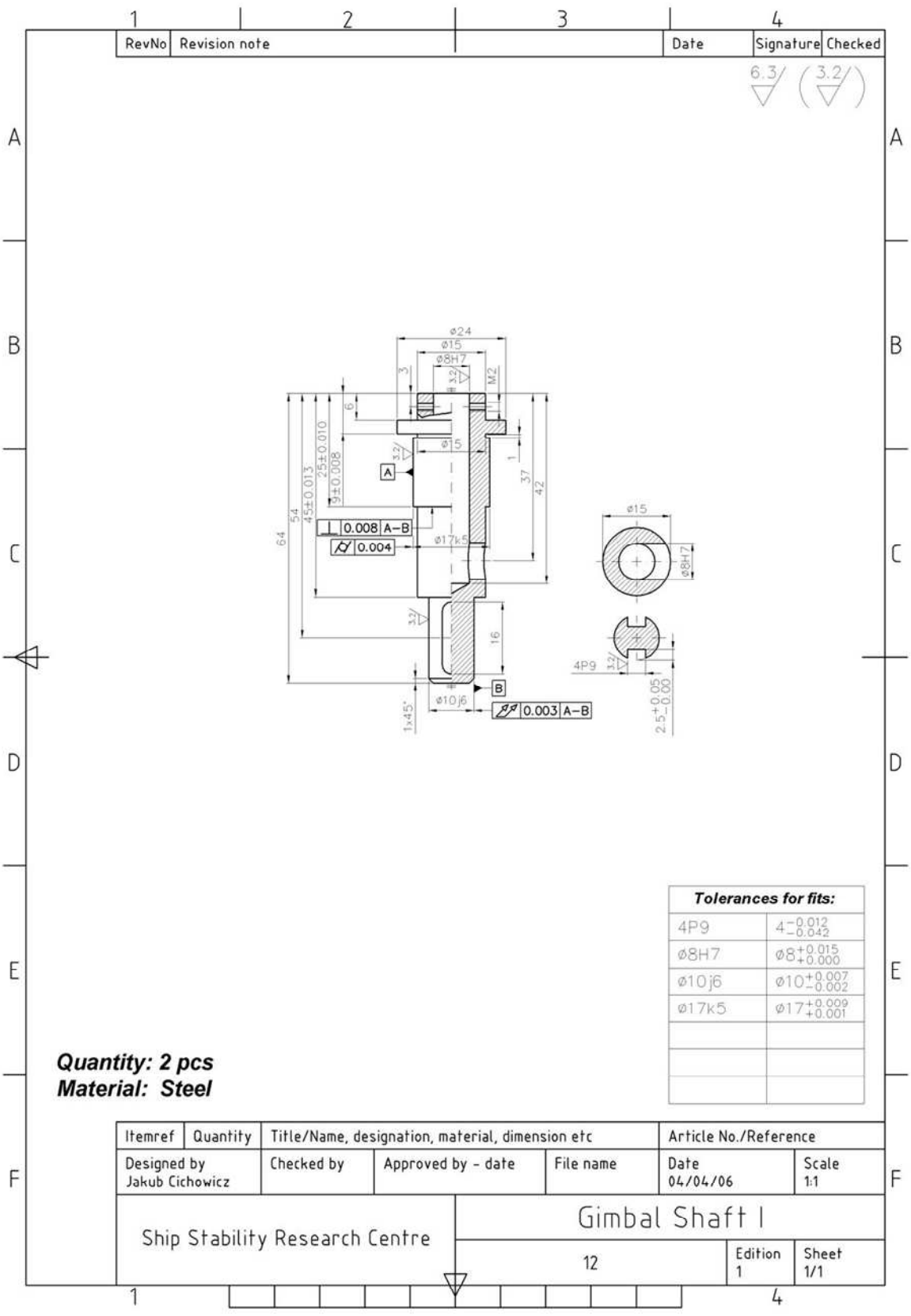
RevNo
Revision note
Date
Signature
Checked
6.3
3.2
ø24
ø15
ø8H7
M2
25±0.010
9±0.008
45±0.013
54
64
0.008 A–B
0.004
ø17k5
ø10j6
0.003 A–B
1x45°
4P9
2.5+0.05 -0.00
Tolerances for fits:
4P9 4 -0.012 -0.042
ø8H7 ø8 +0.015 +0.000
ø10j6 ø10 +0.007 -0.002
ø17k5 ø17 +0.009 +0.001
Quantity: 2 pcs
Material: Steel
Itemref
Quantity
Title/Name, designation, material, dimension etc
Article No./Reference
Designed by Jakub Cichowicz
Checked by
Approved by - date
File name
Date 04/04/06
Scale 1:1
Ship Stability Research Centre
Gimbal Shaft I
12
Edition 1
Sheet 1/1

RevNo	Revision note	Date	Signature	Checked

6.3 (3.2)

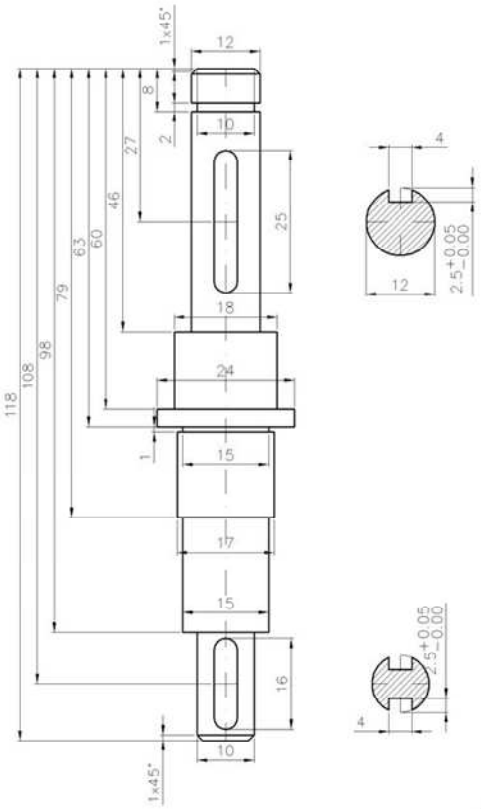

Tolerances for fits:	
4P9	$4^{-0.012}_{-0.042}$
ø8H7	$ø8^{+0.015}_{+0.000}$
ø10j6	$ø10^{+0.007}_{-0.002}$
ø17k5	$ø17^{+0.009}_{+0.001}$

Quantity: 2 pcs
Material: Steel

Itemref	Quantity	Title/Name, designation, material, dimension etc			Article No./Reference	
Designed by Jakub Cichowicz		Checked by	Approved by - date	File name	Date 05/04/06	Scale 1:1
Ship Stability Research Centre				Gimbal Shaft II		
				13	Edition 1	Sheet 1/1

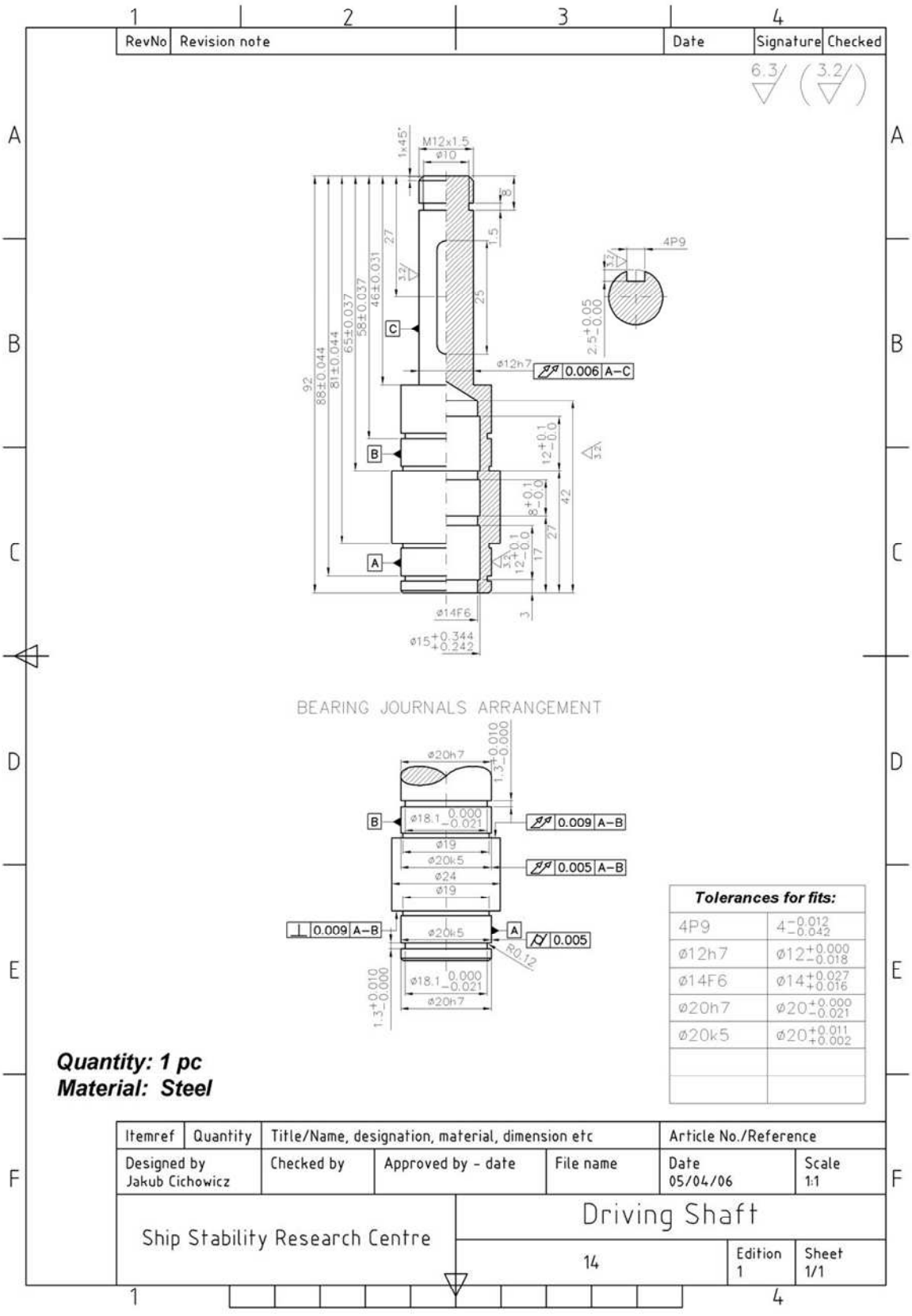
RevNo
Revision note
Date
Signature
Checked
6.3
3.2
M12x1.5
ø10
1x45°
4P9
ø12h7
0.006 A–C
ø14F6
ø15 +0.344 +0.242
BEARING JOURNALS ARRANGEMENT
ø20h7
ø18.1 0.000 −0.021
ø19
ø20k5
ø24
0.009 A–B
0.005 A–B
0.005
R0.12
Tolerances for fits:
4P9 4 −0.012 −0.042
ø12h7 ø12 +0.000 −0.018
ø14F6 ø14 +0.027 +0.016
ø20h7 ø20 +0.000 −0.021
ø20k5 ø20 +0.011 +0.002
Quantity: 1 pc
Material: Steel
Itemref
Quantity
Title/Name, designation, material, dimension etc
Article No./Reference
Designed by Jakub Cichowicz
Checked by
Approved by - date
File name
Date 05/04/06
Scale 1:1
Ship Stability Research Centre
Driving Shaft
14
Edition 1
Sheet 1/1

RevNo	Revision note	Date	Signature	Checked

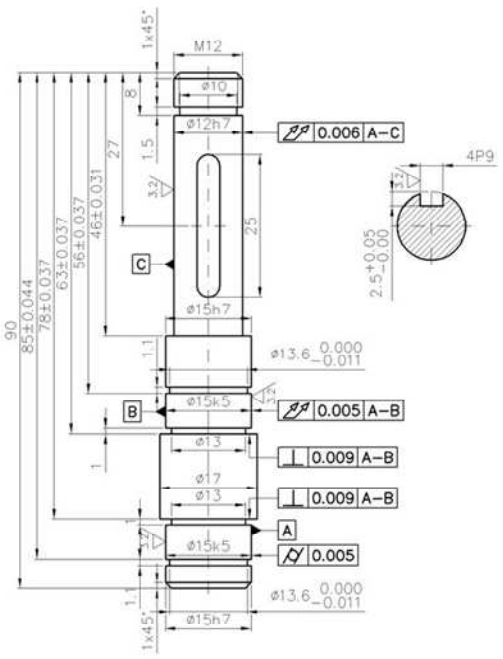

Tolerances for fits:	
4P9	$4^{-0.012}_{-0.042}$
ø12h7	$\varnothing 12^{+0.000}_{-0.018}$
ø15h7	$\varnothing 15^{+0.000}_{-0.018}$
ø15k5	$\varnothing 15^{+0.009}_{+0.001}$

Quantity: 1 pc
Material: Steel

Itemref	Quantity	Title/Name, designation, material, dimension etc			Article No./Reference	
Designed by Jakub Cichowicz		Checked by	Approved by - date	File name	Date 07/04/06	Scale 1:1
Ship Stability Research Centre					Pulley Shaft	
					15	Edition 1 / Sheet 1/1

Appendix B Results summary

Intact, 2 deg, **symmetric** coefficients								
	Frequency	Moment ampl.	Moment phase	Roll ampl.	Roll phase	Sway ampl.	Sway phase	Drift
Run name	[rad/s]	[Nm]	[deg]	[deg]	[deg]	[mm]	[deg]	[mm/s]
Run21	6.0049	8.5559	276.1963	2.0604	99.473	1.8667	87.1666	-0.3712
Run23	4.1236	0.5311	120.2816	3.1971	-42.3	3.4982	-50.9887	0.646
Run24	3.6656	1.5633	-7.1666	2.6524	-9.6271	3.1471	-9.8798	0.0087
Run26	7.4375	16.5065	1063.0464	2.0227	884.4209	1.6611	877.7362	0.228
Run27	8.0476	24.2383	232.8645	2.3741	54.1825	2.073	52.2858	0.6412
Run30	10.6458	39.8077	146.8878	1.9152	-32.5304	1.4985	-29.6223	-0.0391
Run31	10.6431	39.8263	210.2713	1.9429	30.6819	1.2427	40.3092	0.0078
Run35	8.3099	25.0593	128.9789	2.2663	-49.5642	2.0182	-51.1932	0.1565
Run36	8.4547	25.5953	122.485	2.2103	-56.2631	1.9657	-56.7854	0.0017
Run37	7.2786	16.4308	210.6466	2.1558	32.3829	2.0154	26.8907	0.0186
Run38	7.2809	16.4167	306.5093	2.1414	128.5207	2.0539	123.1893	0.153
Run39	2.1808	6.1806	-168.4813	2.5311	-168.3983	2.9019	-167.1329	-0.027
Run45	5.4712	5.8162	126.3054	2.0401	-50.0651	2.2929	-60.6284	0.0399
Run46	5.4669	5.8244	308.2113	2.0219	131.5566	2.2621	122.8626	-0.0587
Run48	5.3834	5.4619	250.2858	2.0281	74.5024	1.959	66.6394	0.0685
Run50	5.18	4.6401	34.046	2.0894	-141.301	2.0212	-150.2524	0.0508
Run52	4.8118	3.3744	42.7634	2.3384	-132.6366	2.7366	-140.3603	0.0044

[a22]	[a24]	[a42]	[a44]	[b22]	[b24]	[b42]	[b44]	Dissipation work
[kg]	[kg.m]	[kg.m]	[kg.m^2]	[kg/s]	[kg.m/s]	[kg.m/s]	[kg.m^2/s]	[J]
-0.622	1.8	1.8	1.2168	-0.5568	-10.3467	-10.3467	3.3362	-0.0558
-0.2486	0.0188	0.0188	1.2452	-0.4073	-6.0869	-6.0869	1.4712	-0.0288
-0.0696	-0.9329	-0.9329	1.2916	-0.0135	-0.1714	-0.1714	0.4189	-0.0098
-0.1577	2.4012	2.4012	1.2057	-0.2966	-6.3674	-6.3674	2.0969	-0.0437
0.0603	1.8783	1.8783	1.3397	-0.1089	-2.0849	-2.0849	1.8798	-0.0725
0.0279	2.7	2.7	1.4876	0.1681	3.7897	3.7897	0.7969	-0.0425
-0.5182	4.0748	4.0748	1.2338	0.3701	10.1808	10.1808	0.0545	-0.0304
0.059	1.7215	1.7215	1.3163	-0.1034	-1.8853	-1.8853	2.1322	-0.0792
0.0815	1.7281	1.7281	1.3311	-0.036	-0.6143	-0.6143	1.7773	-0.0678
-0.1577	1.3693	1.3693	1.2487	-0.3186	-5.8282	-5.8282	2.4404	-0.0589
-0.1679	1.1509	1.1509	1.3122	-0.3217	-5.8059	-5.8059	2.7491	-0.0675
-0.0394	-0.5733	-0.5733	0.0375	0.0329	0.4938	0.4938	-0.158	0.0012
-0.6901	-0.1624	-0.1624	1.3681	-0.6502	-10.0416	-10.0416	3.167	-0.0412
-0.4732	-0.1852	-0.1852	1.4539	-0.5366	-8.2468	-8.2468	2.8127	-0.0378
-0.2134	1.1365	1.1365	1.297	-0.3569	-6.3628	-6.3628	2.8047	-0.0446
-0.2655	1.1507	1.1507	1.2332	-0.3911	-6.9714	-6.9714	2.757	-0.0431
-0.3568	-0.674	-0.674	1.4066	-0.457	-6.7534	-6.7534	2.2776	-0.0347

Intact, 5 deg, **asymmetric** coefficients								
	Frequency	Moment ampl.	Moment phase	Roll ampl.	Roll phase	Sway ampl.	Sway phase	Drift
Run name	[rad/s]	[Nm]	[deg]	[deg]	[deg]	[mm]	[deg]	[mm/s]
Run98	8.0737	43.9378	215.8886	4.3263	37.003	3.7605	34.2842	0.1851
Run96	7.5076	38.8023	261.2656	4.6602	82.7929	3.6138	76.1269	-0.0978
Run93	5.6618	16.8834	319.1751	5.1177	142.7281	5.3436	131.9243	-0.1198
Run92	2.5472	9.8118	-69.1908	4.7221	-69.5738	5.5121	-69.3634	0.078
Run91	2.5484	9.7956	-1218.7401	4.7247	-1219.1262	5.5337	-1219.1674	0.0574
Run90	2.7134	8.5672	-35.638	4.5004	-36.0372	5.2095	-34.8099	0.1023
Run89	2.7081	8.4458	149.7945	4.457	149.6209	5.1461	150.1623	0.2075
Run87	3.1881	5.659	35.3565	4.3136	34.4887	4.8445	33.059	0.0543
Run86	3.1868	5.6372	101.8391	4.3411	101.3058	4.8702	99.5947	0.1514
Run85	3.5402	4.5928	-29.9877	5.7614	-31.2388	6.8892	-31.194	0.0035
Run84	3.5437	4.2942	136.3702	5.4413	134.7278	6.2843	134.801	-0.0579
Run83	3.5941	2.6294	103.5976	3.7632	100.9605	4.5593	97.7575	0.0222
Run79	4.0108	0.3411	583.4946	4.2415	529.957	4.8959	523.4239	0.1849
Run77	4.1395	0.9275	127.1989	5.3242	-31.3229	6.134	-38.4461	0.4356
Run76	4.1401	0.9491	315.9371	5.2771	154.7185	6.2177	147.7556	0.2536
Run75	4.3197	2.5218	302.1382	4.9142	129.3043	5.8734	123.4149	0.0596
Run72	4.5478	4.6553	143.7834	5.1684	-31.0748	5.7849	-38.9663	0.0466
Run71	4.545	4.6516	172.5915	5.1339	-2.9272	5.8806	-9.2716	-0.0981
Run70	4.8946	7.5851	65.2651	4.7339	-110.2497	5.2704	-120.3101	-0.0347
Run69	4.89	7.5583	232.7061	4.6872	57.3664	4.9831	48.2956	-0.0186
Run68	4.865	7.4514	340.3992	4.8374	165.0714	4.941	155.3348	0.1022
Run67	5.0912	10.1162	51.7428	5.0176	-124.1916	5.1602	-134.1049	0.2693
Run66	5.0903	10.1025	67.3575	5.0296	-108.1622	5.1163	-118.3201	0.0225
Run65	5.1351	10.2807	121.6351	4.8609	-53.9729	5.2088	-64.6371	0.1338
Run63	5.3231	12.8405	269.0458	5.1026	93.0457	5.3195	83.3577	0.8434
Run62	5.3431	12.819	35.4505	5.0169	-140.8939	5.3567	-150.4684	0.4729
Run61	6.0507	19.8772	240.3902	4.7074	63.3306	4.665	52.9651	1.2065

[a22]	[a24]	[a42]	[a44]	[b22]	[b24]	[b42]	[b44]	Dissipation work
[kg]	[kg.m]	[kg.m]	[kg.m^2]	[kg/s]	[kg.m/s]	[kg.m/s]	[kg.m^2/s]	[J]
-0.3492	-5.8778	0.1137	1.6929	-0.1462	-2.9766	0.0764	1.5448	-0.2025
-0.4174	-4.1543	0.144	1.5488	-0.2648	-6.0437	0.0855	1.9543	-0.2638
-1.1436	-8.8195	0.2793	1.9028	-0.5645	-9.8494	0.1521	2.6386	-0.2933
-0.75	-11.2139	0.0772	1.157	0.0045	0.0973	0.0207	0.3045	-0.017
-0.7572	-11.2842	0.0802	1.1942	-0.0028	-0.019	0.0212	0.3139	-0.0171
-0.7341	-11.0368	0.0794	1.2115	0.0348	0.5992	0.0166	0.2391	-0.0147
-0.7272	-10.9863	0.0869	1.3161	0.0131	0.2634	0.0072	0.1036	-0.0063
-0.6744	-10.4211	0.0978	1.4872	-0.045	-0.7963	0.0253	0.4066	-0.0203
-0.6739	-10.3985	0.1024	1.5681	-0.0526	-0.9516	0.0164	0.2774	-0.0125
-0.8034	-11.7268	0.1264	1.8457	0.0018	0.0294	0.0191	0.2784	-0.0317
-0.7277	-10.9974	0.1182	1.7883	0.0028	0.0465	0.024	0.361	-0.0367
-0.8604	-11.979	0.1456	1.9686	-0.1366	-2.1643	0.0435	0.6593	-0.0249
-0.858	-10.9051	0.1621	1.9032	-0.2856	-4.688	0.0764	1.2275	-0.0637
-0.8894	-10.8567	0.1654	1.8917	-0.3303	-5.2607	0.0781	1.2232	-0.0991
-0.937	-11.3239	0.1704	1.961	-0.3263	-5.2594	0.0723	1.1499	-0.0884
-0.9363	-11.6467	0.1775	2.0869	-0.3008	-4.7104	0.0757	1.1649	-0.0846
-0.9002	-10.2514	0.176	1.8831	-0.3761	-6.2187	0.086	1.4077	-0.1182
-0.8702	-10.7541	0.1682	1.9621	-0.316	-5.1191	0.0763	1.2216	-0.1022
-1.0941	-10.0725	0.2312	1.9504	-0.5078	-8.4604	0.1206	1.9927	-0.154
-0.8971	-9.2189	0.2077	1.9164	-0.421	-7.2959	0.1146	1.9675	-0.1577
-0.8485	-8.4616	0.1953	1.7962	-0.4126	-7.4853	0.1057	1.9046	-0.161
-0.9124	-8.5789	0.2137	1.8403	-0.4514	-8.0249	0.117	2.0686	-0.1973
-0.9058	-8.3735	0.2202	1.8072	-0.4499	-8.1309	0.1242	2.2263	-0.2175
-1.0901	-9.313	0.2526	1.9184	-0.5296	-9.0524	0.1384	2.3463	-0.2098
-0.9648	-8.8329	0.237	1.8702	-0.4544	-8.3123	0.131	2.371	-0.2504
-1.0188	-9.2815	0.237	1.903	-0.4927	-8.44	0.1322	2.2484	-0.2246
-1.0343	-7.8925	0.26	1.8009	-0.5083	-9.6007	0.1372	2.5784	-0.2628

Damaged, 2 deg, **asymmetric** coefficients								
	Frequency	Moment ampl.	Moment phase	Roll ampl.	Roll phase	Sway ampl.	Sway phase	Drift
Run name	[rad/s]	[Nm]	[deg]	[deg]	[deg]	[mm]	[deg]	[mm/s]
Run107	8.002	14.9765	317.2276	1.7739	137.4349	2.6968	141.528	0.0324
Run110	8.0664	14.8955	279.5137	1.7683	99.6378	2.5989	105.2499	-0.0231
Run112	7.4139	13.4892	238.8897	1.9429	61.1892	2.7079	60.9234	-0.8821
Run113	6.1533	9.4341	257.2546	2.1003	102.2077	4.8317	74.0924	-9.0783
Run114	6.1527	9.3636	297.6562	2.1956	143.4228	4.8114	115.0078	-6.8234
Run118	6.2844	8.6013	7.0564	1.9749	-149.3705	4.0188	-181.7658	-5.5949
Run121	4.6864	5.63	206.5607	2.1737	31.6373	4.6502	31.5702	-1.3498
Run122	4.2272	4.1769	20.7175	2.2894	-156.1981	4.609	-155.2861	-0.9383
Run123	4.2126	4.3752	193.2797	2.2893	16.3287	4.688	16.2496	-0.8306
Run124	3.841	3.4781	205.6604	2.4364	29.6611	4.8878	29.018	-0.4642
Run125	3.8569	2.8925	106.0846	2.2052	-68.3017	4.2707	-68.5686	-0.4251
Run126	3.6116	2.3218	279.9728	2.1322	104.8191	4.2099	103.3994	0.1138
Run127	3.613	2.0839	69.1811	2.1534	-102.8836	4.3302	-103.736	0.012
Run128	3.6114	2.2917	194.4077	2.1307	19.5586	4.3338	18.2892	0.009
Run129	3.1262	1.1396	283.3237	2.3965	119.7155	4.5692	117.082	-0.3749
Run136	2.607	0.0938	-25.5895	1.9327	-81.7179	3.4569	-85.5164	-0.3047
Run137	1.8578	1.2763	-12.6371	2.5065	-17.9489	6.6612	-31.7078	-0.0423
Run138	1.7511	1.1658	-144.3638	2.0475	-149.5138	5.7245	-155.2711	-0.3227
Run139	1.7474	1.2897	1254.2734	2.1257	1246.8016	6.019	1235.8049	-0.4519
Run146	5.4424	7.1329	-1084.7537	1.8506	-1256.2924	4.4477	-1265.0887	-1.4218
Run147	5.4405	7.1689	61.2224	1.7679	-109.1726	4.3079	-110.1394	-1.8905
Run148	6.1333	8.8553	48.2997	2.013	-104.7753	4.8039	-134.1378	-4.9681
Run149	6.1397	8.9765	233.9495	2.0292	79.9901	4.7732	52.1308	-4.1651
Run150	6.1709	8.6951	228.4713	2.0335	73.6059	4.3403	44.0843	-4.698
Run151	5.8235	8.9274	16.1412	1.95	-144.7661	5.2274	-158.9706	-3.9114
Run152	5.8359	9.0209	147.8843	1.9799	-11.9085	5.3319	-24.891	-4.2419
Run153	5.5957	9.2606	182.8192	2.1747	16.2628	5.7286	11.5526	-3.6539
Run154	4.9485	8.3531	107.2087	3.2207	-66.7701	6.7284	-66.913	-2.5313
Run155	4.9393	7.9562	342.3938	3.0664	166.9589	6.368	166.6323	-2.3892
Run156	4.9314	6.9586	254.7304	2.4867	79.2243	5.2614	81.1472	-1.4874
Run157	6.7802	9.7635	150.2344	1.8783	-20.9434	2.6792	-37.3718	-1.9788
Run158	6.8053	10.0923	137.4149	1.89	-34.1498	2.6615	-51.2939	-1.5369
Run159	6.5535	9.6335	64.1556	2.0705	-104.6884	3.1175	-130.6411	-4.2864
Run160	6.553	9.4612	272.8225	2.0449	105.7871	2.985	79.652	-4.3003
Run162	6.4139	9.3061	334.5024	2.1266	172.7825	3.8303	141.515	-7.2333
Run165	8.7306	20.8067	-25.7862	2.1122	152.9318	3.5085	158.445	-0.6011
Run166	9.0193	22.7255	-206.5407	1.9865	-27.3343	3.2664	-20.0781	-0.0783
Run167	9.0224	22.9399	-221.9969	2.053	-42.9214	3.3995	-31.8129	-0.1053
Run168	9.938	26.7674	-82.005	1.9655	97.1149	3.4747	107.038	-0.2961
Run169	9.928	26.8992	-231.4786	1.9441	-52.1999	3.4129	-41.6432	-0.7452
Run172	2.2227	0.5764	134.7583	1.7857	121.8725	2.9831	105.8533	-0.2382
Run173	2.4022	0.3756	136.0649	2.0539	124.1748	3.5297	116.8951	0.0017
Run174	2.3846	0.4398	-87.0472	2.1049	-103.6327	3.6551	-110.979	-0.0759
Run175	2.3982	0.4585	53.237	2.4466	43.443	4.2558	34.2285	-0.6191

[a22]	[a24]	[a42]	[a44]	[b22]	[b24]	[b42]	[b44]	Dissipation work
[kg]	[kg.m]	[kg.m]	[kg.m^2]	[kg/s]	[kg.m/s]	[kg.m/s]	[kg.m^2/s]	[J]
-0.6252	-3.9138	0.3249	3.5855	0.4939	5.7319	-0.0205	-0.2691	-0.0056
-0.7768	-3.207	0.3123	3.3309	0.6384	7.6471	-0.0385	-0.4993	-0.0034
-0.1835	-2.287	0.2576	3.1511	-0.0272	-0.3178	0.1776	2.1633	-0.0576
-15.6382	-10.8274	8.0248	3.5222	-6.1188	-37.6223	3.2518	19.9247	-0.4105
-14.5662	-9.6552	7.4877	3.0213	-5.4392	-36.7241	2.9048	19.4613	-0.4437
-16.0505	-7.2432	7.3717	2.6148	-4.0878	-39.0709	1.9077	18.1231	-0.3379
-1.4823	-12.0924	0.7081	5.7617	-0.0354	-0.0733	0.3453	2.7697	-0.0594
-1.2116	-10.446	0.5828	5.1351	0.1178	0.8824	0.1368	1.2144	-0.0283
-1.2791	-10.9008	0.6525	5.5532	-0.0241	-0.076	0.1643	1.3728	-0.0292
-1.193	-10.3556	0.6325	5.4368	-0.0712	-0.5642	0.1777	1.5288	-0.0324
-1.0487	-9.447	0.5307	4.7483	-0.0193	-0.2285	0.2021	1.9092	-0.0342
-1.1354	-9.9365	0.5902	5.0781	-0.1202	-1.1563	0.1709	1.568	-0.0229
-1.2044	-10.4164	0.5445	4.6097	-0.0768	-0.7064	0.2481	2.1699	-0.0339
-1.2583	-10.7152	0.6165	5.1607	-0.116	-1.0628	0.1863	1.6314	-0.024
-1.0145	-9.0389	0.5009	4.2134	-0.1913	-1.7937	0.2907	2.6188	-0.0421
-0.8006	-7.4767	0.3729	3.4592	-0.1722	-2.0345	0.0934	1.0814	-0.0082
-3.2036	-18.2376	0.9208	5.0676	-0.7557	-7.5247	0.2771	2.5469	-0.0163
-3.3447	-20.4295	0.9072	5.316	-0.2382	-3.1512	0.273	2.1289	-0.0117
-3.6098	-20.6225	0.9474	4.7675	-0.5823	-6.0179	0.4845	3.4786	-0.0195
-3.5192	-15.147	1.715	6.3135	-1.7446	-12.7207	1.0382	7.4672	-0.1042
-2.243	-15.9353	1.0528	6.8811	-0.1432	-1.4479	0.9336	7.1969	-0.1159
-17.9041	-11.4571	9.1235	3.3989	-3.9549	-40.2196	2.1259	21.2019	-0.3944
-16.1329	-11.4105	8.3786	3.4778	-5.07	-38.2049	2.751	20.5962	-0.3938
-14.8224	-8.8015	7.422	2.8896	-4.4681	-37.3427	2.2981	19.1327	-0.3744
-7.789	-17.8441	4.7228	6.3128	-3.3925	-23.3827	2.5772	17.2356	-0.2979
-7.1444	-18.1521	4.5572	6.2361	-2.6803	-21.8259	2.2247	17.8933	-0.3258
-3.2931	-18.3367	1.8244	7.0487	-1.0992	-7.7125	1.5398	11.0187	-0.2549
-1.3699	-11.4429	0.5679	4.7061	-0.0065	-0.1696	0.3328	3.1339	-0.1549
-1.3434	-11.28	0.5699	4.7223	-0.0326	-0.3822	0.3046	2.4006	-0.1063
-1.4725	-11.7757	0.5997	5.3198	0.2596	2.2786	0.2967	2.238	-0.0745
-2.9476	-2.1213	1.4417	2.4563	-1.1816	-17.7476	0.5267	7.9707	-0.1514
-3.1044	-1.8417	1.4661	2.5424	-1.2311	-18.3028	0.5222	7.8468	-0.1505
-6.8718	-2.2673	2.5714	2.252	-1.7289	-27.0625	0.6057	9.6867	-0.2049
-6.4912	-1.7093	2.7326	2.0797	-2.5708	-26.3557	1.0358	10.6717	-0.2295
-12.5506	-4.9477	5.1577	2.3231	-4.2463	-35.2617	1.7323	14.4164	-0.3166
-1.2695	-5.7074	0.5204	3.58	0.8823	9.1292	-0.2174	-2.2705	0.0529
-1.8163	-5.3966	0.6127	4.1408	1.1311	12.2244	-0.1903	-2.1033	0.033
-3.543	-5.2748	0.8306	3.942	1.7036	18.5049	-0.2524	-2.8111	0.0399
-4.0277	-6.7296	0.9403	4.0983	1.9369	19.3491	-0.3011	-3.0633	0.042
-4.3698	-6.513	0.9564	4.2113	1.9387	20.3651	-0.2751	-2.9518	0.034
-0.9013	-5.4945	0.3942	2.7097	-0.5896	-6.7416	0.2079	2.4682	-0.0126
-0.7364	-6.4826	0.3449	3.156	-0.3028	-3.4459	0.103	1.2227	-0.0087
-0.7685	-6.7165	0.3585	3.0918	-0.3031	-3.4871	0.1546	1.7594	-0.0144
-0.8271	-6.6977	0.3566	3.1647	-0.4106	-4.3946	0.1063	1.1828	-0.0104

Damaged, 2 deg, **asymmetric** coefficients								
	Frequency	Moment ampl.	Moment phase	Roll ampl.	Roll phase	Sway ampl.	Sway phase	Drift
Run name	[rad/s]	[Nm]	[deg]	[deg]	[deg]	[mm]	[deg]	[mm/s]
Run193	1.5595	3.6742	-2.8811	5.1878	-4.9151	13.1251	-6.177	0.0302
Run194	1.5602	3.6458	67.8685	5.2044	65.8638	12.976	64.6444	-0.2656
Run195	1.8711	3.1615	-5.105	5.862	-10.3533	14.3423	-20.5024	-1.1911
Run197	2.2124	2.1646	53.8859	6.4384	43.075	12.8789	32.0059	-1.9829
Run198	2.2118	1.3162	-106.9171	4.1199	-117.5785	7.7458	-128.9378	-1.3383
Run199	2.4517	0.7392	5.9292	4.4714	-13.5472	8.4344	-20.4108	-0.9757
Run200	2.4502	0.8326	71.4922	4.8115	51.6116	9.509	37.8394	-1.7227
Run201	2.5742	0.3547	-95.4774	4.4773	-138.5499	8.3648	-146.9373	-1.4446
Run202	2.573	0.4111	22.9809	4.9496	-22.0438	8.3925	-26.9768	-0.7035
Run203	2.7846	0.6966	1044.5953	4.99	891.3874	10.0689	888.3017	-0.7922
Run205	3.2864	2.6938	299.219	4.4342	126.609	8.4688	122.6807	-1.0138
Run206	3.2881	3.0506	-1084.6268	4.7899	-1256.9024	8.8246	-1259.5146	-1.9895
Run208	3.6587	5.6137	24.0907	5.3291	-149.2827	10.1445	-151.2668	-2.0143
Run209	3.549	5.28	203.2525	5.6267	30.2596	11.686	28.1	-3.4072
Run211	4.2721	9.5156	214.2866	4.9978	40.908	10.1314	42.371	-4.5403
Run212	5.0723	14.6661	78.421	4.6522	-95.0072	9.8261	-95.7005	-6.9731
Run213	5.076	14.7941	196.7171	4.4669	23.264	10.8709	22.7784	-7.3516
Run215	10.6373	64.776	-207.8023	3.8776	-28.2666	6.4243	-15.2753	-4.6203
Run217	9.6379	59.3207	-100.6573	4.5265	78.5444	7.7793	88.343	-4.4152
Run218	9.3785	57.4187	-219.4532	4.7654	-40.4898	8.0297	-30.34	-5.7497
Run219	8.8433	53.928	-11.1801	4.924	168.4078	7.4672	179.9415	-3.2021
Run220	8.6889	53.0843	-217.7791	4.9798	-37.7936	8.062	-28.1018	-2.5131
Run221	8.69	52.8605	-122.2575	4.9778	57.4237	7.7569	67.311	-2.9682
Run222	7.9221	44.3387	340.3405	5.4488	161.9278	7.7629	165.7512	-3.2556
Run223	8.3856	46.2729	69.5507	4.8111	-110.205	7.5733	-107.2943	-2.7872
Run224	8.2535	45.4847	249.5447	5.1943	70.3756	7.4786	79.5275	-2.3382
Run225	7.784	39.3492	253.4479	4.9952	75.1798	7.3786	77.1534	-2.6507
Run226	7.6984	38.8988	1433.9839	5.1556	1255.641	7.4277	1257.2126	-3.0491
Run227	6.8719	30.0811	299.1174	5.3952	126.2165	7.3264	110.9106	-12.0583
Run228	7.0229	30.8891	297.4743	5.3158	122.6012	6.8142	112.5753	-8.4873
Run229	6.692	26.3835	219.2957	5.3879	48.7217	6.6199	29.4853	-17.3502
Run230	6.4359	25.2471	34.1181	5.6067	-131.5433	8.7472	-159.298	-34.1391
Run231	6.4979	24.4336	45.798	5.2604	-121.5285	7.8472	-147.3489	-29.001
Run232	6.3957	21.3466	194.939	4.7818	31.0895	8.1365	1.8322	-30.9539
Run233	6.3877	22.405	53.1974	5.0407	-110.8698	8.1152	-139.103	-30.4268
Run234	6.2412	19.3579	243.8739	4.5041	85.2401	8.6138	56.3374	-30.5211
Run235	6.2572	19.9017	6.366	4.6043	-153.2963	8.7367	-182.4596	-31.7816
Run237	6.164	20.1581	273.5584	4.7413	115.8115	9.6296	87.4726	-30.5299
Run238	6.0962	20.5747	236.7283	4.8501	79.591	10.243	53.9584	-28.0234
Run240	5.9957	20.8823	693.5701	4.9788	536.826	11.2263	517.4654	-28.1522
Run241	5.9117	20.6768	192.5252	4.8876	35.4319	11.4126	14.4024	-23.7762
Run242	5.814	21.3526	208.967	5.1544	50.5762	12.0601	33.8474	-24.2638
Run243	5.673	19.8644	101.7496	4.7777	-60.0182	11.8747	-72.2732	-14.2878
Run244	5.4473	19.5229	15.186	5.2913	-150.9695	12.5307	-157.75	-13.7569
Run245	5.5687	19.1036	327.5825	4.7083	164.5092	11.5728	154.8778	-16.058
Run246	5.293	17.9642	111.5814	4.9761	-58.0268	11.3607	-61.3089	-10.9319
Run247	5.1341	16.8095	-330.3622	4.8539	-501.6777	11.907	-504.3339	-9.2796
Run248	4.8222	14.5835	235.7389	5.562	64.3845	12.0198	63.0494	-8.4113
Run249	4.7062	13.4533	215.2091	5.5456	44.4504	11.7365	42.7092	-6.2721
Run251	7.3492	31.6336	189.7933	4.7441	12.8276	6.2548	9.9143	-3.8266

[a22]	[a24]	[a42]	[a44]	[b22]	[b24]	[b42]	[b44]	Dissipation work
[kg]	[kg.m]	[kg.m]	[kg.m^2]	[kg/s]	[kg.m/s]	[kg.m/s]	[kg.m^2/s]	[J]
-2.4887	-17.1535	0.4565	3.1158	-0.0443	-0.5622	0.1363	0.9858	-0.0371
-2.3851	-16.6826	0.4598	3.1873	-0.0705	-0.5321	0.1365	0.9572	-0.0364
-2.4245	-15.824	0.6479	3.9566	-0.5152	-5.2143	0.2468	2.2058	-0.0929
-1.3991	-10.0369	0.4876	3.3672	-0.5733	-5.5488	0.2343	2.2356	-0.1431
-1.1453	-8.4543	0.4439	3.277	-0.4245	-5.3794	0.1644	2.0839	-0.0549
-1.0483	-8.6987	0.4231	3.4532	-0.3346	-3.6285	0.1549	1.6588	-0.0601
-1.5481	-9.561	0.5372	3.5691	-0.7779	-7.519	0.2217	2.1898	-0.0748
-1.0762	-8.4153	0.4442	3.559	-0.4063	-4.604	0.1427	1.6739	-0.0591
-0.6577	-6.2458	0.3412	3.1848	-0.2133	-2.4745	0.1338	1.5325	-0.0787
-1.2464	-10.5001	0.5066	4.1633	-0.2018	-1.9767	0.1654	1.5004	-0.0855
-1.0595	-9.0701	0.5012	4.2199	-0.3045	-2.814	0.1801	1.6442	-0.0837
-0.8941	-8.2072	0.4703	4.2108	-0.1725	-1.8125	0.1705	1.6602	-0.1072
-1.0051	-9.0205	0.5218	4.5274	-0.1464	-1.5822	0.2129	2.0489	-0.1887
-1.3707	-11.2847	0.6206	4.947	-0.2369	-1.808	0.2468	2.0311	-0.1981
-1.2536	-10.6389	0.5697	5.2055	0.1163	1.4491	0.3394	2.7407	-0.3012
-1.428	-11.749	0.7064	5.5841	-0.0441	-0.8515	0.4146	4.1315	-0.4284
-2.2227	-15.9122	0.9643	6.7316	-0.1592	-0.6661	0.5857	4.2783	-0.4133
-6.1192	-4.9814	1.0768	4.3252	2.0778	24.9274	-0.2401	-2.9811	0.1039
-3.5196	-6.1522	0.8579	4.2187	1.8228	18.095	-0.2718	-2.7773	0.1947
-3.4066	-5.711	0.8494	3.9426	1.5083	17.949	-0.2443	-2.9751	0.2606
-2.961	-3.4998	0.6292	3.8566	1.5563	17.3339	-0.1703	-1.9582	0.0995
-2.538	-4.9416	0.5715	4.1716	1.3248	15.3751	-0.1138	-1.401	-0.0012
-2.3785	-4.153	0.5778	4.0095	1.3373	15.1114	-0.1411	-1.6898	0.0747
-0.4322	-2.6722	0.2155	3.2909	0.4315	4.9761	0.107	1.2188	-0.3682
-0.5896	-4.6586	0.3561	3.9068	0.3885	4.4252	-0.0099	-0.11	-0.054
-1.5594	-2.6815	0.2733	3.1793	1.0264	12.3832	-0.0044	-0.1325	-0.1881
-0.3464	-3.3931	0.2569	3.4453	0.2255	2.6201	0.1364	1.522	-0.3265
-0.2756	-2.9148	0.2419	3.2378	0.1764	2.0138	0.1256	1.4489	-0.3185
-2.3552	-1.3399	1.1569	2.635	-1.6117	-15.9751	0.6807	6.7963	-1.0792
-0.9702	-0.6165	0.6222	2.5045	-0.9302	-10.3083	0.4404	4.9114	-0.7962
-2.6977	0.5361	1.3519	1.9018	-1.2138	-17.6105	0.5492	7.8956	-1.2556
-7.979	-2.7494	3.3346	2.2868	-2.1073	-28.9706	0.8348	11.7716	-1.8425
-6.5852	-2.1478	2.7642	2.3001	-1.5825	-26.54	0.6148	10.6956	-1.4939
-10.1968	-4.1005	4.2431	2.4321	-2.132	-32.3163	0.8776	13.245	-1.4746
-8.6396	-3.2482	3.7751	2.3216	-1.4437	-30.0484	0.6016	12.8665	-1.6235
-11.8209	-6.5113	5.6595	2.6522	-5.1892	-33.8734	2.504	16.3526	-1.6044
-11.9523	-6.3973	5.529	2.7185	-4.0685	-34.2233	1.8958	15.9004	-1.6186
-12.5073	-7.9569	6.078	2.9493	-6.2271	-34.3404	3.0805	16.9639	-1.8079
-11.4811	-9.27	5.9951	3.2492	-5.0263	-32.8091	2.7048	17.6759	-1.9609
-8.3952	-12.0312	5.0615	3.9361	-4.637	-26.9823	3.1292	17.8425	-2.1094
-10.0531	-12.6011	5.7851	4.2521	-3.4376	-29.8769	2.1193	18.5124	-2.0231
-7.1325	-13.3796	4.4634	4.6529	-3.3139	-24.1351	2.3436	17.2321	-2.1228
-5.4407	-15.7957	3.4234	5.7935	-1.7363	-18.9088	1.4521	15.262	-1.5855
-2.8544	-14.8705	1.6797	5.787	-1.2721	-9.7497	1.4428	10.3137	-1.3383
-4.0703	-15.775	2.6174	6.0644	-2.4722	-14.3282	2.4108	13.531	-1.3965
-1.9976	-13.9277	1.0943	6.09	-0.4013	-4.5075	0.7204	7.5411	-0.8829
-2.3913	-16.1362	1.1687	6.8414	-0.4266	-3.7614	0.847	6.2238	-0.6721
-1.5551	-12.3865	0.7273	5.3377	-0.2614	-1.5673	0.6563	4.7875	-0.6668
-1.4644	-11.8012	0.7092	5.1495	-0.2773	-1.9646	0.6106	4.9026	-0.6557
-0.1887	-1.2774	0.2991	2.8509	-0.2319	-3.271	0.2119	2.9773	-0.4345